ANALYSIS OF PRODUCED WATER DATA TO MODEL AND IDENTIFY GEOCHEMICAL REACTIONS OCCURRING IN THE RESERVOIR

Yisheng Hu

Submitted for the Degree of

Doctor of Philosophy in Petroleum Engineering

Institute of Petroleum Engineering
School of Energy, Geoscience, Infrastructure & Society
Heriot Watt University
Edinburgh UK

August 2016

ABSTRACT

Water injection has been commonly used to maintain reservoir pressure and improve oil recovery in many oil fields. The equilibrium between reservoir rock and formation brine at initial reservoir conditions would be disturbed by the introduction of a non-native water, which mixes and reacts with the formation brine and interacts with minerals present in the formation. A series of brine/brine and/or brine/rock interactions would then take place in the flow paths from the injection well to the production well, potentially leading to dissolution and/or precipitation of minerals; knowledge of these interactions is crucial for the evaluation and the management of oilfield scale problems. In this thesis, thermodynamic models, reactive transport models and reservoir simulation models are used to identify the geochemical reactions occurring in the reservoir and investigate how the reservoir interactions affect the produced water composition. Brine composition data have been collected from 26 fields, and examples from four selective fields provide the basis for the analysis in this thesis.

For Field X, a typical sandstone reservoir located in the North Sea region, a thermodynamic prediction model was used to calculate the risk of scale precipitation based on a series of individual produced water samples, thus providing an evaluation of the actual scaling risk in these samples, which is then compared with the usual theoretical estimate based on endpoint formation and injection brine compositions, and the erroneous assumption that no reactions in the reservoir impact the produced water composition. The occurrence of barium sulphate precipitation and calcium magnesium ion exchange reaction are identified by the modelling results. The Cation Exchange Capacity was identified as a modest 0.05 mol/kgw (50 meq/L) for this field. Since ion exchange capacity is an important parameter for some chemical EOR method, this a promising technique for EOR evaluation.

An available history matched streamline reservoir simulation model of the Miller Field was then integrated with produced water chemical data. Streamline simulation is applied to better model brine mixing through reducing the numerical dispersion which cannot be effectively controlled in finite difference simulation. A simplified model of barite scale precipitation was included in the streamline simulation, and the calculation results with and without considering barite precipitation were compared with the observed produced water chemical data. The streamline simulation model assumes scale deposition is possible everywhere in the formation, whereas in reality the near production well zones

were generally protected by squeezed scale inhibitor, and thus the discrepancies between modelled and observed barium concentrations at these two given wells diagnose the effectiveness of the chemical treatments to prevent formation.

1D and 2D reactive transport models were developed to identify the geochemical reactions occurring in the Gyda Field where there is a high reservoir temperature and formation water is high salinity. Anhydrite and barite precipitation are identified as the two dominant mineral reactions taking place deep within the reservoir. Anhydrite is deposited due to mixing of formation and injection waters in the area before this zone is cooled, and the precipitated anhydrite is gradually dissolved as the local reservoir temperature is lowered by cool injection water. The dissolved anhydrite then re-precipitates downstream in the at high temperature zones since the propagation of the temperature front is much slower than the brine mixing front. This creates a risk of late life anhydrite deposition in the producer.

Finally, a carbonate reservoir study was performed for Ekofisk field where seawater flooding has been implemented. The 1D reactive transport model provides a good match with observed produced water chemistry data when the primary calcite mineral phase, calcium magnesium carbonate precipitation, temperature change and initial source of CO_2 were modelled. In Ekofisk Field, calcite dissolution drives anhydrite and calcium magnesium carbonate precipitation. The modelled combination of calcium magnesium carbonate precipitation and ion exchange remove magnesium from the brine, also as observed from the produced water data. Simulation results also demonstrate that calcite dissolves quickly at first due to CO_2 partitioning from the hydrocarbon phase into the brine. It was also shown that calcite dissolution is promoted by an increase in sulphate concentration in the injection water due to the coupled anhydrite precipitation.

This body of work develop a methodology for systematically storing and analyzing produced brine data, and using modelling tools to identify what geochemical reactions have taken place. The methodology is then applied to various reservoir scenarios, leading to insights that impact scale management in these systems, and may also have a bearing on chemical EOR methods.

To my beloved mom

for her love, endless support and encouragements.

ACKNOWLEDGEMENTS

I would like to express my sincerest gratitude to my PhD supervisor Professor Eric Mackay for the opportunity, support, encouragement and trust during this study. He is always available to discuss, guide, and support. It would have been very difficult for me to have reached this point in my academic journey, without his leadership and technical criticism, which is highly appreciated. I am fortunate to have been able to work with him. His kindly but rigorous oversight of this thesis constantly gave me the motivation to perform to my maximum ability.

I am also grateful to Foundation CMG and Flow Assurance & Scale Team (FAST) for their support both technical and financial. Without their financial contribution towards the cost of my PhD at Heriot-Watt University, Edinburgh, UK, I would not have been able to complete this study. My gratitude also goes out to FAST 5 and FAST 6 JIP sponsors for their input, financial support for my research.

I would also like to thank my second supervisor Professor Ken Sorbie for his great supervision and his fabulous insight. I would like to express my sincere thanks to Dr. Oscar Vazquez, Dr. Oleg Ishkov, Dr. Lorraine Boak and Mr. Mike Singleton who provided insight and expertise that greatly assisted my research. I would like to thank Ross McCartney, Managing Director of Oilfield Water Services for reviewing work presented to the FAST sponsors. Also thanks to my colleges, Xu Wang, Ayrton Ribeiro, Duarte Silva, Scot Shaw and Nazia Farooqui. I would also like to extend my appreciation to all the other members of the Flow Assurance & Scale Team (FAST) for making my stay at Heriot-Watt, memorable, for my lifetime.

I offer special thanks to Dr. Baard Kaasa from Scale Consult AS and Prof. Colin MacBeth from Institute of Petroleum Engineering of Heriot-Watt University, for agreeing to examine this thesis.

The following software providers are gratefully acknowledged: United States Geological Survey for providing PHREEQC, Computer Modeling Group for providing GEM and supporting software, Schlumberger for providing ECLIPSE100, FrontSim.

Special thanks also go to my parents and grandparents who encouraged and supported me throughout the period of my research. I send you all my love and warm hugs from the distance.

ACADEMIC REGISTRY
Research Thesis Submission

Name*:*	YISHENG HU		
School/PGI:	EGIS/IPE		
Version: *(i.e. First, Resubmission, Final)*	Final submission	Degree Sought (Award **and** Subject area)	PhD Petroleum Engineering

Declaration

In accordance with the appropriate regulations I hereby submit my thesis and I declare that:

1) the thesis embodies the results of my own work and has been composed by myself
2) where appropriate, I have made acknowledgement of the work of others and have made reference to work carried out in collaboration with other persons
3) the thesis is the correct version of the thesis for submission and is the same version as any electronic versions submitted*.
4) my thesis for the award referred to, deposited in the Heriot-Watt University Library, should be made available for loan or photocopying and be available via the Institutional Repository, subject to such conditions as the Librarian may require
5) I understand that as a student of the University I am required to abide by the Regulations of the University and to conform to its discipline.

* *Please note that it is the responsibility of the candidate to ensure that the correct version of the thesis is submitted.*

Signature of Candidate*:*		Date:	

Submission

Submitted By *(name in capitals):*	YISHENG HU
Signature of Individual Submitting:	
Date Submitted:	

For Completion in the Student Service Centre (SSC)

Received in the SSC by *(name in capitals):*			
Method of Submission *(Handed in to SSC; posted through internal/external mail):*			
E-thesis Submitted ***(mandatory for final theses)***			
Signature:		Date:	

TABLE OF CONTENTS

LIST OF FIGURES

LIST OF TABLES

NOMENCLATURE

1D	One-dimensional
2D	Two-dimensional
3D	Three-dimensional
å	Empirical ion-size parameter
a_A	Activity of ion
γ_A	Activity coefficient
r_ϵ	Specific rate
σ	Coefficient based on the reaction stoichiometry
υ_ϵ	Specific reaction rate
z_i	Charge number of ion i
A_ϵ^0	Initial reactive surface area
$E_{\partial\epsilon}$	Activation energy
k_ϵ	Empirical constant
$k_{0\epsilon}$	Reaction rate constant at T_0
m	Amount of solid
m_0	Initial amount of slid
m_A	Molality concentration of A
m_i	Molality of ion i
N_ϵ	Amount of mineral at a given time
N_ϵ^0	Initial amount of mineral
R_ε	Reaction stoichiometry

B	Boron
Ba	Barium
$\dot{B}$	B-DOT parameter
$[Ba]_{FW}$	Barium concentration in formation water
$BaSO_4$	Barium sulphate (Barite)
Ca	Calcium
$CaCO_3$	Calcium carbonate (Calcite)
$CaSO_4$	Carbonate sulphate (Anhydrite)
$CaSO_4.2H_2O$	Calcium sulphate (Gypsum)
C_{con}	Ion concentration in the produced water
C_{FW}	Ion concentration in the formation water
C_{IW}	Ion concentration in the injection water
CEC	Cation Exchange Capacity
Cl	Chloride
CO_2	Carbon dioxide
CO_3	Carbonate
EDTA	Ethylenediaminetetraacetic acid
FW	Formation water
FOPR	Field oil production rate
FWPR	Field water production rate
H^+	Hydrogen
HCO_3	Bicarbonate

H_2O	Water
I	Ionic strength
IAP	Ion Activity Products
IW	Injection water
IWF	Injection water fraction
K	Potassium
K_{eq}	Equilibrium constant
Mg	Magnesium
Na	Sodium
OH^-	Hydroxyl
PWRI	Produced water re-injection
SO_4	Sulphate
$[SO4]_{IW}$	Sulphate concentration in injection water
Sr	Strontium
$[Sr]_{FW}$	Strontium concentration in formation water
$SrSO_4$	Strontium sulphate (Celestite)
SR	Saturation Ratio
SW	Seawater
TDS	Total dissolved solids
V	Amount of Solution
WCT	Water cut

PUBLICATIONS

Yisheng Hu, Eric Mackay and Oleg Ishkov. Predicted and Observed Evolution of Produced Brine Compositions, and Implications for Scale Management. Paper SPE 169765 presented at the SPE International Oilfield Scale Conference and Exhibition held in Aberdeen, United Kingdom, 14 – 15 May 2014.

Yisheng Hu, Eric Mackay and Oleg Ishkov. Predicted and Observed Evolution of Produced Brine Compositions, and Implications for Scale Management. SPE Production & Operations. (In press)

Yisheng Hu, Eric Mackay, Oscar Vazquez and Oleg Ishkov. Comparison of Streamline Reservoir Simulation of Brine Flow, Mixing and Barium Sulphate Induced Formation Damage with Observed Produced Water Chemical Data to Aid Scale Management. Paper SPE 169765 presented at the SPE European Formation Damage Conference held in Budapest, Hungary, 3 – 5 June 2015.

Yisheng Hu and Eric Mackay. Analysis of Mineral Reactions Occurring In the Gyda Field under Seawater Injection with the Help of Geochemical Non-isothermal Model and Produced Water Data. Paper SPE 179911 presented at the SPE International Oilfield Scale Conference and Exhibition, Aberdeen, United Kingdom, 11 – 12 May 2016. (Submitted to SPE Production & Operations)

Yisheng Hu and Eric Mackay. Modelling of geochemical reactions during Smart Water injection in carbonate reservoir. Paper presented at the 78th EAGE Conference & Exhibition, Vienna, Austria, 30 May – 2 June 2016.

CHAPTER 1 INTRODUCTION, BACKGROUND AND THEORY

1.1 Oilfield scale

Average recovery factors from oil fields in the UK Continental Shelf, by the time they reach the end of their productive lives, are in the range 30-50% - i.e. more than half of the original oil in place remains unrecovered by the time the fields are decommissioned (Kokal et al., 2010). Many offshore and some onshore fields have undergone waterflooding, a process which involves injecting water to maintain reservoir pressure and sweep the oil towards the production wells (Craig, 1971; Mitchell et al., 1980; Robert et al., 1982). Much of this injected water, in addition to native reservoir water, is co-produced along with the oil (Sorbie and Mackay, 2000). This produced water can lead to damage in production systems, as a result of inorganic scale precipitation, corrosion, precipitation of naphthenates, generation of H_2S, hydrates formation, etc. Oilfield scale formation has been a significant problem causing loss of oil production since the beginning of the oil industry itself until now (Yeester et al., 1939; Slaton et al., 1965; Weintritt et al., 1967; Mackay and Graham, 2002). Models to predict scaling tendencies have been proposed and methods of scale removal and scale inhibition have been developed through the years (Stiff et al., 1952; Featherston 1959a, 1959b; Charleston 1968; Lasater et al., 1968; Ralston 1969; Vetter et al., 1970). Scale is defined as "a secondary deposit of mainly inorganic chemical compounds caused by the presence or flow of fluids in a system at least partially man-made" (Vetter, 1976). Neither gas scale, such as hydrates, nor organic scales including waxes and asphaltenes are considered in this definition. The formation of mineral scales may be due to a variety of mechanisms.

a. The variation in pressure or temperature during oil and gas extraction
b. Mixing of two or more incompatible waters
c. Evaporation induced reactions

1.2 Types of mineral scales

There are three principal oilfield scales: carbonate scales, sulphate scales, halite scale.

The occurrence of carbonate scale is normally as a result of a decline in pressure or increase in temperature during oil production. The Equation 1.1 shows the fundamental behaviour of calcium carbonate dissolution and precipitation. As the pressure of produced fluid decreases below the carbon dioxide (CO_2) bubble point pressure, CO_2 is removed

and this causes calcite to precipitate. Conversely, an increase of CO_2 leads to the dissolution of calcite. Scale formation in the production tubing will allow pressure to decline further and more scale precipitations then takes place.

$$Ca + HCO_3^- \rightarrow CO_2(g) + H_2O + CaCO_3(s) \quad (1.1)$$

Oil and gas is forced from the subsurface to the surface by natural energy (initial reservoir pressure) during primary recovery. As pressure is depleted over time during oil production, at some point the injection of fluids is necessary to improve reservoir performance. This is referred to as secondary recovery. Seawater injection is popularly used for pressure maintenance and oil displacement in offshore fields due to its ready availability and cost efficiency. The mixing of incompatible injected and formation waters primarily results in sulphate scale formation (Equation 1.2). Sulphate scale, which is another common oilfield scale, usually occurs where the injection water, generally rich in sulphate, is incompatible with the initial formation water containing divalent cations such as barium, strontium and calcium.

$$Ba^{2+}\ (Sr^{2+}, Ca^{2+}) + SO_4^{2-} \rightarrow BaSO_4\ (s)\ (SrSO_4, CaSO_4) \quad (1.2)$$

Halite deposition is a self-scaling process (Equation 1.3). At low water-cuts and high gas flow rate, brine evaporation may cause the remaining total dissolved solids (TDS) to exceed the solubility of the associated minerals, and deposition takes place. This is the most common cause of the formation of halite scale in wells experiencing high temperature and high pressure gas flow (Kleinitz et al., 2001).

$$NaCl_{(aq)} \rightarrow NaCl_{(s)} \quad (1.3)$$

1.3 Reservoir interactions

Mineral scale may form in the perforations, production casing, tubing, and downhole equipment of production wells and anywhere in surface equipment during oil production, which causes significant restrictions to fluid flow, and can even plug wells. **Figure 1.1** exemplifies the places where scale can form in an oilfield. In this scenario there is seawater injection, PWRI, aquifer water, and mixing at the manifold. However, when mineral scale precipitation reactions occur deep within the reservoir it may not prevent fluid (oil, gas and water) from flowing in the subsurface as the pore volume of the whole reservoir is too large to be blocked by the relatively small amount of scale precipitation (Mackay et al., 2005b). Moreover, scale ion stripping caused by the occurrence of mineral

deposition in the reservoir would greatly affect the chemical composition of produced water and thus be beneficial to mitigate the scaling risks in the production well and surface equipment (Paulo et al, 2001; Mackay et al., 2003a; 2003b; 2003c; 2005).

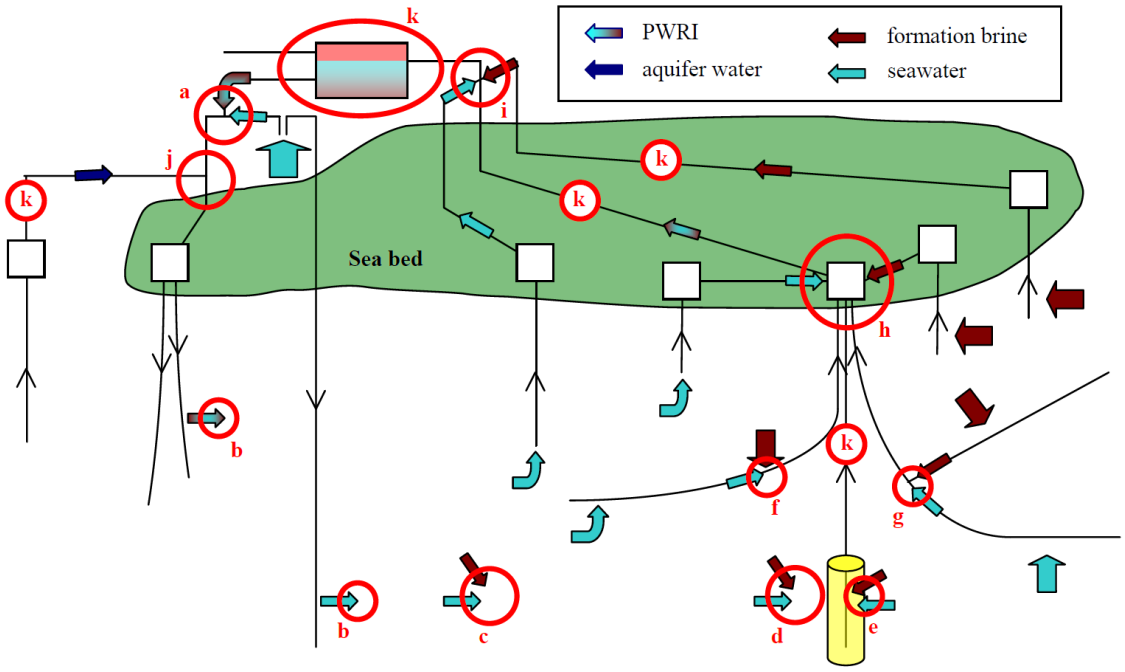

Figure 1.1 Locations throughout the flow system where scale deposition may take place. (Collins et al., 2006). (a) Prior to injection; (b) Around the injection well; (c) Deep in the formation; (d) within the radius of a squeeze treatment; (e) beyond the radius of squeeze treatment (f) In the completed interval of a production well; (g) At the junction of a multilateral well; (h) At the subsea manifold; (i) At the surface facilities; (j) scale formation within a self-scaling brine or mixing with an incompatible formation brines as in b; (k) Downhole tubing or surface processing equipment.

Sulphate (barite, celestite and anhydrite) and carbonate (calcite) mineral scale deposition reactions mentioned above can take place when the injection water is mixing with and displacing the formation water within the reservoir. On the other hand, the composition of the injected water - which may also be out of equilibrium with the reservoir rock substrates - may some fluid-rock interactions to occur.

The composition of seawater generally has a much higher Mg/Ca ratio than occurs for formation water. This larger difference stimulates the interaction between calcium and magnesium. Thus, when the seawater is injected, the equilibrium between the rock and initial formation is disturbed. If the Mg/Ca ratio for seawater is much greater than Mg/Ca ratio in the formation water, the system tends to re-equilibrate the Mg/Ca ratio. Therefore, the occurrence of ion exchange causes magnesium to be absorbed onto the rock from the brine, and in return, calcium is released into the brine from the rock. This behaviour has been observed in many field examples (Smith 1978; Bazin et al, 199; Carlyle et al., 2004).

Dolomitization is defined as the process by which the calcium within the calcium carbonate is partially substituted by magnesium to give calcium, magnesium carbonate (dolomite) mineral (Equation 1.4). This is an important mechanism in certain oilfields (carbonates reservoirs) because this reaction generates reservoir porosity (Zenger et al., 1980). Although there is some debate as to whether dolomite can precipitate from seawater, a variety of studies show that it is possible both in the presence of bacteria (Sánchez-Román et al., 2009) and without their presence (Siegel, 1961). It was reported by Machel et al. (1986) that dolomite formation is thermodynamically favoured in brines of high Mg/Ca ratio and high temperature and the kinetic considerations favour dolomitization under the same conditions. Therefore, with the consideration of the thermodynamics and kinetics, the conditions where a high temperature (normally over 100°C) reservoir injected with seawater (which has high Mg/Ca ratio) can be considered chemically conducive to dolomitization.

$$2CaCO_3(s) + Mg^{2+} \rightarrow MgCa(CO_3)_2(s) + Ca^{2+} \qquad (1.4)$$

Houston et al. (2006) used the dolomitization mechanism to explain the produced water chemical compositions in an oilfield. The occurrence of dolomitization was indicated by the comparison of relative molar depletions and gains in magnesium and calcium respectively (**Figure 1.2**).

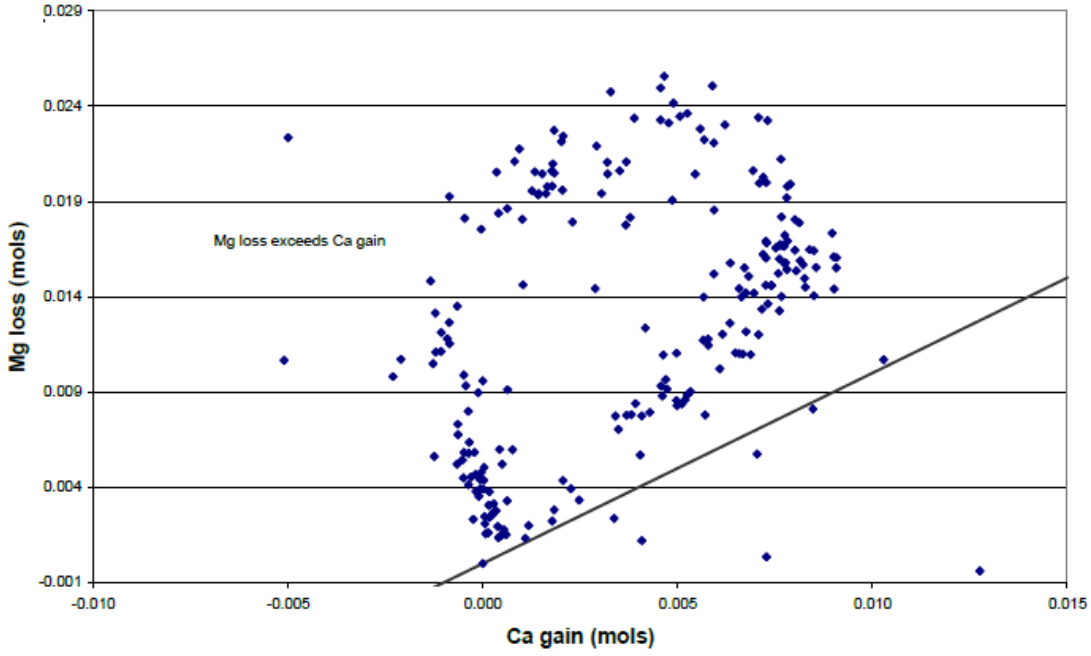

Figure 1.2 Ca and Mg concentrations relative to a 1:1 stoichiometric exchange (straight line) representative of simple dolimitization. (Houston et al., 2006)

MacCartney et al. (2012) demonstrated that incomplete dolomitization in the Veslefrikk field most probably explains the gain of calcium and stripping of magnesium from injected seawater based on geochemical model calculations. The compositions of the high-seawater-fraction produced water samples in the Veslefrikk field were explained by dolomite precipitation causing calcite dissolution and anhydrite precipitation (**Figure 1.3**).

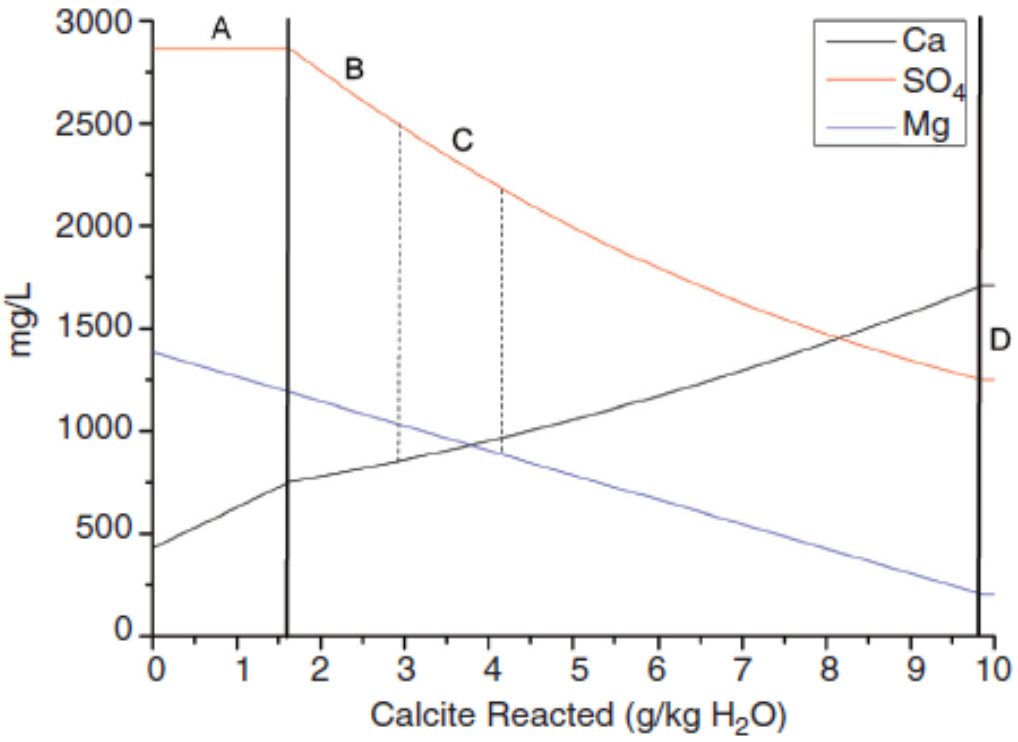

Figure 1.3 Simulation of dolomitization of calcite under Brent reservoir conditions. A is precipitation of dolomite and dissolution of calcite. B is precipitation of dolomite and anhydrite and dissolution of calcite. C is the range of produced-water SO_4 concentrations in reacted seawater. D is equilibrium between calcite, dolomite and anhydrite. (MacCartney et al., 2012)

1.4 Reactive transport model

When the fluid is transported through the porous medium the dissolved reactive constituents can react with the ones present in initial fluid and/or the reactive matrix. Therefore, reactive transport modelling was developed through coupling a variety of chemical reactions with fluid flow transport in the porous medium to understand how the chemical reactions take place during fluid flow and transport and to make quantitative evaluation on the distribution of chemical species and mineral phase both spatially and temporally (Wolery et al., 1979; Reed et al., 1982; Bethke, 1996).

1.4.1 Advection and dispersion

Diffusion, advection and dispersion are normally considered transport processes in reactive transport models. The advection-reaction-dispersion (ARD) equation is usually used to describe the law of mass conservation for a chemical component that is transported (Levenspiel, 1986; Bedient et al., 1999; Appelo and Postma, 2010):

$$\frac{\partial C}{\partial t} = -\upsilon \frac{\partial C}{\partial x} + D_L \frac{\partial^2 C}{\partial x^2} - \frac{\partial q}{\partial t} \tag{1.5}$$

$$D_L = D_e + \alpha_L \upsilon \tag{1.6}$$

where C and q represent species concentrations in fluid and solid phases; υ, x, D_L, $D_e$and α_L represent pore water flow velocity, distance, the hydrodynamic dispersion coefficient, the effective diffusion coefficient and dispersivity, respectively.

1.4.2 Thermodynamic equilibrium

I consider the following general, reversible reaction:

$$eE + fF \leftrightarrow sS + tT \tag{1.7}$$

The distribution of species at equilibrium on the left and right sides of the reaction is given by

$$K_{eq} = \frac{[S]^s[T]^t}{[E]^e[F]^f} \tag{1.8}$$

where K_{eq} is the equilibrium constant, $[E], [F], [S]$ and $[T]$ represent "effective concentrations" or activity for each ion and *e*, *f*, *s* and *t* are molar proportions of compounds *E*, *F*, *S* and *T*. If the concentration of one compound is adjusted, others change to maintain the equilibrium constant (K_{eq}). Chemical equilibrium terms are calculated as a function of temperature in different polynomial equations (Equation 1.9, 1.10 and 1.11) which are used in different simulation codes. K_1-K_5, A1-A_6 and a_0-a_4 are temperature coefficients that area determined for each of the equilibrium constants.

$$\ln(K_{eq}) = \frac{K_1}{T} + K_2 + K_3 \ln T + K_4 T + \frac{K_5}{T^2} \tag{1.9}$$

$$\log(K_{eq}) = A_1 + A_2 T + \frac{A_3}{T} + A_4 \log_{10} T + \frac{A_5}{T^2} + A_6 T^2 \tag{1.10}$$

$$\log(K_{eq}) = a_0 + a_1 T + a_2 T^2 + a_3 T^3 + a_4 T^4 \tag{1.11}$$

In concentrated solutions, ions interact electrostatically with each other, so the stoichiometric coefficients do not reflect reactive availability. In chemical equilibrium calculations the interactions between charges contribute to move the system away from an ideal (dilute) case. These interactions are stronger in concentrated solutions, especially high salinity waters, and therefore require calculation of activity coefficients at these conditions; these calculations are performed using an activity model. The activity of ions is related to the molality concentration by an activity coefficient corrected for non-ideal behaviour. For aqueous solutes, the relation is given by

$$a_i = \gamma_i m_i \tag{1.12}$$

where a_i is the activity of ion i, γ_i is the activity coeffeient and m_i is the molality concentration of i.

In electrolyte solutions, the activity coefficients are influenced mainly by electrical interactions. Much of their behaviour can be correlated in terms of the ionic strength, defined by:

$$I = \frac{1}{2}\sum_i m_i \ z_i^2 \tag{1.13}$$

where z_i is the charge number of ion i, m_i is the molality of i.

The DEBYE-HUCKEL model (Equation 1.14) is proposed to calculate activity coefficient which is expressed as a function of the ion size parameter and ionic strength (Debye and Hückel, 1923).

$$\log \gamma_i = -\frac{AZ_i^2\sqrt{I}}{1+B\text{å}\sqrt{I}} \tag{1.14}$$

where A and B are constants dependent on temperature, å is the empirical ion-size parameter which is a measure of the effective diameter of the hydrated ion and I is the ionic strength of the solution defined in the Equation 1.13.

The DEBYE-HUCKEL equation is applicable for dilute electrolyte solutions (I<0.1). It has been extended to various models with additional terms to calculate activity coefficients for solutions having higher ionic strength. The Davies (1962) equation (Equation 1.15) is one of the extended DEBYE-HUCKEL models that works for up to an ionic strength of about 0.5.

$$\log \gamma_i = -AZ_i^2 \frac{\sqrt{I}}{1+\sqrt{I}} - 0.3I \quad (1.15)$$

The B-DOT equation (Equation 1.16) presented by Helgeson (1969) is another relation commonly used to derivate activity coefficients, which is also an extension of the DEBYE-HUCKEL equation. A B-DOT parameter ($\dot{B}$) which depends on the electrical charge of the species which varies with temperature is included.

$$\log \gamma_i = -\frac{AZ_i^2\sqrt{I}}{1+\mathring{a}B\sqrt{I}} + \dot{B}I \quad (1.16)$$

However, these models consider only the interaction of the species with the solution medium and therefore have limited accuracy in highly saline solutions. B-DOT for example, provides reasonable results for ionic strength lower than 2 mol/kgw in predominantly chlorine solutions (Parkhurst, 1990). On the other hand, the so-called PITZER model calculates activity coefficients by incorporating short-range interactions between ion pairs and triplets. These type of interactions become relevant in solutions with high ionic strength (above 2 to 3.5 mol/kgw) (Langmuir, 1997) and it has been proved that the PITZER model can accurately model them in solutions up to 6 mol/kgw (Pitzer, 1987). In addition, the PITZER model uses a multi parameter approach that can be used to fit the model to experimental data and provide accurate results in high salinity, high pressure and high temperature solutions (Appelo, 2014 and Appelo, 2015).

One way to determine whether a water sample is saturated, undersaturated, or oversaturated with given minerals is to compare the chemical equilibrium constant (K) with the corresponding Ion Activity Products (IAP). Suppose we have the following general dissolution reaction:

$$M + N \leftrightarrow MN \quad (1.17)$$

Where *MN* is the given mineral and *M* and *N* represent anion and cation ions. The ratio of *IAP* and K_{eq} is referred to as the saturation ratio (SR) which is defined as:

$$IAP = a_M \cdot a_N \quad (1.18)$$

$$SR = IAP/K_{eq} \quad (1.19)$$

The saturation index (SI) is defined as:

$$SI = \log(SR) = \log(IAP/K_{eq}) \quad (1.20)$$

Where a_M and a_N are the activities of anion M and cation N, and K_{eq} is the chemical equilibrium constant for the reaction at the solution temperature and pressure.

If SR=1 (SI=0), the solution is in equilibrium with the given mineral;

If SR<1 (SI<0), the solution is undersaturated with the given mineral and the reaction is proceeding from right to left (dissolution);

If SR>1 (SI>0), the solution is oversaturated with the given mineral and the reaction is proceeding from left to right (precipitation).

1.4.3 Chemical kinetics

Thermodynamics can only be used to describe the equilibrium state and where the system should go at equilibrium, but does not explain how fast a chemical reaction reaches equilibrium. If the reaction rate is slower compared to the residence time, the equilibrium for the chemical reactions cannot be achieved. Under the circumstances, the extent of the reaction is controlled by chemical kinetics. Reaction rate is normally defined by a function of reactive surface area, rate constant, and activation energy.

In PHREEQC the overall rate for a kinetic mineral reactions is given by (Parkhurst and Appelo, 1999):

$$R_\epsilon = r_\epsilon \frac{A_\epsilon^0}{V}\left(\frac{m}{m_0}\right) g(C) \tag{1.21}$$

where r_ϵ the specific rate. A_ϵ^0 is the initial surface area, V is the amount of solution, m_0 is the initial amount of solid, m is the amount of solid at a given time. When experimental information is lacking, the specific rate is usually expressed by:

$$r_\epsilon = k_\epsilon\left(1 - (IAP/K_{eq})^\sigma\right) \tag{1.22}$$

where k_ϵ is an empirical constant and IAP/K_{eq} is the saturation ratio (SR). σ is the coefficient based on the reaction stoichiometry.

Equation 1.23 is used to calculate mineral dissolution and precipitation rate in CMG GEM (Computer Modeling Group Ltd, 2015):

$$R_\epsilon = A_\epsilon k_\epsilon\left(1 - IAP/K_{eq}\right) \tag{1.23}$$

where A_ϵ is the reactive surface area, k_ϵ is the rate constant of the reactions, K_{eq} is the chemical equilibrium constant and IAP is the activity product.

The overall rate for the different aqueous species is related to specific reaction rate and reaction stoichiometry

$$r_\epsilon = \upsilon_\epsilon \cdot R_\varepsilon \tag{1.24}$$

The reaction rate constant at temperature of T is calculated by Equation 1.25:

$$k_\epsilon = k_{0\epsilon} exp\left[-\frac{E_{\partial\epsilon}}{R}\left(\frac{1}{T}-\frac{1}{T_0}\right)\right] \tag{1.25}$$

where $E_{\partial\epsilon}$ is the activation energy and $k_{0\epsilon}$ is the reaction rate constant at T_0.

The reactive surface area is given by:

$$A_\epsilon = A_\epsilon^0 \cdot \frac{N_\epsilon}{N_\epsilon^0} \tag{1.26}$$

where A_ϵ^0 is the initial reactive surface area, N_ϵ is the amount of mineral at a given time and N_ϵ^0 is initial amount of mineral.

1.4.4 A simplified model of barium sulphate deposition implemented in FrontSim

FrontSim does not have the capacity to model geochemical reactions, so a simplified model for barium sulphate precipitation was implemented in the streamline simulation model. Modelling the transport of barium and sulphate ions is not a difficult task in FrontSim, as any ion concentrations can be included as passive tracers moving in the water phase (say initial formation water or injected sea water) using existing (supported) tracer codes for FrontSim. Therefore, the key issue here is to introduce a model of the chemical interaction between barium and sulphate. A basic assumption was made that barite scale precipitation takes place instantaneously in the reservoir in order to simplify the calculation – i.e. geochemical equilibrium is assumed in each grid block at each time step. The assumption is reasonably based on the previous studies that the flow rate of fluid deep within the reservoir is low relative to the reaction rate for barite deposition, and there is enough time for the fluid to reach equilibrium within each time step (Brantley et al., 2007). I can then make a further assumption that either barium (if sulphate is in excess) or sulphate ions (if barium is in excess) would be depleted during precipitation of barite in each grid block by the end of each time step.

Assuming that X mmol/l barium and Y mmol/l sulphate are available in the aqueous phase in one grid block during the current time step, then

If X>Y, then

$$XBa^{2+} + YSO_4^{2+} === YBaSO_4 + (X-Y)Ba^{2+} + (X-Y)\ SO_4^{2+} \quad (1.27)$$

And if X<Y, then

$$XBa^{2+} + YSO_4^{2+} === XBaSO_4 + (Y-X)Ba^{2+} + (Y-X)SO_4^{2+} \quad (1.28)$$

The remaining ions (in excess) will be transported downstream in the mobile brine phase at the next time step.

1.4.5 Heat transport model

An exchange of heat that will cause the temperature of the cell to change as transport progresses. Diffusive heat transport will be calculated as a separate process if the temperature in any of the solutions of the transport domain differs by more than 1°C, and when the thermal diffusion coefficient is larger than the effective (aqueous) diffusion coefficient. Otherwise, diffusive heat transport is calculated as a part of aqueous diffusion.

Conservation of heat yields the transport equation for heat, or rather, for the change of temperature. The equation is identical to the advection-reaction-dispersion equation for a chemical substance:

$$R_T \frac{\partial T}{\partial t} = -\upsilon \frac{\partial T}{\partial t} + \kappa_L \frac{\partial^2 T}{\partial x^2} \quad (1.29)$$

where T is the temperature (°C), υ is the pore water flow velocity, R_T and κ_L represent temperature retardation factor and thermal dispersion coefficient respectively. The last two parameters need to be defined for calculating the diffusive part of heat transport. The temperature retardation factor and the thermal diffusion coefficient are defined as:

$$R_T = 1 + \frac{(1-\theta)\rho_s k_s}{\theta \rho_w k_w} \quad (1.30)$$

$$\kappa_L = \frac{\kappa}{\theta \rho_w k_w} \quad (1.31)$$

where θ is the porosity, κ is a term which entails both the dispersion by advective flow and the heat conductivity of the aquifer ($kJ°C^{-1}m^{-1}s^{-1}$), *k* is the specific heat ($kJ°C^{-1}kg^{-1}$), and subscripts *w* and *s* indicate water and solid, respectively.

1.5 Simulation codes used in this study

The software used in this thesis are briefly summarized below.

MultiScale (Kaasa, 1998) is a computer program designed to calculate equilibria in systems containing water, gas, oil and solids. This is an aqueous equilibria model that can predict inorganic scaling tendencies in oilfield production systems. In addition to the aqueous equilibria, it also contains a PVT-model which can calculate bubble point and phase distribution, especially for CO_2 and H_2S. However, the role of the reservoir was neglected in all of thermodynamic modelling work which is based on the fundamental assumption that the potential scale precipitation will be due to pure mixing of formation and injected water in the production well. The equilibrium constant for a given mineral is calculated as a function of temperature based on Equation 1.9 and PITZER activity model was implemented in MultiScale.

PHREEQC (Parkhurst and Appelo, 1999) is a computer program for simulating chemical reactions and transport process in natural waters. The program is based on equilibrium chemistry of an aqueous solution interacting with minerals, gases, solid solutions, exchangers and sorption surfaces, but also includes capability to model kinetic reactions with rate equations. A 1D algorithm consists of dispersion, diffusion and some options for dual porosity media. The most important and biggest difference, relative to many kinds of thermodynamic models, such as Multiscale, ScaleChem and ScaleSoftPitzer, is the capability to define multiple solutions and multiple assemblages combined with the capability to determine the stable phase assemblages, providing a framework for 1D transport modelling. PHREEQC provides a method for simulating the movement of solutions through a column or a 1D flow path with or without the effects of dispersion. The initial composition of the aqueous, gas, and solid phases within the column are specified and the changes in composition due to advection and dispersion coupled with reversible and irreversible chemical reactions within the column can be modelled. It should be note that Equation 1.10 is used to calculate the equilibrium constant in PHREEQC and users have an option to run the PITZER activity model for calculation activity coefficients for high salinity solutions. The Saturation Index (SI) (Equation 1.20)

can be tuned to delay the precipitation or dissolution of a given mineral in PHREEQC, which is equivalent with changing the solubility of the mineral.

FrontSim is a streamline simulation model in which the fluid flow is modelled as a series of saturation fronts moving along the streamline. Streamline simulation (Datta-Gupta and King, 2007) is well developed as an alternative method to conventional finite difference methods for modelling fluid flow in hydrocarbon reservoirs. This is an IMplicit Pressure Explicit Saturation (IMPES) method of simulation in which pressure is solved implicitly over the whole grid. The pressure field is then used to trace the path that a single fluid would follow as it flowed across the reservoir producing streamlines. The saturations are then mapped from the grid on to the streamlines and then these are updated along the streamlines then mapped back to the model grid. This approach has two important features. First the calculation is not subject to the same Courant–Friedrichs–Lewy (CFL) constraint on stability that has to be applied to a finite volume IMPES simulator. This allows the simulator to take much longer timesteps without generating unstable unphysical solutions, with the result that streamline simulation is usually faster than a normal finite volume simulation. Secondly, the saturation solution is not subject to numerical dispersion to the same extent or in the same way that a finite volume or finite difference simulator is. (In fact, some dispersion is introduced by the process of mapping the solution to and from the grid). A consequence of this is that the reservoir model can be coarser (and hence faster to run) without smearing out the zone where the ion concentration has been depleted. Streamline-based flow simulations approximate 3D fluid flow calculations by the sum of 1D solutions along streamlines. The choice of the streamline directions for 1D calculations makes the approach effective for modelling the fluid flow in the geologically complex and heterogeneous system for which fluid flow is dominated by well locations and rates, reservoir rock properties (permeability, porosity and faults properties) and fluid properties (relative permeabilities and viscosities) (Thiele et al, 2001).

CMG GEM (Computer Modeling Group Ltd, 2015) is a fully compositional finite difference simulator that allows chemical reactions, changes in the permeability due to precipitation, and models temperature as well. As a result, it can be used for modelling aqueous phase chemical reactions and mineral precipitation/dissolution. This simulator also includes chemical equilibrium terms that can be a constant or a function of temperature in a polynomial equation (Equation 1.11). Hence, it includes a simplified thermodynamic model. It is important to note that this simplified model neglects the effect

of pressure on the equilibrium constant. For some components at reservoir conditions this approach can lead to large errors. In order to reduce this issue the modeller should adapt these parameters for reservoir conditions. CMG GEM allows the user to choose between the DEBYE-HUCKEL and B-DOT activity models to calculate activity coefficients and change the solubility of a given mineral through tuning the Saturation Ration (SR) (Equation 1.19).

1.6 Comparison of model results related to barite and anhydrite

Three models used in the thesis to calculate geochemical reactions occurring in the flow path, were compared with respect to barite and anhydrite solubility. The three models were the simplified barite deposition model, PHREEQC model with PITZER activity model and CMG GEM model with B-dot activity model,

1.6.1 Comparison of Simplified barium sulphate model with equilibrium model

The simplified model of barium sulphate deposition implemented in the streamline simulation is not an accurate geochemical model. Its calculation results were compared to the equilibrium model (PHREEQC) results to show how large error will be induced by the simplified model. A series of calculations were run based on different barium and sulphate concentrations which are calculated based on varying extent of mixing of formation water (containing 600 mg/l barium) and injection water (containing 3000 mg/l sulphate). **Table 1.1** shows very little difference between the simplified model results and equilibrium model results, so this indicates the assumption made to simplify the equilibrium model is reasonable. This is the case become the solubility of barite is very low.

Table 1.1 The comparison of simplified $BaSO_4$ model and equilibrium model results

IWF, %	Ba, mg/l	SO4, mg/l	BaSO4, mole **Simple model**	BaSO4, mole **Equilibrium model**	Error	Error Percentage
10	540	300	3.2480E-03	3.2470E-03	1E-06	0.0308%
30	420	900	3.1440E-03	3.1440E-03	0	0.0000%
50	300	1500	2.2470E+00	2.2460E+00	0.001	0.0445%
70	180	2100	1.3490E-03	1.3480E-03	1E-06	0.0742%
90	60	2700	4.4980E-04	4.4950E-04	3E-07	0.0667%

1.6.2 Comparison of PHREEQC and GEM chemical equilibrium results

A reservoir model consisting of just five grid blocks was developed using GEM. Initially, all aqueous species in the reservoir were set to 0 and no mineral was present. Saline water containing barium (or calcium), sulphate, sodium and chloride was continuously injected into the first block from the start of the simulation. Injected barium (or calcium),sulphate concentrations were each set to 0.5 mol/kgw, which is a high enough concentration to observe barite (or anhydrite) precipitation, while sodium chloride concentration varies through values 0, 0.5, 1, 2, 3, 4, 5, 6 mol/kgw. The solubility of barite or anhydrite is determined by the concentration of barium (or calcium) which is dissolved in the brine by the time the injected water reaches equilibrium in the last block. The same model was also built in PHREEQC and run with the PITZER database. The experimental data associated with the solubility of barite and anhydrite were compared to the GEM results with the B-DOT model and the PHREEQC results with the PITZER model.

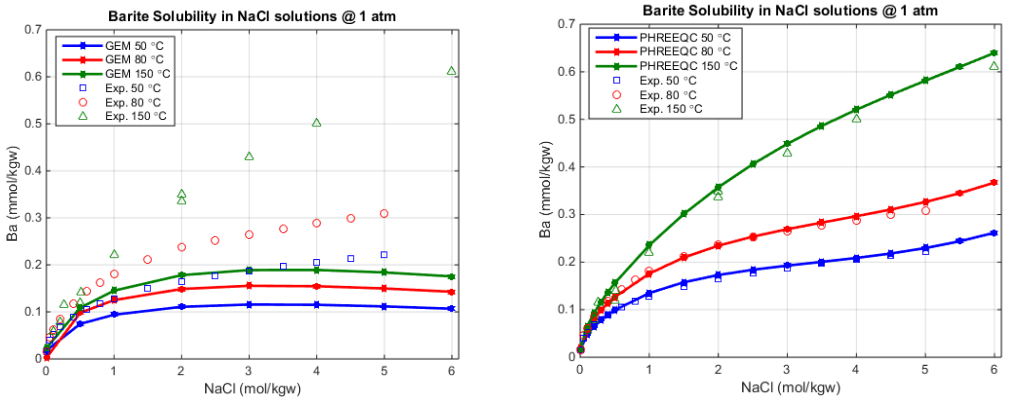

Figure 1.4 Barite solubility using GEM (left) and PHREEQC (right). Experimental data from Templeton, 1960; Uchameyshvili et al., 1966; Blount, 1977.

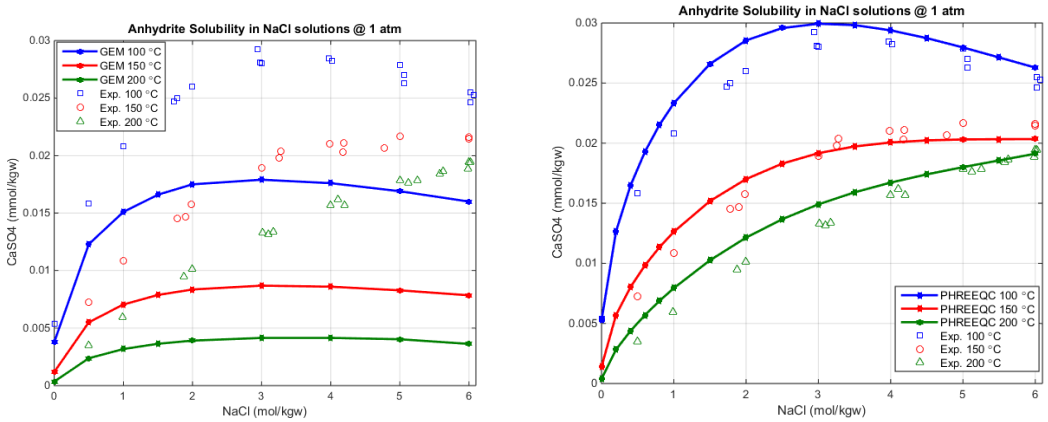

Figure 1.5 Anhydrite solubility using GEM (left) and PHREEQC (right). Experimental data from Block and Waters, 1968; Blount and Dickson, 1969.

The GEM results with the B-DOT activity model underestimate the solubility of barite (and anhydrite) when compared to the experimental data available (Templeton, 1960; Uchameyshvili et al., 1966; Blount, 1977; Block and Waters, 1968; Blount and Dickson, 1969.). In contrast, the PHREEQC results calculated with the PITZER activity model match with the experimental data very well (**Figures 1.4** and **1.5**).

For these geochemical systems described by Equation 1.7, 1.12 and 1.13, the sources of errors are (a) the equilibrium constants and (b) the activity coefficients, because the same molalities were defined in the GEM and PHREEQC models. In the **Figure 1.6** we show that changes in equilibrium constants modify the GEM results slightly, but this is not the major reason for the discrepancies. I performed the simulation using GEM with the equilibrium constants extracted from the PITZER database of PHREEQC. There is a slight modification, but it is obviously not enough to cause the large discrepancies shown in **Figures 1.4** and **1.5**.

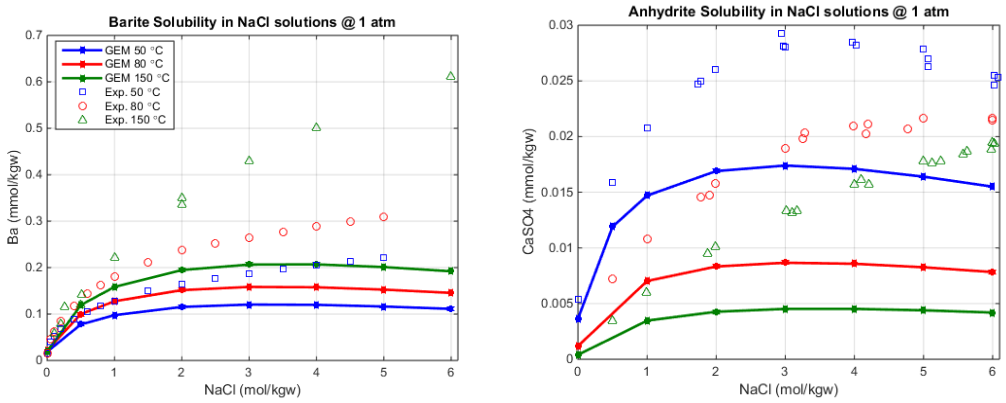

Figure 1.6 Barite (left) and anhydrite (right) solubility using GEM with equilibrium constants from PHREEQC. Experimental data from Templeton, 1960; Uchameyshvili et al., 1966; Blount, 1977 (Barite); Block and Waters, 1968; Blount and Dickson, 1969 (Anhydrite).

The inaccurate activity coefficients calculated by the B-DOT activity model in GEM is the only one reasonable explanation for the errors highlighted in **Figures 1.4** and **1.5**. Therefore, it is identified that for conditions typical of oilfield reservoir systems, the mineral reaction model used in GEM is not accurate, primarily because the activity coefficients are not being accurately determined.

1.7 Literature review of petroleum engineering studies involving reactive transport modelling

Mackay (2003a) applied a flow and reaction simulator to model barite precipitation due to brine mixing in the reservoir and investigated its impact on the produced ion

concentrations. His simulation results indicated that the maximum barite scale precipitated in or near the production well for the case of a vertical well, and the barium concentration in the produced water would not return to the value based on pure mixing of formation and injection water if barium sulphate mineral precipitation occurred in the reservoir. He also found that cross flow caused higher levels of brine mixing in the aquifer, and this lowered the scaling tendency in the wellbore. The reaction rate is only important for accurate modelling of *in situ* precipitation at high flow rate, in the near wellbore region, because the flow rate is so slow deep within the reservoir that the chemical reaction can reach equilibrium (**Figure 1.7**). The presence of an aquifer provides an additional source of scaling ions, but also increases the level of brine mixing in the reservoir.

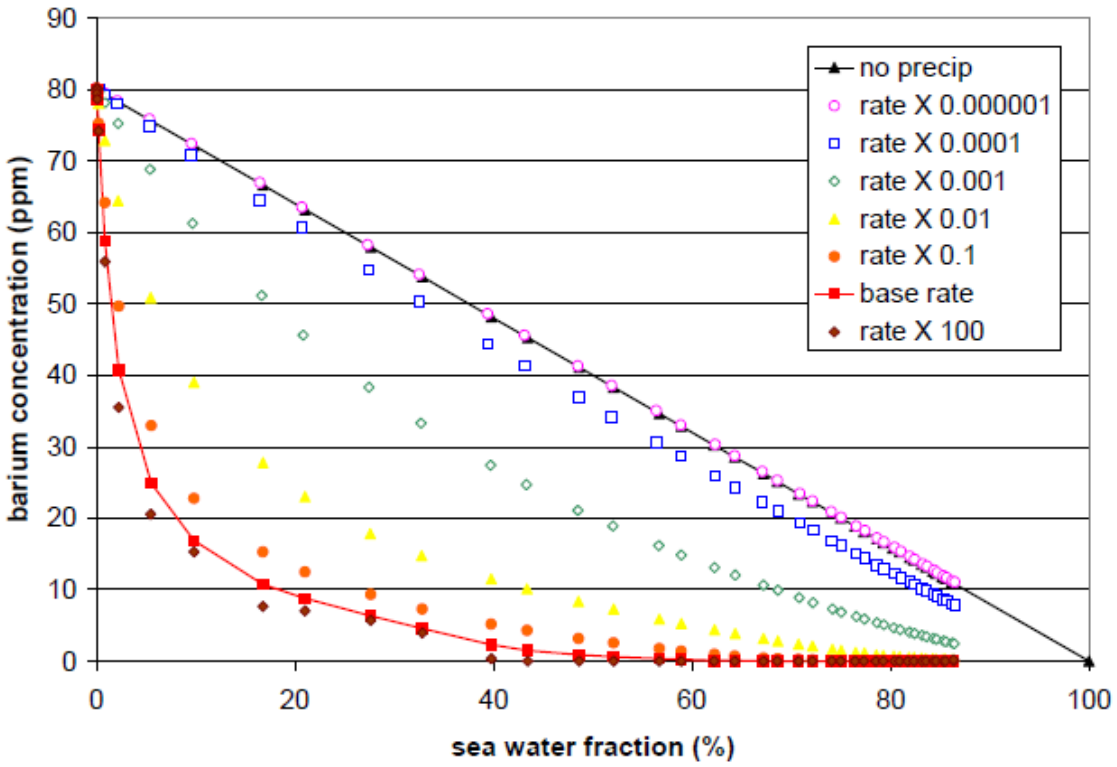

Figure 1.7 Sensitivity to reaction rate. The base case leads to near equilibrium conditions everywhere. However, lower reaction rates would significantly the produced barium concentrations. (Mackay, 2003a)

Gomes et al. (2012) studied the geochemical reactions occurring in the reservoir when the brine was transporting and flowing towards to the well by analysing produced brine compositions from a variety of fields. They developed a new technique to evaluate the impact of ion striping in the reservoir on the scaling potential that considered mineral scale precipitation taking place in the reservoir (**Figure 1.8**). Barium sulphate scaling tendencies were calculated based on different extents of barium/sulphate ion depletion by

the use of a three dimensional surface. They further proposed that anhydrite precipitation could occur in the fields where reservoir temperature is higher than 120°C and formation water had high calcium concentration (>7000mg/l), and that ion exchange led to magnesium being absorbed onto rock surfaces and calcium released into the brine which could promote anhydrite precipitation.

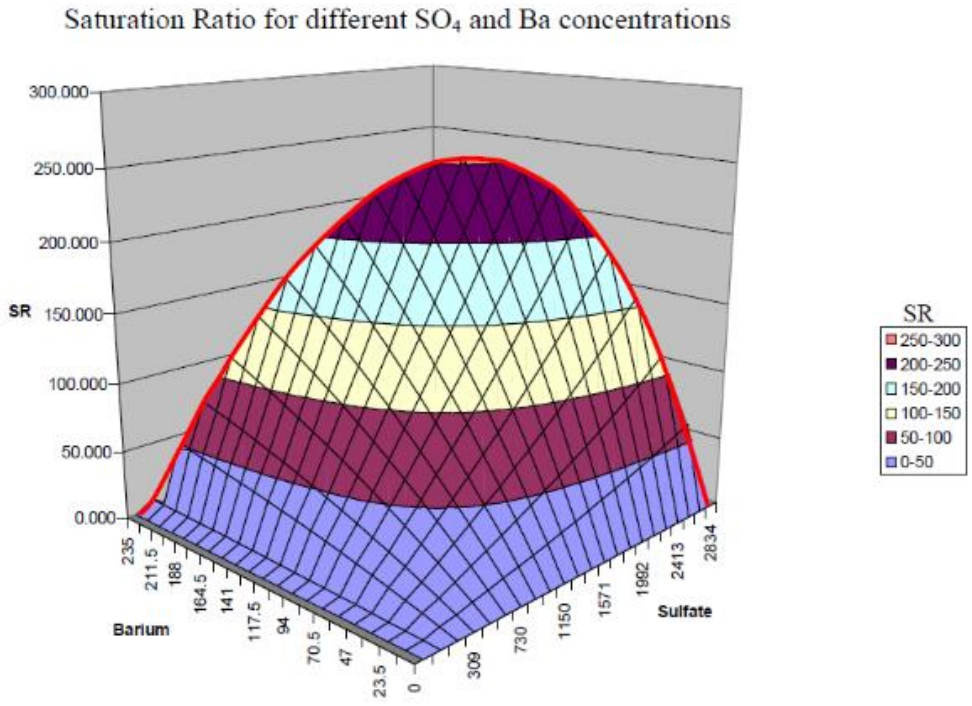

Figure 1.8 Reservoir C, surface response of SR for the full range of mixes of injected water and formation water, and accounting for reservoir stripping effects. (Gomes et al., 2012)

Østvold et al. (2010) conducted a simulation study on whether Utsira formation water (UW; low sulphate) or seawater (SW) should be selected as the injection water for the re-development of the Froy field. They found that barium sulphate and calcium carbonate scales are the dominant scaling risks whether UW or SW is injected through thermodynamic calculations. Two methods were used to predict produced water compositions that accounted for barium sulphate precipitation within the reservoir. The first was a 'semi-empirical approach' in which the barium and sulphate concentrations in historical produced water samples was fitted with an exponential regression and the best-fit line was then used for the estimation of future produced barium concentrations for each well against time. The second method was to combine ECLIPSE with STAR model where STARS was used to model geochemical reactions occurring in the reservoir and

ECLIPSE was used for flow calculations. Their simulation showed that production wells would experience higher scaling risks of barium sulphate in the case of 100% UW injection.

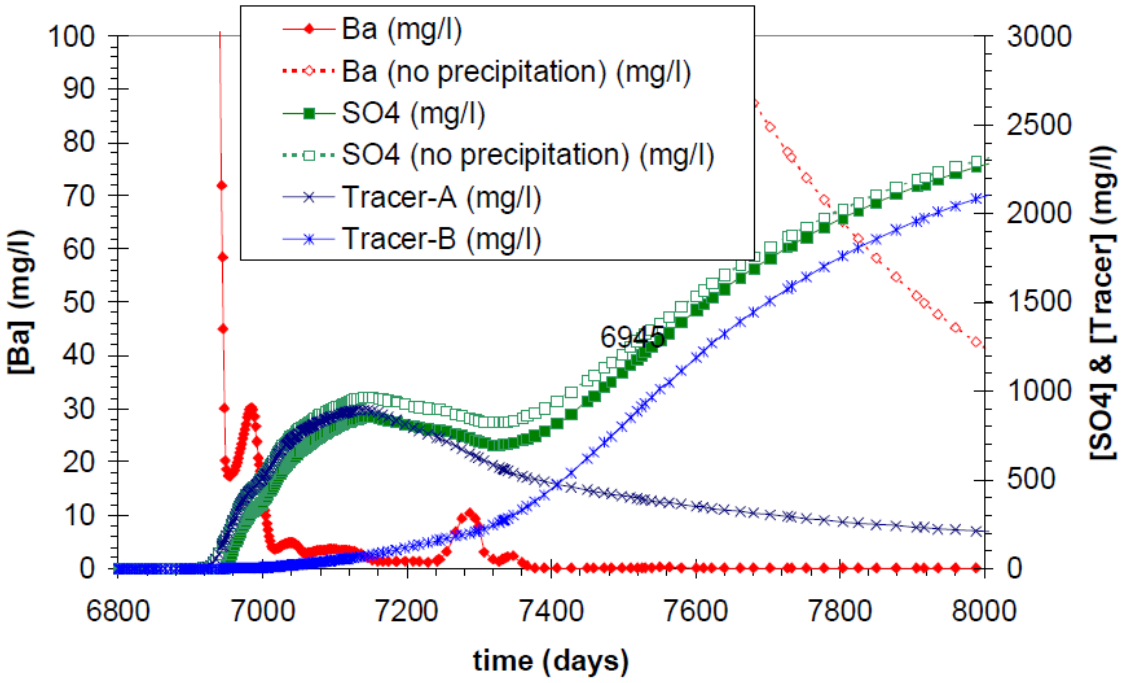

Figure 1.9 Calculation of Ba and SO_4 concentrations in producer well B-01CC versus time with 100% SW injection. (Østvold et al., 2010)

Mackay et al. (2014a) investigated several potential geochemical reactions that took place *in situ* in the carbonate reservoir during CO_2-WAG injection in order to predict the scaling risks. GEM, a reactive transport simulator, was used to develop a two dimensional simulation model and several simulations were run for different recovery methods (Injection of Low Sulphate Seawater, CO_2-WAG injection and Injection of CO_2 only), and different mineralogies. Their main results were that there is a very high scaling risk for barium sulphate at the production well in the case of seawater injection, and the lowest scaling potential for the case of only CO_2 injection, the system pH is buffered by calcite dissolution and is stabilized at a certain value, and dolomite deposition is formed by Ca^{2+} and CO_3^{2-} from calcite and magnesium from seawater (**Figure 1.10**).

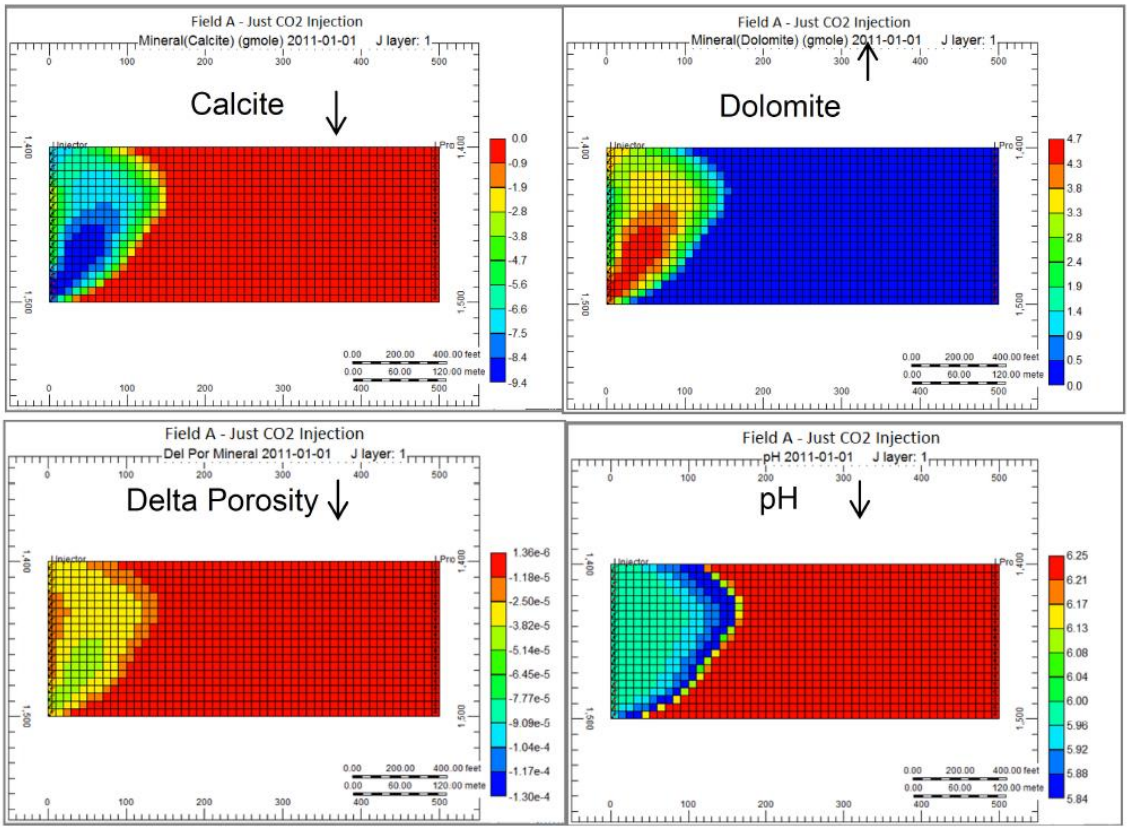

Figure 1.10 System changes after 1 year of CO_2 injection – (a) Calcite, (b) Dolomite, (c) net change in porosity, (d) pH. (Mackay et al., 2014a)

McCartney et al. (2012) conducted an integrated study for interpreting produced water chemistry data and multirate separator tests (MRTs). One dimensional reactive transport modelling was applied to identify possible reservoir interactions to be taking place in the Veslefrikk reservoirs, which accounts for injecting seawater into a flow path containing formation water, mixing and displacing these waters and the effect of potential geochemical reactions on the produced water compositions. The match between observed trends in produced water compositions and those calculated by their simulation model indicated that barite precipitation was the principal reaction occurring in the mixing zone for the Brent model and that ion exchange reactions became more important under high clay content conditions due to the release of barium and strontium from the exchange sites into the brine (**Figure 1.11**). The difference between observed strontium concentration in produced water and those modelled is probably caused by a release of strontium during the dissolution of calcite which was not included in their model.

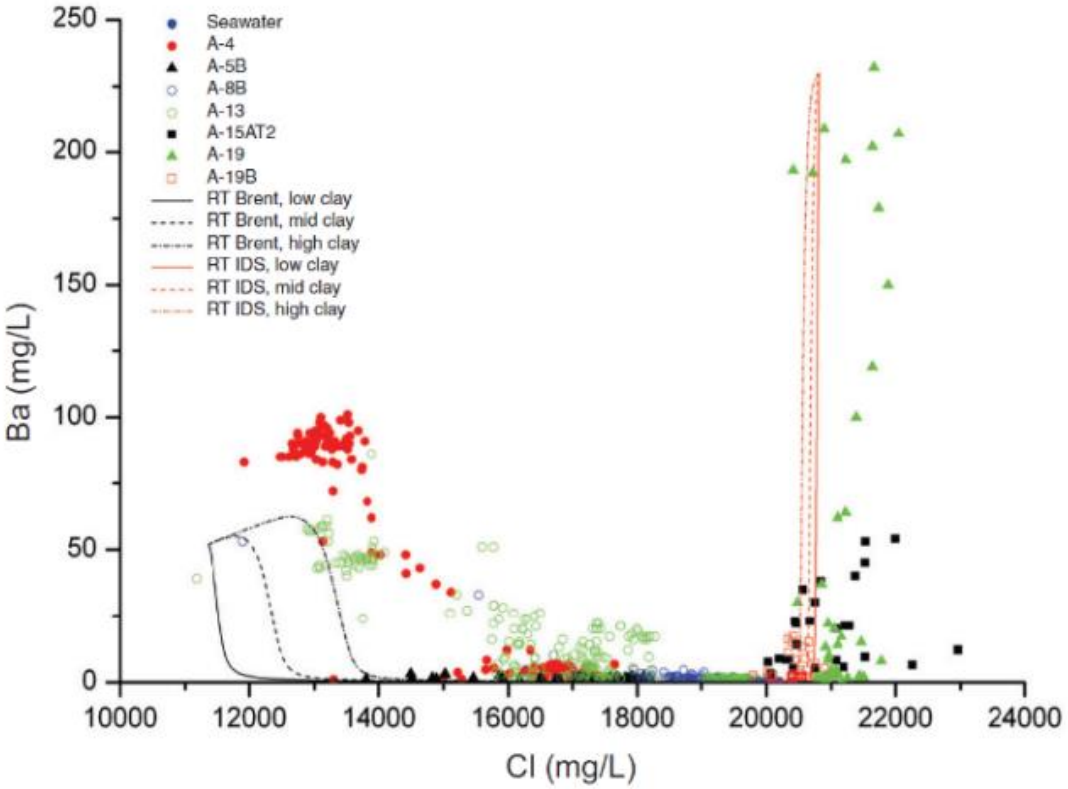

Figure 1.11 Comparison of Ba and Cl produced water analyses from the Brent and IDS reservoirs and simulation produced water analyses from reactive-transport models. (**McCartney et al. 2012**)

1.8 Motivation and Objectives

As reserves in the UKCS decline, and as oil prices vary, increasing attention is paid to the potential to increase recovery and extend field life. Options to increase recovery from brownfield sea water flooded reservoirs include, in order of actual or probable uptake:

1. Improved waterflood management, including drilling of new infill wells to target unswept oil, or pressure depletion to liberate solution hydrocarbon gas;
2. Injection of low salinity water, which has been demonstrated to improve recovery factors by 2-10%, and which has been selected by one operating company as its waterflooding method of choice for all future developments, unless a strong case can be made to the contrary for any specific asset;
3. Injection of polymers, or other chemicals or combinations of chemicals, such as surfactants and alkali, to improve sweep efficiency and mobilise trapped oil;

4. Injection of miscible gas, including hydrocarbon gas and/or carbon dioxide (the latter including the benefit of carbon sequestration), again to improve sweep efficiency and mobilise trapped oil.

Indeed, combinations of the above four options are also considered. In the cases of low salinity water flooding, injection of chemicals and injection of carbon dioxide, geochemical reactions will play a very significant role in determining the success or failure of these enhanced oil recovery (EOR) methods. However, the industry is not well positioned to evaluate these recovery methods because there is a lack of knowledge of what geochemical reactions will take place, and even once the reactions are identified the models are not adequately tuned to enable accurate predictive calculations to be undertaken.

Advanced reservoir simulation software is used to better understand and predict the flow of fluids through reservoir rock, very little modelling of geochemical interactions between the fluids and the host rock is undertaken. This is partially because geochemical reactions are not considered to be important in determining recovery factors for conventional sea water flooding operations. This is also partially because the available geochemical simulators may be tuned to systems close to ambient conditions, but are generally not well tuned to the higher pressures, temperatures and salinities that occur in oilfield systems.

Given the reason that reservoir interactions have a big impact on produced water compositions and the risk of mineral scale precipitations, and also play an important role in chemical enhanced oil recovery methods, the main focus of this thesis is to develop a systematic and searchable database in which produced water chemical compositional data are collected and stored, and to conduct an investigation about what geochemical reactions are taking place within a variety of reservoirs, linked to the reservoir rock mineralogies, thermodynamic conditions such as temperature and pressure, formation water compositions, and injection water compositions. A better understanding of potential reservoir interactions occurring deep within the reservoir would be helpful in predicting produced water compositions and scaling tendencies, and potentially in identification of suitable chemical recovery methods for candidates in future field developments.

1.9 Thesis outline

Chapter 1 gives an introduction to general review of scale formation and reactive transport model, research motivation, objectives and thesis outline.

Chapter 2 describes the background and motivation to develop the produced water database and its structure. The statistics of key characteristics of reservoir fields in the produced water database were described. Possible *in situ* reactions were discussed and summarized based on the observation of field data.

Chapter 3 presents a produced water dataset for a typical and normal sandstone reservoir in which chemical compositional data have been recorded from repeated produced water samples. This chapter provides insights into what components are involved in the *in situ* geochemical reactions that occur as the brines are displaced through the reservoir, and how the precipitation and dissolution of minerals and the ion exchange reactions occurring within the reservoir can be identified. This information is then used to better evaluate the scale risk, especially focusing on sulphate scales that deposit at the production wells due to the mixing of incompatible formation and injection brines.

Chapter 4 presents a fully three dimensional reservoir simulation study for the Miller Field to evaluate brine flow and mixing processes occurring in the reservoir, using an available history matched streamline reservoir simulation model. The displacement of injection water and the behaviour of the produced water in two given production wells were further investigated through adding conservative natural tracers. A model of barite scale precipitation was included in the available streamline reservoir model, and the simulation results with and without barite precipitation were compared with observed data (barium and sulphate concentrations in the produced brine), and various possible locations of scale deposition (barite) for different kinds of data (simulated and observed) were summarized.

Chapter 5 demonstrates the understanding of mineral reactions occurring in the Gyda field where there is high initial temperature and high TDS (especially calcium) in formation water. Anhydrite precipitation is the dominant mineral reaction within the reservoir and is largely dependent on temperature, with reservoir temperature, which initially is very high (160°C), decreasing gradually due to cold injection water (25°C). Thermal modelling was added to the 1-D model in order to evaluate the effect of non-isothermal processes and heat transport on the geochemical reactions, especially the anhydrite mineral reaction. The 1-D base case model was extended to be a 2-D vertical cross section model where two layers with high and low permeabilities were assigned and how the difference in horizontal permeability in the two layers affects brine mixing of formation and injection water and geochemical reactions were discussed.

Chapter 6 demonstrates particular work on analysis of produced brine data from a North Sea chalk field and associated modelling. With the help of the valuable produced water dataset and some basic reservoir properties, a one dimensional reactive transport model is developed to identify what *in situ* reactions were taking place in the carbonate reservoir triggered by seawater injection. The effects of calcite dissolution on the sulphate scaling reactions due to incompatible brine mixing and the potential occurrence of carbonate mineral precipitation induced by calcite dissolution were highlighted.

Chapter 7 presents a three-dimensional reactive transport modelling study to investigate the geochemical process during seawater/ altering seawater with different sulphate concentrations injected into a carbonate reservoir which helps understanding the possible mechanism behind Smart Water injection. A series of calcite and anhydrite mineral reactions are investigated and discussed in detail. At the early stage, CO_2 partitioning from the hydrocarbon phase into the brine causes significant calcite dissolution. This process can be enhanced by increasing sulphate concentration in the injection water. Sulphate concentration in the injection has a significant impact on whether the calcite is continuously dissolved, or not, after the CO_2 front passes by. In the modelling cases including thermal transport, reservoir temperature is cooled by injection water, compared with isothermal cases, thus anhydrite precipitation and calcite dissolution are affected.

Chapter 8 gives the conclusions of this research and provide some suggestions for the future work.

CHAPTER 2 PRODUCED WATER DATABASE

2.1 Introduction

In oilfields where scaling problems exist, produced water samples are routinely collected and submitted for chemical compositional analysis on a regular basis (monthly, weekly, sometimes daily) to aid with identification of potential flow assurance problems and assist overall management of the well stock. At the end of the productive lives of these fields generally nothing further is done with these. However, this produced water compositional data contains clues about geochemical interactions that occur as the various waters are displaced through the reservoir rock.

Over the past two decades of research into oilfield scale management, produced water chemical composition data from some fields have been collected as part of individual field studies. For operating companies effort is required in collecting and putting into context such field data, but the data itself does not tend to be as sensitive as hydrocarbon compositional data, and hence there is generally a preparedness to supply such data for research purposes. Indeed, often there is a desire by operators for their field data to be used in this research, so that there may be an opportunity for lessons learned to be applied to their specific assets.

There is thus an opportunity to collect the data from many fields worldwide for which it is available, and organise it in a systematic and searchable database, so that trends common to various fields can be identified. There is also an opportunity to significantly extend this database, although the window of opportunity is limited in that as fields reach the end of their operational lives, less attention is paid to collecting, or storing, or being able to retrieve such data.

Once these produced water chemistry data have been collected, a systematic analysis of the database may well reveal that there are common trends across specific types of fields and formations. This may prove invaluable when assessing scale management options in these and similar fields undergoing development worldwide. This information may also prove useful for analysis of the various chemical and altered brine composition recovery methods, in that some categories of field may be amenable to one type of recovery method, whilst others may not, based on the geochemical reactions occurring that can be deduced from the produced water data.

Furthermore, such a systematic grouping of reservoir types, linked to the mineralogies of the rock in these reservoirs, would help inform what types of laboratory experiments need to be performed to generate the thermodynamic and kinetic data that are required for accurate reactive transport simulations of such fields. This would be a key enabler in not only modelling scaling behaviour in such fields, but also potentially in identification of suitable chemical recovery methods for candidate fields, and the optimisation of the engineering plan (choice of injection chemicals, concentrations, well locations, timing of injection, etc).

In the past a database of *formation water* compositions has been developed for the North Sea (Egeberg and Aagaard, 1989; Bjørlykke and Gran, 1994; Moss et al., 2003; Warren and Smally, 1994). Whilst a very useful resource, this database only contains the static compositions of the reservoir brines before any fluids are injected, and hence contains little or no information as to what geochemical reactions will occur as non-native fluids are injected and interact with the rock. This new *produced water* database will contain information on how waters have interacted with rocks in all types of North Sea and other worldwide formations, data that will have cost many millions of pounds to collect and analyse over decades of sampling, and yet which otherwise would be lost.

A database that can be used to inform and validate laboratory geochemistry experiments, based on measurements made by the subsurface exploration and production industry, may have benefits a long time into the future, in terms of maintaining appropriate scale management and also of maximising recovery opportunities in the maturing oil industry.

2.2 Structure of produced water database

The basic structure of the produced water database has been developed and more than 50,000 measured samples from 26 fields around the world have been collected and put into the database. The structure of the database includes data plotting and analyses tools in order to make data storing, searching, filtering and plotting efficient and effective. The structure of the database is shown in **Figure 2.1**.

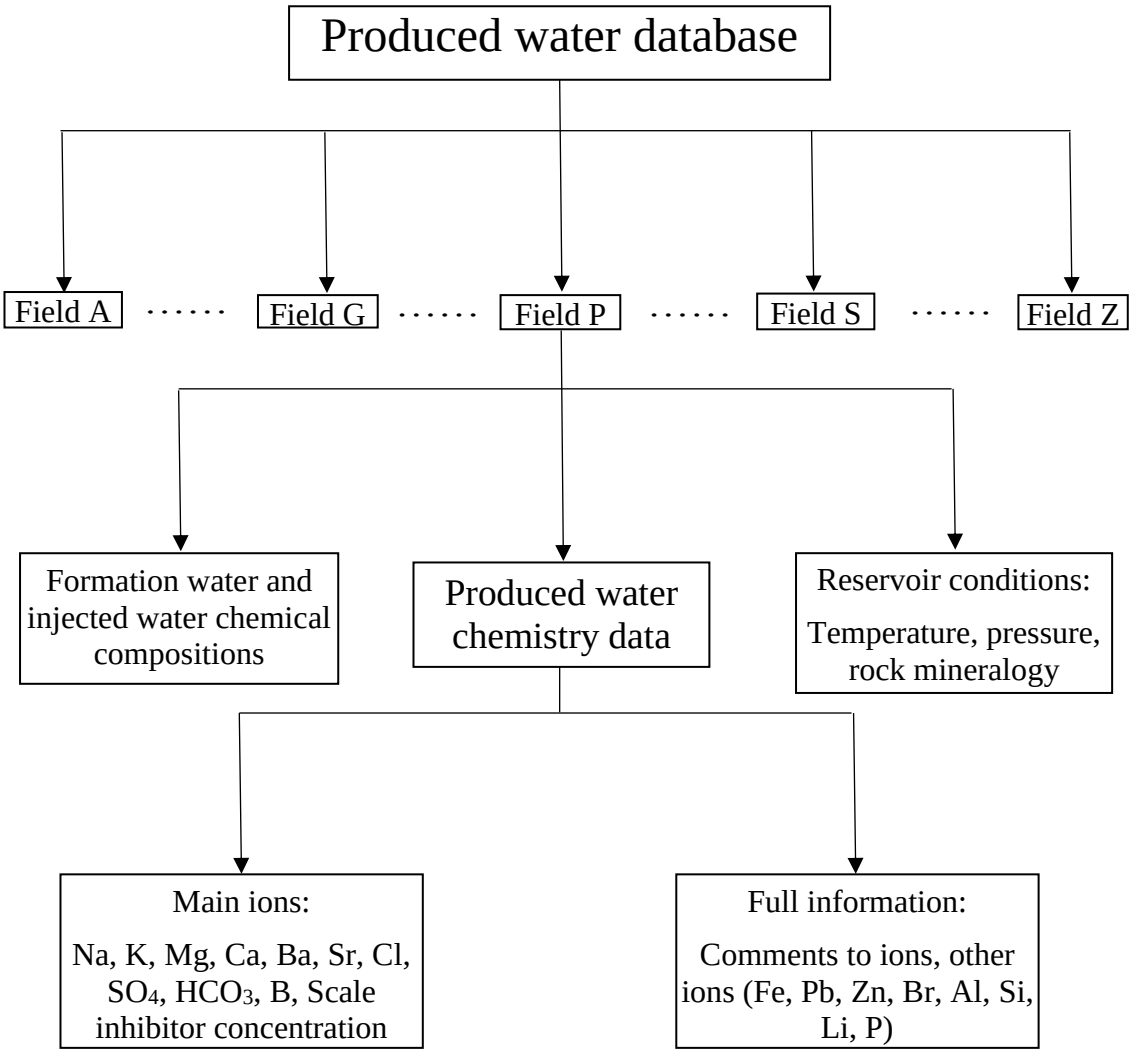

Figure 2.1 The structure of produced water database.

In the database, data for each field are stored in one unit (one file folder); each unit contains three files. The three files contain produced brine data; formation and injected brine compositions; and reservoir conditions including temperature, pressure, and mineralogy. The first file is the most vital and core to the database, because it contains the various measurement results for each sample that has been analysed.

The file of produced brine data contains two sheets. In the first sheet, called "Main Ions", basic information about the sample is stored, such as sample date and well name, and sodium, potassium, magnesium, calcium, barium, strontium, chloride, sulphate, bicarbonate, boron and residual scale inhibitor concentrations (**Figure 2.2**). This focuses on data that reservoir engineers and production chemists will pay attention to when evaluating the oilfield scale risk. This allows a quick look at the main scaling risks in the field. It is generally considered that these main ions would have been involved in some geochemical reactions in the reservoir. Clearly erroneous or noise data are removed from

this sheet. The data will be filtered in this sheet if more than one concentration for single water sample are provided.

Field	Well	Date	Na	K	Mg	Ca	Ba	Sr	Cl	SO4	HCO3	B	SI
		13/03/1994	13530	3800	190	38	120	30	28486	540	74	53	21
		02/04/1994	13950	940	150	36	120	25	23360	390	93	53	7.5
		22/04/1994	14460	800	150	46	110	29	22900	77	145	55	12
		10/05/1994	13940	750	140	49	75	29	22930	9.2	120	54	36
		05/06/1994	14220	830	170	41	99	29	23380	190	68	55	1.5
		19/06/1994	13920	750	140	52	93	31	23020	50	105	55	4.2
		01/07/1994	13670	700	130	50	90	28	22890	53	170	54	5.8
		01/08/1994	13720	680	130	52	92	29	22970	17	180	53	92
		01/08/1994	13730	680	130	53	92	29	22850	11	170	54	275
		22/09/1994	14330	700	140	57	94	30	22780	12	190	55	385
		22/09/1994	14290	700	140	57	93	30	22560	12	157	55	85
		03/11/1994	13790	670	130	54	89	28	22780	9.8	145	54	92
		05/12/1994	13870	690	130	54	89	29	22630	12	225	54	39
		09/01/1995	14300	690	140	55	90	30	22960	150	205	56	55
		17/01/1995	13910	680	130	55	95	30	22770	12	215	52	29
		26/01/1995	13570	680	130	55	85	29	22940	10	235	56	68
		01/02/1995	13720	680	130	55	98	29	22980	9.7	225	52	27
		10/02/1995	14090	730	140	56	87	31	22990	10	220	54.1	34
		21/02/1995	13920	715	135	56	91	30	22950	11	240	55.5	18
		04/03/1995	14050	715	135	57	93	31	22970	10	215	54.4	36
		13/03/1995	14090	710	135	58	90	30	22700	9.9	225	53	8.9
		31/03/1995	14170	745	140	56	90	32	22610	10	250	54.9	8.9
		15/04/1995	14580	725	135	57	92	31	23280	22	275	56.8	7.6
		01/05/1995	13520	680	130	35	200	29	21810	43	220	49.4	10
		02/06/1995	14010	680	155	2.9	87	27	22780	120	130	51.8	9.4
		07/08/1995	13390	715	425	14	165	22	22700	1080	245	36.3	19
		15/08/1995	13640	665	220	19	95	26	22590	400	180	48.2	13
		20/08/1995	13910	670	185	35	91	28	22640	270	205	50	25
		31/08/1995	13710	660	165	45	97	30	22600	210	240	51.6	3.8
		25/09/1995	13930	690	175	41	89	30	22350	295	240	50.5	21
		02/10/1995	14200	625	150	41	83	28	22930	280	i/s	49.9	4.2
		10/10/1995	13760	670	165	45	89	29	22980	205	200	52.5	20
		14/10/1995	13870	680	170	45	90	29	22690	210	205	52	3.4
		21/10/1995	13370	655	160	45	84	29	22820	180	205	51	23
		18/11/1995	12930	645	175	38	81	27	22130	290	225	47.6	27
		25/11/1996	13360	660	180	39	83	28	22310	305	235	49.4	43

Main ions | Full information | Sheet3

Figure 2.2 Screenshot of "main ions" sheet in the produced brine database (Field, well and laboratory names have been blanked out).

However, all data supplied are preserved in the second sheet, called "Full Information" - data integrity is ensured by not altering any of the supplied data when it is stored in this sheet (**Figure 2.3**). Apart from the main ions mentioned above, iron, lead, zinc, lithium, bromine, silica, phosphorus, and aluminium concentrations of produced water samples are stored in the "Full Information" sheet. This information may not be related with common reactions focused on in this thesis, but they may be useful for some other studies, such as silica concentration for silicate scale formation and iron, lead, zinc for sulphide scale precipitation. It should be noted that the availability of data varies in different fields. In addition, one column is added next to the column for ion concentration to comment what measurement was used for obtaining the data. For example, the sulphate concentration in produced water samples can be measured by ICP or DIONEX. Which

method has been used is crucial for some fields which has potential sulphide scale problems, so comments about the sulphate concentration are needed. In some cases, there are more than one concentration value provided for each ion, so all of them are stored in this sheet.

The collection of produced water data is the first step in developing a general and universal study of produced ion trends and reservoir reactions, and is the foundation of the more detailed analysis presented later in this thesis. Common trends across specific types of fields and formations are identified; these trends may, and the factors that cause them may only, be identified if sufficient data from many types of reservoir fields worldwide have been collected, plotted and analysed. The more extensive the database, the powerful a tool it will prove in identifying common trends, and perhaps what causes these trends. It may be difficult to develop an accurate understanding of the processes that will take place within any given reservoir before production commences, so in such a scenario a produced brine database may be a very helpful tool, if behaviour in analogue fields can be studied and compared.

Field	Well	Date	Fe	Comm	Pb	Comm	Zn	Comm	Li	Comm	Br	Comm	Si	Comm	P	Comm	Al
		13/03/1994							2				69		0.41		<1
		02/04/1994							2.5				33		<0.06		<0.2
		22/04/1994							2.5				24		<0.15		<0.5
		10/05/1994							2.4				19		0.18		<0.5
		05/06/1994							2.4				21		0.18		<0.5
		19/06/1994							2.3				19		<0.15		0.5
		01/07/1994							2.3				19		65		<0.5
		01/08/1994							2.3				18		<0.15		<0.5
		01/08/1994							2.3				18		<0.15		<0.5
		22/09/1994							2.4				21		0.22		<0.5
		22/09/1994							2.4				18		0.32		<0.5
		03/11/1994							2.4				18		0.18		<0.5
		05/12/1994							2.3				18		<0.15		<0.5
		09/01/1995							2.5				18		<0.15		<0.5
		17/01/1995							2.4				17		0.61		<0.5
		26/01/1995							2.3				18		0.23		<0.5
		01/02/1995							2.5				17		<0.15		<0.5
		10/02/1995							2.4				18		<0.15		<0.5
		21/02/1995							2.5				18		<0.15		<0.5
		04/03/1995							2.5				18		0.19		<0.5
		13/03/1995							2.5				18		<0.15		<0.5
		31/03/1995							2.4				17		<0.15		<0.5
		15/04/1995							2.4				19		0.18		<0.50
		01/05/1995							2.3				17		<0.15		<0.50
		02/06/1995							2.2				20		0.64		<0.50
		07/08/1995							1.9				42		110		<0.50
		15/08/1995							2.1				24		41		<0.50
		20/08/1995							2.2				20		28		<0.50
		31/08/1995							2.3				19		14		<0.50
		25/09/1995							2.2				20		19		<0.50
		02/10/1995							2.1				17		230		<0.50
		10/10/1995							2.2				18		8.9		<0.50

Main ions | Full information | Sheet3

Figure 2.3 Screenshot of "full information" sheet in the produced brine database. (Field, well and laboratory names have been blanked out).

Table 2.1 describes the statistics of some key characteristics of these fields. More than 50000 produced water sample data from 26 fields worldwide have been collected. Most

of the fields in the database are sandstone reservoirs located in the North Sea where there has been seawater injection. Although there are also carbonate fields and one example of a steam flood, the database will continue to be expanded and developed beyond the end of this PhD project.

Table 2.1 Statistics of characteristic of reservoir fields in current produced water database.

Field ID	Location	Reservoir type	Injection brine	Number of wells	Number of samples	
A	North Sea	Sandstone	Seawater	28	2798	
B	North Sea	Sandstone	Seawater	2	247	
C	Brazil	Sandstone	Seawater	10	66	
D	Angola	Sandstone	Seawater	10	1431	
E	Angola	Sandstone	Seawater	9	758	
F	North Sea	Sandstone	Seawater	5	1540	
G	North Sea	Sandstone	Seawater	132	19782	
H	Brazil	Sandstone	Seawater	7	40	
I	North Sea	Sandstone	Seawater	31	1334	
J	North Sea	Chalk	Seawater	128	2825	
L	North Sea	Sandstone	Seawater	1	410	
M	North Sea	Sandstone	Seawater	2	92	
N	Angola	Sandstone	Seawater	7	639	
O	North Sea	Sandstone	Seawater	22	13067	
P	North Sea	Sandstone	Seawater	16	10133	
Q	North Sea	Sandstone	Seawater	12	294	
R	North Sea	Sandstone	Seawater	21	2275	
S	North Sea	Sandstone	Seawater	3	1046	
T	North Sea	Sandstone	Seawater	12	2815	
U	North Sea	Sandstone	Seawater	1	25	
V	North Sea	Sandstone	Desulphated seawater	6	872	
W	Angola	Sandstone	Seawater	3	224	
X	North Sea	Sandstone	Seawater	4	203	
Y	North Sea	Sandstone	Seawater	5	530	
Z	Kuwait	Dolomite	Steam	25	640	
26				**502**	**64086**	**TOTAL**

2.3 Typical initial analysis of generated plots

Produced water chemical compositional data were processed using the Reacting Ion Toolkit (Ishkov et al., 2009), and plots generated for interpretation - for example concentration of ion X vs concentration of ion Y, or concentration of ion Z vs IWF - to enable us make an estimate of formation water compositions and calculation IWF. In the plots generated by this toolkit, the vertical/horizontal green dashed lines correspond to the ion (X/Y axis) concentrations in formation and injection water.

2.3.1 Identification of water sample preserved with different content of EDTA

Three main trends have been observed in any of the plots involving Sodium, for example the barium vs sodium plot shown in **Figure 2.4**. It is concluded that Na-EDTA with different concentrations has been used to preserve produced water samples, and that three sodium concentration ranges exist, corresponding to samples without EDTA (identified in the data set as not stabilised and highlighted with the red arrow), samples with a lower concentration of EDTA (highlighted with the purple arrow) and samples with a higher concentration of EDTA (highlighted with the blue arrow).

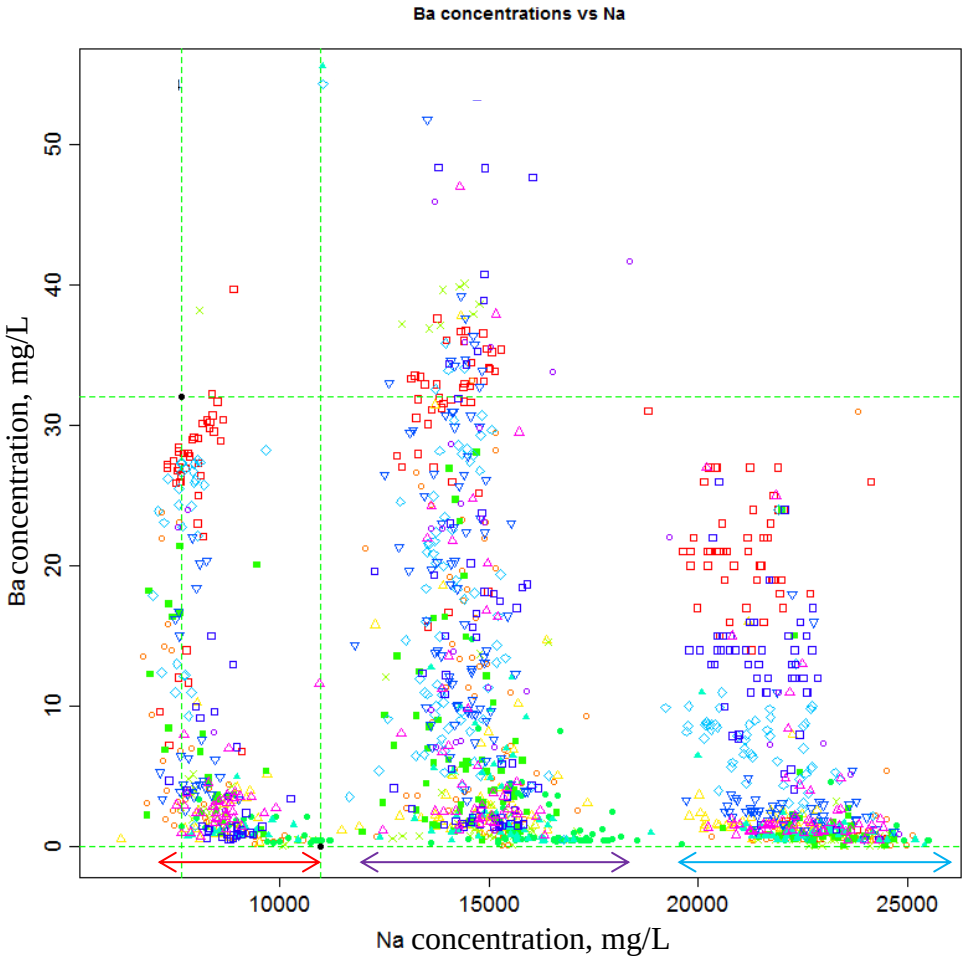

Figure 2.4 Ba concentration vs Na concentration for all samples from all wells. Note the three sets of characteristic behaviour, suggesting samples preserved with two concentrations of Na-EDTA, and a further set of samples not preserved with Na-EDTA.

Taking into account that samples were preserved with different concentrations of EDTA, it is necessary to filter and rearrange the data in order to make full use of the produced brine data and generate plots that can be more readily understood. **Table 2.2** presents such data as were made available and were used to generate the plots. EDTA would form

complexes with any divalent cations in solution, thereby reducing the free ions available to participate in the crystallization process and lowering the supersaturation.

The measurement of barium and Strontium from samples preserved by EDTA is more reliable because addition of EDTA would reduce the amount of barite and celestite that could precipitate once the sample has been collected (Shaughnessy et al., 1983). However, the Na concentration would be increased due to the addition of EDTA, so samples without EDTA are used for plots with sodium on the ordinate.

Table 2.2 Availability and filtration of data. (Data used for plotting highlighted with a red tick).

	without EDTA		**with EDTA**	
Ions	Data availability	For plotting	Data availability	For plotting
Na	√	√	√	✗
Ca	√	√	✗	✗
Mg	√	√	√	✗
Ba	✗	✗	√	√
Sr	✗	✗	√	√
Cl	√	√	✗	✗
SO_4	√	✗	√	√
B	√	√	√	✗

2.3.2 Estimation and validation of formation water composition

Formation and injected water compositions have been supplied. Identification of formation water composition in particular can be challenging, since samples of formation water can be difficult to obtain, they may be contaminated by drilling fluids, reactions may have taken place during or after the process of extracting the brine from the formation, or the sample may not have been preserved adequately. Thus, supplied formation water samples should be reviewed carefully within the context of how the samples were collected and analysed, and accounting for the conditions under which the brine would have originally migrated into the formation, and any subsequent reactions that would have led to the equilibrium state before any wells were drilled (McCartney et al., 2005). Formation water samples were not available for this study, and thus the accuracy of the supplied formation water composition was simply checked by seeking consistency in the analysis of the ions vs ions plots for the produced water samples - i.e. the supplied formation water composition was compared with the composition achieved by extrapolating compositions in produced water samples to zero IWF (the lowest

chloride concentration). Clearly this has the limitation that any reactions that have affected the composition of the produced samples, or any inaccuracy in identifying the IWF associated with each sample, will limit the accuracy of the extrapolated formation water composition. Nonetheless, it provides a useful qualitative consistency check, even if quantitatively it is not a precise method.

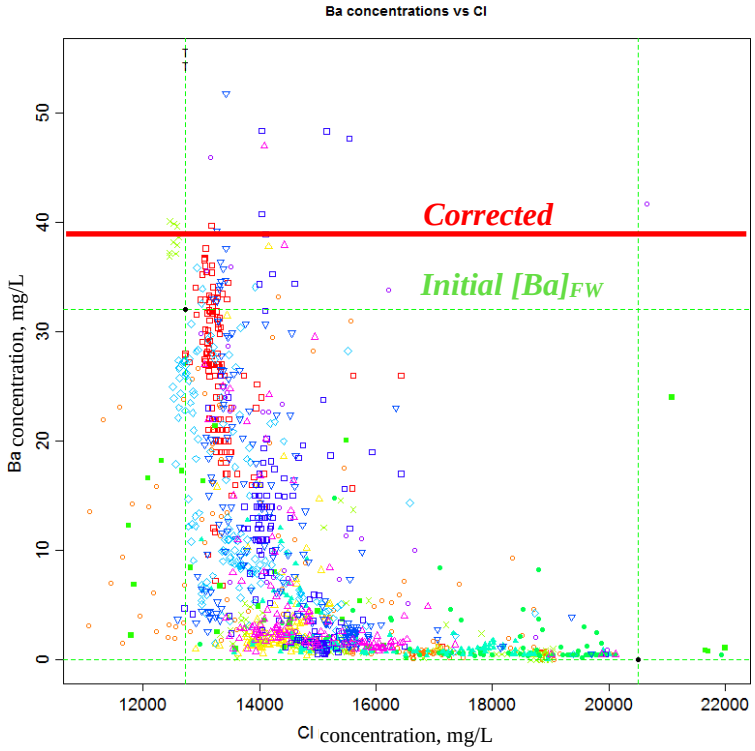

Figure 2.5 Ba concentration vs Cl (including initial $[Ba]_{FW}$ and corrected $[Ba]_{FW}$), showing Ba is very reactive.

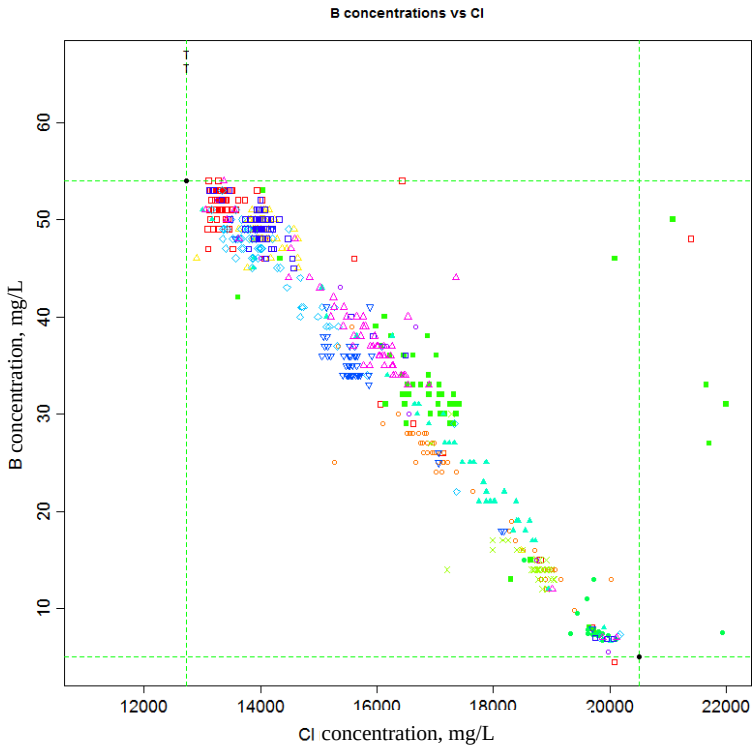

Figure 2.6 B concentration vs Cl concentration, suggesting both B and Cl are conservative ions.

There is a doubt about the reported barium concentration in the formation water. This is one of the most important parameters for scale prediction, control and management, and so due care must be paid to accurately measuring it. In **Figure 2.5**, which is a plot of barium vs chloride, some data points with low chloride concentrations, meaning low injected water fractions, exceed the initial barium concentration (32 mg/L) supplied. From the data, approximately 40 mg/L would appear to be a consistent value for barium concentration in the formation water, indicated by the red straight line. It may be noted that there are some samples with higher barium concentrations, up to 52 mg/L, but that these tend to be in samples taken at very low IWFs. The fact that a chelating agent is used in preserving samples raises the possibility that for samples with a significant IWF, and hence containing sulphate, barite crystals may have formed before the brine reached the treated zone, and some of these crystals may have passed through the system to the sampling point without further growth or deposition due to the presence of the inhibitor. Once the sample was captured, it would then be possible that the chelating agent would dissolve the crystals. Thus a precise determination is not possible, but the balance of evidence from the data, particularly those taken at low IWFs, suggest that a barium concentration in the formation water of approximately 40 mg/L is consistent with the observed data. In the same way, the boron concentration in the formation water (FW) and the injection water (IW) could be estimated based on the observations in **Figure 2.6**.

The updated formation water and injection water compositions are shown in **Table 2.3**.

Table 2.3 Updated FW and IW chemical composition data. (Updated values highlighted in red).

Constituents	Formation water (mg/L)	Injected water (mg/L)
Na	7679	11000
Ca	636	400
Mg	88	1300
Ba	32 ⇨ 40	0
Sr	95	0
Cl	12727	20500
SO_4	25	2800
B	54	5
K	191	400

2.3.3 Calculation of Injection Water Fraction

Injection water fraction (IWF), indicating the extent of injection water breakthrough at producers, plays an important role in oilfield scale prediction and management. Thus, four different methods (Schmidt et al., 1990; Webb et al., 2004) have been used to evaluate injected water fraction for all wells, based on measurements of chloride, boron and sodium concentrations (Equation 2.1), and on the Reacting Ions method (Ishkov et al., 2009); the results are shown in **Figure 2.7**. First of all, we can identify that the injected water breakthrough curves, distinguished by different colours for the different methods, are *generally* in good agreement. However, it should be noted that there is not precise agreement, and that this can occur for a variety of reasons. The accuracy of the analytical methods can vary - for example there tends to be greater scatter in reported sodium concentrations than in chloride concentrations. Furthermore, as we shall note later, there may be variations in the local formation water composition throughout the field, which would then lead to systematic differences between wells. Also, some of the ions may not be completely conservative, and while any changes due to reactions may be relatively small if the ion is present at high concentrations to begin with, this can lead to some discrepancies. For example, sodium is known to take part in ion exchange reactions, but in relatively high salinity brines typically the concentration change is too small to be detectable on a consistent basis – nonetheless, such changes may cause some differences when comparing different ion trends, as here. Overall the data suggests that chloride, boron and sodium may be conservative ions and are not involved in geochemical reactions to a significant extent in this system, or that if they are involved in reactions, reactions

that remove them from solution are balanced by reactions that add them to the solution. In addition, it is probable that there is minimal $CaSO_4$ precipitation in the reservoir, since assuming only barite deposition in the Reaction Ions method gives a match to the other methods of determining injection water fraction.

$$IWF = \frac{C_{con}^{(ion)} - C_{FW}^{(ion)}}{C_{IW}^{(ion)} - C_{FW}^{(ion)}} \tag{2.1}$$

where $C_{con}^{(ion)}$, $C_{IW}^{(ion)}$ and $C_{FW}^{(ion)}$ are conservative ion concentration in the sample, ion concentration in injection brine and ion concentration in formation brine respectively.

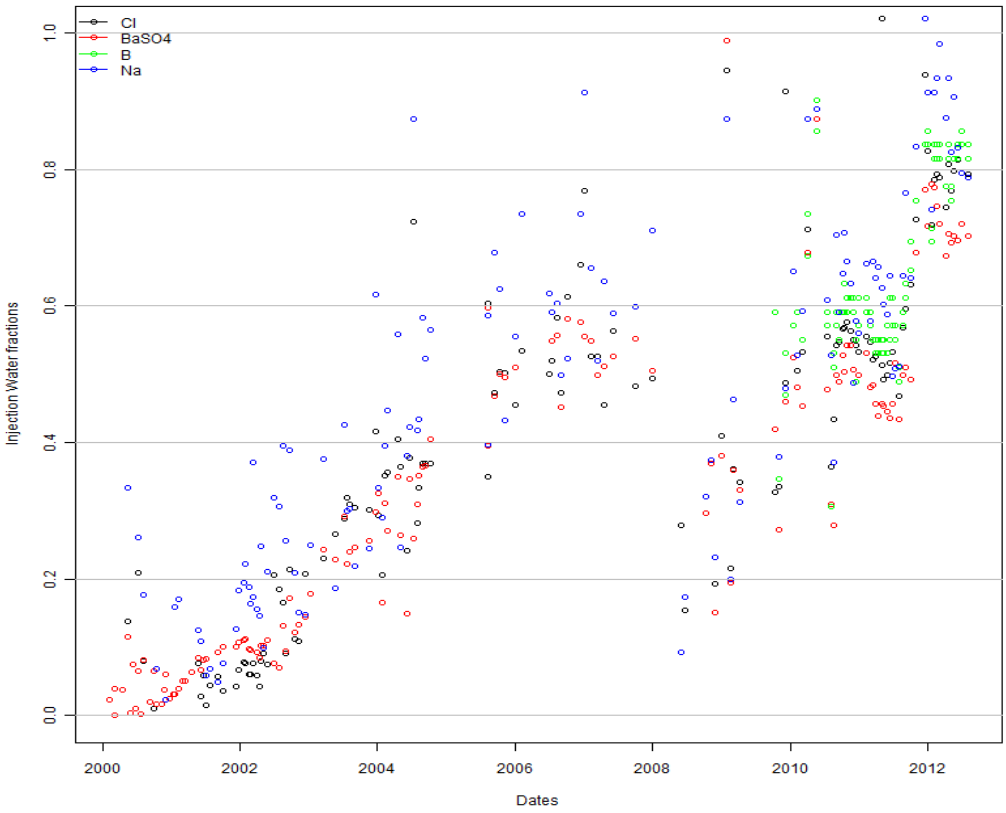

Figure 2.7 IWF vs dates for Well 1 using four methods (three based on ion concentrations for Cl, B and Na, and one using the Reacting Ions method based on the assumption that SO4 is only consumed in reactions with BaSO4).

CHAPTER 3 EVOLUTION OF PRODUCED WATER COMPOSITIONS IN FIELD X

3.1 Introduction

In this chapter, a study of the individual ion trends in the produced brine, using the types of plot developed for the Reacting Ions Toolkit (Ishkov et al., 2009), provides insights into what components that are involved in *in situ* geochemical reactions as the brines are displaced through the reservoir. Thermodynamic calculation are run based on produced water data and formation/injection water compositions to obtain actual scaling tendency and theoretical scaling tendency respectively. The comparison of theoretical and actual results indicates that geochemical reactions taking place in this given reservoir lead to ion depletion that greatly reduces the severity and potential for scale formation. However, ion exchange reactions are also observed, and these also affect the scale risk, and the effectiveness of scale inhibitors in preventing deposition. Additionally, comprehensive analysis using a geochemical model is used to predict the evolution of the produced brine compositions at the production wells, and to test the assumptions about which *in situ* reactions are occurring. A good match between the predictions from this geochemical model and the observed produced brine compositions is obtained, suggesting that the key reactions included in the geochemical model are representative of actual field behaviour. This helps to establish confidence that the model can be used as a predictive tool in this field.

3.2 Background

Field X is located in the northern North Sea, and covers an area of 70 km^2. The reservoir is part of the Middle Jurassic Brent Group sandstone with hydrocarbon source rock being the Upper Jurassic Kimmeridge Clay Formation, the principal source rock for the area. The reservoir sandstones generally have good porosities and permeabilities and are sealed by the Upper Jurassic Humber Group shales. The production zone is within the Middle Jurassic Brent sandstones at the relatively shallow depth of about 2440 meters and has an average porosity of 21%. Field X, which is at an initial reservoir pressure of 246 bar and initial reservoir temperature of 112^oC, is initially under normal hydrostatic pressure and therefore has very low natural drive and is undersaturated. As a result, water injection and gas lift play an important role in oil recovery. Water injection has been used from the outset at a rate of around 100,000 barrels/day to maintain reservoir pressure and maximize

recovery.

Injected water, in this case North Sea seawater, is chemically incompatible with the formation water in this reservoir. Barium and strontium in the formation water may react with sulphate in the injected seawater and precipitation of barite and celestite would take place. Therefore, produced brine sampling has been conducted to monitor for scale precipitation and a large dataset of produced water chemical compositions has been produced, and has been used here to understand what geochemical processes occur during water injection into the reservoir. The production wells are under active scale management by means of scale inhibitor squeeze treatments and regular brine composition and scale inhibitor returns monitoring.

3.3 Validation of formation water composition

The formation water compositions have been updated in **Table 2.3**. The quality of the updated formation water composition is validated by making some thermodynamic calculations of the formation water and identifying the saturation state of the given minerals. It is normally known that the formation water is in a chemical equilibrium with the reservoir rock in the initial reservoir conditions, which indicates that the saturation index of the given minerals should be approximately 0 or less than 0 (if the given mineral is not present in the reservoir mineralogy) in a chemical modelling of the water compositions.

Table 3.1 Saturation Index of anhydrite, barite, celestite and gypsum based on formation water composition

$[SO_4]$ in Formation water	SI(Anhydrite)	SI(Barite)	SI(Celestite)	SI(Gypsum)
25 mg/l	-1.75	0.4	-1.26	-2.25
10 mg/l	-2.15	0	-1.65	-2.65

In **Table 3.1**, it can be found that the saturation index of barite is 0.4 (> 0) when sulphate concentration in formation water is considered to be 25 mg/l and barite would be precipitated by formation water itself. This is not correct based on the fact that the equilibrium among water, oil and reservoir rock has reached. Therefore, the sulphate concentration in formation water was lowered to decrease the saturation index of barite. When the estimated sulphate concentration is 10 mg/l, the formation water equilibrate with barite mineral and would not precipitated. The corrected FW and IW compositions

have been included in **Table 3.2**.

Table 3.2 Updated FW and IW chemical composition data. (Updated values highlighted in blue).

Constituents	Formation water (mg/L)	Injected water (mg/L)
Na	7679	11000
Ca	636	400
Mg	88	1300
Ba	40	0
Sr	95	0
Cl	12727	20500
SO_4	25 ⟹ 10	2800
B	54	5
K	191	400

3.4 Behaviour of ions in produced brine

Plots of ion concentrations vs IWF are presented here. As mentioned previously, IWF has been calculated based on chloride. From **Figure 3.1** and **Figure 3.2** it can be seen that there is not strong evidence that boron and sodium are involved in reactions, although the boron data do suggest that there may be small but consistent differences in the formation water compositions for different wells. Such differences in boron concentration in formation brine compositions are not unusual, and have been reported previously (Mackay et al., 2000). The sodium data are sufficiently scattered, with no consistency between wells, that in this study no significant reactions could be inferred. Ba, as a common scaling ion, attracts attention.

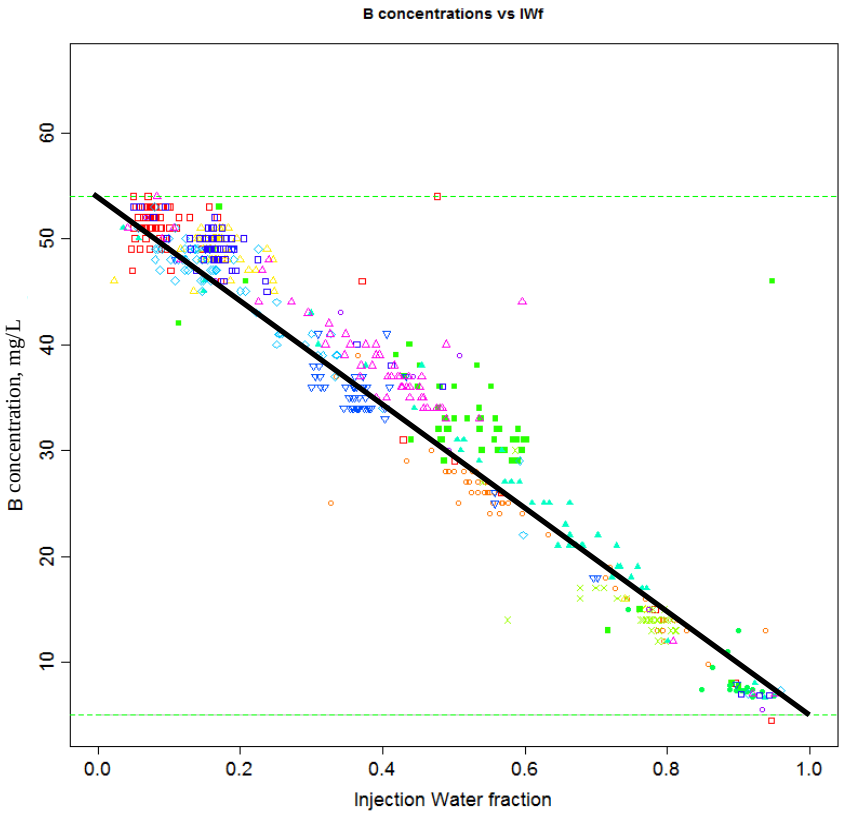

Figure 3.1 B concentration vs injection water fraction for ten wells (identified by colours in this and subsequent plots).

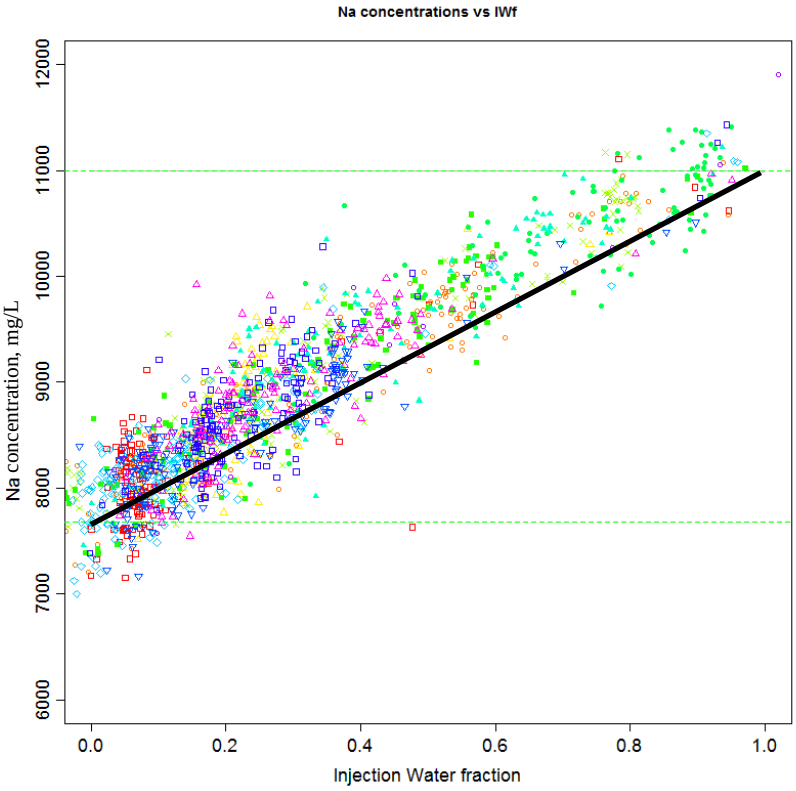

Figure 3.2 Na concentration vs IWF for samples without EDTA.

The plot in **Figure 3.3** shows a steep decline of barium concentration at low IWF (0% ~20%), and then barium concentration is observed to remain very low in the produced brine from 30% IWF and above. This kind of Ba trend is typical of seawater flooded sandstone reservoirs which contain Ba rich formation water. The reason for this typical Barium trend is that barium begins to react with sulphate in the injected water and precipitates as barite. Moreover, barium concentration in the initial formation water is low relative to sulphate concentration in the injected water, and as the reaction is limited by the availability of barium, only very small concentrations of barium are produced at high injected water fractions. Significant barium stripping in the produced water due to barite scale precipitation occurring in the reservoir was observed in the Froy Field (Østvold et al., 2010), Gyda field (Mackay et al., 2006; McCartney et al., 2007) and Veslefrikk field (McCartney et al., 2012).

Strontium sulphate is another common scale caused by incompatible mixing of FW and IW. For this field (see **Figure 3.4**), just a small amount of celestite precipitates at lower IWF values, and then the data suggest that some of it dissolves at high IWF, which is reflected by the "S" curve of the stontium trend in the plot. (stontium concentrations from one well show higher stontium concentrations at low IWFs - this possibly reflects a local variation in the stontium content in the formation water.) Overall, this general characteristic stontium trend has been observed in many oil fields within our database. In the Veslefrikk field, produced water that is a mixture of formation water and injected seawater, gains stontium in the reservoir, which probably results from dissolution of celestite and/or calcite. (McCartney et al., 2012) However, it was reported that stontium concentrations lie on its seawater-formation water mixing line and stontium was not involved in geochemical reactions in the Gyda field. (Mackay et al., 2006; McCartney et al., 2007)

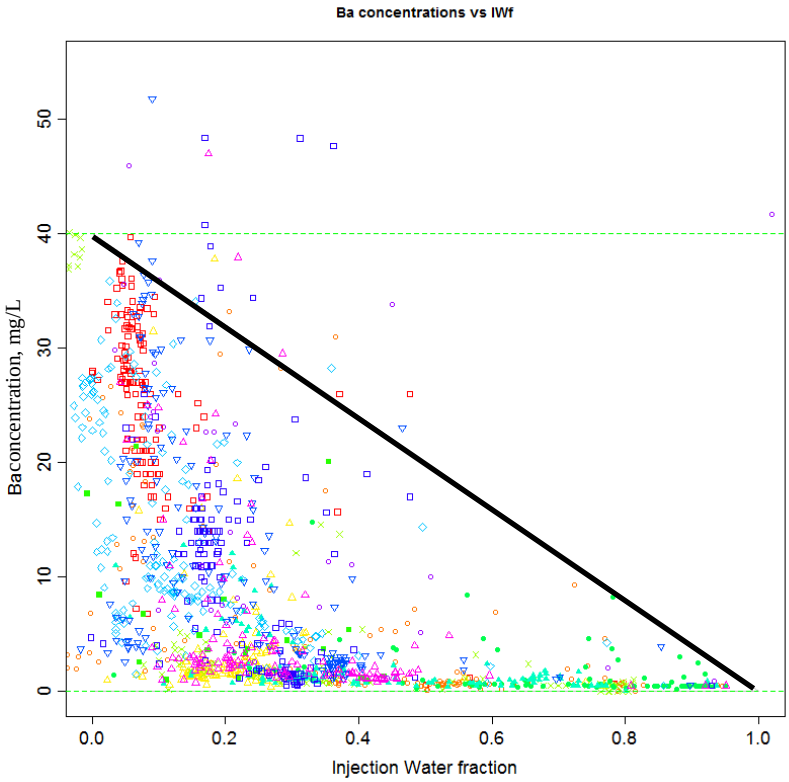

Figure 3.3 Ba concentration vs IWF showing evidence of $BaSO_4$ precipitation at all IWFs.

The depletion of magnesium has been noted and investigated in some publications with respect to the analyses of produce water chemistry. Dolomitization and/or cation exchange were believed to be main mechanisms of magnesium stripping in some fields. (Mackay et al., 2006; McCartney et al., 2007; McCartney et al., 2012) Here we just consider calcium-magnesium ion exchange, since there is lack of information on bicarbonate and carbonate concentrations, then sulphate mineral reactions are the focus in this study and Magnesium sulphate is very soluble at these reservoir conditions. **Figure 3.5** shows that there is very little magnesium stripping relative to its seawater-formation water mixing line. However, the evidence is that calcium-magnesium ion exchange does occur, although the reaction is not strong. Considering the FW and IW compositions, we can identify that this field is one with an unusually low TDS in the FW (around 23,000 mg/L), which is even lower than the TDS of the injected water (North Sea seawater). In our current database, this is the only field where formation water has a lower TDS than the injected water. Therefore, there is reason to believe some characteristic differences with behaviours in other fields may exist.

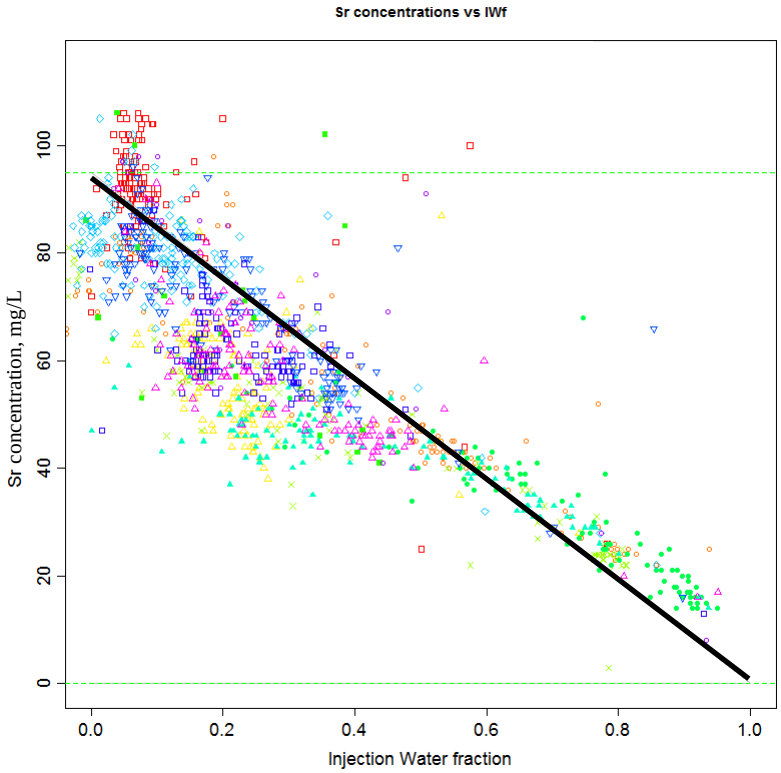

Figure 3.4 Sr concentration vs IWF showing evidence of $SrSO_4$ precipitation at low IWFs, and $SrSO_4$ dissolution at high IWFs – leading to a characteristic "S" shape profile.

In oilfield systems calcium is generally more abundant in formation waters than magnesium, and is involved in a greater number of reactions, which is consistent with the more scattered data points shown in **Figure 3.6**. First, the deviation from its seawater-formation water mixing line reflects calcium ions being released from rock into the flowing brine, which is in accordance with what we have observed and summarized from the magnesium plot described above, and the assumption that ion exchange reactions are taking place. As a whole, the calcium trend rises steadily, followed by a smooth decrease. Therefore, the maximum amount of ion exchange was reached at the highest calcium concentration, corresponding to about 50% IWF, and this is also consistent with biggest variation in magnesium (shown in **Figure 3.5**). Secondly, as noted above, calcium is generally one of the ions involved in the greatest number of reactions, and other reactions, such as calcium carbonate dissolution and precipitation may cause increases or decreases, respectively, in the measured calcium concentrations. It is possible that some calcite precipitation occurs at low IWFs as pressure is decreased, but this is sometimes exceeded by reactions that increase the calcium concentration. This secondary precipitated calcite, or any primary calcite cements may then be dissolved at higher IWFs. A quantitative

analysis would require consideration of bicarbonate and CO_2 concentrations, which data were not available to this study.

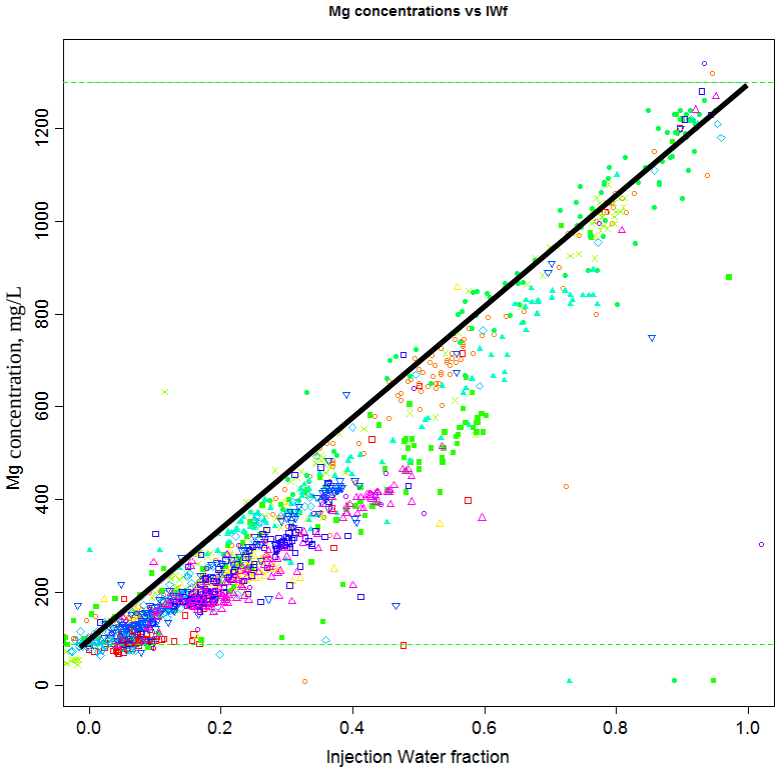

Figure 3.5 Mg concentration vs IWF showing evidence of loss of Mg from solution due to ion exchange reactions.

The sulphate trend, shown in **Figure 3.7**, is influenced by the association of barium, strontium and calcium, because barite, celestite and anhydrite are commonly occurring oilfield scales. $[Ba]_{FW}$ (barium concentration in formation water) (= 40mg/L) and $[Sr]_{FW}$ (strontium concentration in formation water) (= 100mg/L) lead to a relatively low consumption of sulphate {$[SO_4]_{SW}$ (sulphate concentration in seawater) = 2800mg/L}. The consumption of sulphate is so low relative to $[SO_4]_{IW}$ that we can hardly detect any deviation in the sulphate trend compared to its mixing/dilution line. In fact, sulphate concentrations are usually observed to be almost on the seawater-formation water mixing line in sandstone reservoirs, such as Froy field (Østvold et al., 2010), Veslefrikk field (McCartney et al., 2012) and Miller field (Houston et al., 2006; Fu et al., 2012). No evidence of H_2S was presented in the data set supplied by the operator for this study. Although it is possible that iron bearing minerals could retard the propagation of H_2S, at a reservoir temperature of 112^oC the bacteria would generally have to be thermophilic for souring at the production wells to pose a challenge. In any case, under these conditions, it is the sulphate mineral reactions that will tend to dominate in terms of any alteration in

the sulphate content, other than due to simple dilution, and as IWF increases sulphate is soon in excess for any such reactions.

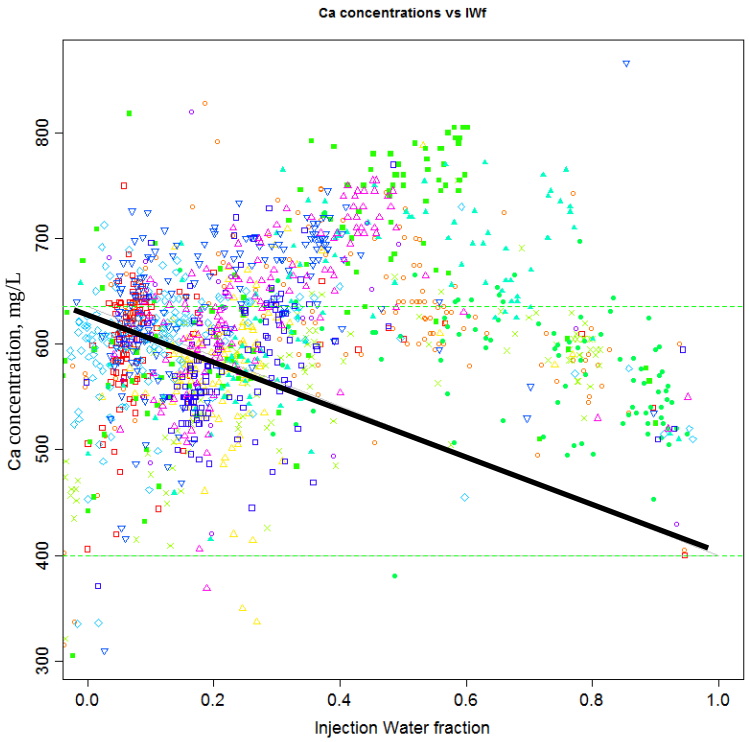

Figure 3.6 Ca concentration vs IWF showing evidence of increase of Ca in solution due to ion exchange reactions.

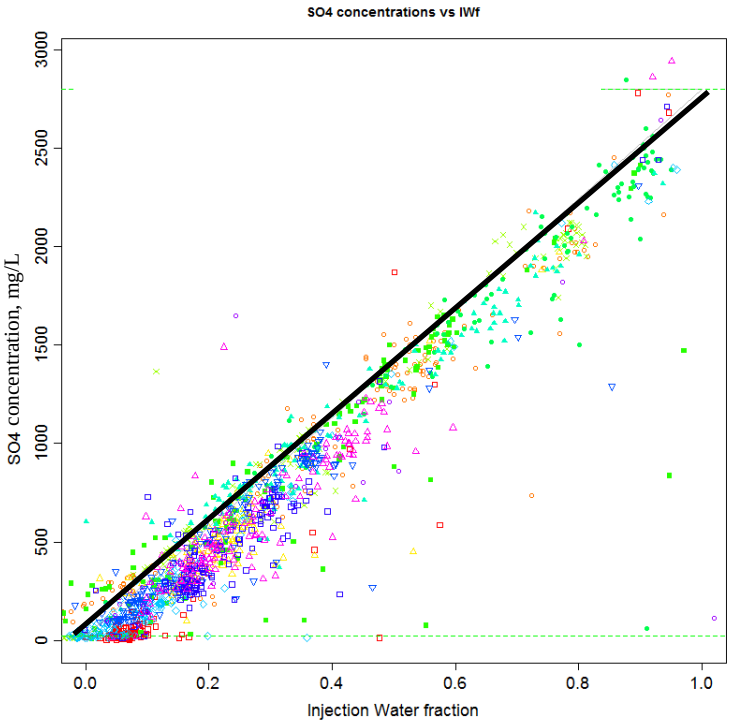

Figure 3.7 SO_4 concentration vs IWF, which is little affected by $BaSO_4$ precipitation, this only evident at low IWFs.

3.5 Thermodynamic model

3.5.1 Conventional method

The scaling tendency can be measured by the potential maximum amount of precipitation and by the Saturation Ratio (SR) which is defined by Equation 1.18 and 1.19. The risk of scale formation depends both on the SR and the local environment. Over-saturation (SR > 1) means that the system is no longer in chemical equilibrium and the force that drives scale precipitation is greater at larger values of SR.

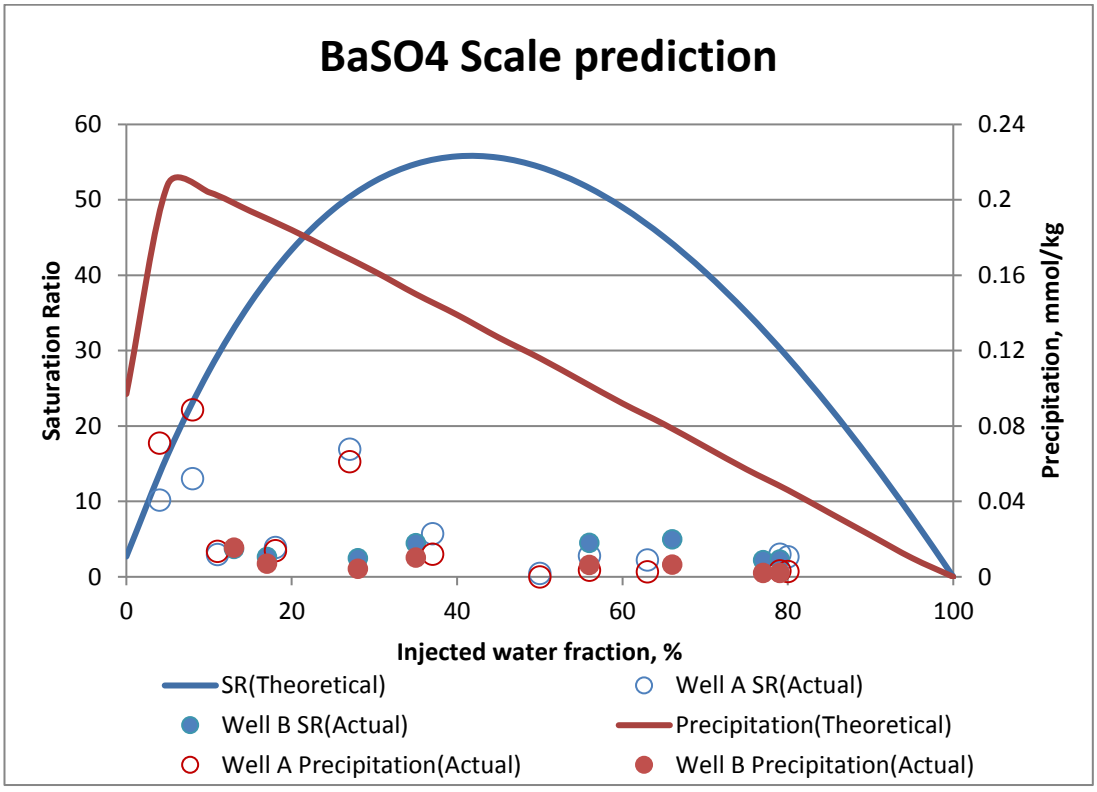

Figure 3.8 Comparison of Saturation Ratio and amount of precipitation for $BaSO_4$ at two wells.

Thermodynamic models have been widely developed for evaluating and predicting scaling tendencies in oilfield based on the composition of formation and injected water and the extent of their mixture (Yuan et al., 1993; Oddo and Tomson, 1994; Kaasa, 1998). In this chapter, a thermodynamic scale prediction code (Kaasa, 1998), MultiScale, was used to calculate SR and mass that would precipitate based on various ratios of mixing of FW and IW. The thermodynamic model results in **Figure 3.8** and **Figure 3.9** (SR values for barite and celestite) show that the greatest driving force for the reaction to occur

(which corresponds to the maximum saturation ratio) is at 40-45% SW for both barite and celestite. However, the results of the thermodynamic equilibrium calculations (with amount of precipitation calculated in mmol/kg) in **Figure 3.8** and **Figure 3.9** also show that the greatest mass of precipitation of barite occurs at a SW fraction in the produced water of 8-10%, whereas the maximum mass of celestite precipitation occurs at 40% SW fraction. The thermodynamic model results in **Figure 3.10** show that no anhydrite precipitation takes place due to the relative low temperature and low calcium concentration.

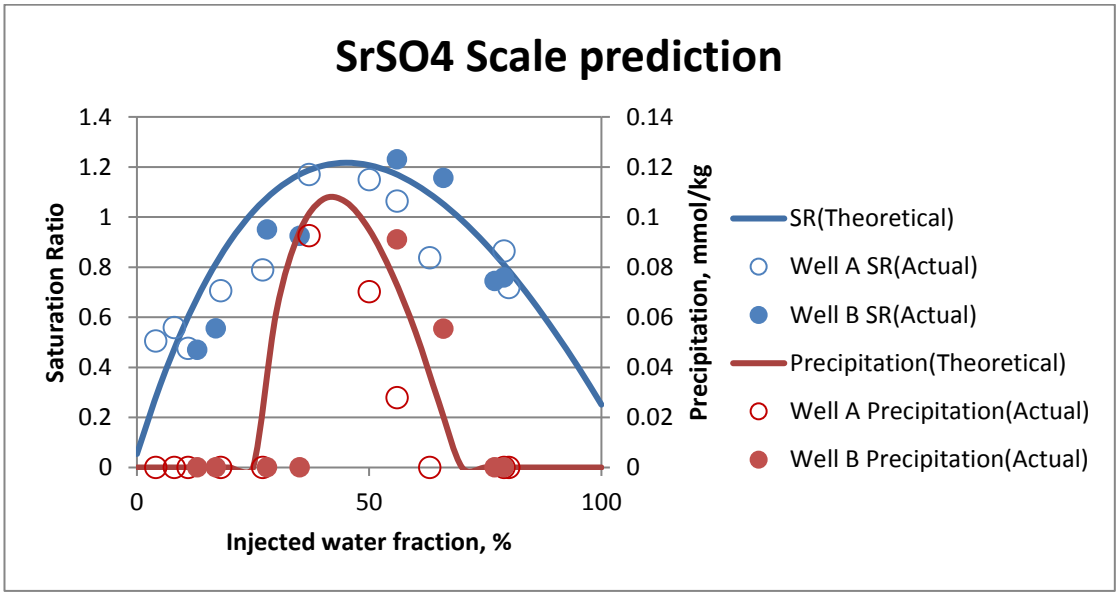

Figure 3.9 Comparison of Saturation Ratio and amount of precipitation for $SrSO_4$ at two wells.

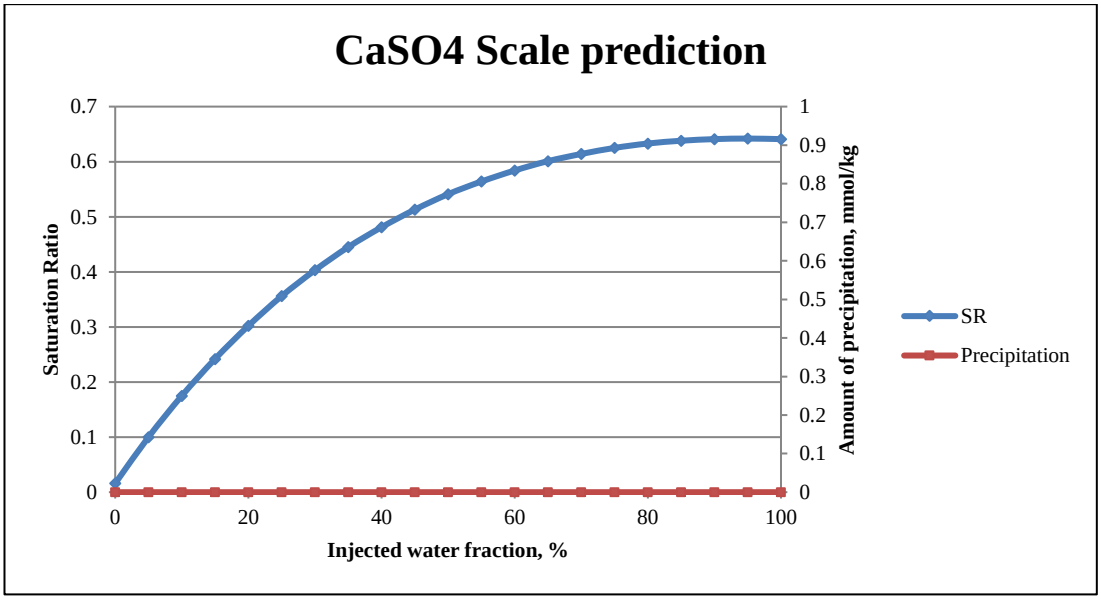

Figure 3.10 The Saturation Ratio and amount of precipitation for $CaSO_4$ scale prediction.

From the perspective of the thermodynamic modelling, barite scale formation is the most severe scale problem as the Saturation Ratio and amount of precipitation are greater than for the other scales. celestite precipitation does occur but is not strong, and anhydrite does not show any scaling potential at all. In summary, scale prediction calculations using the thermodynamic model are consistent with what we have concluded based on the analysis of the produced brine geochemistry database.

3.5.2 New method

As mentioned above, the conventional scale prediction method is to use the thermodynamic model based on the endpoint FW and IW compositions to model scale formation in the wellbore, calculating saturation ratios for various mixtures of FW and IW, ranging from 100% FW to 100% IW; however, this neglects any *in situ* geochemical reactions that took place because at least some of the brine mixing occurred within the reservoir (Gomes et al., 2012). The geochemical reactions taking place in the reservoir are critical and generally beneficial for scale control and management, because some common scaling ions could be stripped deep within the reservoir and would not have the opportunity to react and be precipitated in the wellbore or production tubing (Sorbie and Mackay, 2000; Paulo et al., 2001; Mackay et al., 2003; Mackay et al., 2006, Vazquez et al., 2013). Two wells in this field have been analysed by using an improved method to understand and interpret which geochemical reactions are occurring and their impact on the produced brine composition.

First of all, as is normally done and shown in **Figure 3.8** and **Figure 3.9**, the profiles of Saturation Ratio and maximum mass of precipitation as a function of seawater fraction are calculated using the thermodynamic model, based on the assumption that mixing only takes place in the wellbore, and none of the ion concentrations are decreased or increased due to precipitation or any other geochemical processes in the reservoir or after sampling. This is the *theoretical scaling prediction*.

Next, the produced brine data were used as single points to calculate the above parameters, which were then plotted versus seawater fraction based on chloride. This can be regarded as *actual scaling prediction* based on sampling of a brine mixture which had the opportunity to react in the reservoir, and did, but as it entered the wellbore any further reactions were stopped because the brine passed through a zone where scale inhibitor was present and desorbing. The brine was then sampled topsides and further preserved, and thus the composition used in the calculation reflects the outcome of any geochemical

activity that took place in the reservoir, but is unaffected by scale deposition in the production system. This calculation thus indicates the scaling tendency as the brine mixture reaches the well, accounting for any loss of scaling ions in the reservoir, and identifying what remaining scale risk there is in the well that requires inhibition. This calculation of the potential scaling tendency in the well is lower than the theoretical scaling prediction using the normal mixing calculations because it takes account of the impact of reactions in the reservoir. Therefore, the differences between the theoretical and actual scaling predictions indicate the outcome of scale precipitation in the reservoir at field conditions. This information is very useful in building reactive transport models that include the key geochemical reactions occurring in the reservoir.

The MultiScale results in **Figure 3.8** and **Figure 3.9** for the two wells show the calculated SR and amount of precipitation (single point values) for barite and celestite in the two wells based on observed produced water samples are both lower than their theoretical scaling prediction (smooth lines). This indicates that fluid/fluid and fluid/rock interactions have actually taken place and led to ion stripping or depletion, such as due to barite and celestite precipitation. Moreover, barium stripping due to barite scale formation within the reservoir would be much stronger than stontium stripping as it also can be seen in **Figure 3.8** and **Figure 3.9** that the deviation for celestite is evidently less than that for barite. As a result, there is evidence of geochemical processes that alter the brine composition before the brine mixture reaches the production well. Under this circumstance, the scaling risk to the production well or separator could be very much reduced, which would be critical for scale evaluation, prediction and management.

3.6 One dimensional reactive transport model

The role of the reservoir was neglected in all of thermodynamic modelling work which is based on the fundamental assumption that the potential scale precipitation will be due to pure mixing of formation and injected water in the production well. However, it has been reported in some recent publications that both of brine mixing and geochemical reactions take place within the reservoir and the chemical composition of produced water would then be altered by them before arriving at producers (Paulo et al., 2001; McCartney et al., 2005; Houston et al., 2006; Mackay et al., 2006; Gomes et al., 2012; Fu et al., 2012). Thus, it is important to reveals some fluid/fluid and fluid/rock interactions occurring in the reservoir through combining produced water chemical compositional data with a geochemical model.

PHREEQC (Parkhurst, et al., 1999 is then applied to investigate the effect of geochemical reactions on the produced water composition during the mixing and movement of injection water and formation from injector to producer.

The field being considered in this chapter is a sandstone reservoir, but no details of reservoir mineralogy were available. The mineral composition of reservoir sandstone is normally dominated by quartz. Feldspars, composed mainly of K-Feldspar with minor amounts of plagioclase and some clay (Illite and Kaolinite) are often present in the bulk rock (Morgenthaler et al., 2008; Bybee, 2009). Normally the increase in pH resulting from seawater injection is not enough to dissolve quartz and feldspar so there is little possibility of dissolving quartz/feldspar and subsequent silicate mineral precipitation during conventional seawater flooding. Due to this and due to the formation/injection water compositions, and based on the previous evaluation of the produced brine analyses, the dissolution/precipitation of barite and celestite were considered likely to be the main reactions occurring in the reservoir. Also, ion exchange was assumed where sodium, K, barium, calcium, stontium and magnesium may be involved, but particularly sodium, K, calcium and magnesium.

Table 3.3 gives the Cation Exchange Capacity (CEC) of common soil constituents (Appelo et al., 2010). Clay minerals show a wide range in CECs depending upon mineral structure, structural substitutions and the specific surface of the mineral accessible to water. However, full modelling of precipitation and dissolution reactions and ion exchange processes evidently requires some knowledge of the distribution of the primary minerals in the reservoir, and of the appropriate parameters such as CEC, ion-exchange selectivity coefficients, CO_2 content in the hydrocarbon phases, etc. (McCartney et al., 2012). Furthermore, the impact of mixing can only be fully reflected by accounting for three-dimensional flow in the reservoir, and such calculations will only be accurate if numerical dispersion effects can be overcome, which is generally not possible in a full field reservoir simulation model. Thus a simplistic approach was used here, using a one dimensional reactive transport model, limited by lack of mineralogical data, simply to identify whether, by a qualitative assessment, consistency with the previously proposed geochemical reactions could be achieved. Clearly a non-unique solution might be achievable, and thus this activity can deliver consistency of evidence, not definitive proof of the geochemistry of the system.

Table 3.3 Cation exchange capacities of common soil and sediment materials (Appelo and Postma, 2010).

	CEC, meq/kg
Vermiculite	1000-2000
Montmorillonite	800-1200
Illite	200-500
Chlorite	100-400
Glauconite	50-400
Halloysite	50-100
Kaolinite	30-150

Bearing these caveats in mind, in this case the single phase (water) the one dimensional reactive transport model was used, where the keyword EXCHANGE defines exchange properties and can be used to calculate the composition of an exchanger. EXCHANGE defines moles of exchangers (X^-), but the concentration depends on the amount of solution (default is 1 kg water). Injection of water with the IW composition into a one-dimensional single phase water system was simulated, where the initial *in situ* water has the FW composition. Based on different possible exchangers, magnesium and calcium ion trend behaviours in the effluent or sink of the one-dimensional system were obtained. **Figure 3.11** and **Figure 3.12** show the variation in X has a larger effect on calcium than on magnesium, since calcium has a larger Molecular Weight and smaller range of concentrations. It should be noted that the objective here is not to seek an exact match to the field data. Indeed the field data represents samples taken from many wells with varying flow paths and patterns, potentially different initial FW compositions (albeit the relative constant IW compositions can be assumed since seawater is used), and potentially different distributions of the various mineral phases in different sectors of the field, at all length scales. **Figure 3.11** and **Figure 3.12** indicate that the reactions specified previously could indeed be occurring, although these reactions do not necessarily represent an exhaustive list, and indeed to achieve a match on calcium trends, it is likely that a full carbonate model would have to be used. However, it can be identified that there is a possible range of values of the exchanger for this field which is consistent with the observed data (and which reflects lower exchanger sites and thus relatively weaker Cation Exchange Capacity when compared to other fields in our database).

It may be noted that the operator used Ca/Mg ratio as one of the measure of IWF in this case, because of the potential for ion exchange and the reaction including calcium, this could give erroneous results.

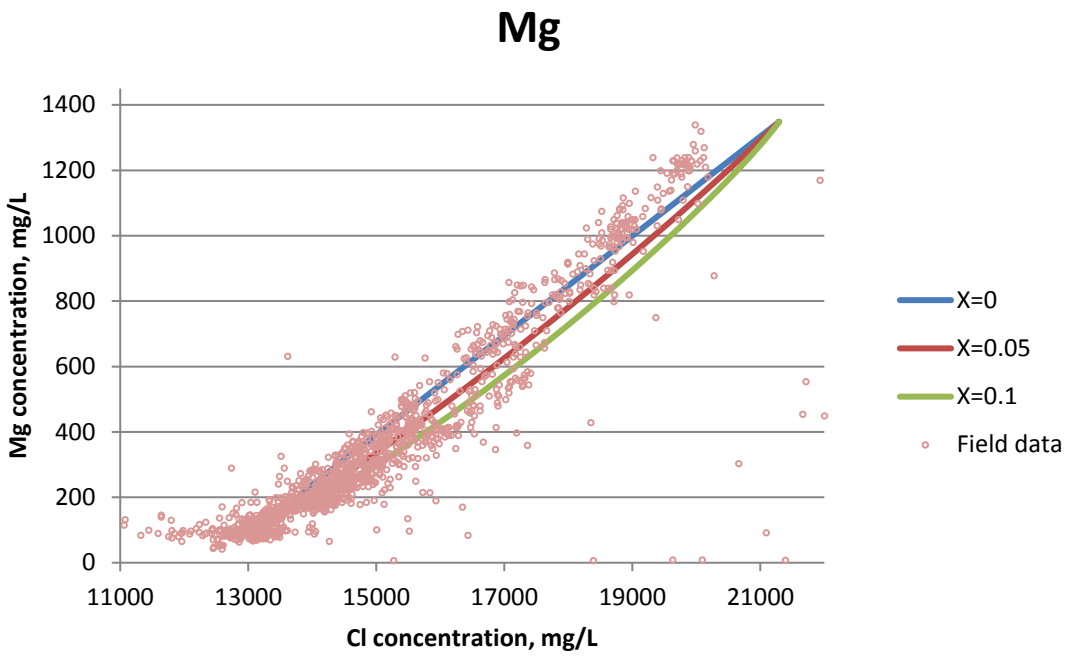

Figure 3.11 Comparison of simulation results and field data for Mg vs Cl plots.

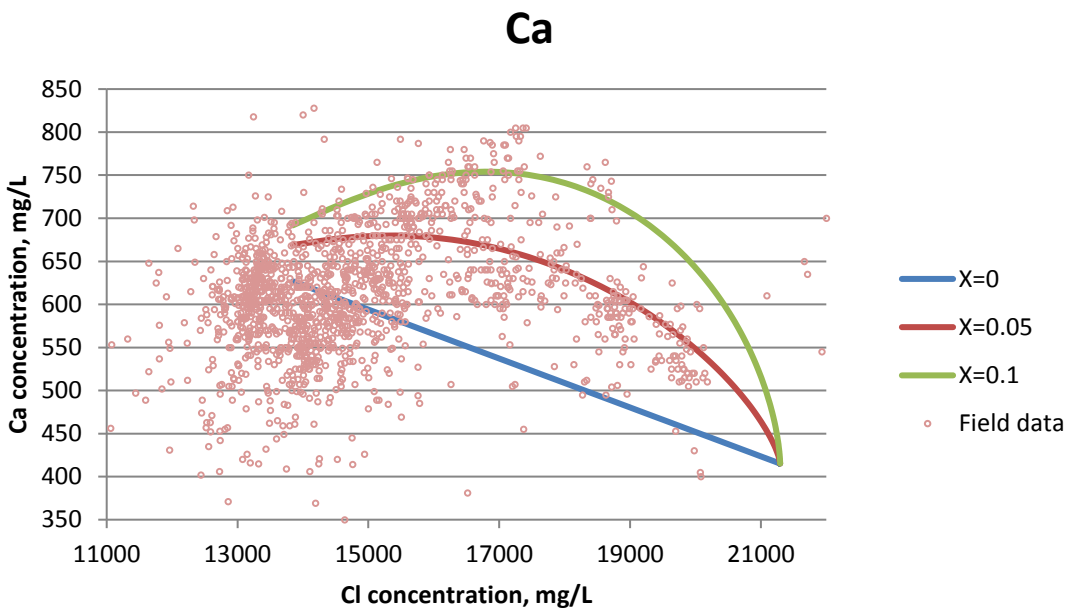

Figure 3.12 Comparison of simulation results and field data for Ca vs Cl plots.

Saturation Index is defined as Equation 1.20. In this word, tuning Saturation Index is used as a proxy changing for the solubility of minerals. By default the solution is saturated with the given mineral when SI = 0. The precipitation will be delayed if we increase the saturation index (>0), which is same as increasing the solubility of the mineral. On the other hand, if the saturation index is declined (<0), the mineral will be deposited earlier, which is equivalent to decreasing its solubility. The relationship between initial (by

default) and updated solubility (tuning) can be described as

$$K_{sp_{NEW}} = K_{sp_{INI}} \times 10^{SI} \quad (3.1)$$

When Saturation Index (SI) for minerals is held at default (0), the initial calculations did not provide a good match for barium, stontium and sulphate concentrations, and it is suspected that this was due to barite and/or celestite having higher/lower actual solubilities than used in the initial calculations. Thus, the calculations were repeated using the same reactions but adjusting the SI at which these minerals precipitated in the reservoir. In this context, increasing SI is used as a modelling technique equivalent to increasing the solubility of minerals, and vice versa, decreasing SI is used to reflect a decrease in solubility.

To achieve a match of the barium behaviour in the produced brine, the SI of barite has to be adjusted away from its default value of 0, as shown in **Figure 3.13**, reflecting incorrect initial solubility for these reservoir conditions. However, a good match of the stontium trends could not be achieved, regardless of any manipulation of the SI alone, as shown in **Figure 3.14**. There are various possible causes for this phenomenon. As already mentioned, the model used is a one dimensional geochemical simulator, and it is not possible to provide a perfect match for each ion's behaviour if differences in the flow and mixing processes occurring in a three dimensional reservoir are important. The fact that achieving a match in the one dimensional problem would prove so problematic suggests that the characteristic stontium behaviour may indeed be strongly dependent not only on the parameters characterising the geochemical reactions, but also on the evolution of the flow and mixing patterns in the reservoir. On the other hand, the match for the sulphate behaviour in **Figure 3.15** suggests that while brine mixing and *in situ* barite precipitation have an impact on the sulphate trends, variations from one well to another and as a consequence of different mixing patterns do not have a large impact.

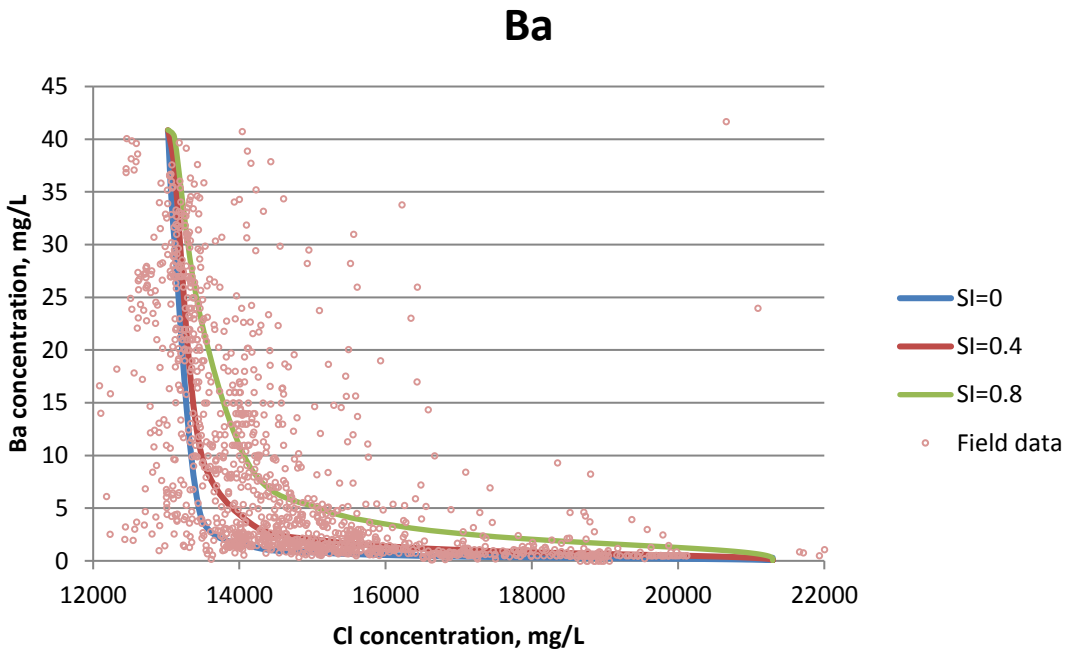

Figure 3.13 Comparison of simulation results and field data for Ba vs Cl plots.

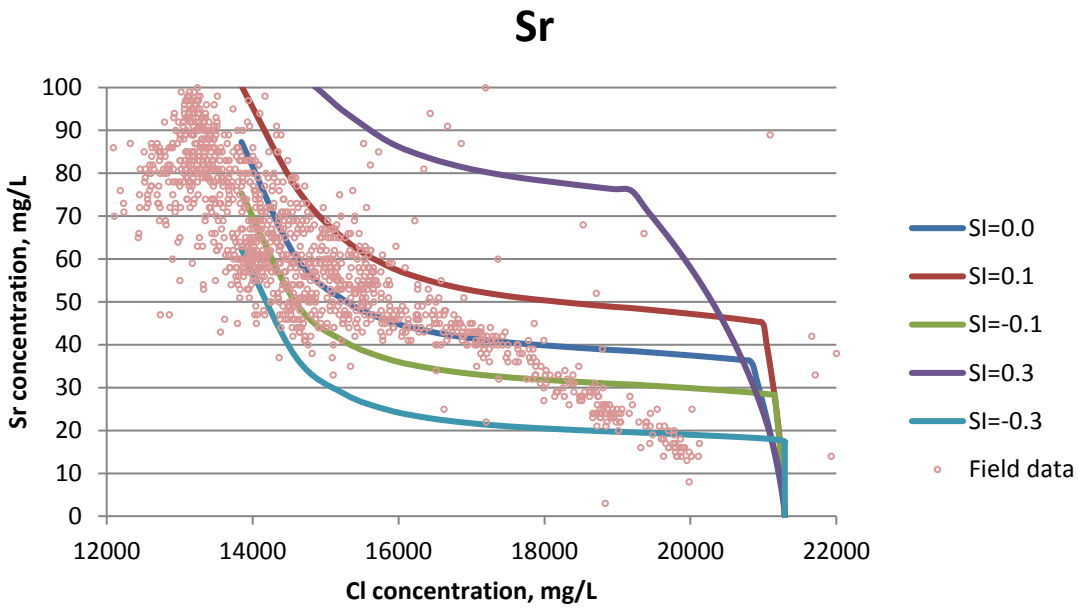

Figure 3.14 Comparison of simulation results and field data for Sr vs Cl plots.

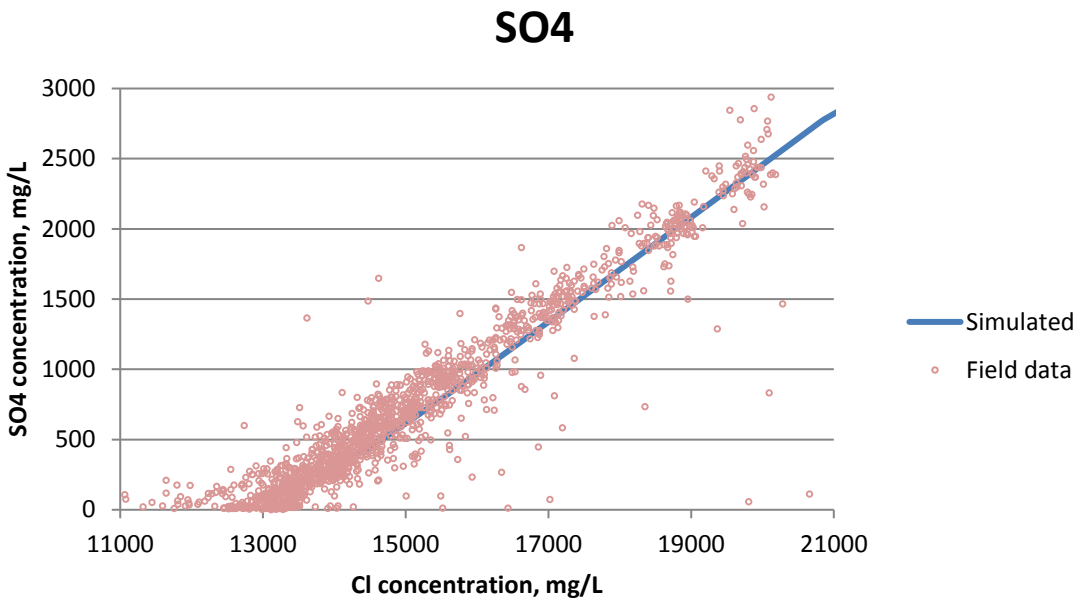

Figure 3.15 Comparison of simulation results and field data for SO4 vs Cl plots.

3.7 Conclusions

A specific field study was undertaken for produced brine chemistry analyses, scale prediction by use of MultiScale and produced water chemistry matching by PHREEQC. The study has led to the following conclusions about reservoir interactions in this field which are also applicable to most normal North Sea sandstone reservoirs:

1. Barium sulphate has been precipitated within the reservoir, but barite scale formation is still the most severe scale problem in the producer, although relative to other fields it is not very severe.
2. There is mild celestite precipitation, but this may re-dissolve at higher IWFs,
3. Anhydrite precipitation can generally be neglected here, but $CaCO_3$ deposition probably occurs (calcium quite reactive).
4. Some Ca/Mg ion exchange occurs, but is not strong compared to other fields.
5. Calcium is very reactive, so the operator should *not* use the Ca/Mg ratio to IWF. Chloride is much more reliable based on results of polynomial fitting for IWF calculations, or Reacting Ions can also be used.

CHAPTER 4 STREAMLINE RESERVOIR SIMULATION OF THE MILLER FIELD

4.1 Introduction

Geochemical data was initially used to investigate reservoir continuity, compartmentalization and origin of produced formation water by Slentz et al. (1981). Huseby et al. (2005) improved the reservoir simulation model through making use of geochemical data, and a better match with regard to produced sulphate$^-$ concentration was provided based on tuning the length of a fault. This process was also studied for the Janice field, and produced water chemistry was added as an extra constraint in the history matching process and two kinds of uncertainties on geology and water allocation between injectors were assessed based on the comparison of calculating seawater fraction from a simulation model and from observed produced water composition (Vazquez et al., 2014). However, geochemical data were only regarded as natural conservative ions and the possible geochemical reactions involving them were not considered in these publications, because the authors used a conventional reservoir simulator, such as ECLIPSE, that does not have a chemical reaction model, and so only the flow transport and brine mixing were calculated. Some applications were demonstrated by Delshad et al., (2003) using UTCHEM, a three-dimensional reservoir simulator, for studying the brine mixing and transport of barium and sulphate ions and barium sulphate scale precipitation taking place within the reservoir and Paulo et al. (2001) and Mackay et al. (2014b) applied the flow and reaction simulator to model barite precipitation. However, observed produced water chemical data were presented to compare with simulation results in only a limited number of modelling studies (Mackay et al., 2003c).

In this chapter, not only a natural conservative tracer, such as chloride$^-$, but also some reacting ions, such as Ba^{2+} and SO^{2-}, have been integrated into a three-dimensional streamline reservoir simulation study in which barium sulphate scale precipitation can be allowed to occur in the reservoir.

4.2 Reservoir Description and Field Development

The Miller field, located in the southern part of the south Viking Graben (Blocks 16/7b and 17/8b), covers an area of 40km^2 in the central North Sea. The production of the Brae field, located to the west of the Miller field, has caused a significant reduction of reservoir pressure in the Miller field, despite their different oil water contacts. The Miller reservoir

is in the Upper Jurassic Brae Formation turbidite sands, similar to the Brae Formation reservoirs in South and Central Brae. It is sealed by the Upper Jurassic Kimmeridge Clay Formation, which is also the source rock (Poynton et al., 2004).

Reservoir quality is approximately 80% net-to-gross. Porosity of 14%~18% is exhibited and permeability ranges from 200mD to over 1000mD (Poynton et al., 2004). Reservoir pressure is 45,000 kPa and reservoir temperature is 121°C. CO_2 contributes 20%mol to oil from the Miller field and the gas contains significant volumes of CO_2 – up to 20% by volume. Moreover, hydrogen sulphide is also present at up to 360 ppm in the gas phase (Rooksby, 1991; Smalley, 1994).

The mineral composition of the reservoir sandstone is dominated by quartz (>90%). Feldspars, composed of mainly K-Feldspar with minor amounts of plagioclase, compromises 1–3 % of the bulk rock. The rest of the bulk rock is made up of clays (Illite and Kaolinite, 3%), rock fragments and wood fragments. Quartz cements are also common (in ranges 2~3% and 0~4% respectively) (Marchand et al., 2001, 2002).

Development wells include 15 producers and 6 injectors. Oil production started in 1987 and seawater injection to maintain reservoir pressure started in August 1992. Significant water breakthrough occurred in 1996. The composition of formation water and seawater has been presented in **Table 4.1**. The mixing of formation water rich in barium (and some strontium) and seawater rich in sulphate injected to displace the oil leads to barite and some celestite precipitation within the reservoir or in the production tubing and casing or in the separator. In particular, the barium concentration (>600 mg/l) in the formation water is extremely high relative to other North Sea fields, which is why severe barite scaling problem occurred in the Miller field (Bourne et al., 2000).

Table 4.1 Chemical composition of formation water and injected North Sea seawater for Miller field.

Constituents	Formation water (mg/l)	North Sea seawater (mg/l)
Na	25898	10890
Ca	307	428
Mg	82	1368
Ba	643	0
Sr	39	7
Cl	41767	19800
SO4	4	2960
B	18	4
K	1100	460
HCO_3	2050	124

4.3 Analysing and Modelling of Geochemical Data

More than 10000 produced water chemical compositional data measurements were collected from 16 wells from 1998 to 2006. Chloride is usually regarded as a conservative ion and can be a natural tracer to track brine flowing within the reservoir, although some studies indicated that chloride may be involved in some interactions with clay minerals in the rock such as anion exchange (Kleven and Alstad, 1996). Injection water fraction (IWF) was introduced and calculated based on the difference of chloride concentration in formation and injected water (Equation 2.1) in order to provide a better understanding of geochemical data, and then provide knowledge that can be used in validating the flow calculation in the reservoir simulation model.

In the first section, the analyses of produced water compositional data from the Miller Field are presented and a 1D reactive transport model is developed to study possible geochemical reactions taking place within the reservoir through matching model results with observed produced water data.

Barium, as a common scaling ion, attracts focus. **Figure 4.1** shows that there is a progressive decline in barium concentration at low IWF (0% ~50%), then barium concentration can be observed to remain very low in the produced brine from 60% IWF and above. Barite precipitation is the only one reaction in which barium is involved in the model. As a whole, this kind of barium trend is similar to some typical barium behaviours which have been frequently observed in other seawater flooded North Sea sandstone reservoirs (Paulo et al., 2001; Mackay et al., 2006; Houston et al., 2006; Gomes et al., 2012). However, in the Miller field, the depletion in barium at all seawater fractions is significantly lower than observed previously in other fields. One reason for this particular barium trend is the extremely high barium concentration (>600 mg/l) in the formation water. Although barium concentration in the initial formation water in Miller is still low relative to sulphate concentration in the injected water, barium becomes the limiting ion at a higher IWF then in other systems, and thus the relative decrease in barium concentration appears less.

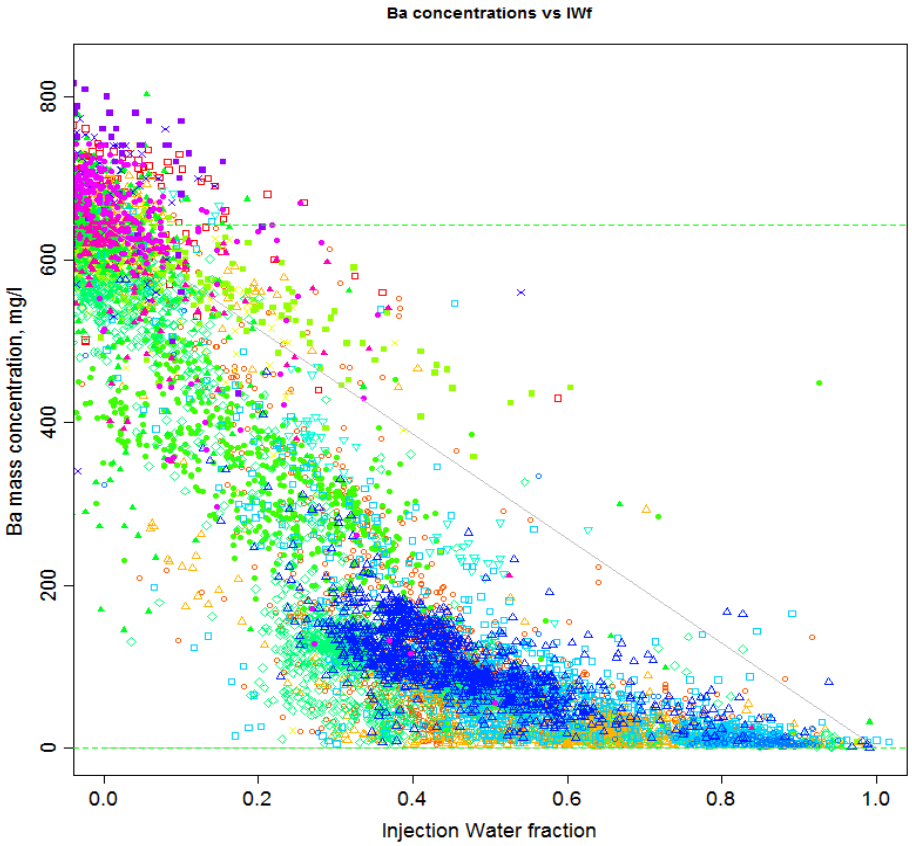

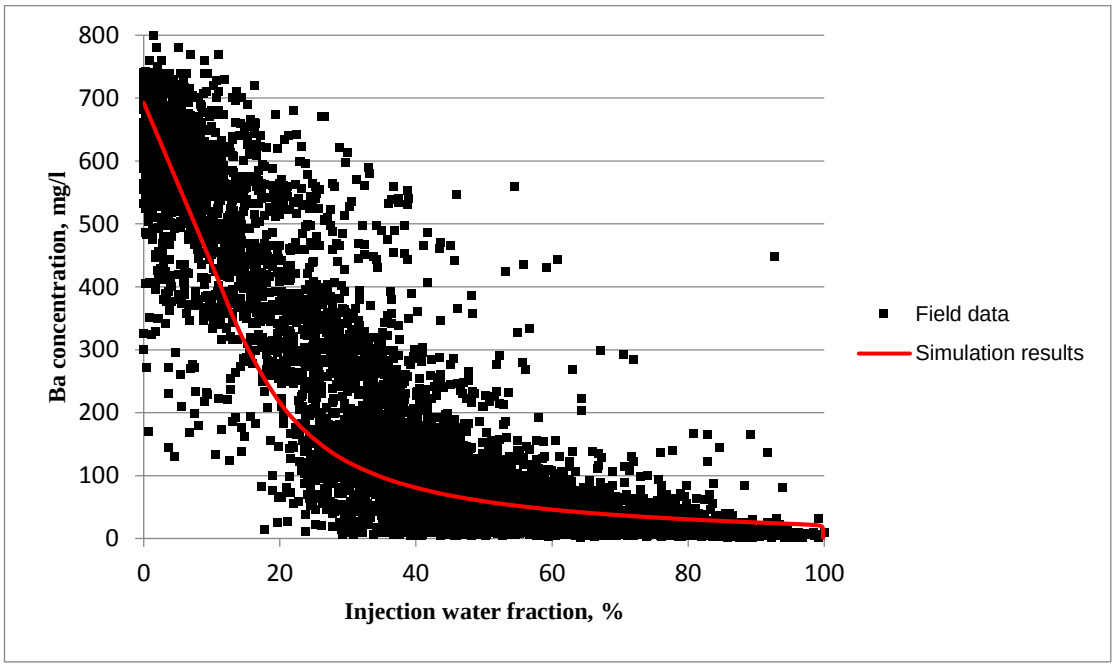

Figure 4.1 Barium concentration vs Injection Water Fraction for different wells. Observed field data are identified for each well by colours (top) and comparison with PHREEQC simulation results (bottom).

For this field, see **Figure 4.2**, there is large range of strontium concentrations in the formation water from 30 mg/l to 80 mg/l, but there is not sufficient evidence that there are two distinct types of formation water in the field and that mixing of them has occurred. Produced strontium concentrations decline almost linearly, relative to the non-reactive mixing line and the trend behaves as a shape of “S” which has been mentioned and observed in the previous chapter. This implies that a small amount of celestite scale precipitation forms at relatively low IWF (<50%) and some of it dissolve again at high IWF (68~80%).

For this field, the produced water contains much less magnesium than expected by pure dilution (see **Figure 4.3**). Magnesium can be involved in some geochemical reactions, such as dissolution and precipitation of dolomite, brucite deposition and ion exchange. All of these three possible involving magnesium reactions were included in the 1D reactive transport model, but the dolomite and brucite mineral precipitation were not observed and the only geochemical reaction for this loss in the system is multicomponent ion exchange.

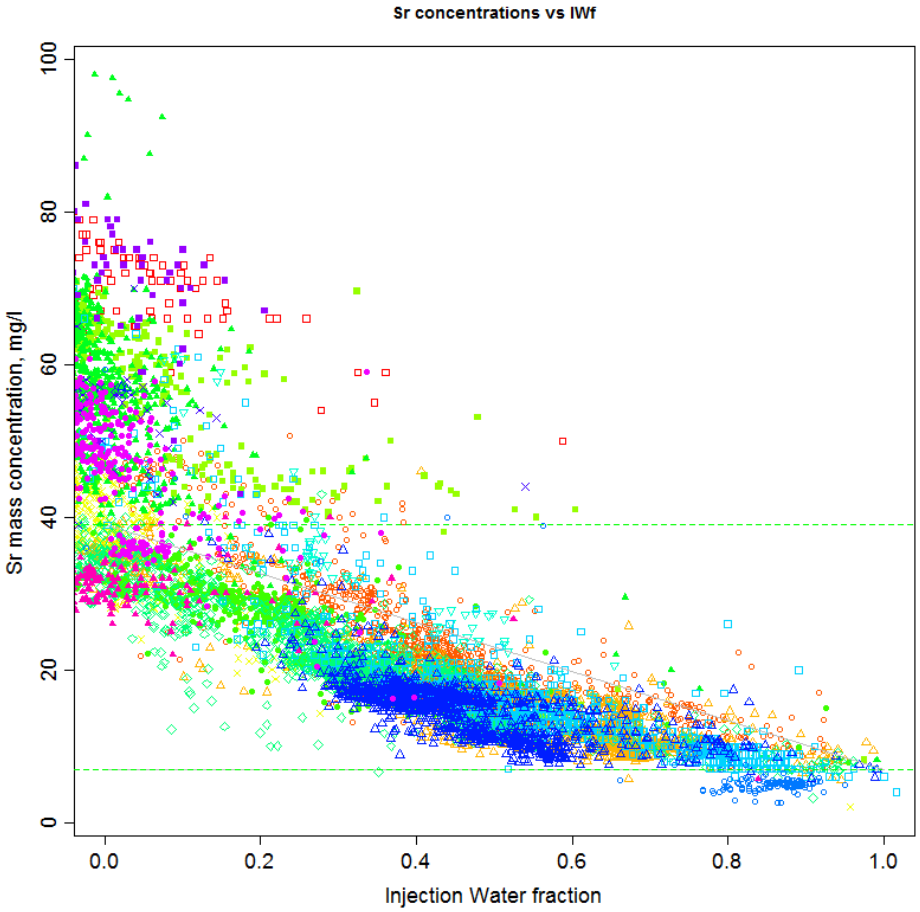

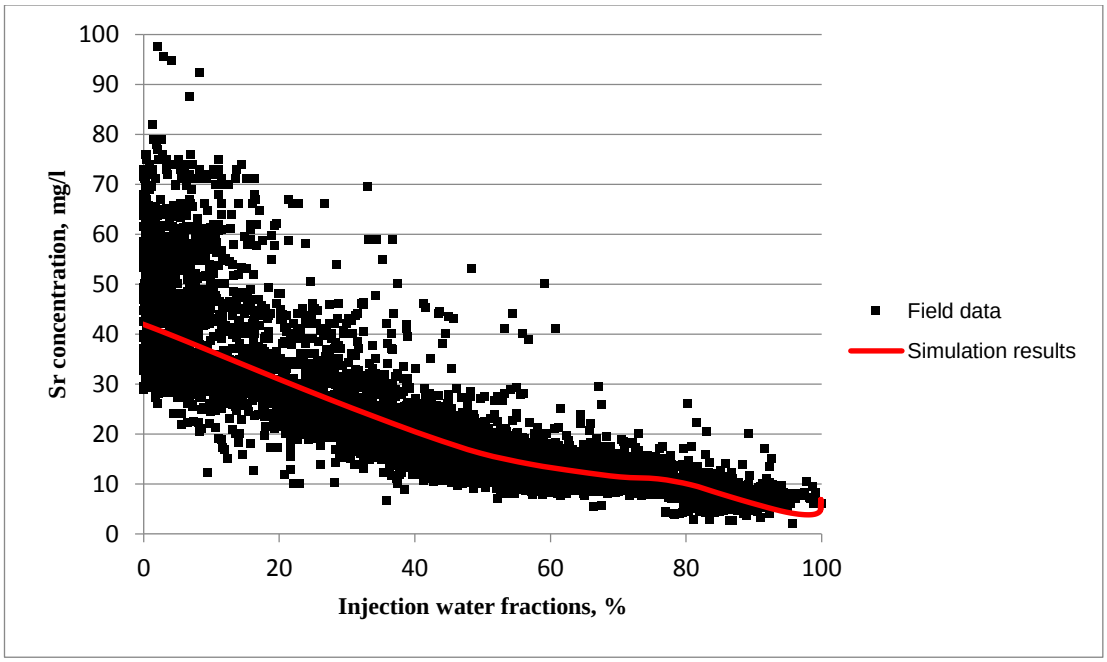

Figure 4.2 Strontium concentration vs Injection Water Fraction for different wells. Observed field data are identified for each well by colours (top) and comparison with PHREEQC simulation results (bottom).

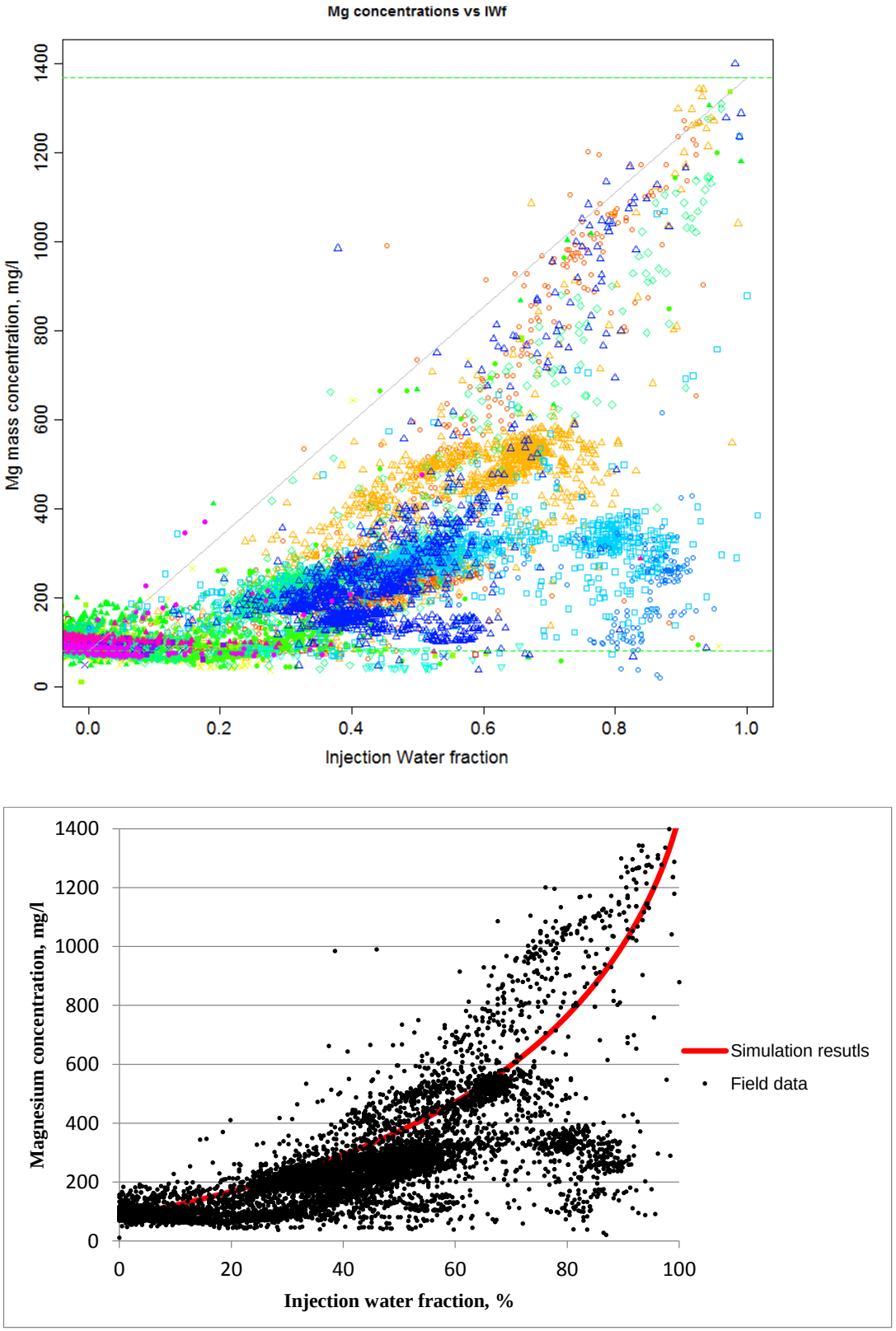

Figure 4.3 Magnesium concentration vs Injection Water Fraction for different wells. Observed field data are identified for each well by colours (top) and comparison with PHREEQC simulation results (bottom).

For **Figure 4.4**, the calcium concentration in formation water varies from 380 mg/l to 630 mg/l across the reservoir. On the whole, the calcium concentration has increased, compared with its simple mixing line, which may be the cumulative effect of multicomponent ion exchange, dolomitization, dissolution and/or precipitation of calcite and anhydrite precipitation. Based on the 1D reactive transport model, multicomponent ion exchange is the primary reason of the increase in calcium concentration. Although some calcium could be released into brine by the dissolution of calcite, there is no evidence to show the substantial presence of calcite in the reservoir mineralogy.

The sulphate trend shown in **Figure 4.5** is determined by the combination of barium, stontium and calcium, because barite, anhydrite and celestite are commonly occurring oilfield scales. $[Ba]_{FW}$ (= 600mg/l) and $[Sr]_{FW}$ (= 80mg/l) lead to a relatively low consumption of $[SO_4]_{IW}$ = (2800mg/l), and at low injection water fraction (<60% IWF) the consumption of sulphate concentration is so low relative to $[SO_4]_{IW}$ that we can hardly identify any deviation from its mixing/dilution line. However, from 60% IWF and above, significant sulphate stripping occurs, which is obviously not caused by just barite and celestite scale formation, since the barium and strontium concentrations are in fact *reducing* at these higher IWFs. 1D reactive transport model results suggest the precipitation of anhydrite at high IWF (>80%).

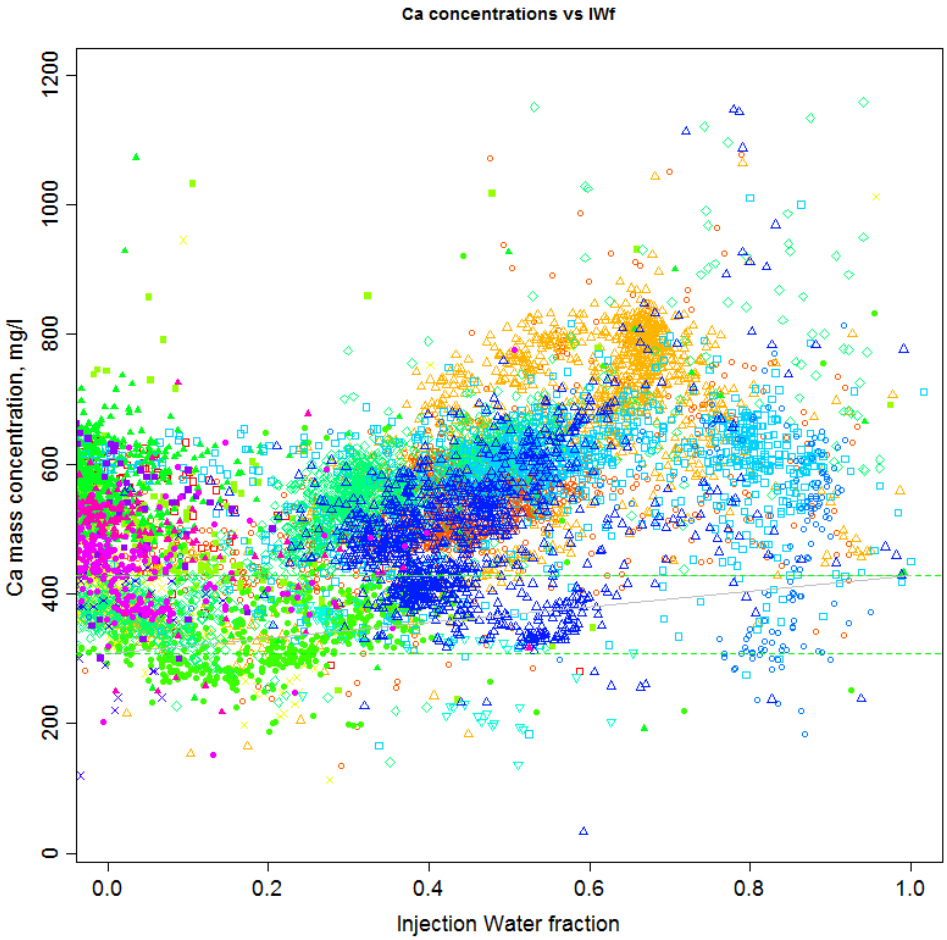

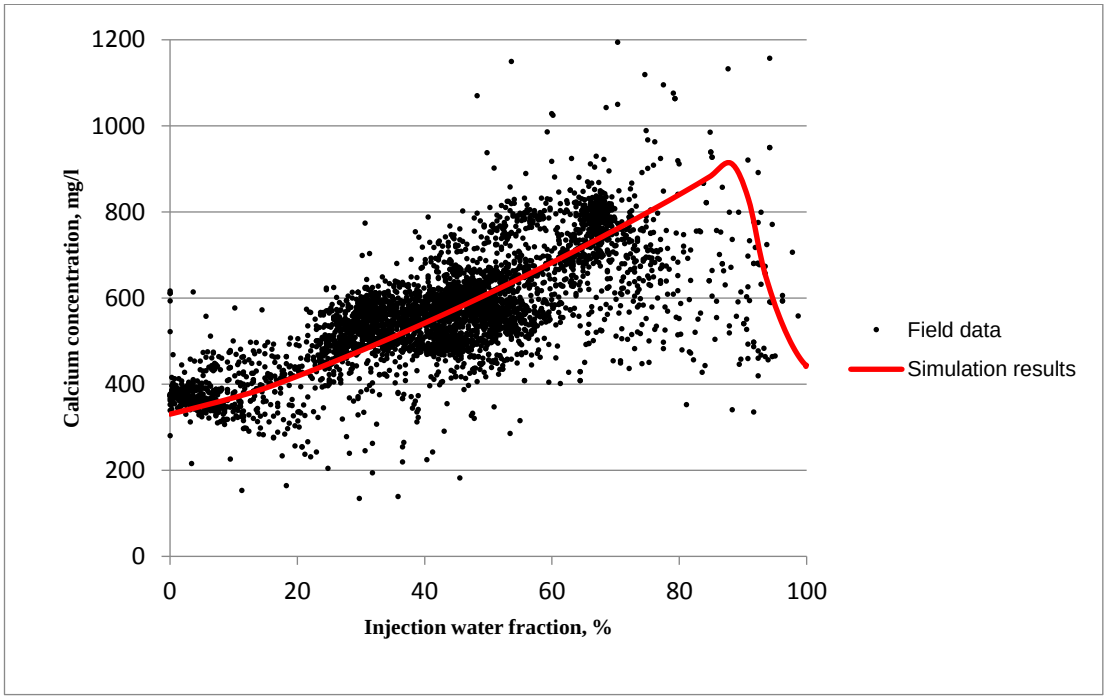

Figure 4.4 Calcium concentration vs Injection Water Fraction for different wells. Observed field data are identified for each well by colours (top) and comparison with PHREEQC simulation results (bottom).

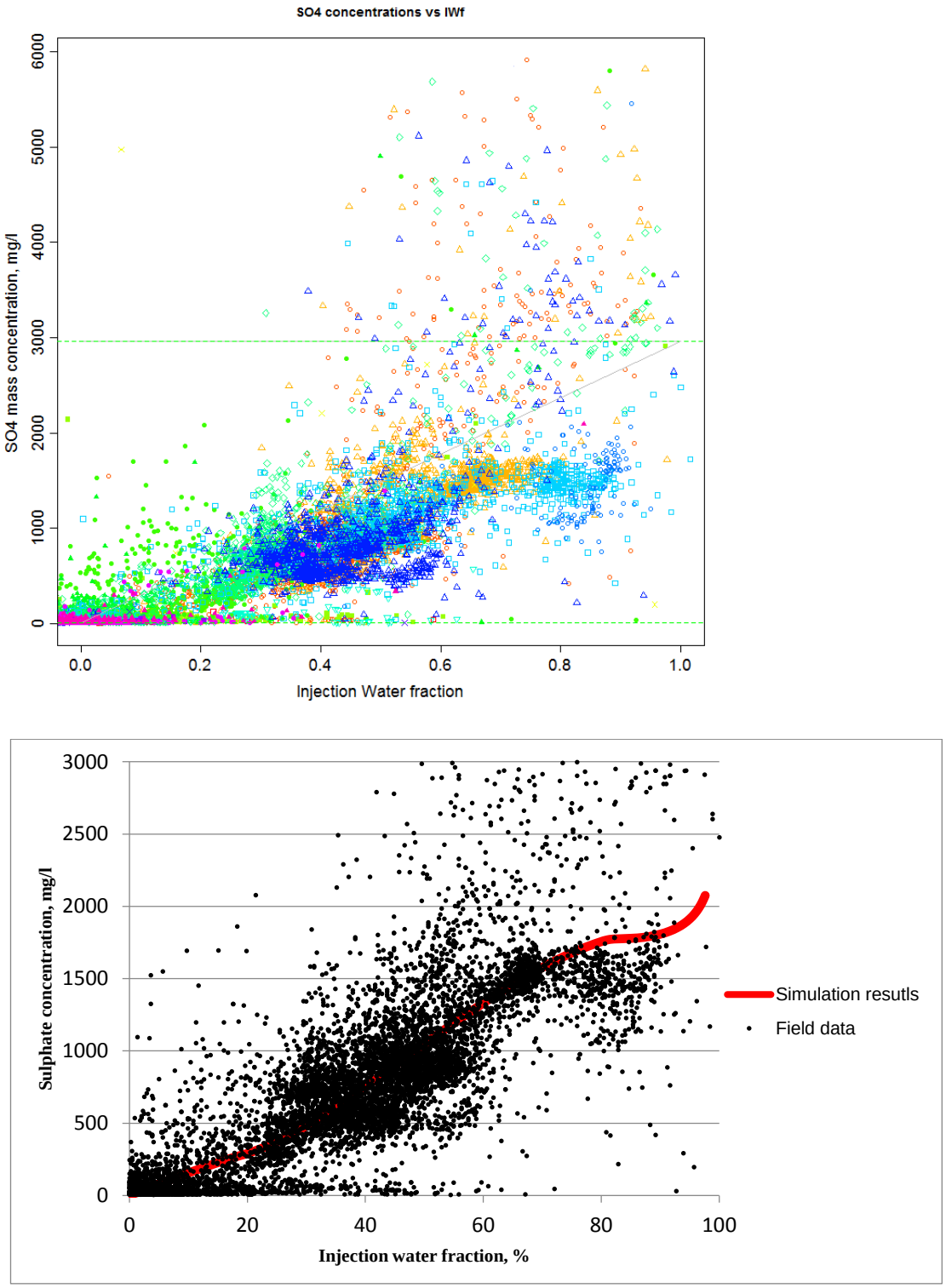

Figure 4.5 Sulphate concentration vs Injection Water Fraction for different wells. Observed field data are identified for each well by colours (top) and comparison with PHREEQC simulation results (bottom).

4.4 Systematic Reservoir Study

A history matched streamline (FrontSim) model of the Miller Field was made available,

in addition to the large geochemical dataset presented above. There is then an opportunity to perform a systematic three dimensional reservoir study for the Miller field to evaluate brine mixing and flow transport in the reservoir, and also investigate barium sulphate precipitated deep within the reservoir and its impacts on the chemical composition (barium and sulphate) of produced water. The advantage of this streamline simulation is that numerical dispersion is general reduced by streamline modelling relative to conventional finite difference modelling. In particular, the input of numerical dispersion on component transport can be controlled in streamline simulation in a way not possible in finite difference simulation.

4.4.1 Reservoir Model

The three-dimensional reservoir model consists of 155,040 grid cells – 76 × 60 × 34 in the x, y and z directions, respectively. In this model there are eight injectors, controlled by surface flow rate targets, and 15 producers, controlled by the observed liquid rate (oil + water), and their locations are shown in **Figure 4.6**. Two producers, A12 and A14, are studied in detail in the case study presented here.

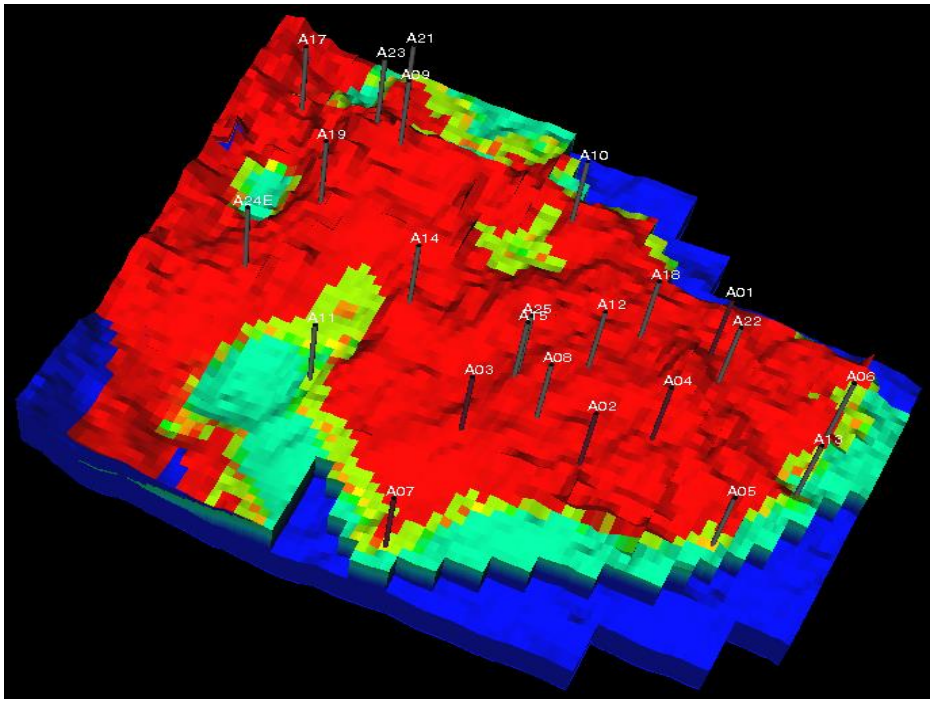

Figure 4.6 Top view of Miller reservoir simulation model. Wells A12 and A14 are of particular interest in this study.

Generally, the matching of modelled total field oil/gas/water production rates and bottom hole pressures to observed values should be achieved in conventional history matching

of reservoir simulation models. The first step in this study was to check that the available FrontSim reservoir model of the Miller field is well history matched. To do this, it was run to verify its accuracy based on the above mentioned targets. In **Figure 4.7**, it can be seen that the simulation results for field oil production rate (FOPR) and field water production rate (FWPR) obviously represent a reasonable match with observed oil and water production rates, respectively.

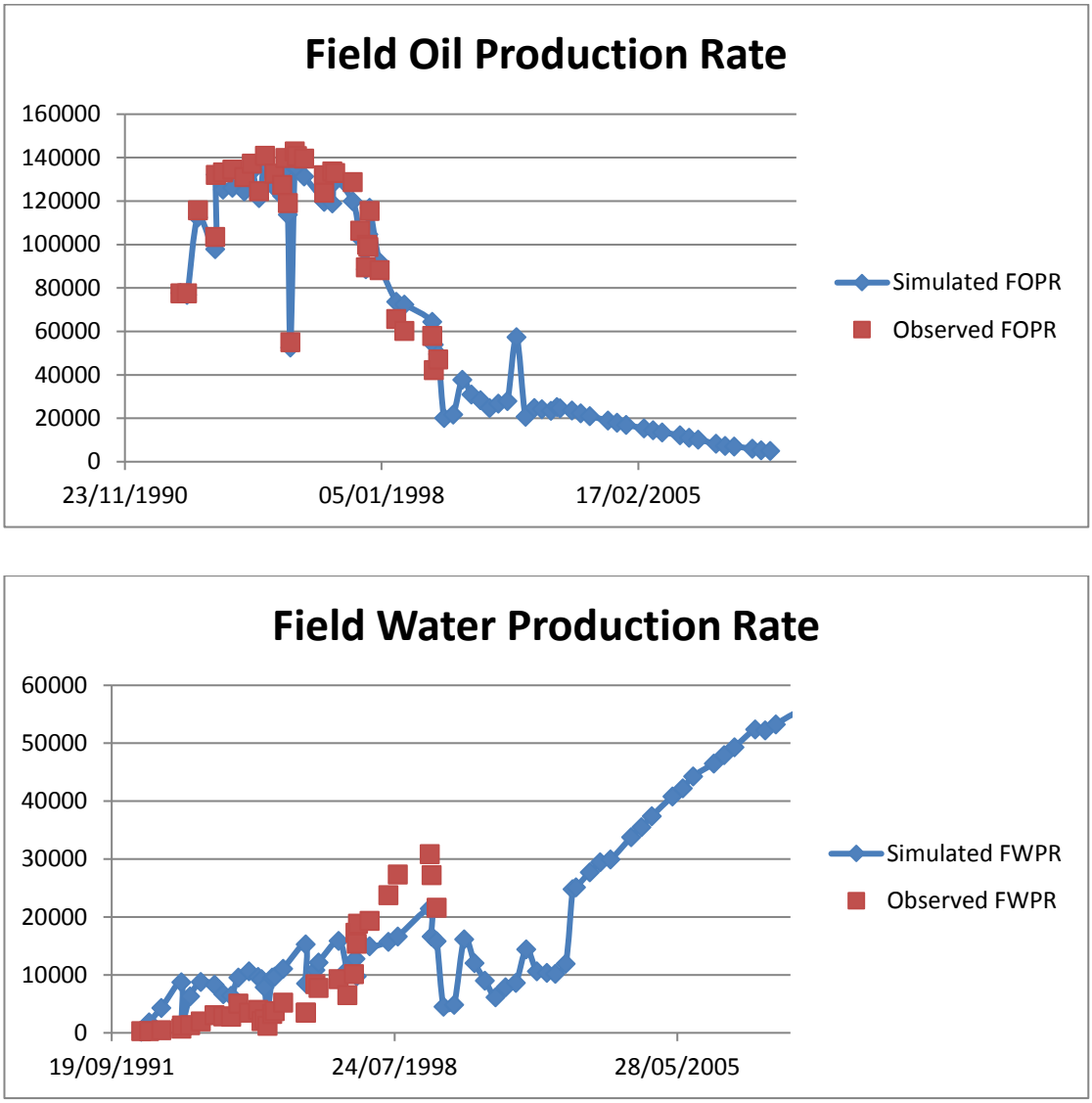

Figure 4.7 Simulated and observed Field oil (FOPR) (top) and water (FWPR) (bottom) production rates vs. Time.

4.4.2 Flow Transport and Brine Mixing In the Reservoir

The injection water fraction (IWF) is defined as the ratio of the flow rate of injection water (usually seawater) production to the flow rate of produced water containing formation water and injection water. Production chemists often consider the IWF as a

critical parameter used to assess the movement of injection water and the propagation of a mixing zone, and therefore the degree of brine mixing, in order to evaluate and predict the scale risk in the production wells.

In this study of the Miller field, a produced water chemistry dataset was made available and the IWF has been obtained through the ion tracking method based on chloride (Equation 2.1). Then we compare IWF calculated based on observed produced water data and that simulated in the history matched model to develop an understanding of how the injected seawater displaces and mixes with initial formation water in the three dimensional reservoir model, and investigate if there is an opportunity to improve the history matched reservoir model.

At first, a natural conservative tracer, named SO, was added to injected water at all injectors in the history matched reservoir model, and the concentration of tracer was set to 0 mg/l and 2780 mg/l in the formation water and injection water, respectively, which is based on assumption that tracer is regarded as sulphate. Although in reality sulphate is not conservative and reacts with barium, strontium and calcium to precipitate as barite, celestite and anhydrite, we would not compare observed and simulated sulphate concentrations, but IWF. Consequently, the concentration of dummy tracers could be given any value and then rescaled, without affecting any of the following analysis.

Secondly, in order for us to track injection water from each specific injector, and to identify where the injection water produced in one specific producer comes from, specific tracers were included in the injection water of each specific injector. For example, water tracer SO1 is present only in the injection water for injection well A1. The concentrations of all tracers in all the injection wells are the same for convenience.

Figure 4.8 presents good matches to water cut (observed water cut only available before 7 years) and IWF between observed and calculated values of these parameters for well A12, despite some deviations of calculated IWF from the observed, which are probably due to samples being taken immediately after squeeze treatments. (The makeup fluid for squeeze treatments in Miller was seawater.) It is shown that a slow increase in the IWF has been observed and this well is producing ca. 50% injection water after 10 years of production, and for the remaining six years of the well's life, which suggests that much of the produced water is coming from the aquifer.

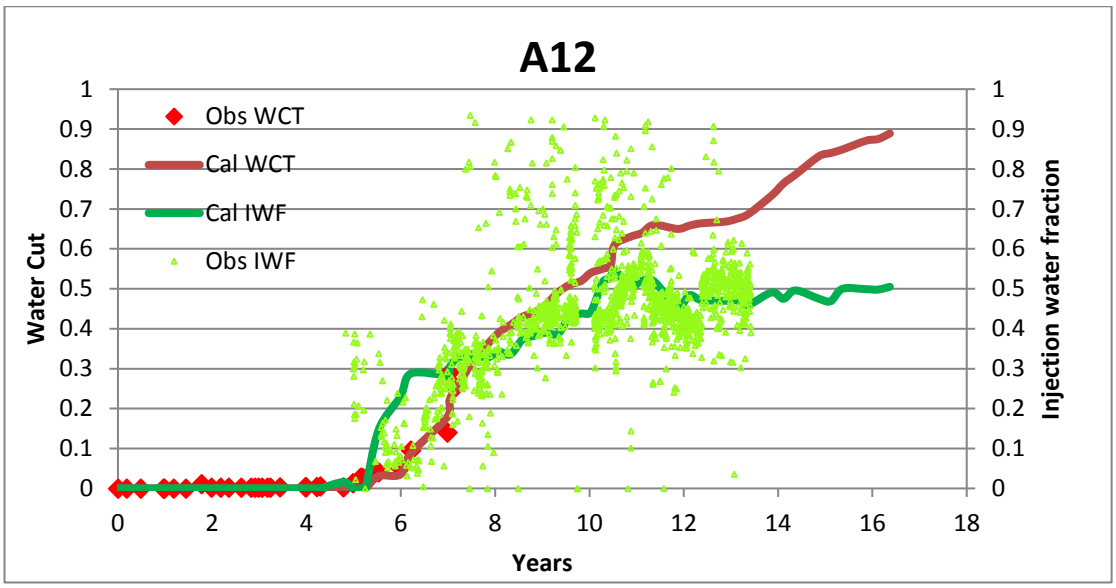

Figure 4.8 Water cut (WCT) and injection water fraction (IWF) vs. time for the modelled results and historically observed data in Well A12.

The sources of injection water produced at well A12 calculated by the history matched reservoir model are reported in **Figure 4.9**; injection water produced at well A12 is initially all coming from well A5, then a combination of A5 (~75%) and A13 (~25%), and then during the period from 8 to 11 years, there is a rapid rise in injection water from well A10, with the other sources decreasing accordingly. Finally, the main source of injection water (~90%) has been well A10.

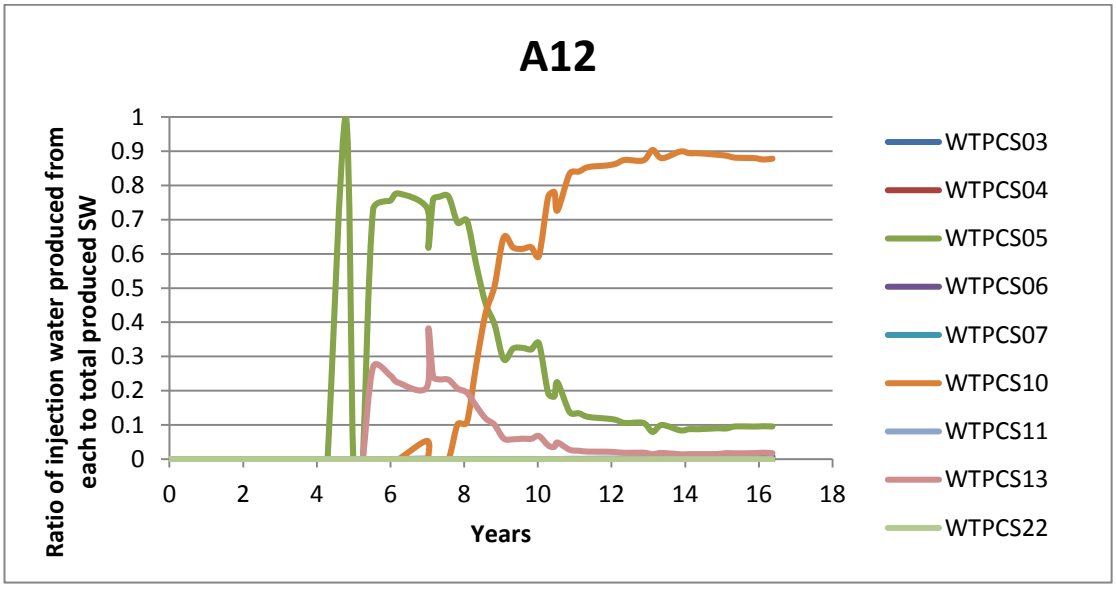

Figure 4.9 Source of injection water produced at Well A12 – initially support comes from well A05, then predominantly from A05 but also from A13, support from these eventually being replaced by breakthrough of injection water from A10.

It can be seen in **Figure 4.10** that the injection water fraction for well A14 is more poorly matched, although there is a reasonable match to water cut after the initial one year delay between observed and predicted water breakthrough. In the reservoir model, the IWF increases only slowly, and just accounts for around 30% of the overall water production rate at the end of the well life, although based on observed produced water chemical data, the IWF increases very sharply after 4 years of production, and finishes in the 60% - 70% range. Based on simulation results of the available history matched reservoir model shown in **Figure 4.11**, it is concluded that the majority of produced injection water at well A14 is from injector A11 alone, suggesting much less mixing of brines than would have been the case for well A12. However, the poor match to IWF implies that some injection water from other injectors (A03, A07 or A24E) might be produced at this well (A12) in reality. The other possibility to cause the lower calculated IWF by the reservoir model is that the water produced at A12 coming from the injection well A10 was underestimated in the streamline model.

A better match of calculated and observed IWF would be expected if the flow paths between the injectors (A03, A07, A10, A11 and A24E) and the producer (A14) are more accurately modelled, and thus, while an attempt has been to made to match the model to water cut, more information on the reservoir could have been obtained if a match to IWF had also been attempted, thus yielding a more accurate and powerful predictive tool.

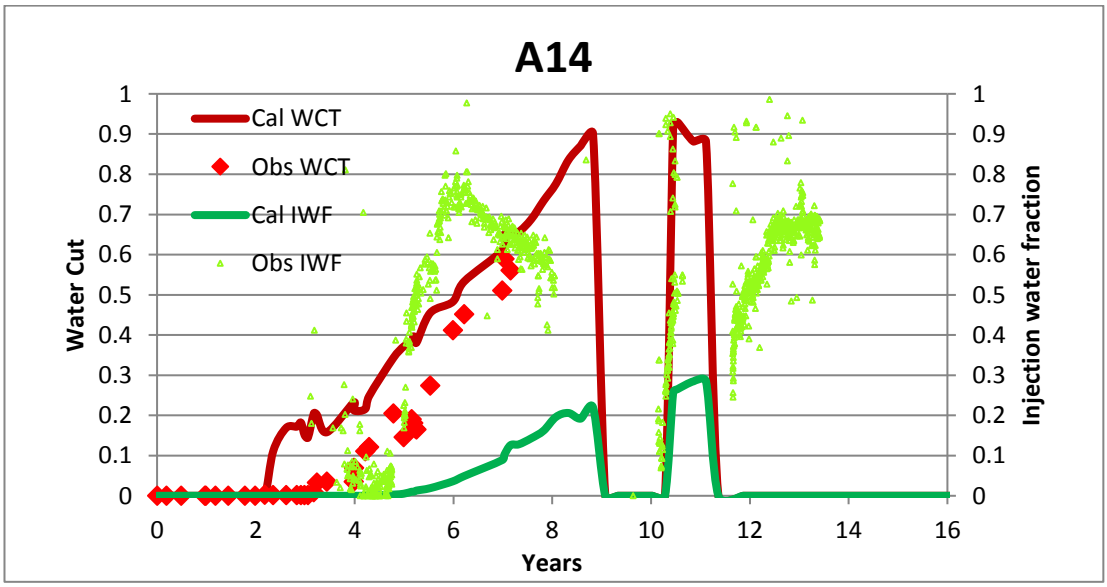

Figure 4.10 Water cut (WCT) and injection water fraction (IWF) vs. time for the modelled results and historically observed data in Well A14

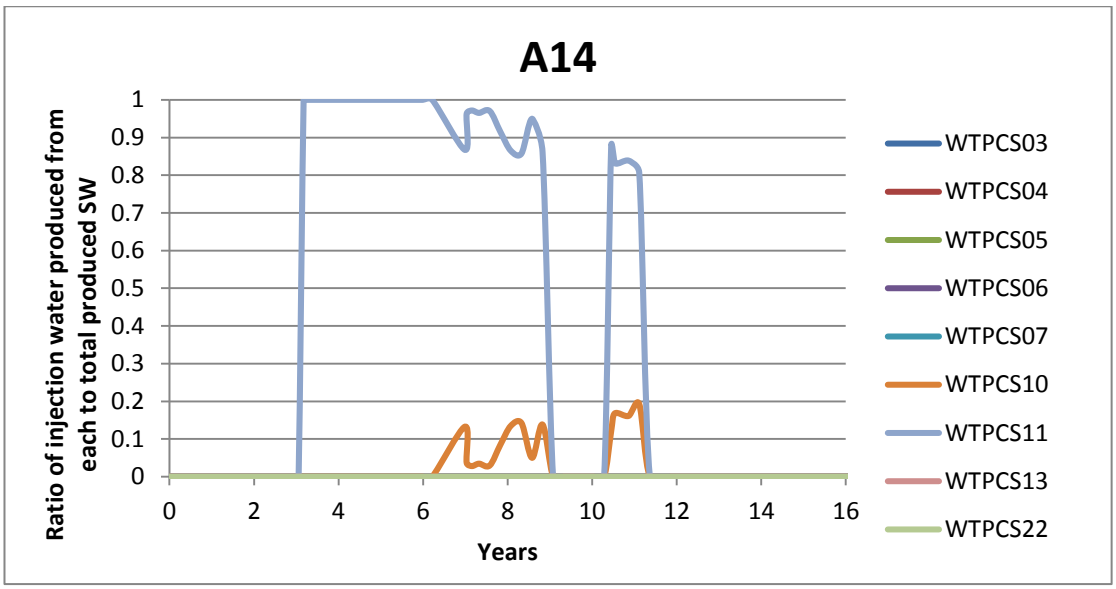

Figure 4.11 Source of injection water produced at Well A14. Most support comes from well A11, with less than 20% from well A10.

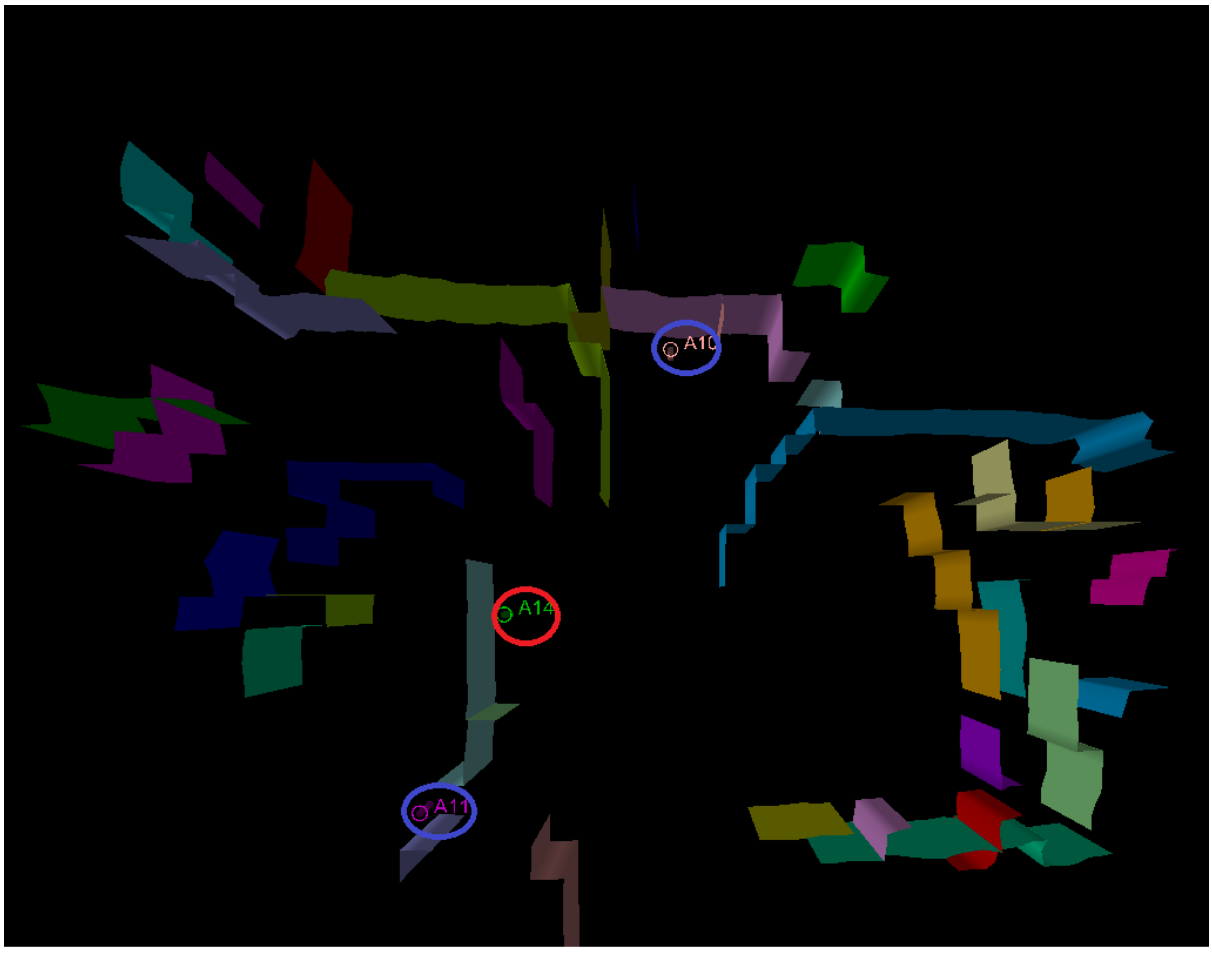

Figure 4.12 Areal view of reservoir showing the locations of faults and wells.

The available reservoir model is a history matched model, so we need to make sure that the adjustment of reservoir properties for matching IWF will not have a significant influence on other history matching targets, such oil and water production rates. Moreover, one of the biggest uncertainties that affect water movement in the path from injector to producer is the presence of faults, and their properties. The transport of injection water is obviously obstructed to some extent by faults located between injectors and producers, so a better match to IWF could probably be obtained through modifying fault properties and/or location (**Figure 4.12**). This can also be regarded as an additional method of improving reservoir simulation by using produced water chemical data.

4.4.3 Modelling of Barite Precipitation Deep Within the Reservoir

Keywords exist in FrontSim that allow it to be used for modelling barite precipitation. The history matched reservoir simulation model of another field had been adapted by Hassane (2013) to model the impact of barite precipitation and deposition deep within the reservoir, and the impact on the produced barium and sulphate concentrations, and similar modifications were made for the Miller field in this study. The model of barium sulphate deposition (Equation 1.27 and 1.28) was simplified based an assumption that either barium (if sulphate is in excess) or sulphate ions (if barium is in excess) would be depleted during precipitation of barite in each grid block by the end of each time step.

4.4.4 Results and Discussion

The simulation was first performed without including the barite precipitation reaction in the reservoir to provide a "no scaling" reference. Both barium and sulphate are regarded as conservative ions and the calculated concentration changes are due purely to dilution by mixing of water with different compositions (formation and injection waters), which was realized in the FrontSim model by adding two passive and non-reactive tracers with barium and sulphate concentrations in formation water and injection water, respectively. The variations in barium and sulphate concentrations in the produced water against time or IWF are shown in the **Figure 4.13 ~ 4.17** as red and green triangles, respectively.

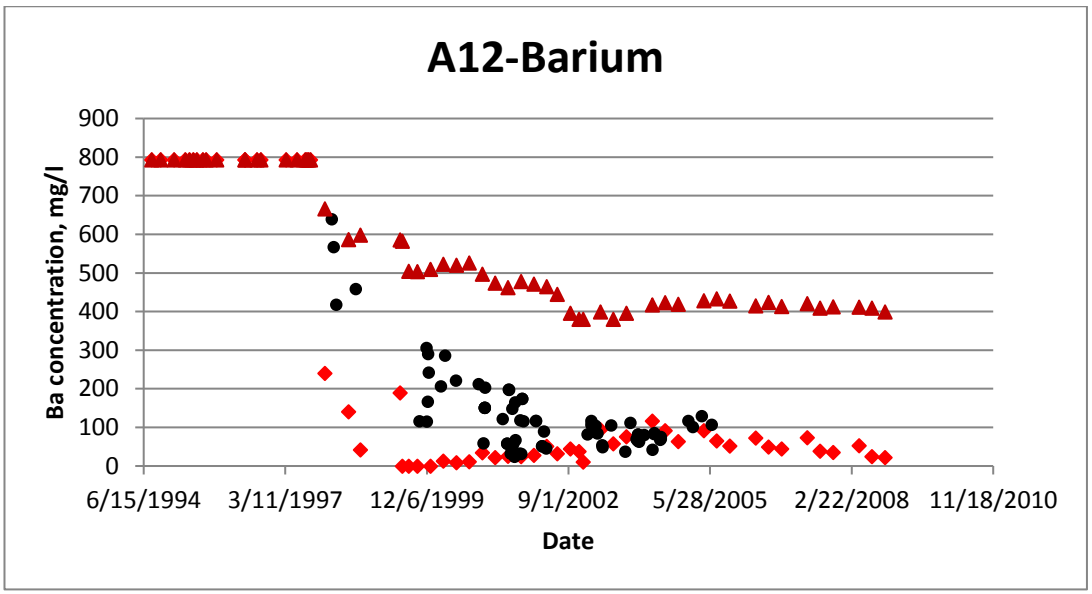

Figure 4.13 Observed barium concentrations (black circles), modelled barium concentrations by pure dilution (red triangles) and modelled barium concentrations with reactions (red diamonds) vs. time for Well A12.

Then the simulation was repeated but barite deposition was allowed to occur deep within the reservoir. The red and green diamonds in the following figures are used to symbolize produced barium and sulphate concentrations, respectively. The observed barium and sulphate concentrations in the produced water samples were plotted in the following four figures, shown using black circles.

For well A12, produced barium and sulphate concentrations against time have been calculated with relatively high confidence since good matches to water cut and IWF have been obtained using the available reservoir simulation model. However, although well A14 is reasonably well matched to water cut, the poor match of observed and simulated IWFs means that plots of ion concentrations vs time (See **Figure 4.15**) are inaccurate. Thus, instead of ion concentrations vs time, ion concentrations as a function of IWF (seawater fraction) have been plotted in **Figure 4.16** and **Figure 4.17** for well A14.

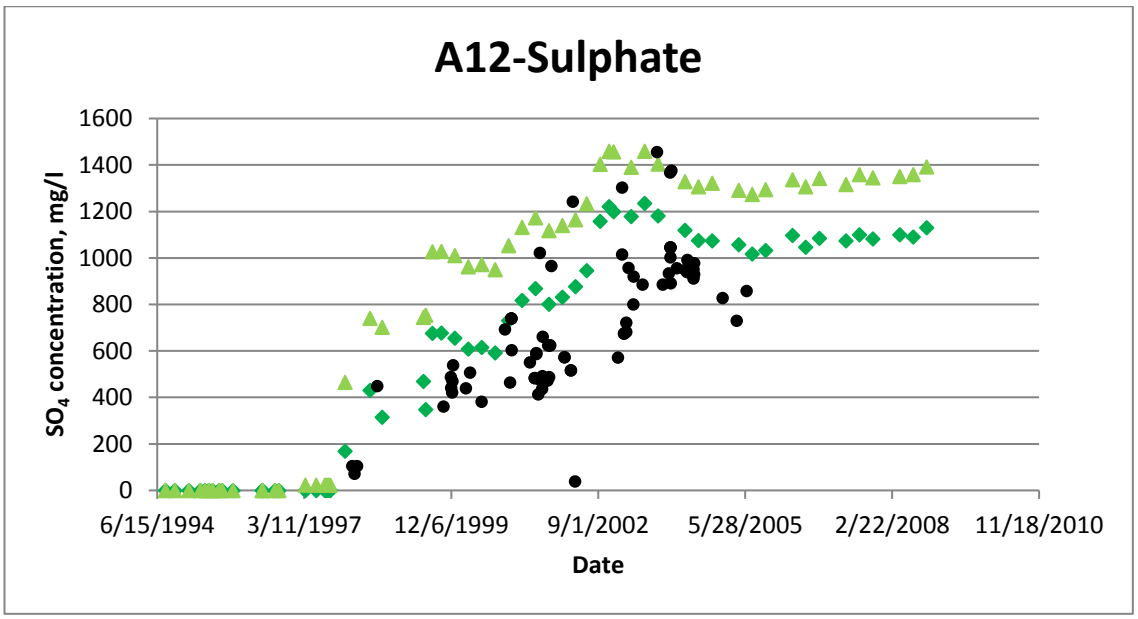

Figure 4.14 Observed sulphate concentrations (black circles), modelled sulphate concentrations by pure dilution (green triangles) and modelled sulphate concentrations with reaction (green diamonds) vs. time for Well A12.

For well A12, barium and sulphate concentrations in the produced water remain at their levels in the formation water as the well was only producing formation water during the initial period from March 1994 to September 1997. Therefore, there is no deviation between simulated ion (barium and sulphate) concentrations with and without barite precipitation. However, significant barium and sulphate depletion due to barite scale precipitation in the reservoir is evident after injected seawater breakthrough takes place in September 1997. This can be seen by comparing results of simulations allowing barite deposition to occur with simulation results with pure dilution only.

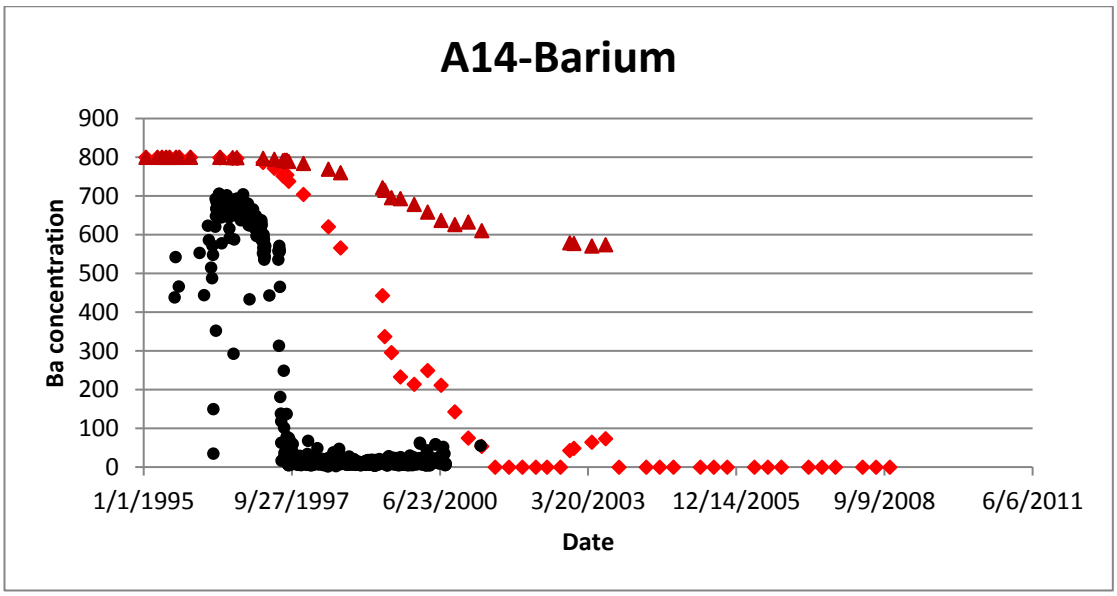

Figure 4.15 Observed barium concentrations (black circles), modelled barium concentrations by pure dilution (red triangles) and modelled barium concentrations with reactions (red diamonds) vs. time for Well A14.

The observed barium and sulphate concentrations in the produced water samples are presented in this study, which allow us to evaluate the difference of observed and simulated barium and sulphate levels. In reality, scale inhibitor squeeze treatments have been implemented with such a high frequency for this well, because of its high scale risks (mainly barite precipitation), that most of the time the well should be protected by scale inhibitor present in the near wellbore formation and in the wellbore, except should the scale inhibitor concentration have dropped to values lower than the MIC (minimum inhibitor concentration) before a repeat treatment was performed. It should be noted that the model assumes barite deposition can take place at all times and at all locations in the reservoir (including in the near well formation), but not in the wellbore itself. Thus the model will tend to over-predict ion stripping if there is mixing in the near production well zone, but, conversely, will predict ion concentrations higher than observed if in reality there were scaling in the well itself.

It is evident in **Figure 4.13** and **Figure 4.16** that at the beginning of injection water breakthrough the observed barium concentration is significantly higher than the calculated one assuming barite deposition. Two possible explanations are proposed for this discrepancy. At first, in our reservoir model barite precipitation was allowed to occur within the entire reservoir, but in reality the near wellbore formation has been protected with scale inhibitor. Therefore, as noted above, the model would overestimate the amount

of barite scale deposition in the reservoir and this probably has resulted in the observed discrepancy. Secondly, the flow rate would be significantly higher when reservoir fluids flow close to the producer compared to when they flow deep within the reservoir, and thus the fluids possibly do not have sufficient time to reach equilibrium, which also results in an overestimate of the removal of barium and sulphate within the reservoir.

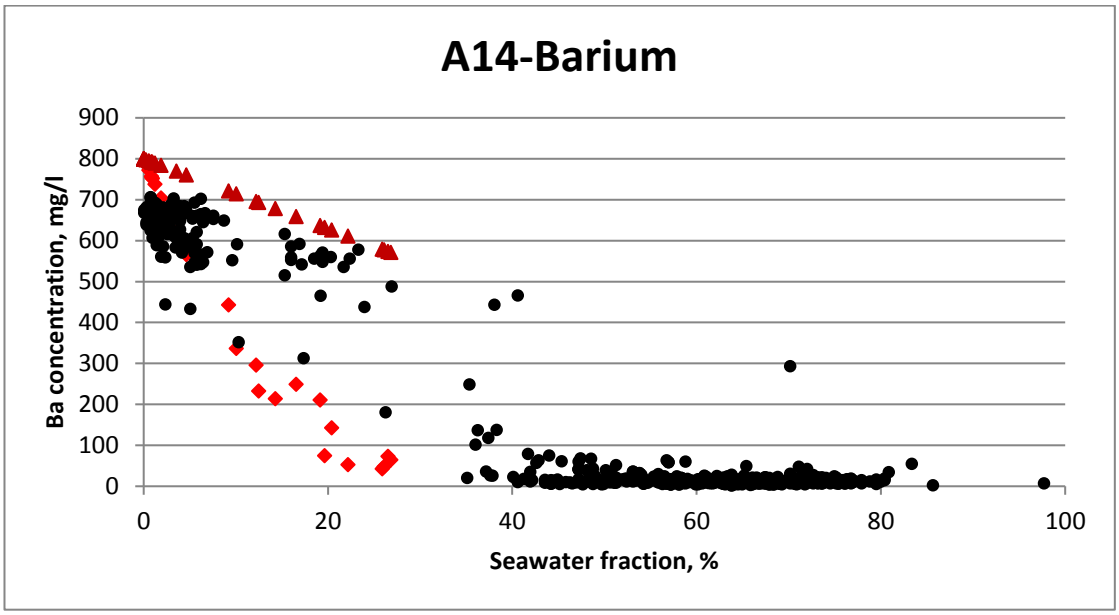

Figure 4.16 Observed barium concentrations (black circles), modelled barium concentrations by pure dilution (red triangles) and modelled barium concentrations with reaction (red diamonds) vs. seawater fraction for Well A14.

However, it can be seen in **Figure 4.14** and **Figure 4.17** that observed sulphate concentrations are located below calculated ones, even when accounting for barite precipitation. This is consistent with the fact that in reality sulphate ions are also consumed by precipitation of celestite and/or anhydrite, but these two deposition reactions were not included in our reservoir model. However, it could simply be that data for A14 are uncertain.

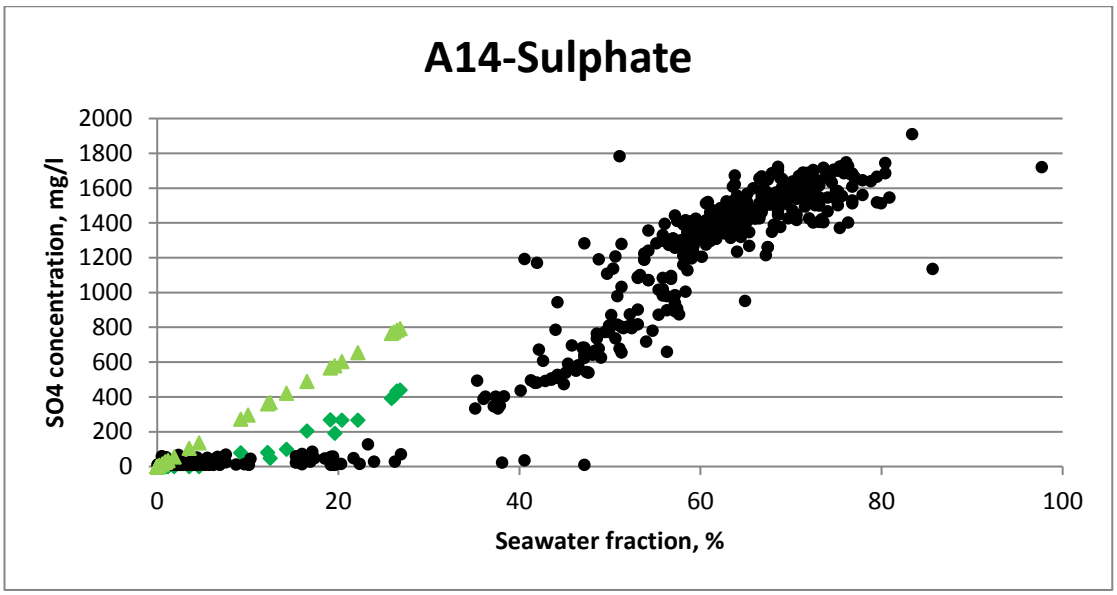

Figure 4.17 Observed sulphate concentrations (black circles), modelled sulphate concentrations by pure dilution (green triangles) and modelled sulphate concentrations with reaction (green diamonds) vs. seawater fraction for Well A14.

The different possible locations of scale precipitation for four kinds of data have been summarized in **Table 4.2**. For the first kind of data, pure mixing and dilution were assumed to provide the base line (although in reality this could not happen with scaling ions if the system were oversaturated). Most of the observed data were measured from produced water samples with scale inhibitor concentration higher than MIC, although some of the time the produced water was not effectively protected by scale inhibitor.

Table 4.2 Summary of various types of data observed and simulated

Location of precipitation / Type of data	Deep within in the reservoir	Near wellbore formation	in the wellbore
No precipitation	NO	NO	NO
Obs data(no squeeze treatment)	YES	YES	YES
Obs data(successful squeeze treatment)	YES	NO	NO
Barite precipitation included	YES	YES	NO

4.5 Impact of Squeeze Treatments on the produced brine chemistry

Based on the information described above and other publications (Bourne et al., 2000; Wylde et al., 2005; Poynton et al., 2004), it is clear that the Miller field has a high potential for very severe barite scale problems and moderate celestite and calcite scaling tendencies, which then necessitates scale inhibitor squeeze treatments to control the scale deposition in the near well bore formation and production tubing.

Observation and evaluation of variations in scaling ion concentrations, such as for barium, is an important way to assess the effectiveness of squeeze treatments. Commonly, the changes in ion concentrations of produced brines result from two major factors, which are pure dilution (mixing of injection and formation water) and some certain chemical reactions (precipitation is generally focused on). The former one is constantly changing as injection water is displaced within the reservoir, and the latter one is impacted by scale inhibitor squeeze treatments. What we concentrate on here are the variations in produced barium concentrations resulting from scale inhibitor squeeze treatments, but not the impact of formation/injection water mixing.

Diluted barium concentrations were calculated based on seawater fraction, then the differences between observed and normalized barium concentration have been obtained to indicate barium stripping, wherever in the reservoir and production system this takes place. In **Figure 4.18** and **Figure 4.19**, we plot observed barium concentrations in produced brine, normalized barium by pure dilution and the difference against time. After seawater breakthrough (July 1998 in this case) there is a steady decrease in produced barium, and various inhibitor squeeze treatments have limited success in increasing barium concentration to the values which would be expected from pure mixing of formation and injected seawater, since some barite precipitation already took place deep within the reservoir where there has not been protection due to squeezed inhibitor, even if squeeze treatments were implemented successfully. However, it can be seen in **Figure 4.18** and **Figure 4.19** that most of the time the decline in barium stripping post-treatment is observed, which implies a positive response to squeeze treatments.

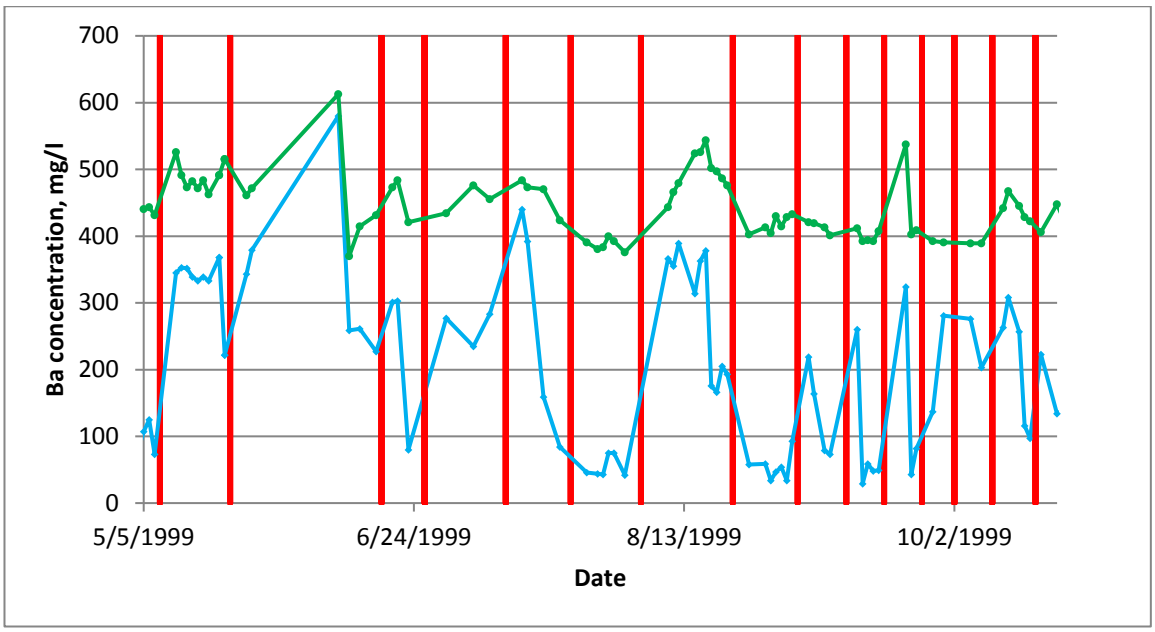

Figure 4.18 Observed barium concentrations (blue line) and barium concentrations calculated based on dilution only (green line) as a function of time (squeeze treatments marked by red lines) for Miller field.

Figure 4.20, which highlights certain treatments (purple arrows), shows that barium concentrations decrease slightly in the first water sample after treatment, but then they would increase considerably. Moreover, it can be seen in **Figure 4.21** that the total barium stripping (indicated by the difference in barium concentration between observed and calculated based on pure dilution) corresponding to these certain treatments (purple arrows) decreases, which implies that treatments were more or less successful. The fact that the increases in barium concentrations are not observed in analysis of some of these produced water samples suggests that they are the flowback from squeeze treatments, mainly consisting of seawater that has been pumped into the producer well and then produced back again, and the brine has not been displaced across the reservoir and had the opportunity to interact with a large volume of matrix rock.

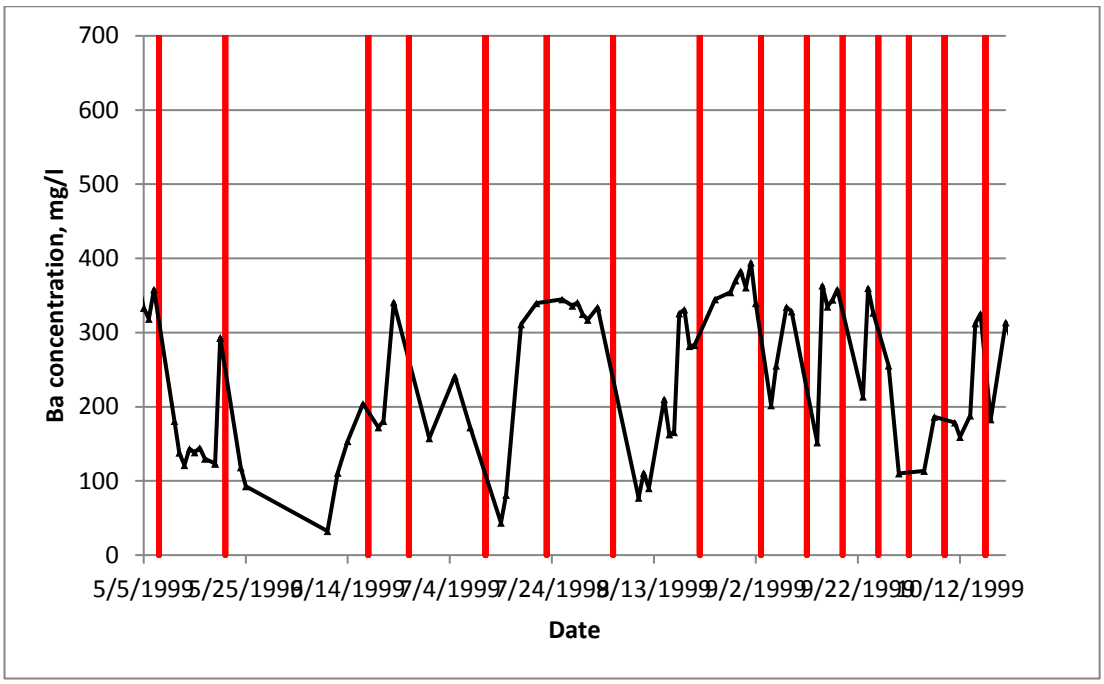

Figure 4.19 Difference in barium concentration between observed and calculated based on dilution, indicating barium striping as a function of time (squeeze treatments marked by red lines) for Miller field.

Figure 4.20 Observed barium concentrations (blue line) and barium concentrations calculated based on dilution only (green line) as a function of time (squeeze treatment marked by red lines) for Miller field.

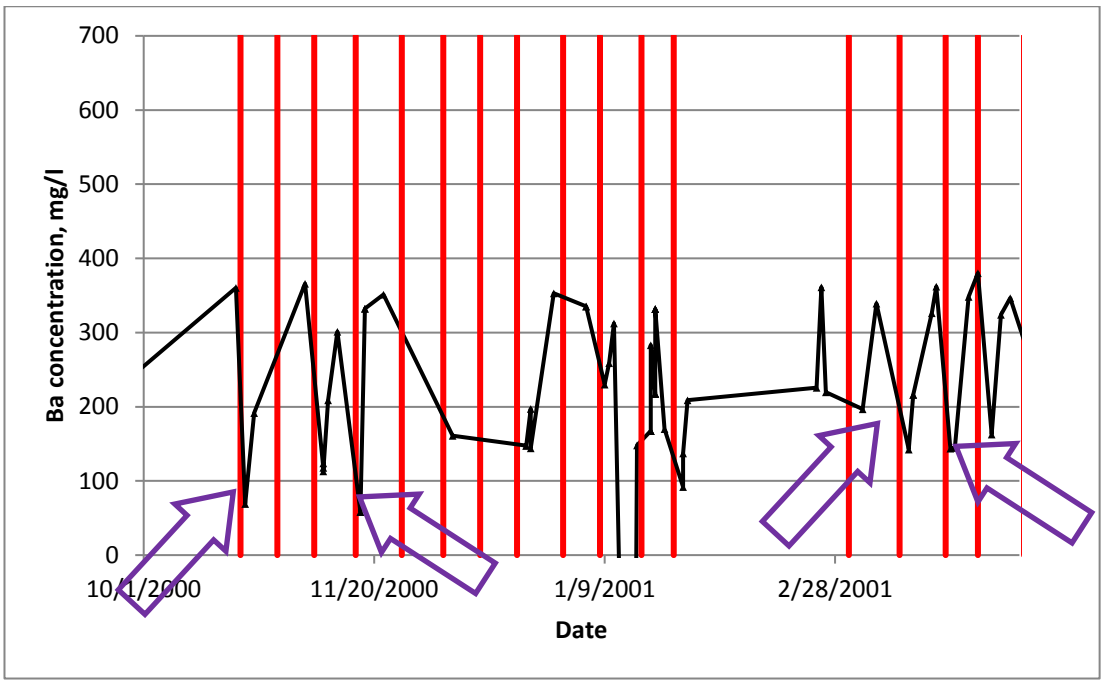

Figure 4.21 Difference in barium concentration between observed and calculated based on dilution, indicating barium striping as a function of time (squeeze treatments marked in red lines) for Miller field.

4.6 Conclusions

The streamline simulation model is applied to identify the brine mixing front, quantitatively evaluate the amount of barite precipitated within the reservoir and predict ions (barium and sulphate) concentrations in the produced water.

In the case study presented here, five ion behaviours from 16 wells were available. Each of them was displayed based on IWF with the help of cross plots, and possible geochemical reactions were then simulated and validated in the one dimensional reactive transport model PHREEQC.

A well history matched reservoir model for the Miller field initially provided a good match with respect to oil and water production rates, and then it was assessed using IWF as a basis for comparison, this being calculated based on observed produced water chemical data and on simulated tracer components. One well (A12) gives a reasonable match, but a poor match have also been obtained for another well (A14).

The source of produced water was further studied through tracking movement of injection water from different injectors. For wells A12 and A14, the detailed profiles of injected seawater breakthrough were described; the movement of the brine mixing front and potential scaling problems were also discussed.

Barium sulphate scale precipitation is modelled and included in the FrontSim model; then the altered chemical composition of produced water can be investigated and predicted. Different kinds of observed and simulated data were summarized and their differences and implication for scale management were further discussed.

CHAPTER 5 MINERAL REACTIONS OCCURRING IN THE GYDA FIELD

5.1 Introduction

The Gyda field is a deep, hot, heterogeneous and intensely faulted oilfield in the North Sea, and Mackay et al. (2006) suggested the occurrence of magnesium/calcium ion exchange in Gyda field based on analysing the produced water data collected from well A20. However, the full produced water chemistry dataset of Gyda field presents some different kinds of ion behaviour trends in different regions. Ion exchange and barite precipitation cannot fully explain the produced ion behaviours. Therefore, it is worth reviewing the produced water dataset in detail and studying what *in situ* geochemical reactions have taken place.

In this chapter, produced brine chemistry data from 16 wells in the Gyda field are plotted and analysed in combination with general geological information and the reservoir description. Three possible classes of formation water compositions in different regions of the Gyda field have been identified by analysis of the produced water dataset. A one dimensional reactive transport model is developed to identify the possible geochemical reactions occurring within the reservoir triggered by seawater injection, then extended with the inclusion of thermal modelling and also to be a two dimensional vertical cross section model. Thermal modelling is included to evaluate the effect of non-isothermal processes and heat transport on the geochemical reactions, especially the anhydrite mineral reaction. I have investigated how the difference in horizontal permeability in the two layers affects brine mixing of formation and injection water and geochemical reactions.

5.2 Reservoir description

The Gyda field is located at the North-Eastern margin of the North Sea Central Trough, on the Norwegian Continental Shelf (Block 2/1) (**Figure 5.1**), 270 km southwest of Stavanger and 43 km northeast of Ekofisk Centre. When the production of oil began in July 1990, it was known to be the deepest, hottest and lowest permeability oilfield in the North Sea at that time (Rothwell et al., 1993). Peak oil production of 20,100 m^3/day was achieved during 1993. BP Norway Ltd operated the Gyda field until Talisman-Energy Norge took over operatorship in 2003. The Gyda field is currently operated by Talisman-Energy Norge (61%) on behalf of DONG (34%) and Norske SEDC A/S (5%).

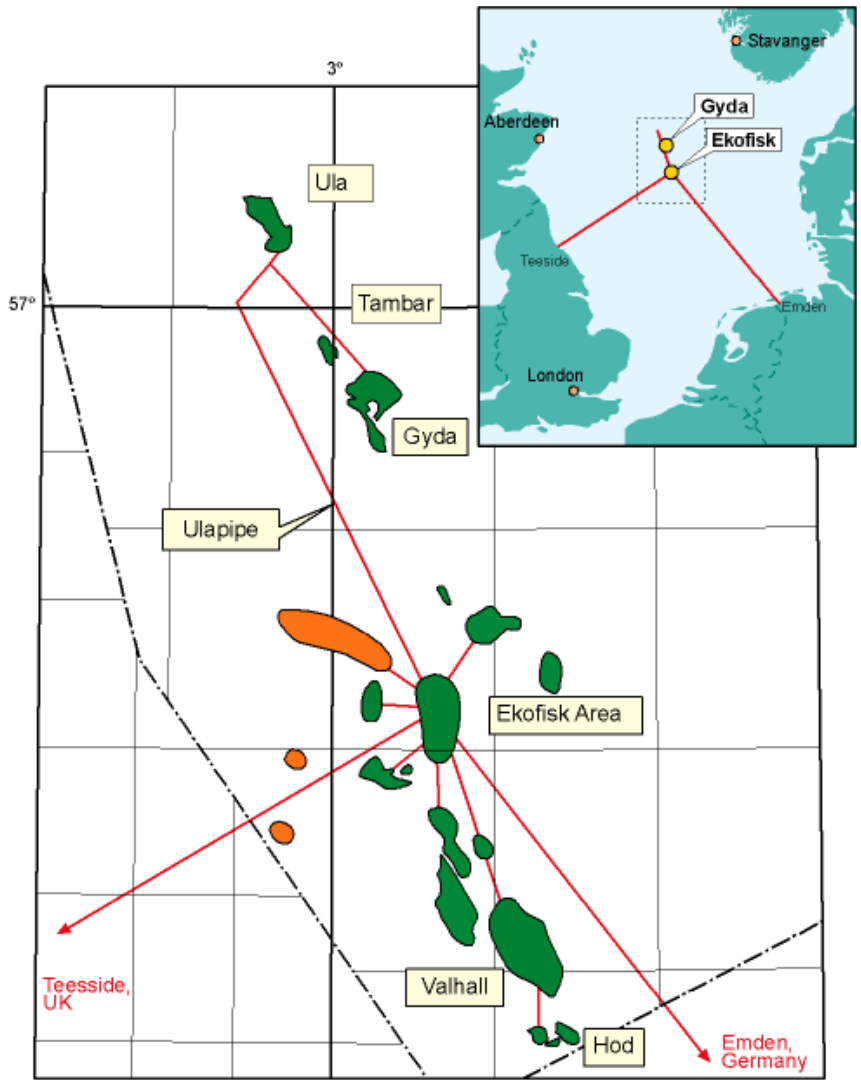

Figure 5.1 Location of the Gyda field.

The reservoir is within Upper Jurassic shallow marine sands at a depth of 3650-4180 m. It is sealed by the overlying Kimmeridge aged Mandal formation, which is also the source rock. The initial temperature was 160°C at 4155 m and initial pressure was 604.5 bar at 4155 m in this field. Average permeability is 30 mD, although the bulk of the reservoir has a permeability of less than 10 mD, but with local high permeability streaks exceeding 1000 mD. It is therefore very heterogeneous - an important consideration for our study.

The Gyda field can be divided into three regions with different structural styles: down-dip (the north-western area), crest (the central area) and Gyda south (the southern area); additionally the C-sand area has a dip-closure in the west of the down dip area. (**Figure 5.2**) The Crest was initially developed in the early 1990s, and high water-cuts have been

observed at most of the wells in the Crest and down-dip areas, higher oil production rates were maintained for longer in the Gyda south area (Rothwell et al., 1993).

The reservoir consists of four depositional units (A to C, **Figure 5.3**). The A-sand is in the bottom with a high permeability zone at the top. The permeability in the top of the A sand is up to 1000 mD while the base can be 1 mD and below. The B-sand is the middle sand, and in general has poor reservoir quality. The best parts of the sand have permeability around 30 mD, while majority is around 1 mD. The C-sand on the top pinches out towards the crest of the field, and varies in reservoir quality. The C-sand is interbedded with calcite stringers, and the western parts have very good quality reservoir rock (up to 800 mD), but the eastern parts have poor reservoir quality, equivalent to the B-sand **(**Stanghelle, 2009**)**.

Three kinds of hydrocarbon, 40°API asphaltene rich black oil (GOR of 1100 scf/stb), an oil with GOR of 2000 scf/stb and a near critical fluid (GOR > 3000 scf/stb), have been proven in the crest and down-dip, southwest and Gyda south area, respectively. The crudes also contain H_2S and CO_2 (Rothwell et al., 1993).

Gyda is produced with water injection as the main displacement mechanism for the main part of the field, and pressure support from the gas cap and the aquifer are drive mechanisms for other parts of the field. Two examples of Gyda formation water compositions have been presented by Mackay et al. (2006) and McCartney et al. (2007). It was also noted that initial reservoir formation water composition varies across the field due to water-rock interactions in the reservoir and the barium concentration in the formation water was observed to range from 266 mg/l to 1150 mg/l (Mackay et al., 2006**)**.

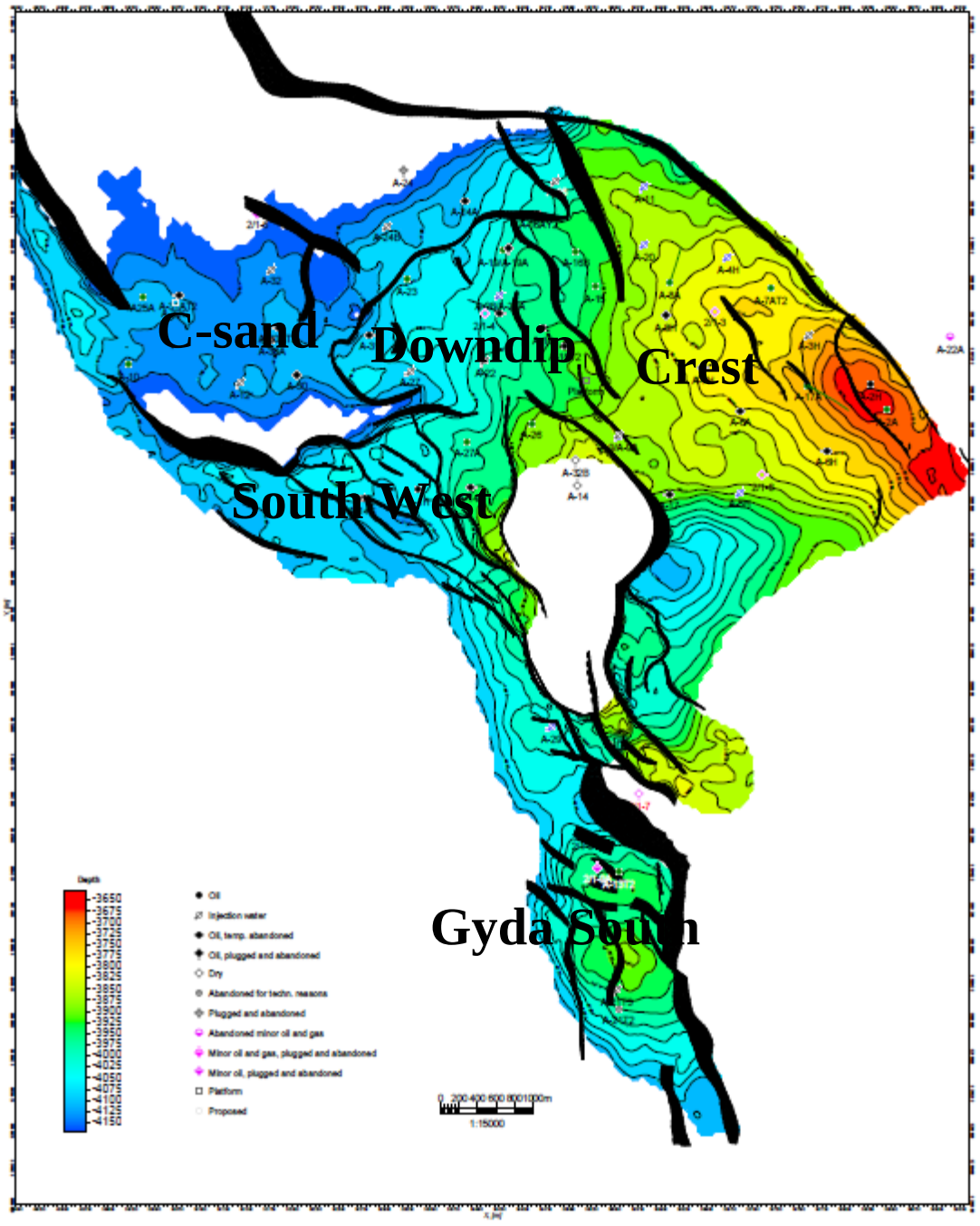

Figure 5.2 Gyda field map showing regions, well locations and faults.

5.3 Produced brine chemistry

A full understanding of the produced brine dataset of Gyda field has not been developed although two produced water datasets at well A-20 in the crest area and well A-13 in the central part of Gyda south were introduced and analysed by Mackay et al. (2006) and McCartney et al. (2007) respectively.

Produced brine samples from 16 production wells have been collected and measured, which contain concentrations of sodium, potassium, calcium, sulphate, magnesium, barium, strontium, iron, chloride, bicarbonate, zinc and pH. Chloride is normally considered to be a reliable natural tracer to track the percentage of formation water and injected seawater that is present in the produced water sample, and there is a big difference in the chloride concentration of formation water and injection water. Therefore, plots of each ion concentration against chloride concentration were made for all of the produced water data from the Gyda field.

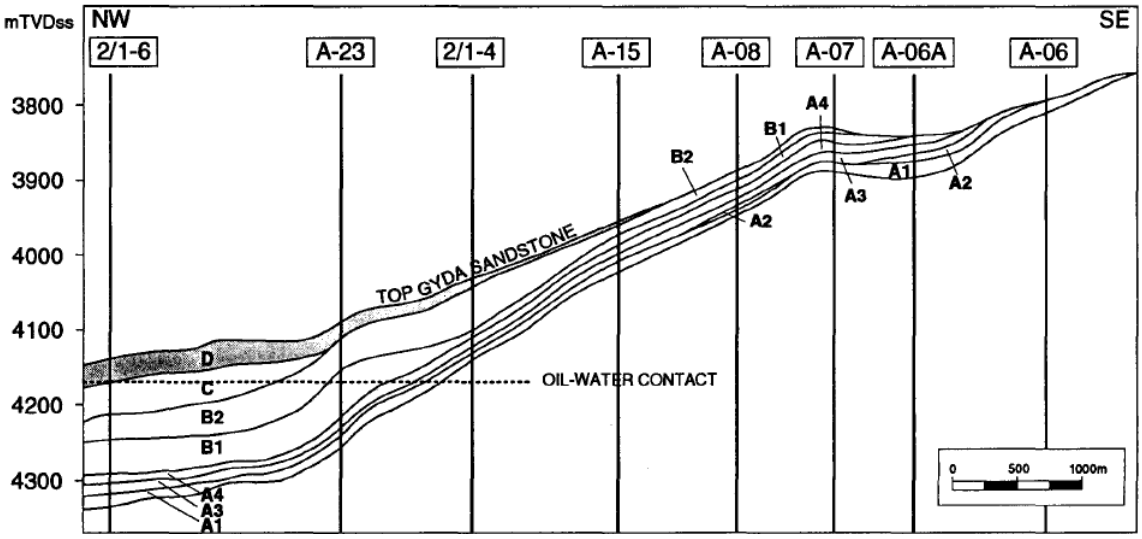

Figure 5.3 Schematic northwest (down-dip) to southeast (crest) cross-section showing continuity of the reservoir zones.

5.3.1 Classification of formation water

As noted above, there are variations in reservoir formation water compositions across the field, so there is an opportunity to make a basic classification and estimation of formation water compositions based on coupling produced water ion behaviours of the full field with general information on geological information, hydrocarbon types and well locations.

In **Figure 5.4-5.6**, sodium, calcium, sulphate show consistent behaviour in all wells in Gyda, but there are some obviously different types of trends for magnesium, barium and stontium that can be observed in **Figure 5.7-5.10**. First of all, well A13 presents an unusual produced water compositional trend, with high initial barium and strontium concentrations and relatively low magnesium concentration, which is consistent with the fact that A13 is the only one well drilled in the area of Gyda south and its formation water composition could be distinct from the other wells. Secondly, similar ion behaviours are

observed in most of the produced water samples collected at wells located in the down dip and crestal areas, such as wells A4, A20, A15 etc. This is considered as the main field, and these wells have the lowest barium and strontium, and the highest magnesium concentrations. Finally, there are some uncertainties in the formation water compositions of well A1 (red circle), A30 (blue triangle) and A32 (purple cross). Geologically, the properties of faults play a key role in blocking fluid flow between the C sand and the south west area, and this can lead to the variation in formation water compositions. From **Figure 5.8 and 5.9**, although the zones are believed to have similar compositions from the produced barium and stontium ion behaviours, in fact three magnesium concentrations in the formation water can be identified from these two regions in **Figure 5.7**.

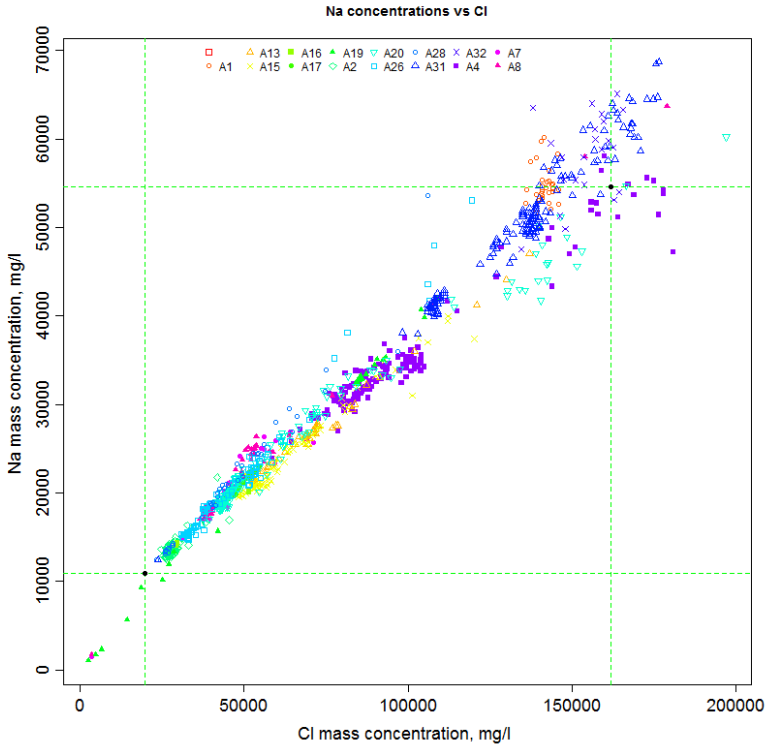

Figure 5.4 Sodium concentration vs chloride concentration (wells in colours).

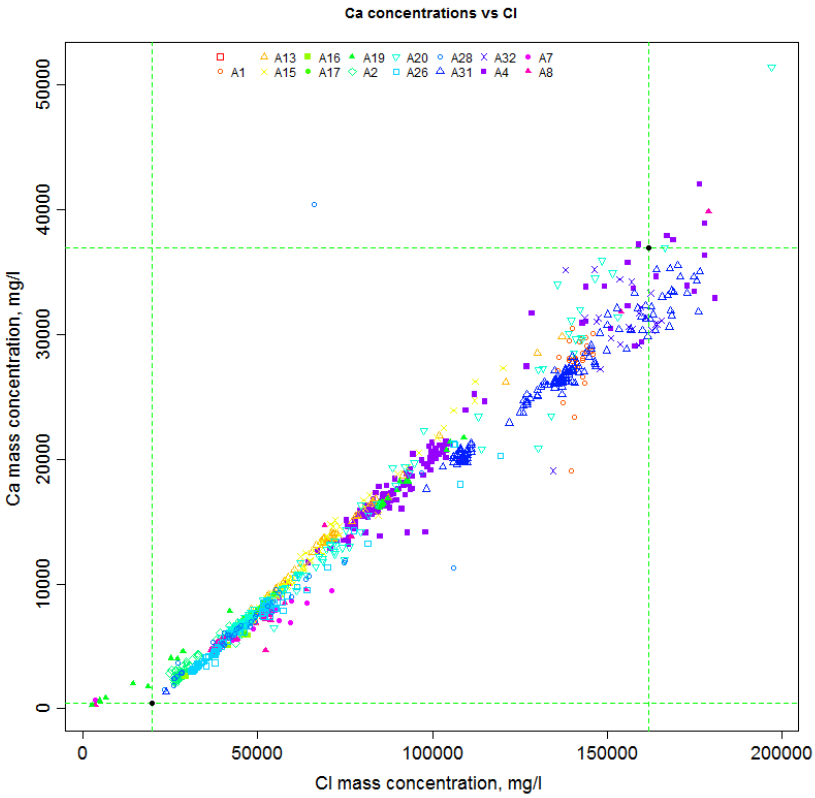

Figure 5.5 Calcium concentration vs chloride concentration (wells in colours).

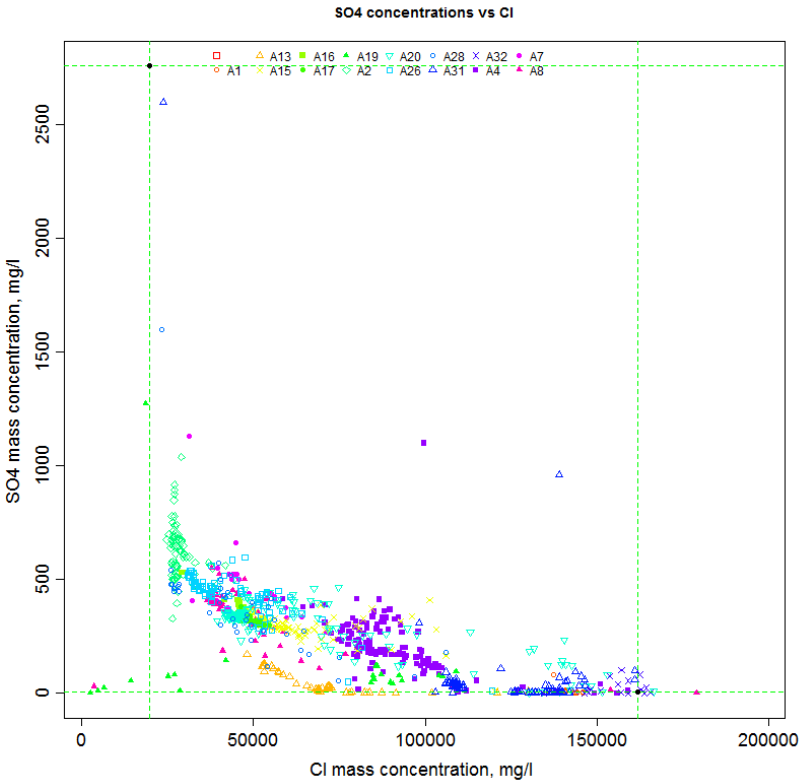

Figure 5.6 Sulphate concentration vs chloride concentration (wells in colours).

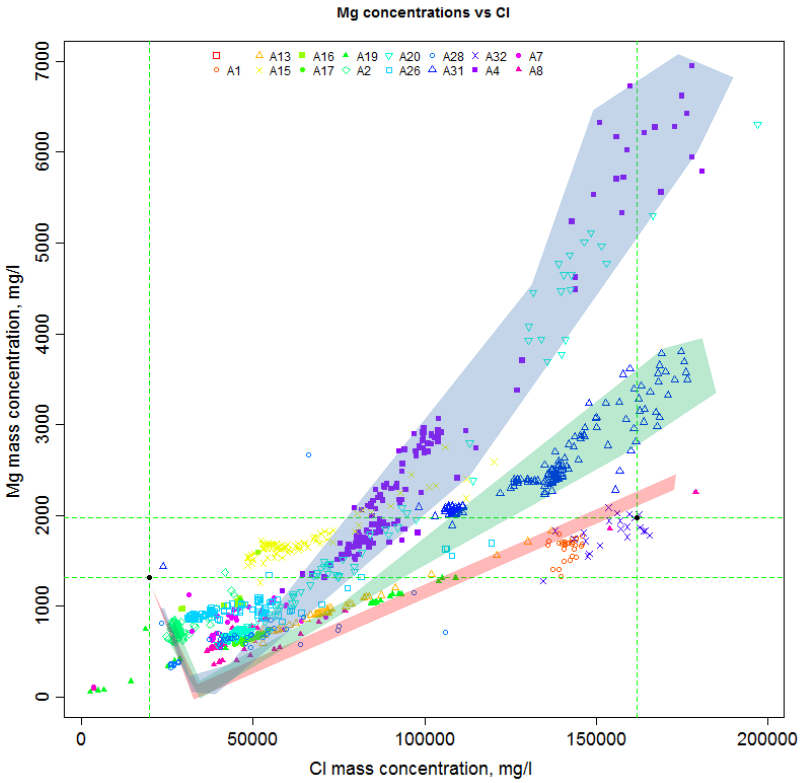

Figure 5.7 Magnesium concentration vs chloride concentration (wells in colours).

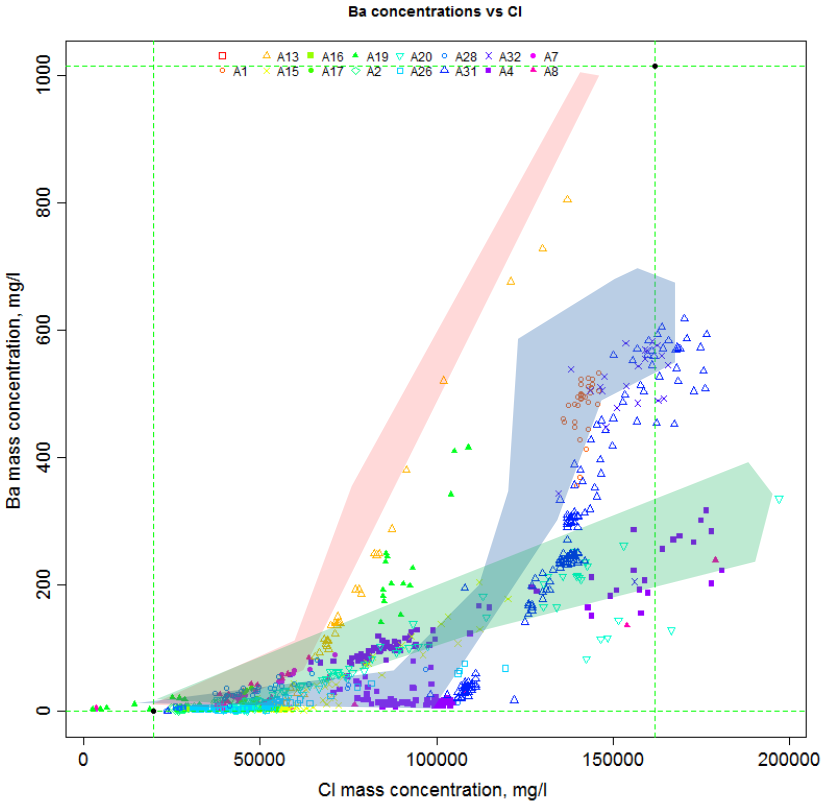

Figure 5.8 Barium concentration vs chloride concentration (wells in colours).

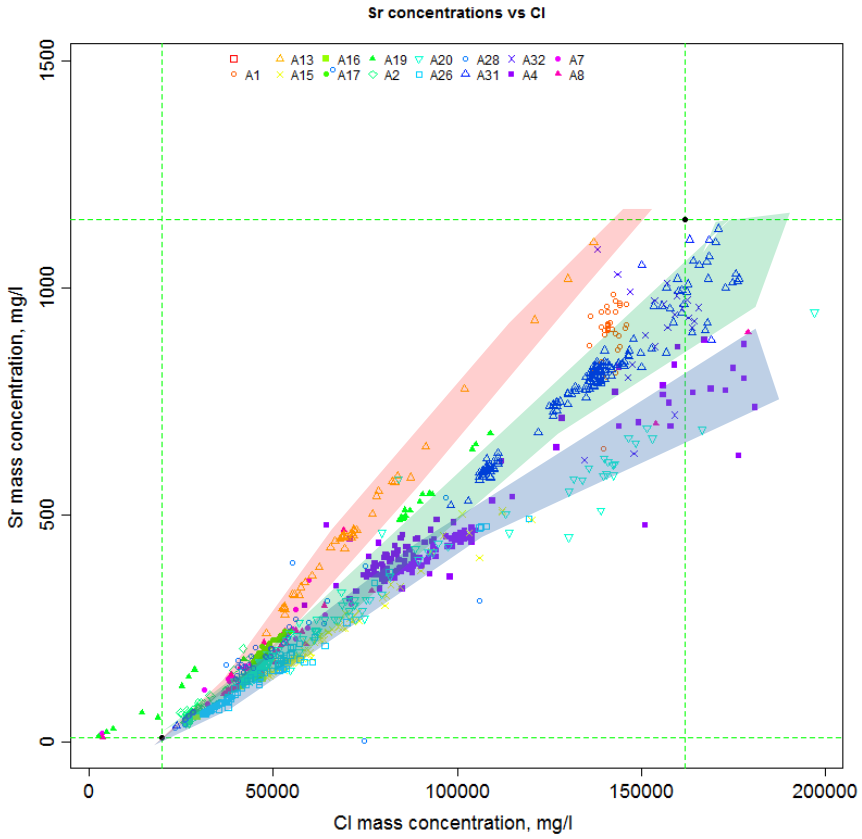

Figure 5.9 Strontium concentration vs chloride concentration (well in colours).

An estimate was made of the three possible classes of formation water compositions in different regions of the Gyda field on the basis of two examples of formation water compositions presented by Mackay et al. (2006) and McCartney et al. (2007). The updated formation water compositions are illustrated in **Table 5.1**, in which barium, stontium and magnesium concentrations vary across the field, although the concentrations of other ions are more or less similar. In **Table 5.1**, FW1, FW2 and FW3 are corresponding to formation water present in the region 1, 2 and 3 respectively.

Table 5.1 Formation water and injected seawater compositions.

	FW1	FW2	FW3	Seawater	FW1	FW2	FW3	Seawater
	mg/l	mg/l	mg/l	mg/l	mmol/l	mmol/l	mmol/l	mmol/l
Na	65340	54560	65340	11470	2.842134	2.37323	2.842134	0.498917584
K	5640	6000	5640	460	0.144252	0.153459	0.144252	0.011765217
Ca	36900	36900	36900	428	0.920705	0.920705	0.920705	0.010679176
Mg	7000	1970	3700	1368	0.288007	0.081053	0.152232	0.056284715
Ba	350	1015	610	0.1	0.002549	0.007391	0.004442	7.28189E-07
Sr	880	1290	1085	8.2	0.010043	0.014723	0.012383	9.35859E-05
Cl	181000	162000	176100	19700	5.105351	4.56943	4.96714	0.555665247
SO_4	0	0	0	2960	0	0	0	0.030814075
HCO_3	79	79	79	124	0.001295	0.001295	0.001295	0.002032227
pH	5.46	4.75	5.46	8				

Table 5.2 Identification of formation water types.

Region 1(Downdip + Crest)	Region 2(Gyda South)	Region 3(C sand + South west)
Well A-2	Well A-13	Well A-1
Well A-4		Well A-30
Well A-6		Well A-32
Well A-7		
Well A-8		
Well A-15		
Well A-16		
Well A-17		
Well A-18		
Well A-19		
Well A-20		
Well A-22		
Well A-23		
Well A-26		
Well A-28		
Well A-29		
Well A-31		

5.3.2 Ion behaviours in produced brine

As is normally observed, sodium concentrations lie on the pure dilution mixing line of formation water and injected seawater, although sodium may be involved in multicomponent ion exchange. Stontium, as a potential scaling ion, also showing a linear relationship with chloride, and the stontium concentrations are located on the mixing line, indicating low mineral reactivity involving stontium in the reservoir. In addition, Ca is also close to its pure dilution line, but this is probably because the initial calcium concentration is so extremely high that the relative effects of any reactions are difficult to

identify. Apart from these three ions, Mg, Ba and SO_4 are all depleted relative to their pure mixing lines during seawater injection.

5.4 Scaling tendency from thermodynamic modelling

In the thermodynamic simulation undertaken using MultiScale (Kaasa, 1998), North Sea seawater was mixed with three types of formation water, respectively, from different regions of the Gyda field. In these calculations the mixing of formation water and seawater was assumed to take place instantaneously and the impact of transport and mixing from injector to producer was not considered in these MultiScale calculations.

Figure 5.10-5.12 show the saturation ratio and maximum predicted mass of scale as a function of IWF. The main scaling risks resulting from the mixing of formation and injection water are barite and anhydrite precipitation. celestite would not be precipitated even if a saturation ratio greater than one was calculated in the absence of calcium and barium, due to sulphate being the limiting ion in the presence of calcium and barium. The scaling tendencies for the seawater mixes with the three kinds of formation brines are quite similar for anhydrite but differ for barite since the barium concentration in the formation waters varies across the field. High barium concentration leads to high scaling tendency for barite deposition.

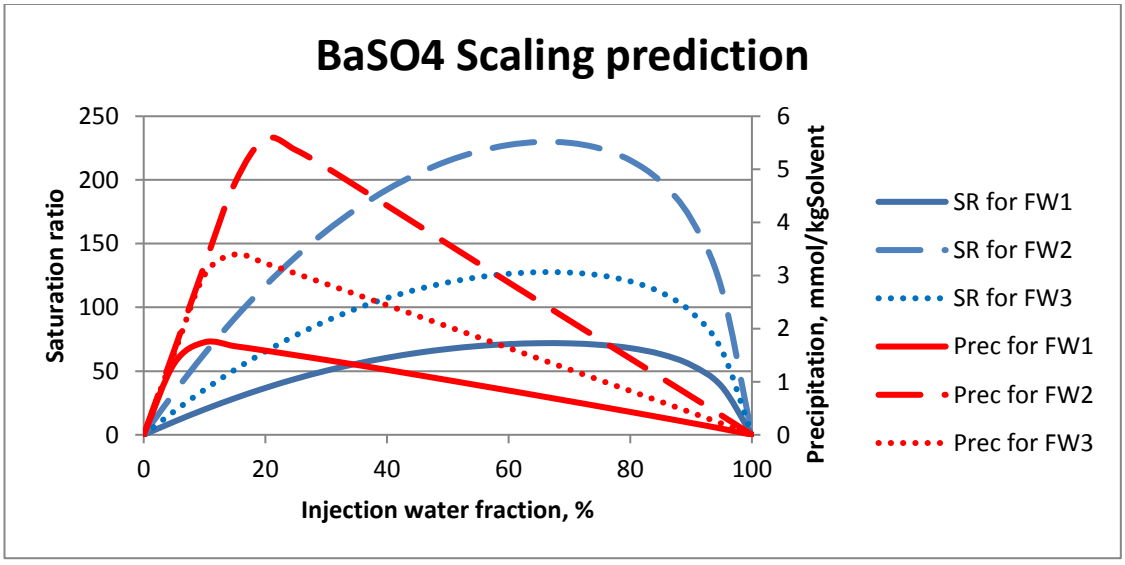

Figure 5.10 Saturation ratio and maximum predicted mass of barium sulphate for different regions (FW1 for Region1, FW2 for Region 2 and FW3 for Region 3).

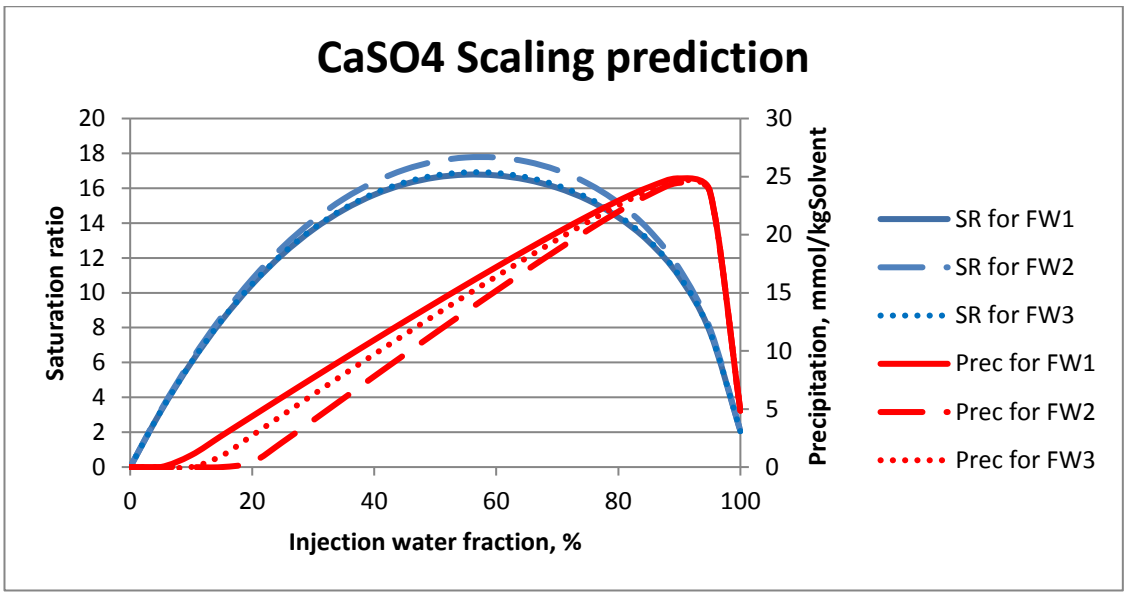

Figure 5.11 Saturation ratio and maximum predicted mass of calcium sulphate for different regions (FW1 for Region1, FW2 for Region 2 and FW3 for Region 3).

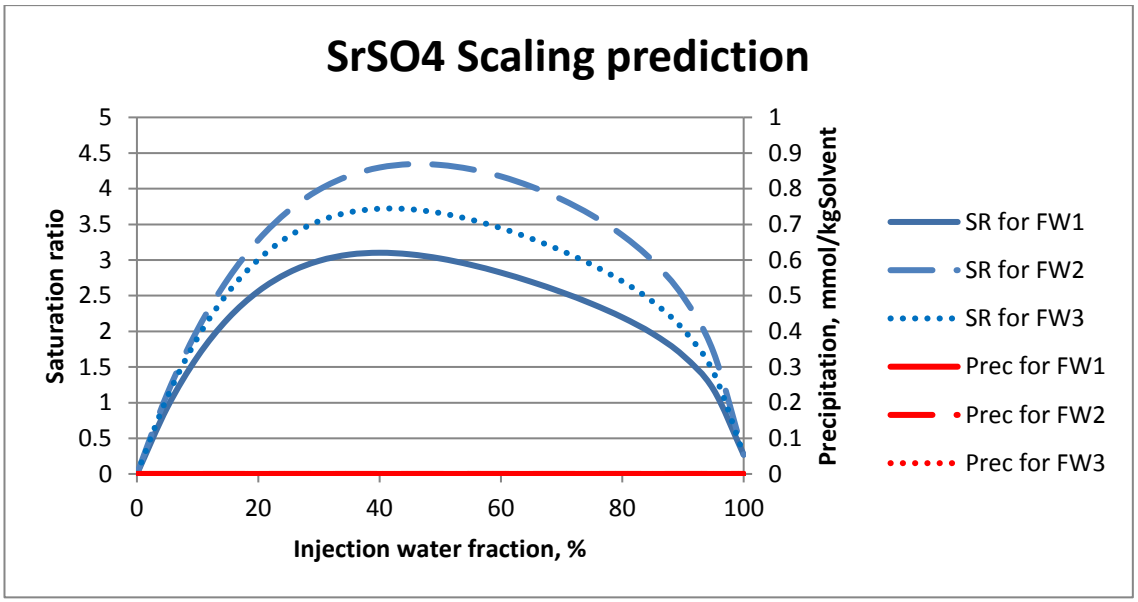

Figure 5.12 Saturation ratio and maximum predicted mass of strontium sulphate for different regions (FW1 for Region1, FW2 for Region 2 and FW3 for Region 3).

Some produced water data with varying injected water fractions were used to calculate single point scaling tendencies using MultiScale. The extent of geochemical reactions occurring within the reservoir can be implied by the difference between the mixing and the single point calculation results if all of the produced water samples were assumed to be protected by squeezed scale inhibitor in the near-well region and the wellbore. From **Figure 5.13-5.18**, it can be observed that barite and anhydrite scaling would be

significantly lowered by reservoir interactions in the three regions. The impact of the reservoir interactions on the scaling tendency for anhydrite is uniform, but the impact on the saturation ratio and predicted mass of scale for barite varies quite significantly. The impact of geochemical reactions within the reservoir is determined by many factors, including factors that affect the extent of brine mixing such as reservoir heterogeneity, and is not just a consequence of the formation and injection water compositions; it is therefore a major challenge to model the chemical reactions occurring inside the reservoir properly.

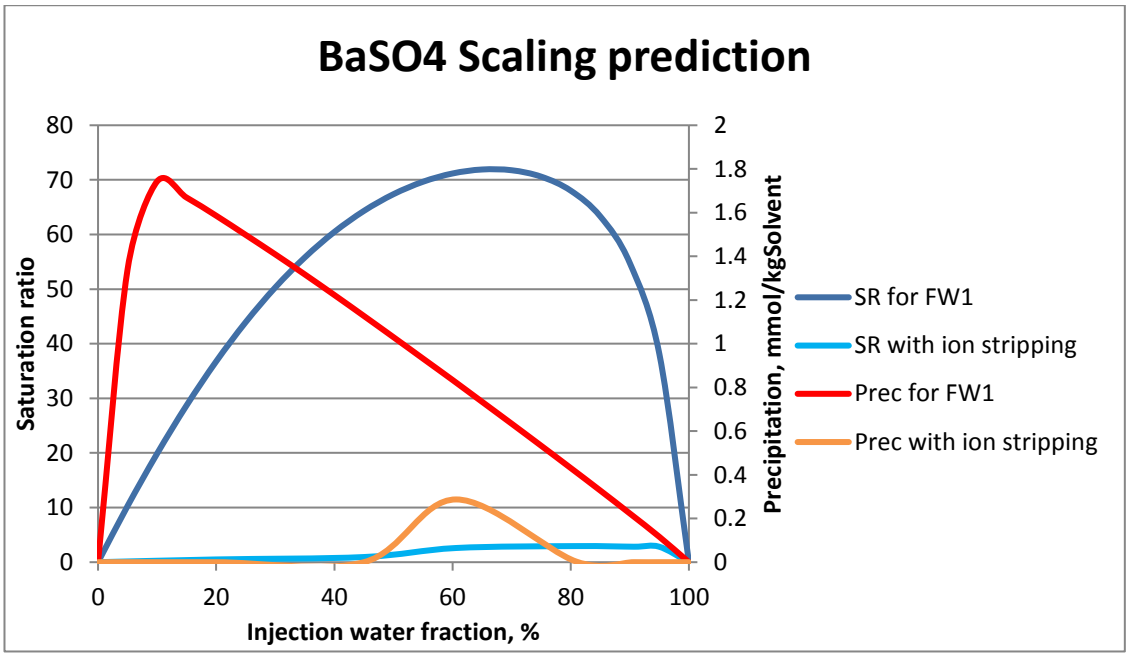

Figure 5.13 The comparison of scaling tendency prediction of barium sulphate by mixing and single points calculation for region 1.

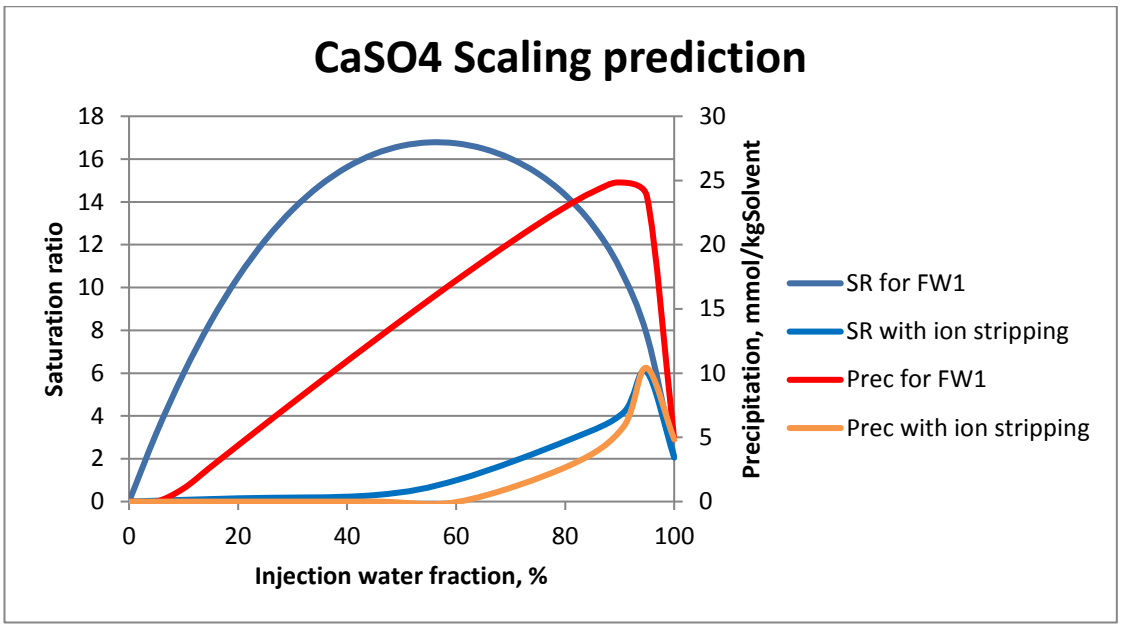

Figure 5.14 The comparison of scaling tendency prediction of calcium sulphate by mixing and single point calculation for region 1.

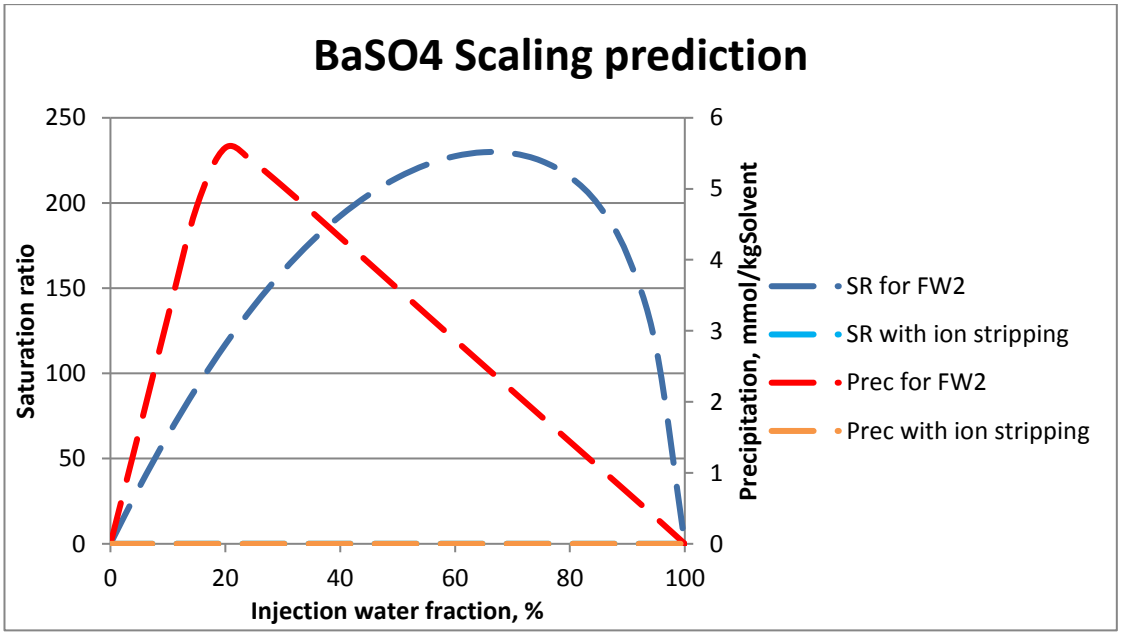

Figure 5.15 The comparison of scaling tendency prediction of barium sulphate by mixing and single point calculation for region 2.

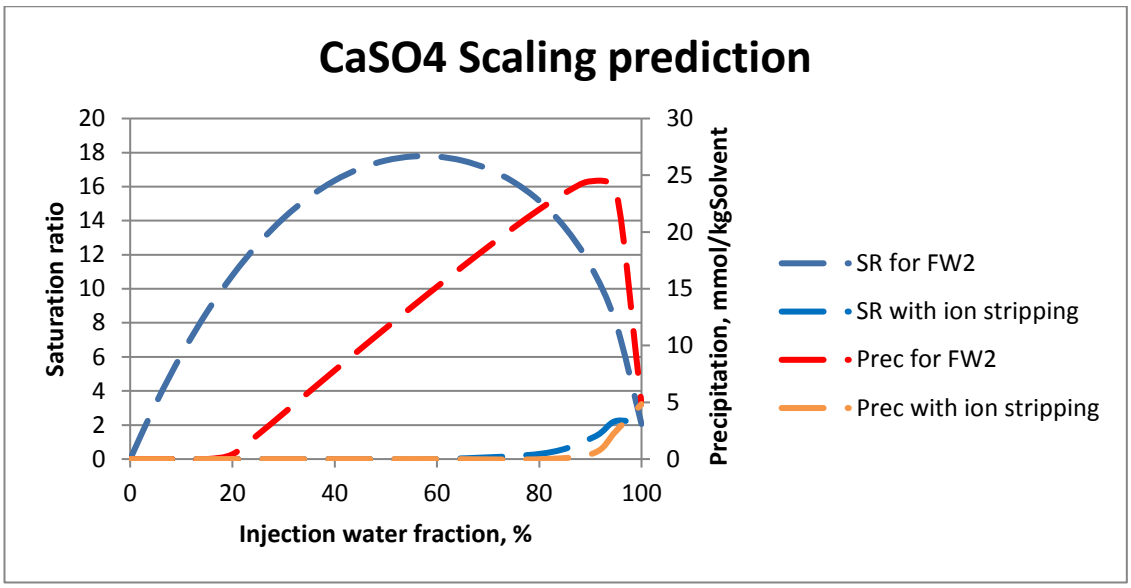

Figure 5.16 The comparison of scaling tendency prediction of calcium sulphate by mixing and single point calculation for region 2.

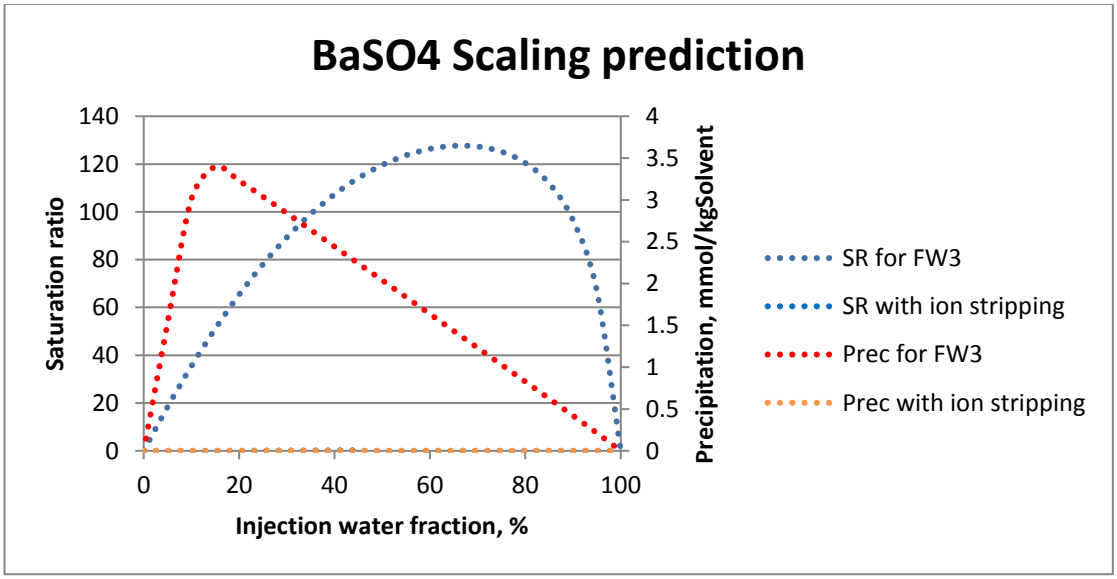

Figure 5.17 The comparison of scaling tendency prediction of barium sulphate by mixing and single point calculation for region 3.

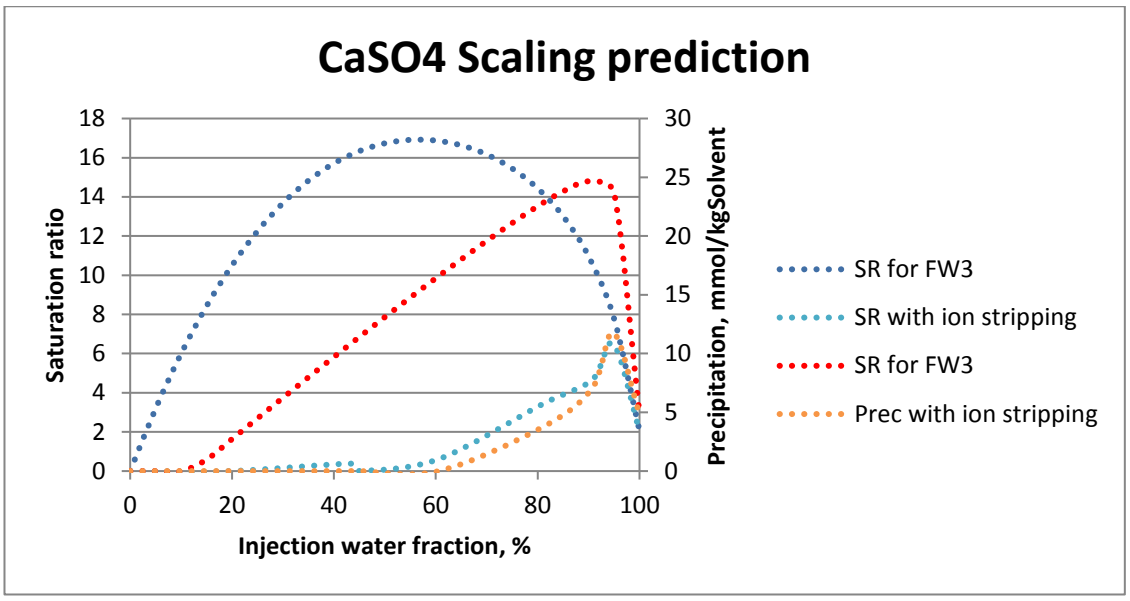

Figure 5.18 The comparison of scaling tendency prediction of calcium sulphate by mixing and single point calculation for region 3.

5.5 GEM modelling study

Various thermodynamic models have been developed to simulate and predict what chemical reactions will occur due to mixing of incompatible formation water and injection water, how severe the scaling potential is and how much scale deposition would take place. These thermodynamic models have been improved to include more and more mineral reactions and the databases they use have been validated and updated by experimental results.

Mackay et al. (2002) identified that it is important to locate where scale precipitation takes place and not just calculate the scaling tendency and maximum amount of scale deposition based on brine mixing that ignores *in situ* effects. The stripping of scaling ions resulting from geochemical reactions deep within the reservoir was realised to be beneficial for scale control and management as it does not cause a significant decrease in porosity and permeability and so does not block fluid flow deep in the reservoir, but it can lower the concentration of scaling ions reaching the producer, and thus lower the scale risk in the near well region and the wellbore itself. Therefore, in recent years, one-dimensional reactive transport modelling has been undertaken to simulate mineral reactions along the single flow path where injected seawater was displacing and mixing with formation water (Vazquez et al., 2013; Fu et al., 2012; McCartney et al., 2006).

Although simulation results from one-dimensional models can provide a reasonable match with produced water data and explain the impact of mineral reactions occurring in the reservoir, they cannot account for complex in fluid (oil + gas + water) on three dimensional flow in porous media coupled to the various mineral reactions. Therefore, it is better to model the mineral reactions through use of a three-dimensional reactive transport reservoir simulator which provides the opportunity to study the behaviour of geochemical reactions in the three-dimensional reservoir, including the impact of the reservoir heterogeneity. In this study, the commercial compositional reservoir simulator CMG GEM was used to simulate *in situ* reservoir interactions during seawater injection into the Gyda field. However, to initiate the geochemically modelling study, we follow the above cited authors and start with a one-dimensional reactive transport model to identify the key reactions qualitatively, and the full impact of horizontal and vertical heterogeneity is accounted for later.

5.5.1 Model description

The dimensions of the base case model were 1000 m x 20 m x 90 m, as presented in **Figure 5.19**. The key parameters of the model and reservoir properties are summarized in **Table 5.3**.

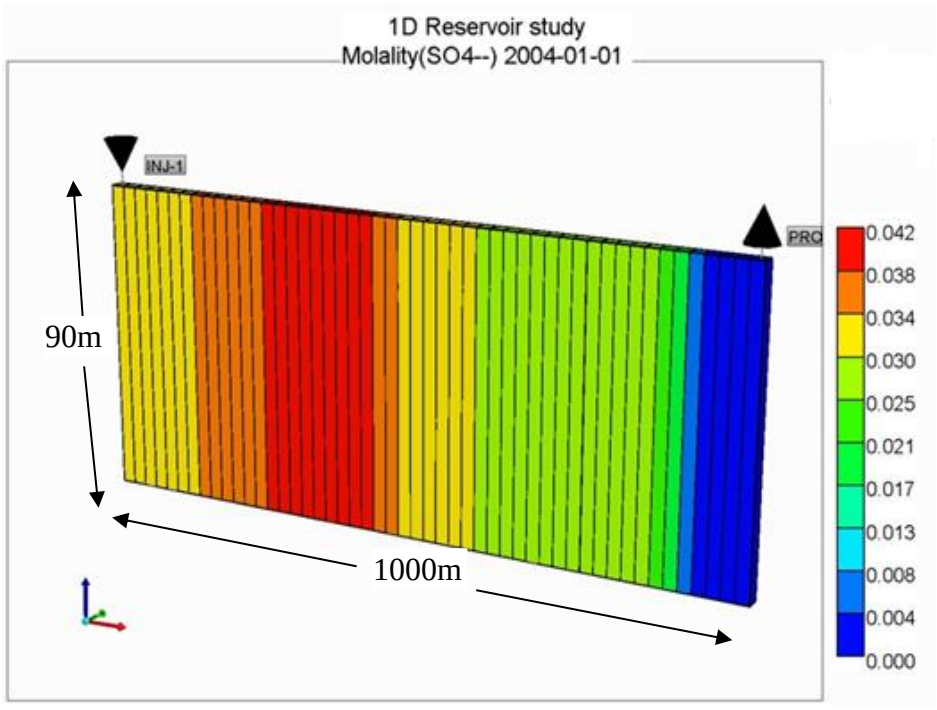

Figure 5.19 Overview of GEM model.

Table 5.3 Summary of model properties.

Model parameters	Assigned value
Number of blocks	50 x 1 x 1
Block size	20 x 20 x 90
Depth to Reservoir Top	4155 m
Initial Pressure	60400 kPa
Initial Temperature	160 ^{o}C
Porosity	20%
Horizontal permeability	200 mD

5.5.2 Geochemical reactions

The aqueous chemical equilibrium reactions and mineral reactions listed in **Table 5.4** were included in the model.

Table 5.4 Summary of chemical reactions included.

Mineral dissolution and precipitation reactions	Aqueous equilibrium reactions
Barite = (Ba^{++}) + (SO_4^{--})	$CO_2(aq) + H_2O = (H^+) + (HCO_3^-)$
Celestite = (Sr^{++}) + (SO_4^{--})	$(OH^-) + (H^+) = H_2O$
Anhydrite = (Ca^{++}) + (SO_4^{--})	$(CO_3^{--}) + (H^+) = (HCO_3^-)$
Calcite + (H^+) = (Ca^{++}) + (HCO_3^-)	
Dolomite + 2 (H^+) = (Ca^{++}) + (Mg^{++}) + 2 HCO_3^-)	

5.5.3 One-dimensional base case

Figures 5.20-5.26 show produced ion concentrations predicted by the original and by an updated one-dimensional model for three types of formation water compositions for different regions of the Gyda field, which are also compared with their own pure mixing lines of formation water and injected seawater, as well as observed concentrations from produced water samples. Reactions involving chloride bearing minerals were not included in the model, so chloride can be used as an indication of injected water fraction in the produced brine. Chloride concentrations decrease from ~180000 mg/l (right) to 19800 mg/l (left) in response to increasing injected seawater fraction.

Both of the modelled and observed sodium concentrations appear to lie on or near the sodium pure mixing line. This is in accordance with what is normally observed in most of the North Sea oil fields studied to date, because sodium is hardly involved in any

mineral reactions except for halite precipitation. However, in this study the process of multicomponent ion exchange (MIE) at the rock surface may lead to the release of sodium, but the sodium is in such excess that the relative impact of MIE on the overall sodium concentration is difficult to identify, given the very high sodium concentration in the formation water.

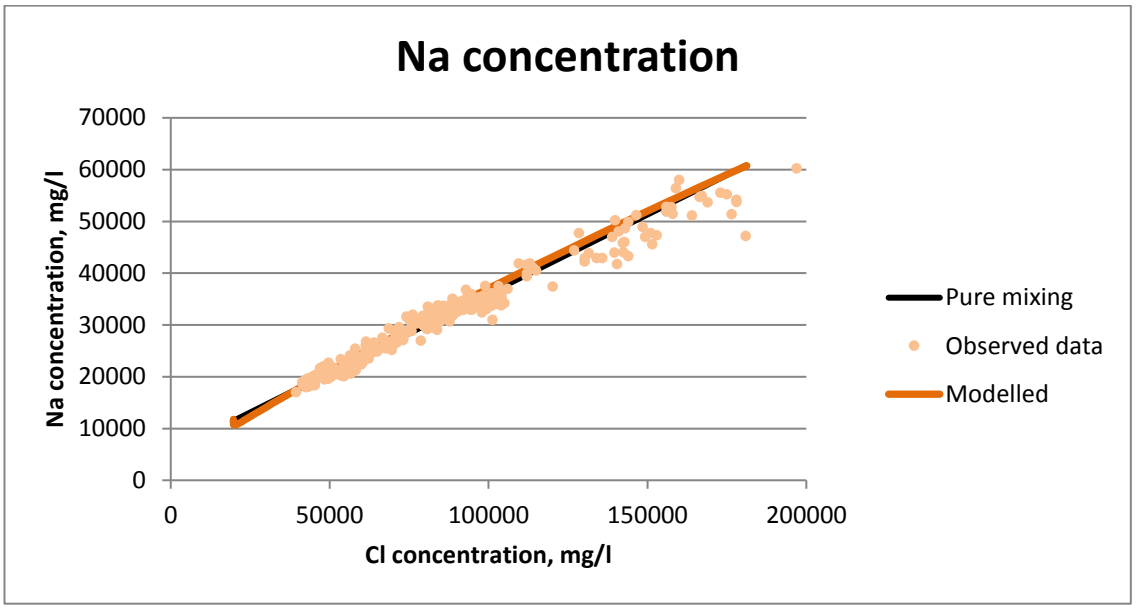

Figure 5.20 Modelled and observed sodium concentration in produced water for region 1.

Calculated and observed stontium in the three regions decreases almost linearly with the decline in chloride concentration, although celestite has been allowed to precipitate or dissolve in the model. This suggests that there is hardly any loss of strontium in the produced brine other than merely due to the effects of dilution.

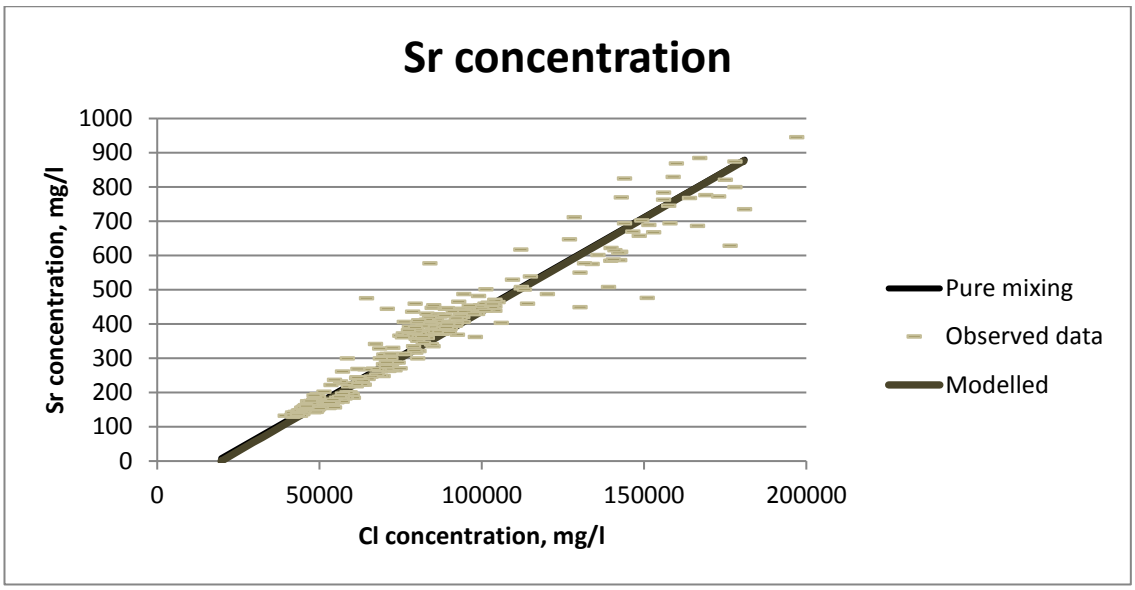

Figure 5.21 Modelled and observed strontium concentration in produced water for region 1.

In contrast to stontium, it is incorrect to summarize that calcium is not involved in any mineral reactions, although the same situation with stontium is presented for calcium where the deviation of modelled calcium from pure dilution is hardly observable. Calcium is liberated as the result of calcite dissolution (in models where calcite is included as a primary mineral) and also released from rock surface into brine due to MIE (where this process is modelled). In addition, calcium is consumed by the precipitation of anhydrite, which will be discussed in detail below. The reason why it is difficult to identify the difference between modelled calcium concentration and its pure dilution line is very similar to the situation with sodium (due to the excess of the ion relative to the reaction or reactions).

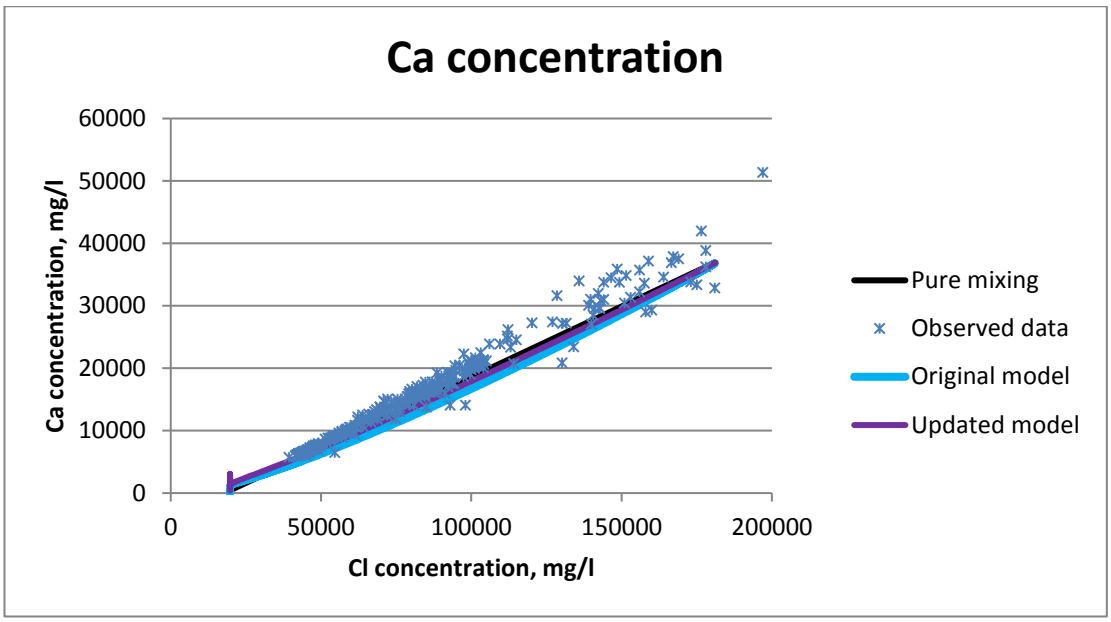

Figure 5.22 Modelled and observed calcium concentration in produced water for region 1.

It is clear that magnesium is remarkably depleted relative to the pure dilution line, so there must be some geochemical reactions involving magnesium taking place. Cation exchange, particularly calcium/magnesium interaction was initially proposed to explain magnesium stripping, on the basis of large differences of Mg/Ca ratio in formation water and injected seawater; this was then simulated by a reactive transport model to match with field data (Mackay et al., 2006). McCartney et al. (2007) conducted a further study using geochemical and reactive transport modelling to evaluate the role of MIE and dolomitization during seawater injected into Gyda field, in addition to more straight forward brine mixing effects. However, there remains some debate as to whether or not the process of dolomite precipitation can take place over production timescales, and some of the literature suggests that it is only likely to occur on geological timescales rather than production time frames. **(**Meister et al., 2011**)** This is because otherwise the assumption has to be made that the solubility of dolomite in the actual reservoir is much lower than experimental data suggests. In other words, dolomite precipitation can be found only if its equilibrium constant is significantly decreased in the thermodynamic database of the model, which was also illustrated by McCartney et al., (2007). Therefore, MIE, dolomite deposition and the combined effect will be discussed in detail based on the simulation results.

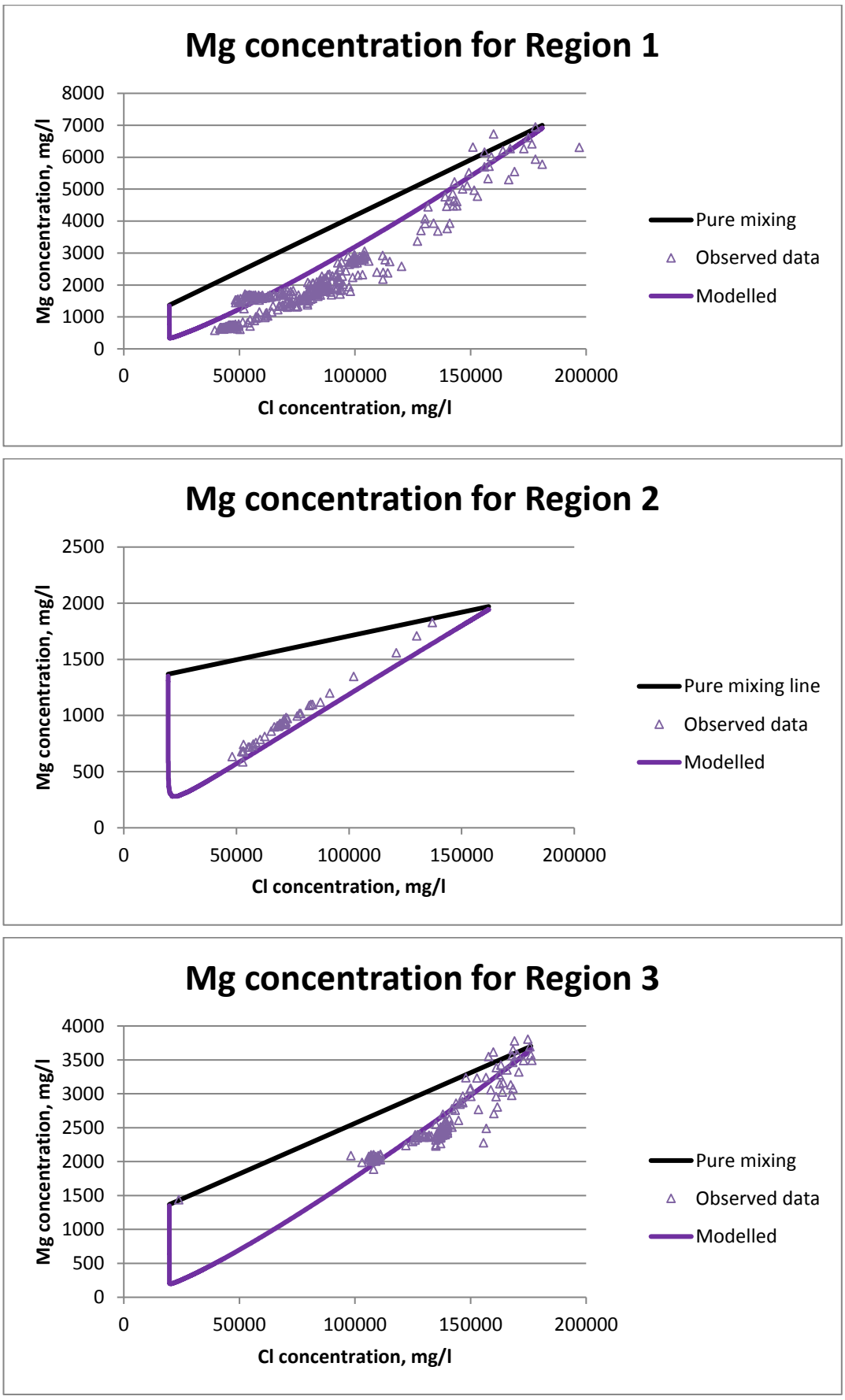

Figure 5.23 Modelled and observed magnesium concentration in produced water for region 1,2 and 3.

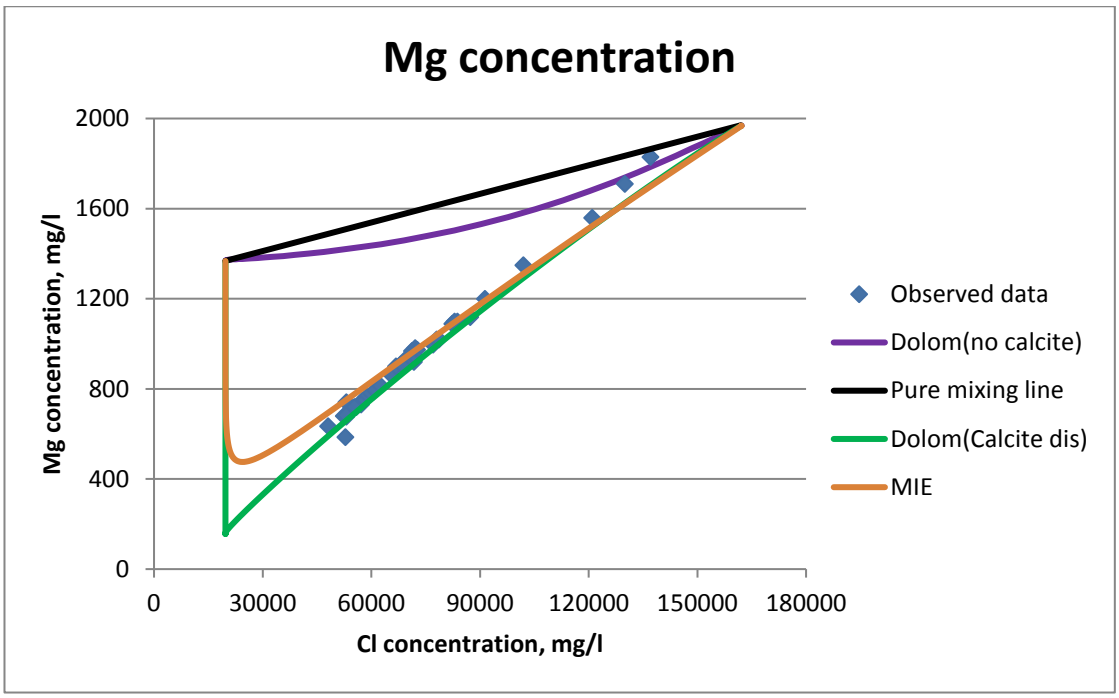

Figure 5.24 Simulated magnesium concentrations in produced water from various kinds of models based on formation water in region 2.

It can be seen from **Figure 5.24** that reasonable matches with observed magnesium concentration through modelling of multicomponent ion exchange or dolomite mineral reaction with calcite present initially are achieved, but it is difficult to obtain a match with observed data if calcite is not defined as a primary mineral phase in the case that includes modelling of dolomite precipitation. This implies that the occurrence of dolomite precipitation largely depends on the presence of calcite in the initial reservoir mineralogy (discussed in chapter 1). This is also consistent with the fact that similar magnesium stripping has been observed from the produced water data of carbonate reservoirs which are predominantly made up of calcium carbonate. In the case of Gyda field, dolomite precipitation would probably take place in or close to calcite stringers, but multicomponent ion exchange may be the dominant reason of magnesium stripping in the region with abundant clays. In addition, it is possible that magnesium removal is caused by the combination of dolomite precipitation and multicomponent ion exchange. Tuning both of the cation exchange capacity (CEC) and dolomite solubility can control the total modelled magnesium concentration in the produced brine although the solution will be non-unique. Therefore, what *in situ* chemical reactions involving magnesium were taking place would be determined by the distribution of clays and calcite stringers in the reservoir.

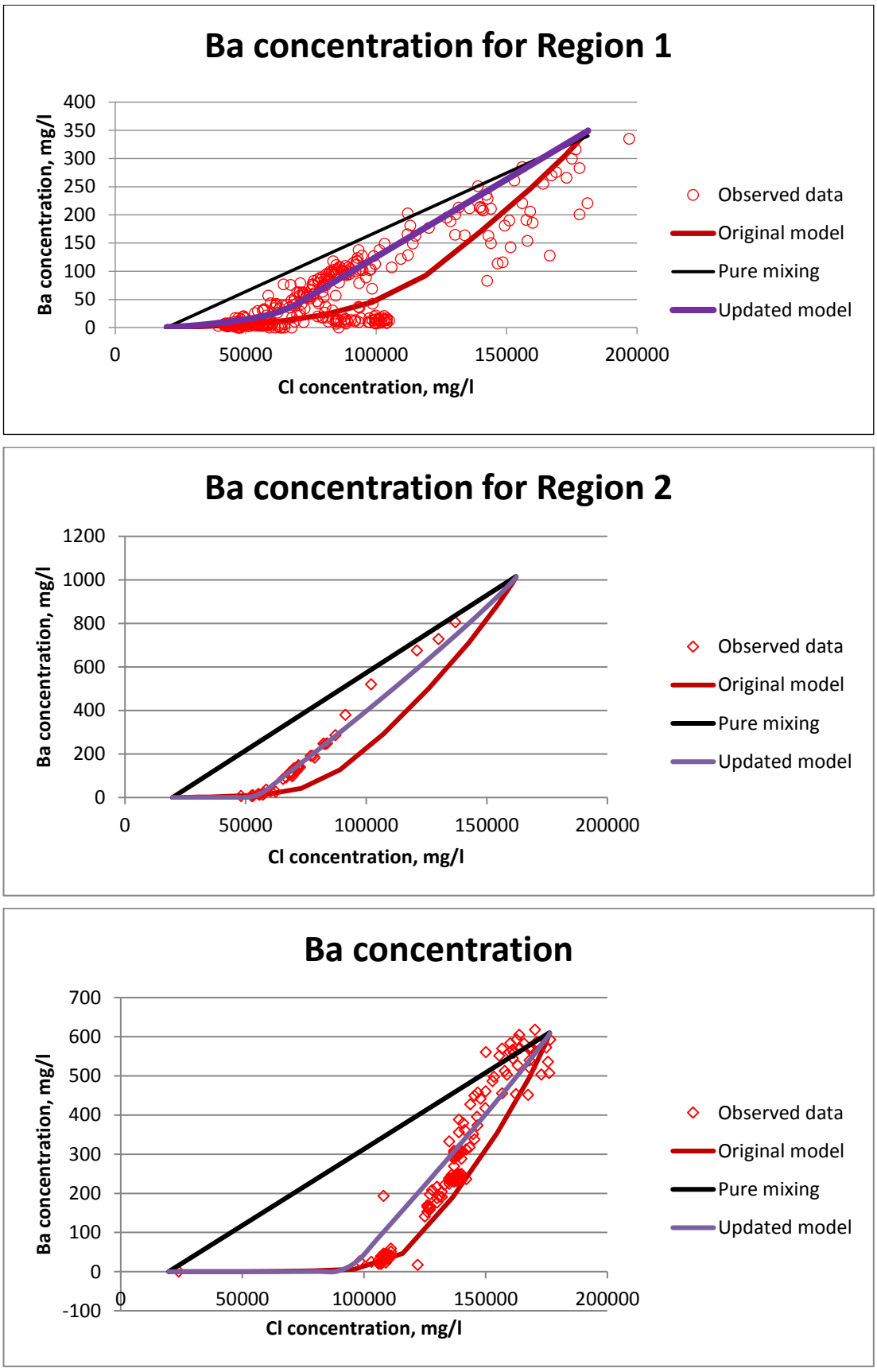

Figure 5.25 Modelled and observed barium concentration in produced water for region 1, 2 and 3.

In **Figure 5.25**, the calculated barium concentrations for the three regions fall substantially below the values predicted by pure mixing of injected and formation water,

but the trends simulated by the original model are not in agreement with observed concentrations for all three regions. Thus the Saturation Ratio (SR) of barite was increased to delay the precipitation of barite and produce more barium in the effluent. Based on Equation 1.19, the relationship between the solubility and SR of a given mineral is further presented in Equation 5.1:

$$K_{sp_{NEW}} = K_{sp_{INI}} \times SR \tag{5.1}$$

where $K_{sp_{NEW}}$, $K_{sp_{INI}}$ and SR represent the corrected equilibrium constant, initial equilibrium constant and the Saturation Ratio defined in the model.

Initially, the SR is 1 by default in the original model. In the updated model, the SR of barite was tuned to 1.5, which indicates the solubility of barite has risen to 1.5 times. Thus, an updated produced barium concentration profile (shown by the purple line) was obtained to show a better match with the measured concentrations. It should be noted that sulphate is a limiting ion, and barium and calcium are in excess for barite and anhydrite precipitation reactions, respectively, and barium is competing with calcium for the availability of sulphate in the brine.

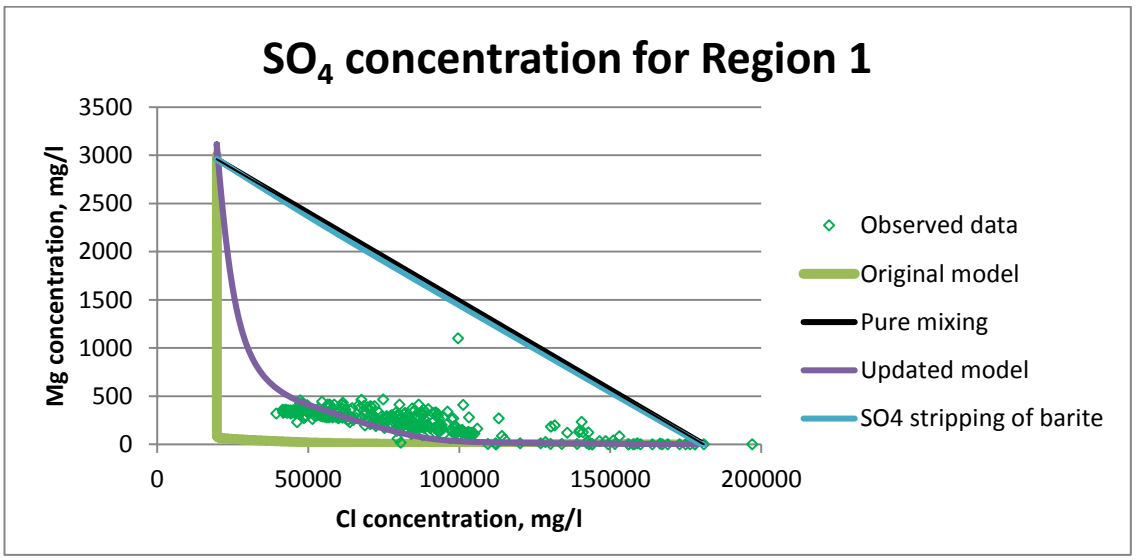

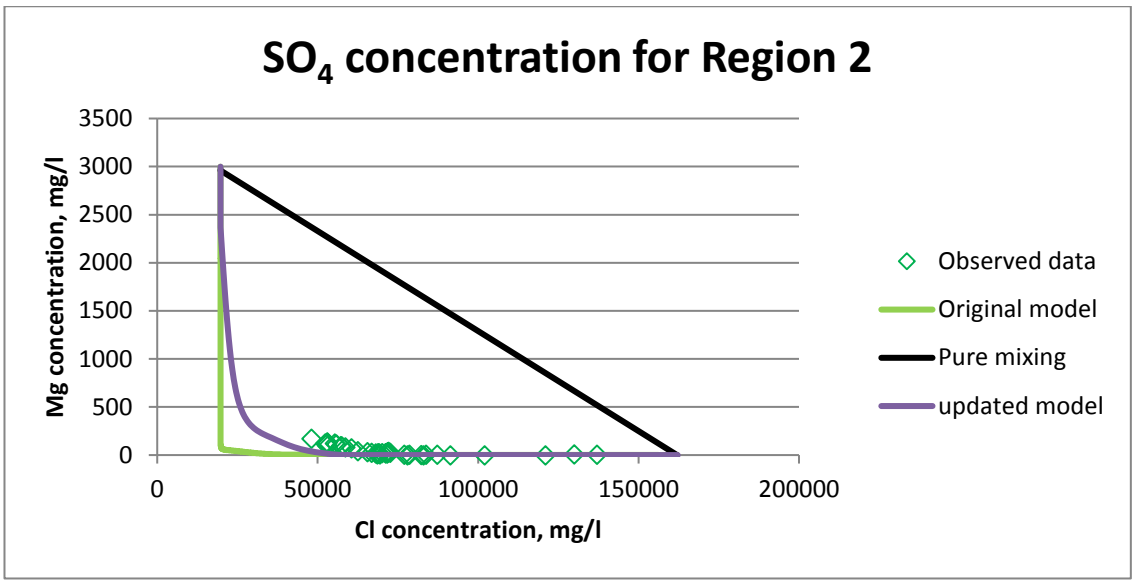

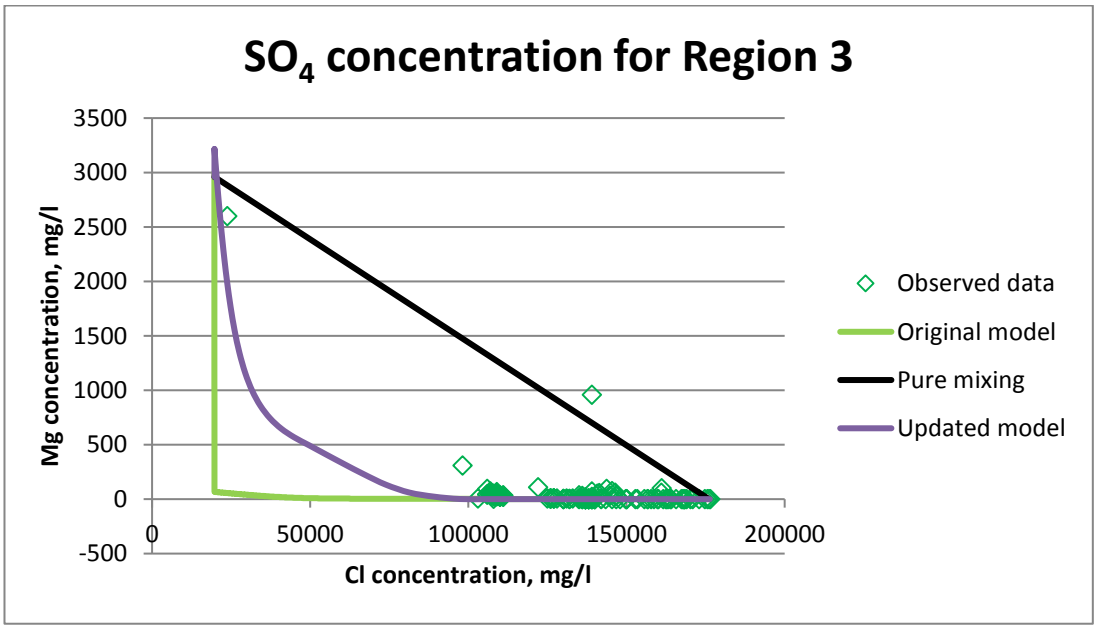

Figure 5.26 Modelled and observed sulphate concentration in produced water for region 1, 2 and 3.

In **Figure 5.26** we can find that the modelled concentration of sulphate in the produced brine significantly deviates from its pure dilution line, which is abnormal behaviour in sandstone reservoirs where produced sulphate usually lies close to its pure mixing line in spite of significant barite precipitation (Houston et al., 2006; Fu et al., 2012), due to the fact that it is usually in excess. This type of sulphate depletion is more commonly observed at carbonate reservoirs, such as Ekofisk. From **Figure 5.26 (Region 1),** the difference between the blue line and the black line reflects the amount of sulphate stripping caused by barite precipitation, and the deviation between the blue line and the purple line indicates sulphate removal due to anhydrite precipitation. It can be concluded

that over 95% of sulphate was depleted by anhydrite deposition and the occurrence of barite just accounts for ~5% of the sulphate stripping. Therefore, the produced sulphate trends are mainly determined by anhydrite mineral precipitation.

For all three types of formation waters, there is some more loss of sulphate in the original model than observed in the produced water samples, so tuning saturation ratio of anhydrite to delay its precipitation is needed. The Saturation Ratio of anhydrite (Equation 5.1) was increased to 2.0 in the *updated model* (shown by the purple line) to provide a reasonable match of sulphate although observed calcium concentrations did not present large deviation from simulation results obtained by the original model. In summary, there is a competitive relationship between barium and calcium to react with sulphate in the Gyda field because sulphate is limited here, and this is the biggest difference with geochemical processes occurring in other normal sandstone reservoirs where sulphate is in excess and barium is limited due to very low occurrence of anhydrite precipitation. The balance between barite and anhydrite precipitation must to be modelled and understood in order to provide a better match of produced ion behaviours. In turn, these presented matches for barium, calcium and sulphate give confidence that the interpretation of the produced water data is that barite and anhydrite mineral reactions are occurring.

In this study, there exist geochemical reasons for the discrepancy between predicted barium and sulphate concentrations and observed data from produced water samples. First of all, it may be questioned whether or not the basic and common thermodynamic database (equilibrium constants) is applicable for predicting the solubility of anhydrite, gypsum and calcite over wide ranges of temperature, pressure, and ionic strength with mixed electrolytes (particularly at reservoir conditions with high temperature high pressure high brine salinity) (Dai et al., 2014). Therefore, to use log K values as a fitting parameter in a specific case study focusing on geochemical reactions taking place deep within the reservoir is justifiable at least when the experimental results on mineral solubility under the specific reservoir conditions are not available. Moreover, the Pitzer activity model has not been included in the latest version of the GEM reservoir simulator and so instead the available B-dot model has been used in this study, although it has been proved that the Pitzer model can accurately model activity coefficients in solutions with high ionic strength (up to 6 mol/kgw) (based on the comparison of PHREEQC and GEM chemical equilibrium results described in the chapter 1). The use of the Pitzer model can possibly be approximated by using higher log K values (implemented by increasing SR).

Equally, there are other reasons for deviations from 1D simulation (e.g. reservoir brine and flow mixing which will be discussed later in the 2D vertical model case study)

5.5.4 Non-isothermal case

As noted above, anhydrite precipitation is the dominant mineral reaction taking place deep within the reservoir in the Gyda field, which is the main reason why particular ion behaviours (especially sulphate and calcium) are observed in the produced brine. Two key factors that cause extensive anhydrite deposition are the relatively high reservoir temperature (160°C) and the high initial calcium concentration (36900 mg/l). It has been reported from many experimental data that the solubility of anhydrite is sensitive to temperature while the solubility of barite and celestite vary just slightly with temperature. **(**Blounot et al., 1968; 1977; Reardon et al., 1986**)** This can also be identified by investigating the thermodynamic databases in the models.

It is known that reservoir temperature does not usually change much during oil production due to depletion, but the reservoir rock is cooled by injection water at lower temperature (typically ~25°C) and so the reservoir temperature declines as cold water is injected. It is therefore necessary to investigate the impact of temperature propagation resulting from cold water injection on the geochemical reactions and the evolution of the produced ion concentrations in the Gyda field.

Thermal calculations can be conducted by using GEM from version 2015 onwards, in which the equations governing temperature can be solved simultaneously with the flow and reaction equations. An energy balance with convection, conduction and heat loss terms are included in the thermal model of GEM.

Thermal properties of a substance, which include heat capacity, thermal conductivity, thermal diffusivity and the coefficient of thermal expansion, connect temperature and heat flow. Heat capacity and thermal conductivity of reservoir rock used for our modelling are 885.77 J/kg.K and 1.73 J/m.s.K, respectively, which are default values in GEM and are widely used for normal sandstone reservoirs. The non-isothermal model was extended on the basis of the second type of formation water in region 2.

5.5.4.1 Anhydrite

As can be seen from **Figure 5.27**, temperature at the outlet of the system (cell 50,1,1) declines constantly with continuous injection of cold seawater. The change in temperature

occurs much later than the evolution of produced ion concentration and is retarded due to heat exchange with the reservoir rock and as a function of the rock heat capacity. When injected seawater mixes with formation water, the chemical composition of the mixed brine changes immediately; however, it takes some time to lower the temperature of reservoir rocks. This is the reason why propagation of the temperature front is much slower than the brine mixing front. Therefore, geochemical processes taking place at the leading edge of the brine mixing zone will be not be affected by temperature changes due to cold injection water.

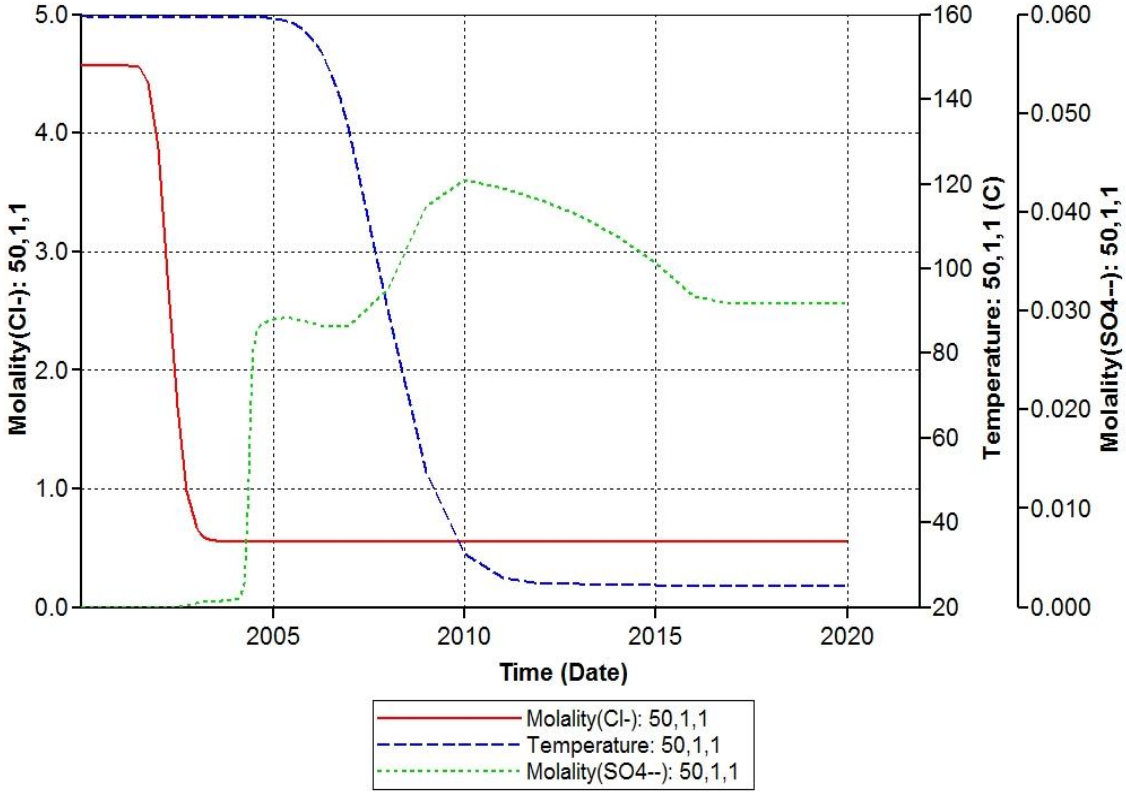

Figure 5.27 The comparison of mixing and temperature fronts, and produced sulphate behaviour.

Anhydrite can be precipitated from injected seawater itself, indicating that anhydrite precipitation can take place even if the IWF is 100% provided it is heated up to the reservoir temperature of 160°C. This has been reflected in **Figure 5.28** (red lines) and in **Figure 5.29**, which show the results of an isothermal calculation where the entire system is at a temperature of 160°C at all times. Here the amount of anhydrite precipitation in the whole system increases monotonically during seawater injection from the start of injection, and it must therefore be precipitated in the region close to the injector as soon as the seawater is injected into the reservoir. Indeed the precipitation takes place close to the injection well, and the brine reaches equilibrium before propagating far into the

reservoir, and so in this one-dimensional system the majority of the precipitation will be located around the injector. (In a three-dimensional system this behaviour will be different, since there will be more widespread mixing of (still) sulphate rich injection and calcium rich formation water as streamlines converge towards the production well.

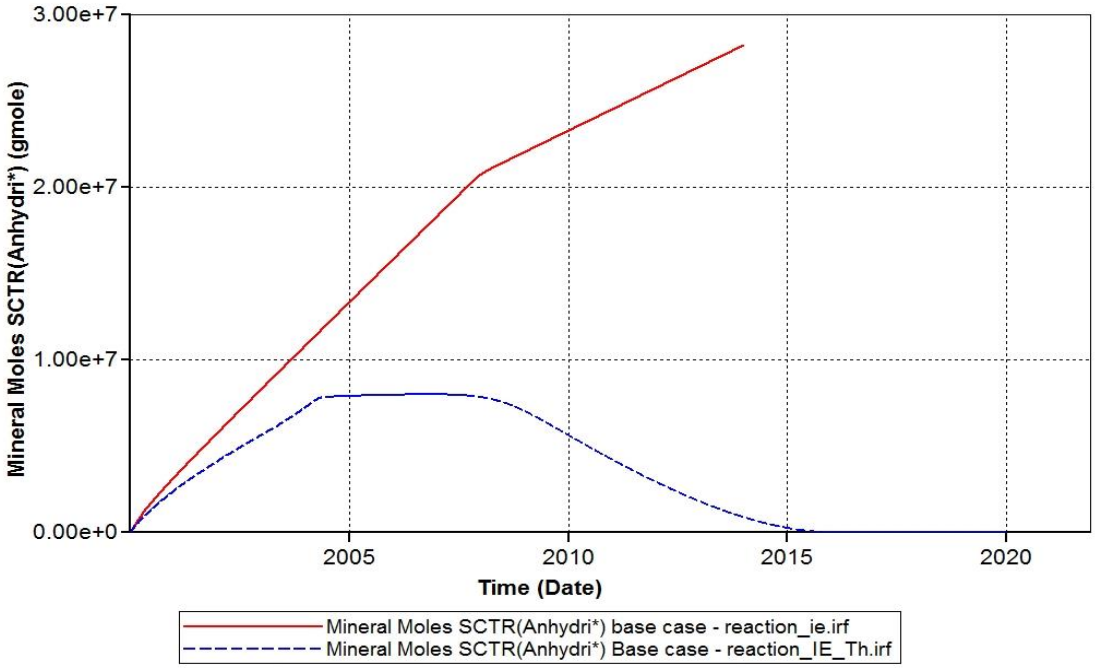

Figure 5.28 Total mass of anhydrite precipitation in the whole field.

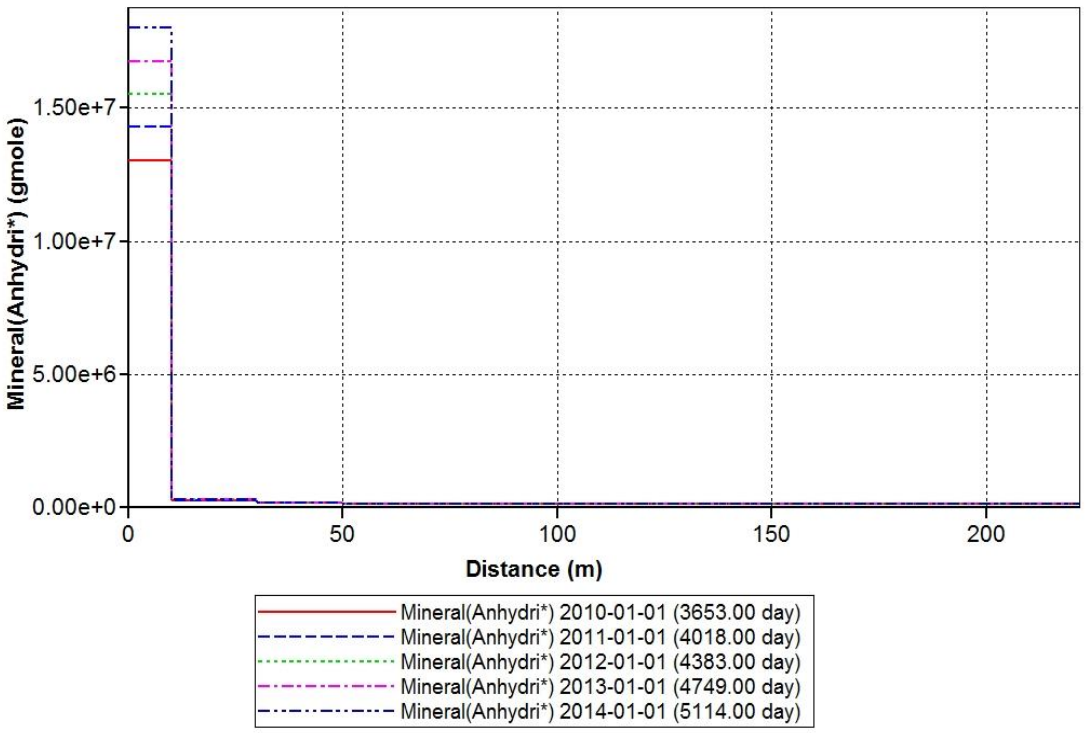

Figure 5.29 The amount of anhydrite precipitation in each block [injector (0m) and producer (1000m)].

However, in the case where thermal modelling was included, there will be a delay in the precipitation of anhydrite as the injection water heats up in the reservoir (slower increase in the mass of anhydrite precipitated), and then subsequently the anhydrite that precipitated in the hot zone will dissolve as the more slowly travelling cool front passes over it, as shown in **Figure 5.28 (**blue line**)**.

The amount of anhydrite precipitation in each block is shown in **Figure 5.30**, which suggests that anhydrite deposited in the area close to the injector before this zone was cooled, is then dissolved as the local reservoir temperature is lowered by the continuous flow of cold injection water. The dissolved anhydrite then re-precipitates again downstream in the area at high temperature (closer to the producer).

The key point is that the precipitation front travels faster than the dissolution front, since the transport of components is faster than heat transport. Sulphate ions ahead of the thermal front will travel faster than the thermal front, and so will travel at the velocity of the fluid until they interact with calcium ions, predominantly due to mixing between the injection and formation water, and so precipitate anhydrite in the hot zone. Sulphate ions

behind the thermal front, which are in solution as a consequence of subsequent anhydrite dissolution that occurred during cooling, will also travel faster than the thermal front, and so will overtake it to reach the hot zone. Once there they may again precipitate to form anhydrite, but in this circumstance they will precipitate due to the presence of calcium ions that were part of the same dissolution process, not so much due to brine mixing with the formation water, which by then will have been displaced.

Eventually all of the deposited anhydrite will be re-dissolved, should the entire reservoir temperature be lowered to 25°C. The modelled sulphate trend (green line shown in **Figure 5.27**) is consistent with this interpretation. The concentration rises initially as seawater breaks through, then reaches a temporary equilibrium at the reservoir of approximately 160°C, and then increases again as sulphate that is a product of dissolution of anhydrite breaks through, before decreasing to the injection concentration as the entire system reaches equilibrium. This also therefore suggests that the producer could experience very high sulphate concentrations (even higher than that in injected seawater), and then the sulphate concentrations will drop. However, it is unlikely that a well will be produced for such a length of time that the entire inter well region has been cooled, and so production will probably stop at some point before this.

However, in a heterogeneous system, it is possible that although the thermal front does not reach the producer, in a high permeability layer the elevated sulphate concentrations may be observed after a period of suppressed sulphate concentrations. Additionally, it is possible that infill wells may be drilled in the cooled zone.

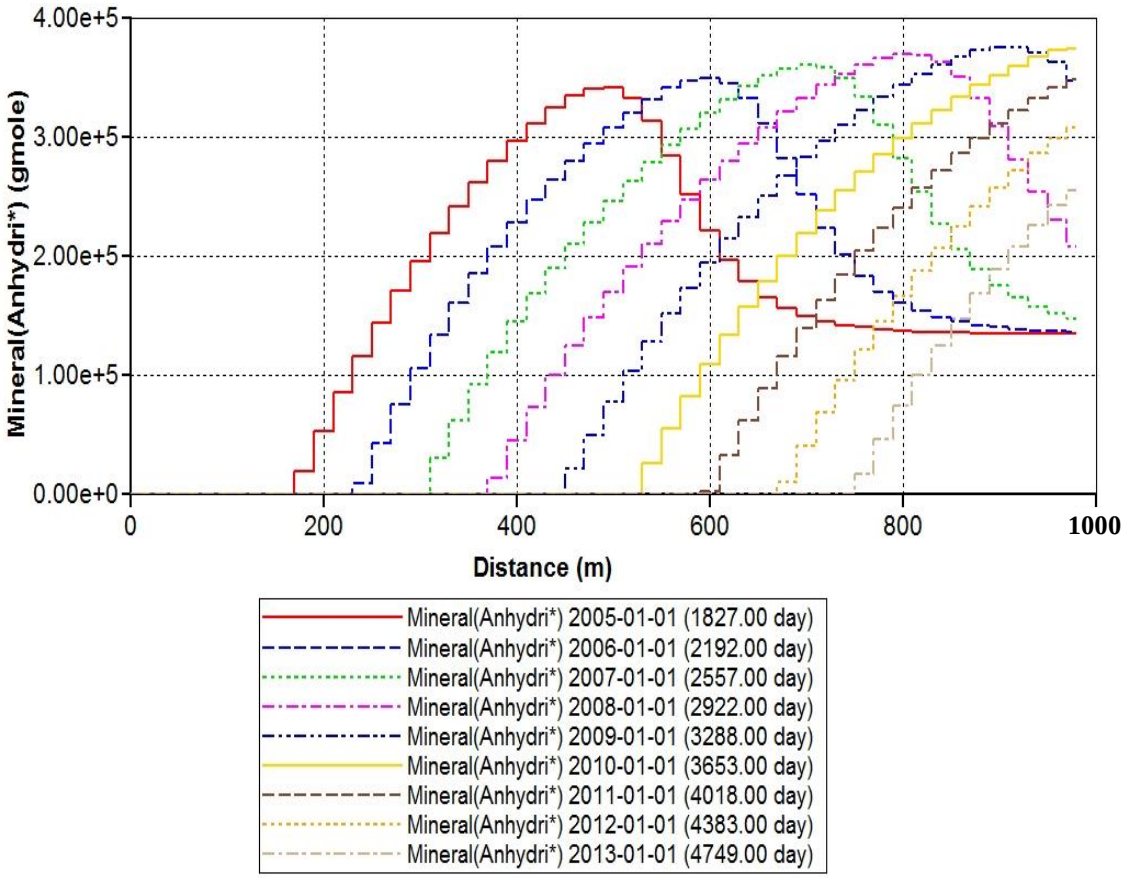

Figure 5.30 The amount of anhydrite precipitation in each block [injector (0m) and producer (1000m)].

5.5.4.2 Gypsum

The occurrence of anhydrite mineral reaction in the isothermal and non-isothermal system has been covered in the detailed discussion in the previous section. In this section we study both of anhydrite and gypsum precipitation and dissolution dependent on temperature as well as the conversion of gypsum to anhydrite, and anhydrite to gypsum.

From **Figure 5.31**, the solubility of anhydrite decreases monotonically with increasing temperature, but that of gypsum increases with increasing temperature below ~50°C and decreases with increasing temperature in the high temperature range. The overlapping (the shadow) in the gypsum and anhydrite solubility curves represents the transition temperature (Hardie, 1967).

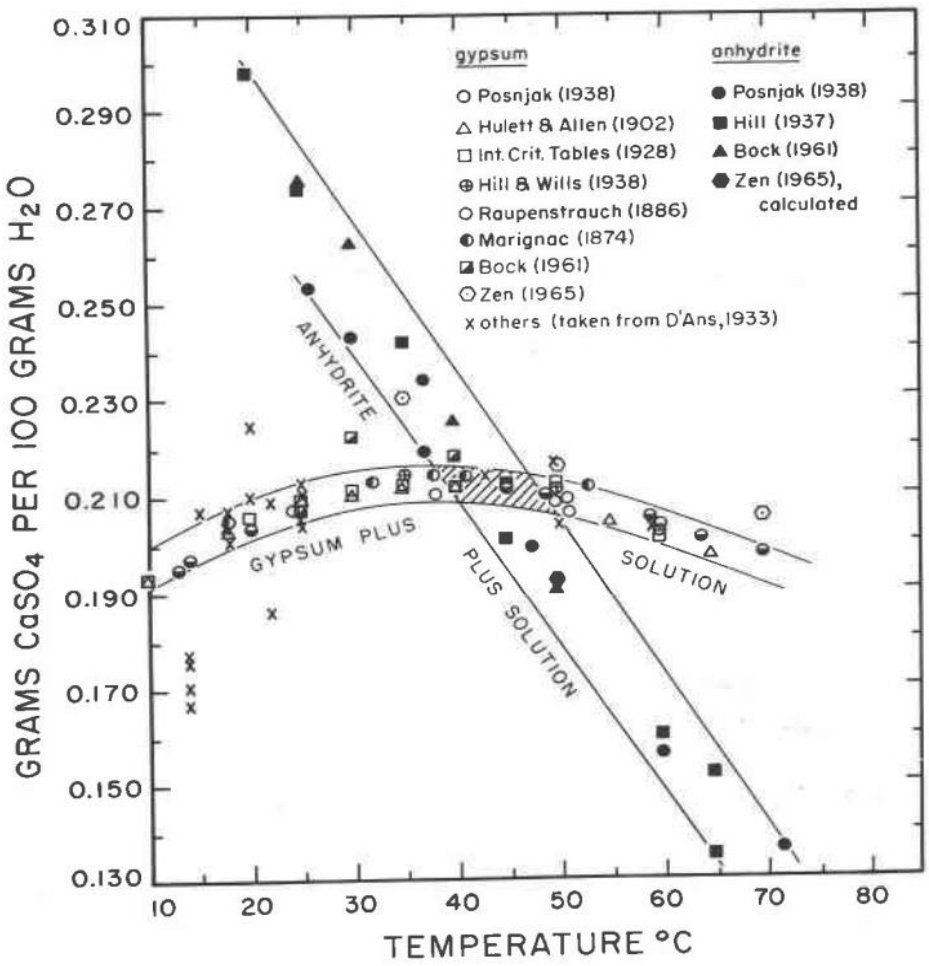

Figure 5.31 The solubility relations of gypsum and anhydrite in the system CaSO4-H2O as a function of temperature at atmospheric pressure: a compilation of previous work. (Hardie, 1967)

In the isothermal model, the gypsum did not precipitate, and so the same simulation results would be obtained, whether the gypsum mineral reaction was included or not. For Gyda field being consider here, the reservoir temperature is 160°C that is over the transition temperature (40~50°C), so the solubility of anhydrite is much lower than that of gypsum, and most of the calcium and sulphate in the brine are consumed by the precipitation of anhydrite.

However, in the case where temperature is decreased by cool injection water, a small proportion gypsum precipitates when temperature is lowered to be below the transition temperature. This is reflected in **Figure 5.32** which presents the total mass of anhydrite and gypsum in the whole system with and without including gypsum mineral reaction. The amount of gypsum in each block from injector to producer is shown in **Figure 5.33** so as to make a better understanding of the process of gypsum precipitation and dissolution. The gypsum began to be precipitated when the temperature was lower than

the transition temperature. This was then dissolved when the brine was undersaturated with gypsum as the calcium concentration would decrease once the anhydrite previously precipitated was completely dissolved. Therefore, the gypsum mineral reaction is determined by not only temperature but also the anhydrite precipitation/dissolution process. Anhydrite deposition would compete with gypsum precipitation, but anhydrite dissolution could give rise to higher calcium and sulphate concentration in the brine which benefits gypsum precipitation.

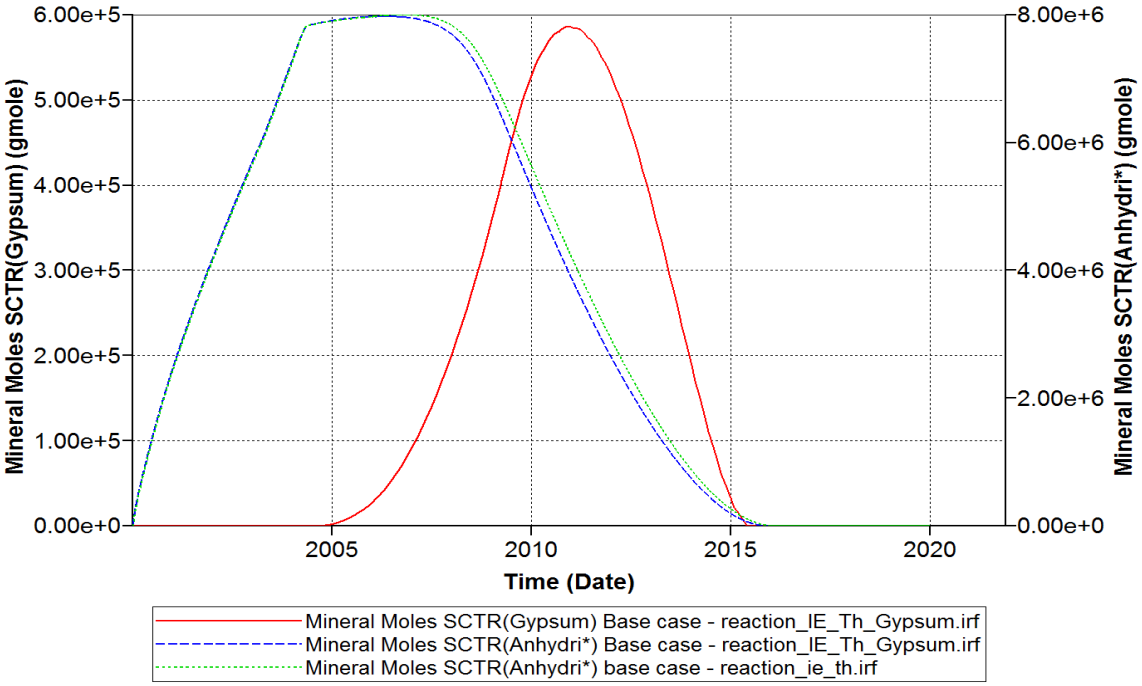

Figure 5.32 Total mass of anhydrite and gypsum precipitation in the whole field with and without gypsum mineral reaction.

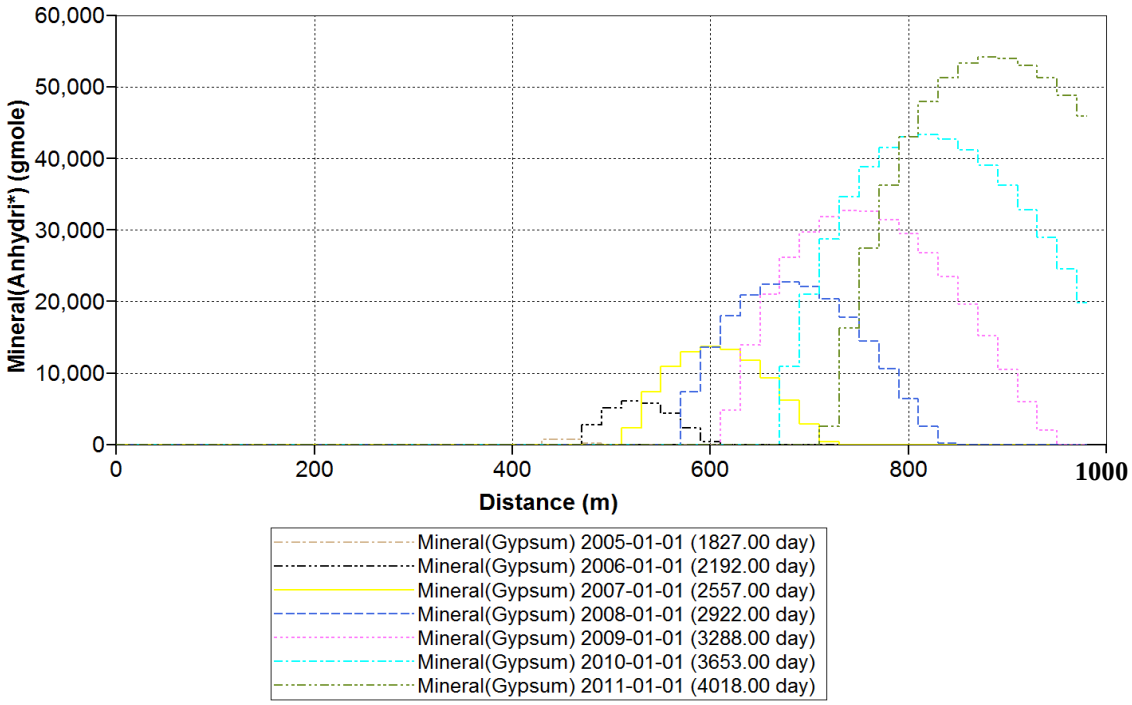

Figure 5.33 The amount of gypsum precipitation in each block [injector (0m) and producer (1000m)].

5.5.5 Two-dimensional vertical case

Geochemical reactions have been modelled and simulated along a single flow path in the one-dimensional base case model described above, but oil reservoirs are heterogeneous and may be composed of several layers with different porosities and permeabilities, etc. Therefore, the brine mixing and chemical reactions could take place in a variety of flow paths from injection well to production well, and each flow path will deliver water with a different IWF. These flow paths will converge near or in the producer, resulting in mixing because injection water may flow faster and break through earlier in the high permeability layers than the low permeability layers. There is thus an opportunity to extend our one-dimensional base case model to a two-dimensional vertical model with two layers (with high and low permeabilities). A number of simulations have been run in order to evaluate the impact of the vertical and horizontal communication on brine mixing, and the occurrence of chemical reactions on the produced brine composition. (**Figure 5.34**)

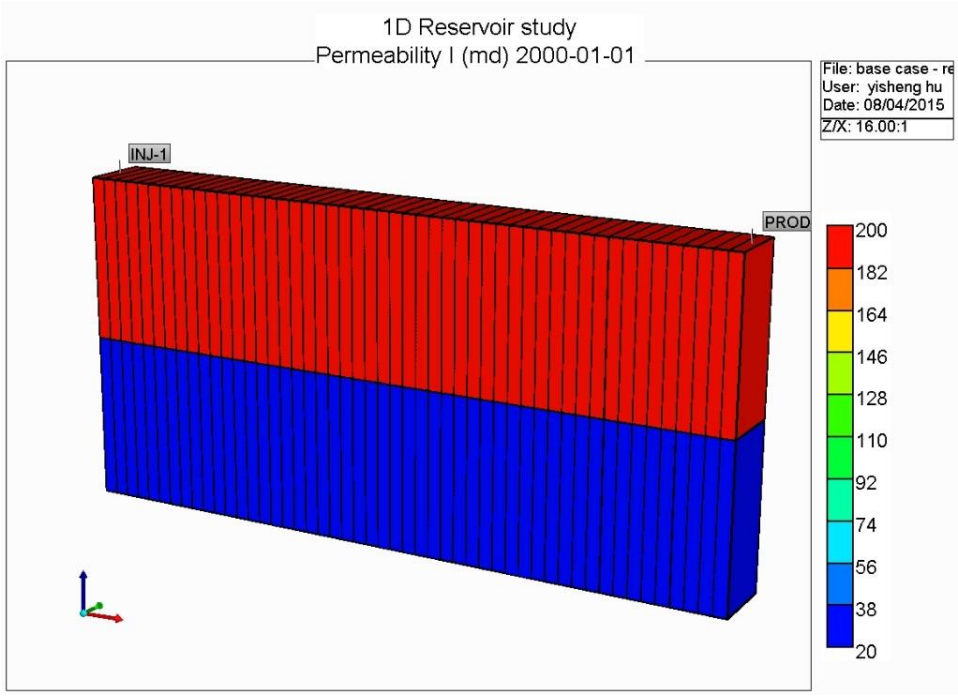

Figure 5.34 Overview of 2-D vertical model.

In the first sensitivity case, the horizontal permeability of the top layer is fixed at 200 mD, and that of the bottom layer is varied - 20, 50, 100, 150 and 200 mD (the latter being equivalent to the homogenous base case); vertical flow is prevented by setting a complete permeability barrier in the vertical direction (i.e. kv/kh = 0). This may occur in a reservoir where an impermeable (shale) layer is located between two perforated layers with different physical properties.

In **Figure 5.35** and **5.36** we focus on the chloride and barium concentrations. In the homogenous base case (pink line) the produced water composition experiences an evolution from formation water to injection water directly in one stage, since the flow rate in both layers is identical. However, in the heterogeneous cases the produced water composition varies from formation water to injection water composition in stages, with an intermediate "plateau" period before the injection water composition is attained. The two parts of the curves are in response to brine mixing from the bottom layer (high permeability) and top (low permeability) layers, with the injection brine breaking through first in the high permeability layer; the length of the plateau is determined by the difference in physical properties of the two layers. The higher the permeability of the bottom layer, the smaller the difference between the two layers, and so the shorter the plateau period.

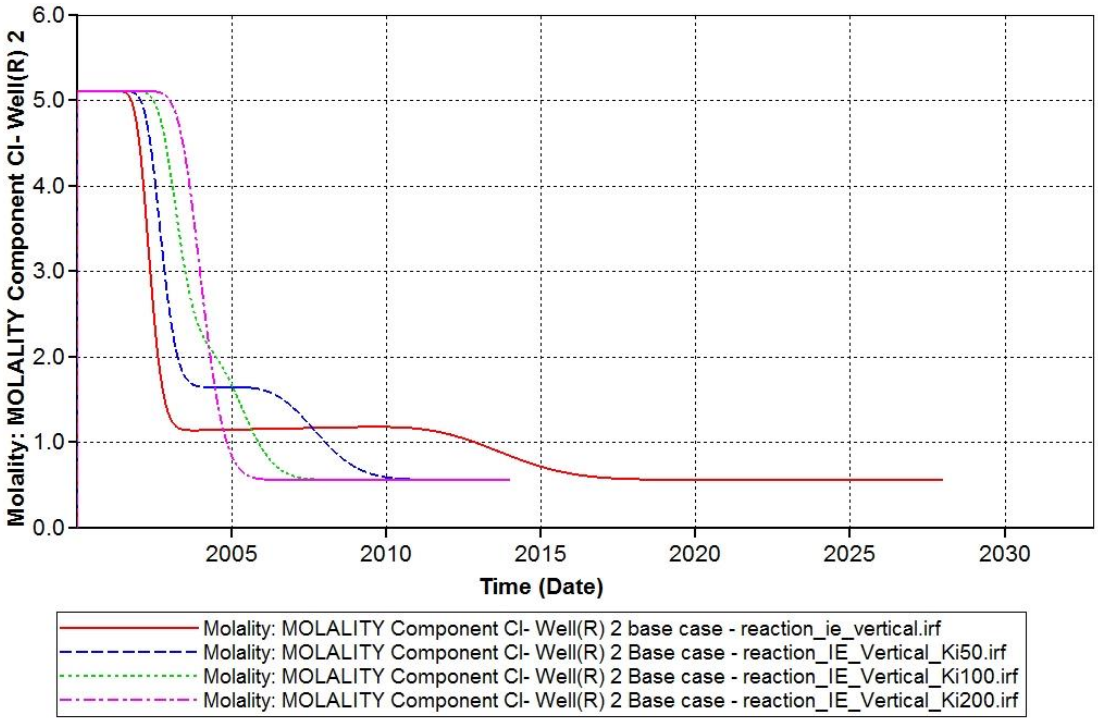

Figure 5.35 The evolution of produced chloride concentration with varying permeability of bottom layer.

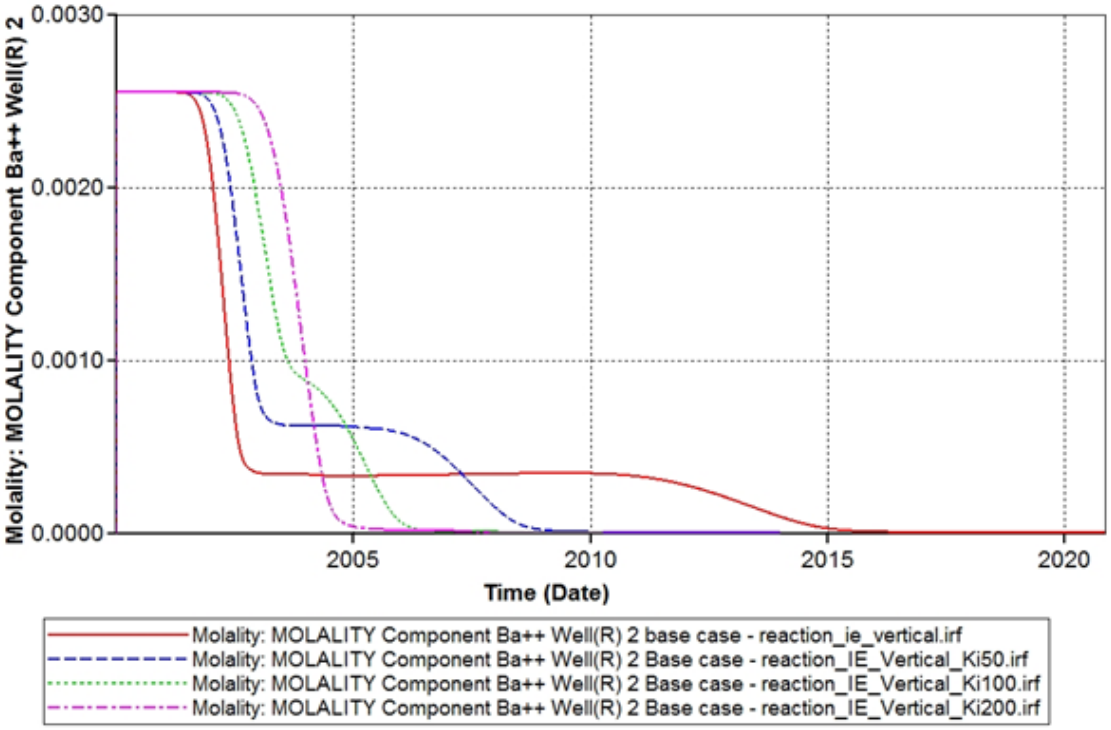

Figure 5.36 The evolution of produced barium concentration with varying permeability of bottom layer.

Barium concentrations were plotted against chloride concentrations in **Figure 5.37** so as to illustrate what the impact of horizontal heterogeneity on chemical reactivity is. It is clear that less ion stripping relative to the pure mixing line (black line) means less precipitation and higher concentration of scaling ions that reach the production well in the two-dimensional vertical model with heterogeneity. This makes scale management more difficult, as it demonstrates that more scale precipitation will occur in the wellbore in a heterogeneous system such as this. It is worth noting that it is not the system with the highest degree of heterogeneity (low permeability of 20 mD), but the one with the intermediate degree of heterogeneity (low permeability of 100 mD), that will produce the highest scaling ion concentrations.

In summary, in the one-dimensional reactive transport model where chemical reactions are allowed to occur in a single flow path, the possible impact of geochemical reactions was overestimated since mixing at the producer due to difference in arrival times along different streamlines is not considered. In other words, a more realistic heterogeneous model will identify that higher scaling ion concentrations may be observed in the production wells under real reservoir conditions than would be predicted by a one-dimensional model.

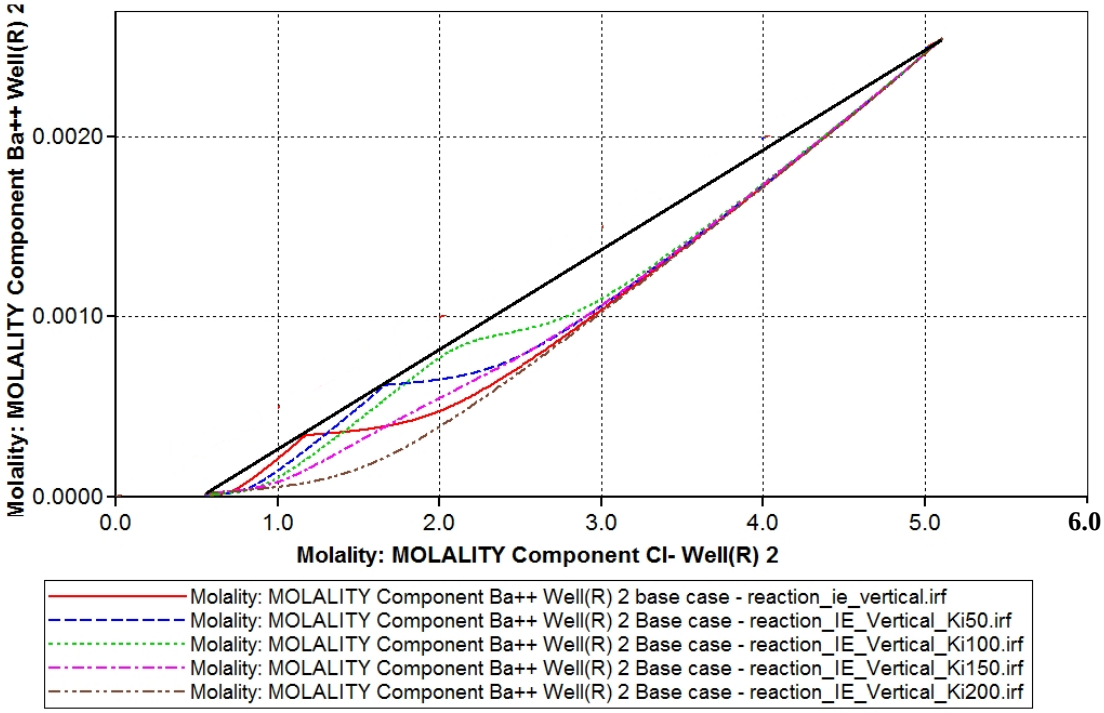

Figure 5.37 Barium concentrations vs chloride concentrations with varying permeability of bottom layer.

A second sensitivity study addresses vertical permeability, where two layers with fixed horizontal permeability (100 mD and 200 mD) were defined, but where the vertical communication was varied, ranging from 0 mD to 200 mD. **Figure 5.38** suggest that there is not a big discrepancy in produced water composition with varying vertical permeability (from 20 mD to 200 mD). The variation in vertical communication has a much smaller impact on the brine mixing and evolution of produced water composition than varying the horizontal permeability. Most of the brine mixing occurs laterally and not vertically, even in the case with a vertical permeability of 200 mD (dark blue line), so the produced brine composition and the occurrence of geochemical reactions is largely determined by horizontal mixing processes, and not by mixing in the vertical direction.

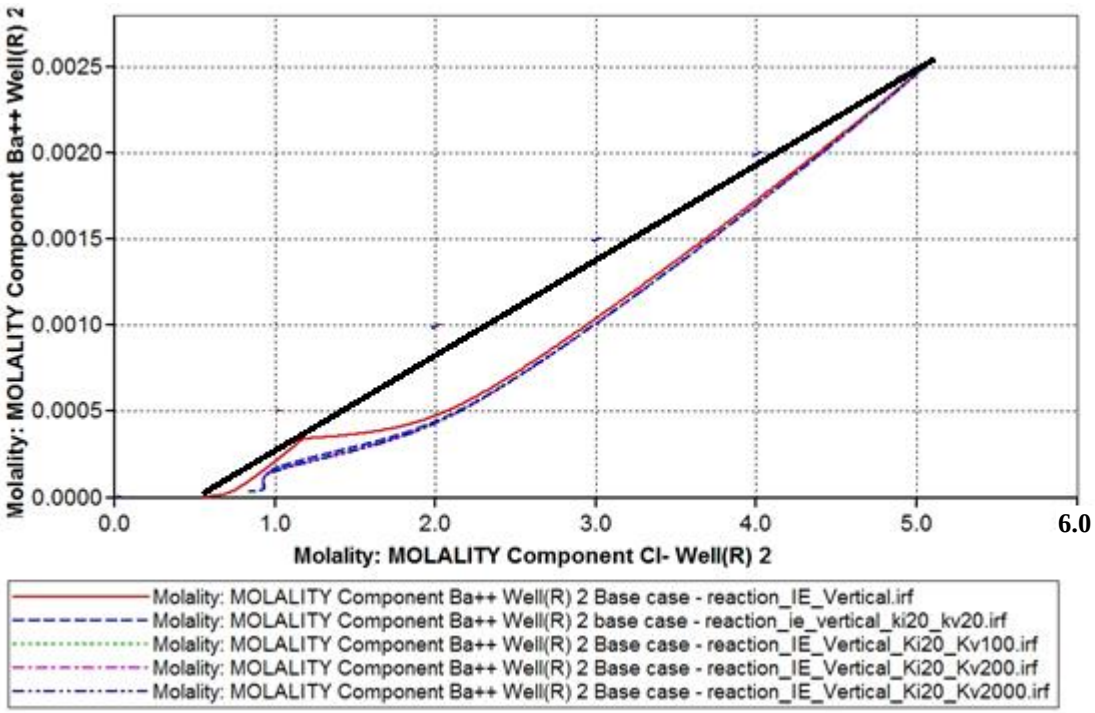

Figure 5.38 Barium concentrations vs chloride concentrations with varying vertical permeability.

5.6 Conclusions

Gyda is a relatively deep, hot, heterogeneous and intensely faulted oilfield in the North Sea with generally poor reservoir quality and considerable structural complexity, according to the reviewed geological information. Various formation water compositions have been identified by analysis of the produced water dataset, collected from 16 wells.

It is understood that one formation water is present within the Downdip and Crestal area, where there is good reservoir connectivity. The second formation water is in the South Gyda region, and it is significantly different from the other two. There is some uncertainty in the formation water composition in the C-sand and South West regions, since analysis shows similar compositions to the main reservoir section, with the exception of magnesium.

CMG GEM, a commercial compositional reservoir simulator, is used to model various chemical equilibria and mineral precipitation/dissolution reactions occurring in the Gyda field. This provides an opportunity to simulate geochemical reactions and fluid flow using a reservoir simulator, and lays the foundation for coupling modelling of geochemical reactions and fluid flow using the full field reservoir simulation model. The following are the conclusions of this modelling study of the Gyda field and analyses of produced water data.

1. Anhydrite and barite precipitation were the two dominant mineral reactions taking place deep within the reservoir. Sulphate is the limiting ion, with barium and calcium in excess during anhydrite and barite deposition. This is the reason for the produced sulphate profiles, with almost no sulphate being produced in some wells, up to IWFs of 40-50%; thereafter the sulphate concentration remains low, and the trend is dissimilar to the trends in other sandstone reservoirs in the North Sea region and elsewhere. The solubilities of anhydrite and barite for the three formation waters were increased through increasing the SR of anhydrite and barite. Thus, a reasonable match between modelled and observed barium and sulphate concentrations in the three regions have been provided.
2. Celestite mineral reaction was not predicted, although the strontium concentration in the formation water is very high relative to other North Sea sandstone reservoirs. This is because strontium is unable to compete successfully with barium and calcium in the sulphate mineral precipitation reactions.
3. Magnesium stripping may be a result of multicomponent ion exchange, dolomite precipitation or a combination of both. The simulation results illustrate that the occurrence of dolomite precipitation mainly depends on the presence of calcite, so the dolomite can probably be precipitated in or close to the calcite stringers. Multicomponent ion exchange dominates the removal of magnesium in reservoir rocks with abundant clays.

4. Reservoir temperature was lowered during cold water injection. The solubility of anhydrite increases at lower temperature, and anhydrite will gradually dissolve in response to the movement of the temperature front, which is much slower than the formation/injection water mixing front.
5. The extent of mineral precipitation within the reservoir can be reduced by the heterogeneity; the modelling shows that the extent of ion stripping caused by mineral reactions in the reservoir is greatest when simulating a single uniform layer. Brine mixing and the occurrence of geochemical reactions due to vertical mixing were not observable, even when assigning a high vertical permeability in a heterogeneous model.

CHAPTER 6 GEOCHEMICAL REACTIONS OCCURRING IN EKOFISK FIELD

6.1 Introduction

In previous chapters, studies were all focused on sandstone reservoirs where the mineral composition is normally dominated by quartz. Feldspars, composed mainly of K-feldspar with minor amounts of plagioclase and some clay (Illite and Kaolinite) may also be present in the bulk rock. Normally the increase in pH resulting from seawater injection is not enough to dissolve quartz and feldspar so there is little possibility of dissolving quartz/feldspar and silicate scales during conventional seawater flooding. However, in carbonate reservoirs where calcite and/or dolomite are mainly present in the reservoir rock, they are readily reacted with injected brine (including seawater). Not only fluid/fluid interactions, but also fluid/rock interactions need to be considered when conducting a geochemical study on a carbonate reservoir. Compared with sandstone reservoirs, more extensive reservoir interactions may be occurring in the carbonate system. Mackay et al. (2014a) used the geochemical modelling of CO_2-WAG injection in predicting the scaling potential in carbonate reservoirs. However, the produced water data were not presented and compared with the simulation results. Multicomponent ion exchange reaction was not considered in the geochemical model, which probably led to higher magnesium concentration in the effluent. In addition, it was not correct that only gypsum mineral reactions was modelled for consuming calcium.

Therefore, a full produced water dataset collected from the Ekofisk field, a chalk reservoir, is presented and analysed in this chapter. A one dimensional reactive transport model is developed to model any possible fluid/fluid and fluid/rock interactions taking placing in the reservoir when seawater is injected into the oil leg or close to the oil water contact, and the produced water chemistry simulated by model is well matched with observed data.

6.2 Field description

The Ekofisk field in the Norwegian sector of the North Sea is an overpressured naturally fractured chalk reservoir. The reservoir consists of two fine-grained limestone producing formations, the Ekofisk formation (Danian Age) and the Tor formation (Maastrichtian Age), separated by a thin, impermeable Tight Zone (Agarwal et al., 1999). A pilot water injection project began in April 1981 in the highly fractured Tor formation and in the

Lower Ekofisk in June 1986. Field wide waterflooding started in 1987 (Hallenbeck et al., 1991).

The Ekofisk is a low permeability fractured chalk reservoir with matrix permeabilities which ranges from 0.1 to 10 md. Effective permeabilities are 2 to 50 times the chalk matrix permeability. Vertical permeability ranges from 0.1 to less than 0.01 times that of the horizontal effective permeability. Reservoir porosities range between 30% and 45% (Christian et al., 1993).

Five major geological layers are present in the Ekofisk and there are three layers in the Tor formation. The upper three Ekofisk layers are referred to as EA, EB and EC. These intervals are characterized by high silica content, chert lenses, 25-30% porosity and moderate fracturing and in total average ~400 feet thick. These are referred to as the Upper Ekofisk. The Lower Ekofisk is the fourth Ekofisk layer, referred to as Layer ED. This interval is characterized by uniform porosity distributions in excess of 30%, water saturations initially below 10%. The thickness is typically in excess of 100 feet. The fifth and lowest layer in the Ekofisk Formation is known as the 'Tight Zone' (Layer EE). This layer varies between 50 and 100 feet in thickness, and is composed of low porosity, low permeability autochthonous chalks which restrict pressure communication between formations throughout most of the field. A cross-section of the pilot wells showing the five Ekofisk layers is presented in **Figure 6.1**. The Tor is sub-divided into three layers, the uppermost of which (the TA layer) is primarily composed of reworked chalk sediments and forms the best reservoir quality. Porosities between 25 and 35% and water saturations between 15 and 30% are typical, with between 300 and 500 feet of oil bearing chalk at the crest of the structure (Sylte et al., 1988).

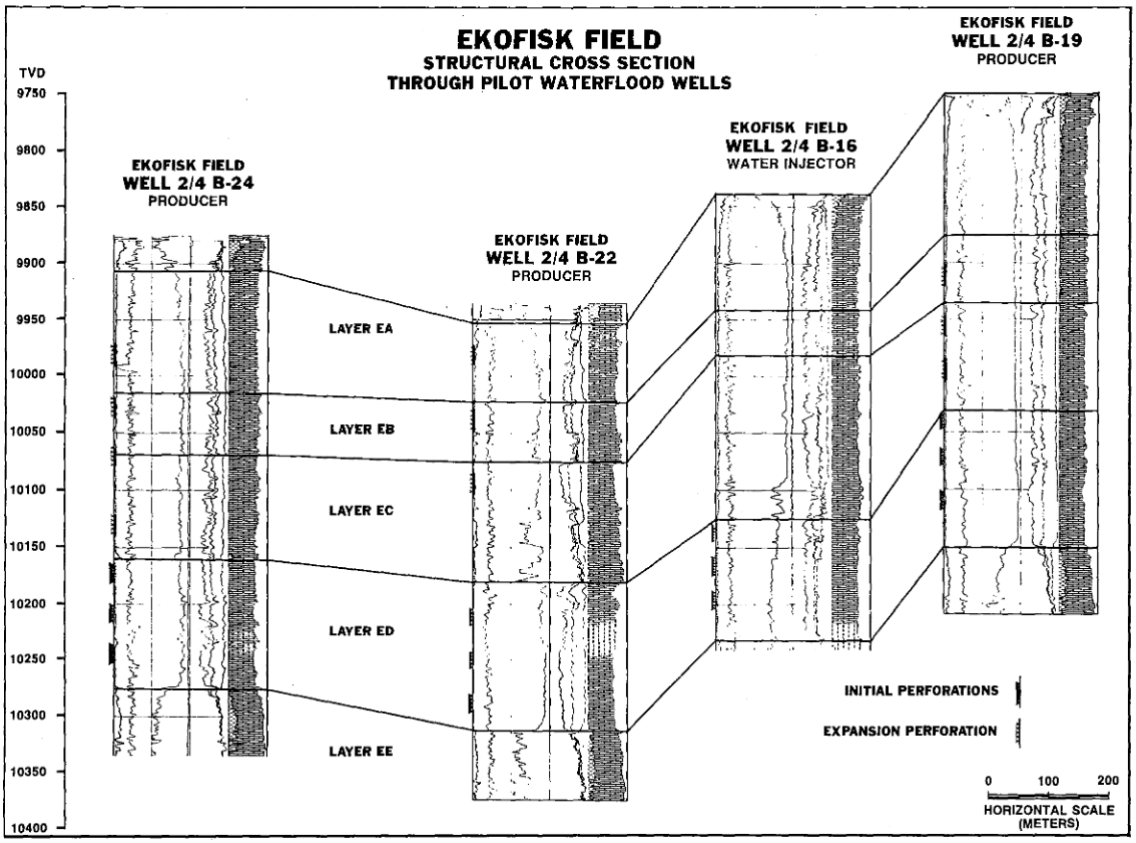

Figure 6.1 Cross sectional view of CPI's through the Ekofisk formation (Sylte et al., 1988).

6.3 Produced water chemistry

Produced water started to be sampled in the Ekofisk field from 1993 in order to monitor the evolution of produced brine and assess potential scale risk in the production wells. Information including pH, resistivity and aqueous component concentrations were collected in the produced water dataset of the Ekofisk field, where more than 2880 produced water sample data were stored from over 110 wells.

The big difference in chloride concentration between formation water and injection water makes it a potentially reliable natural tracer to identify how much of the produced water is coming from formation water and/or injection water, so each sampled ion concentration was plotted against the corresponding chloride value to detect if there is any loss or gain of this ion in the produced brine besides the effects due to pure dilution of formation water and injection water.

Sodium, calcium, strontium and barium concentrations in the produced water all decline with the decrease in chloride concentration. However, magnesium and sulphate are significantly depleted in the produced water since their behaviours appear to lie much

below their pure mixing lines. Slight barium stripping can be observed relative to its pure mixing line.

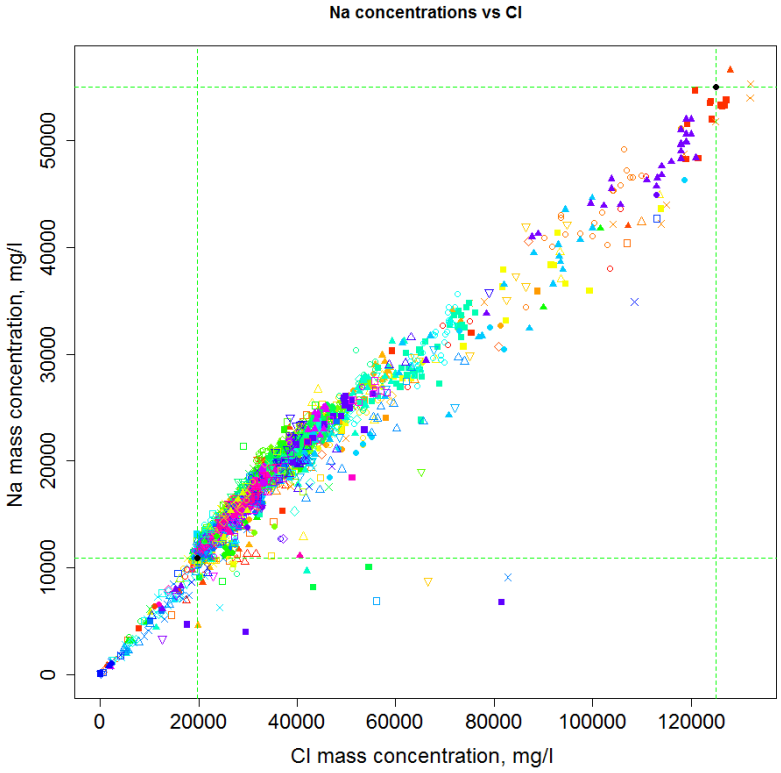

Figure 6.2 Sodium concentration vs Chloride concentration (different wells identified by colours).

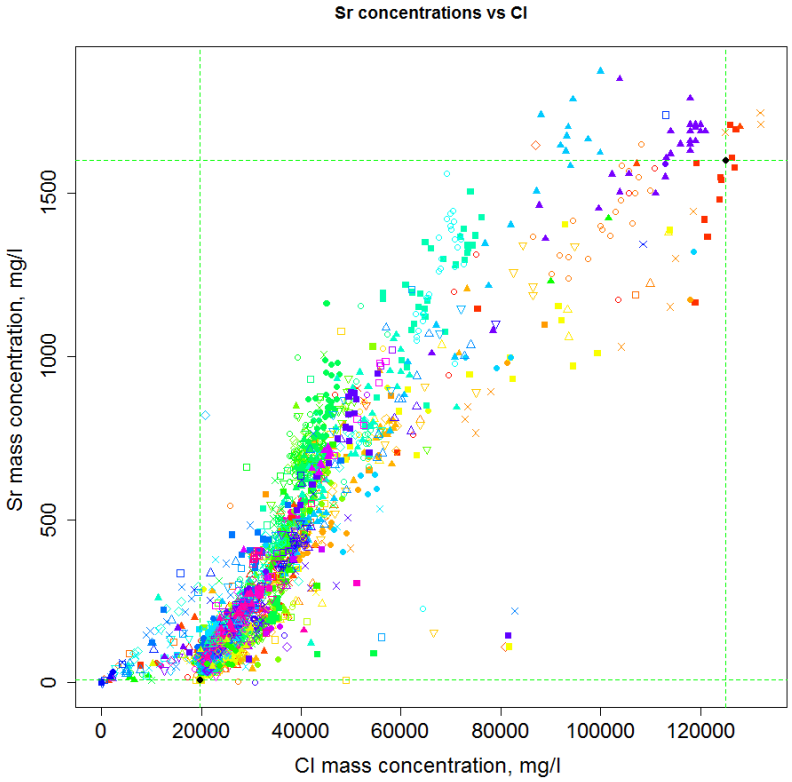

Figure 6.3 Strontium vs Chloride (different wells identified by colours).

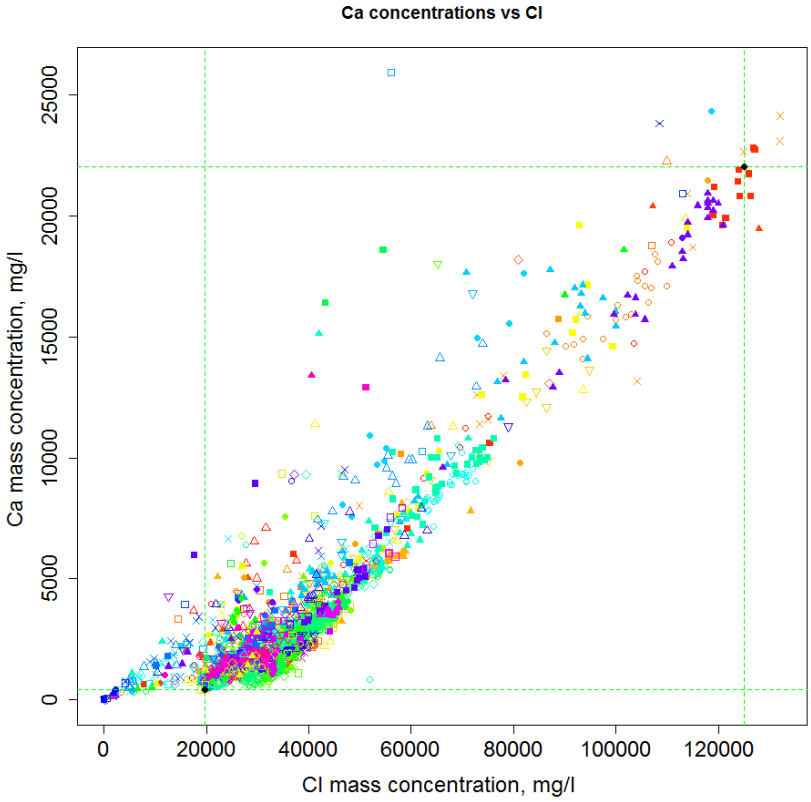

Figure 6.4 Calcium vs Chloride (different wells identified by colours).

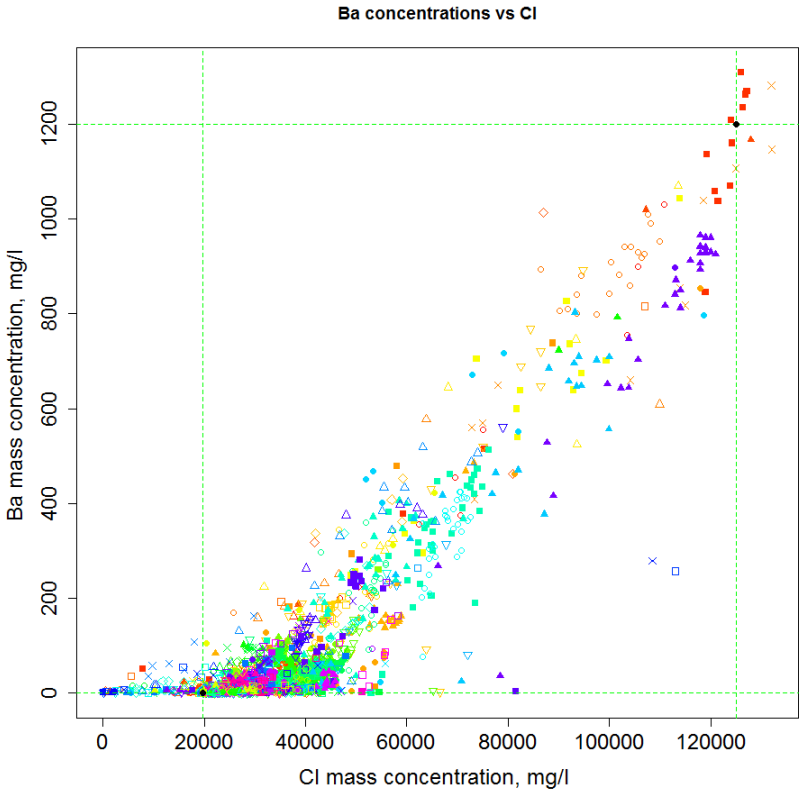

Figure 6.5 Barium vs Chloride (different wells identified by colours).

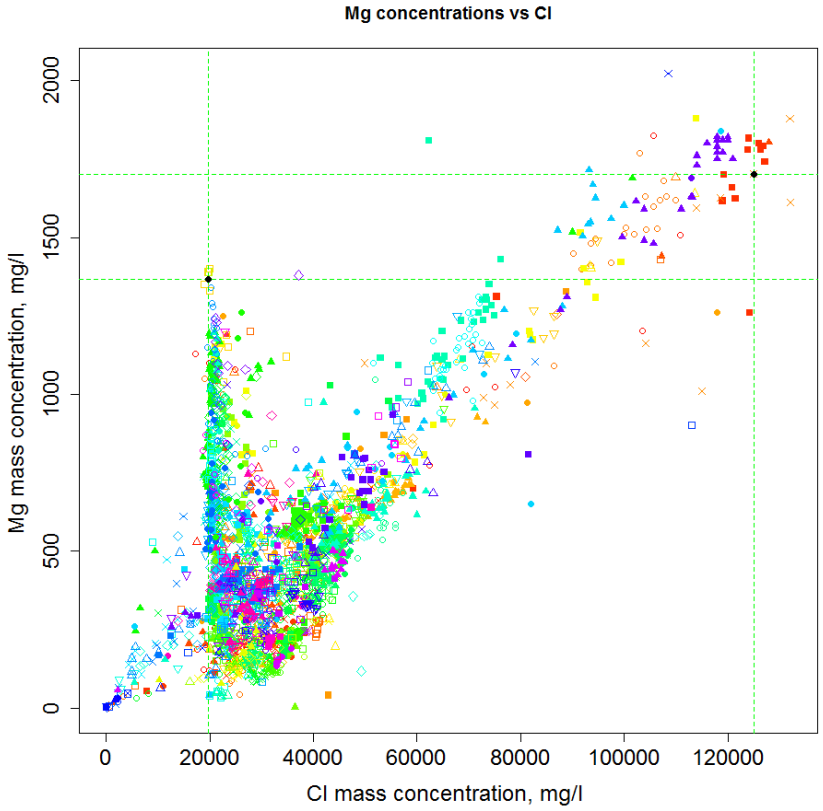

Figure 6.6 Magnesium vs Chloride (different wells identified by colours).

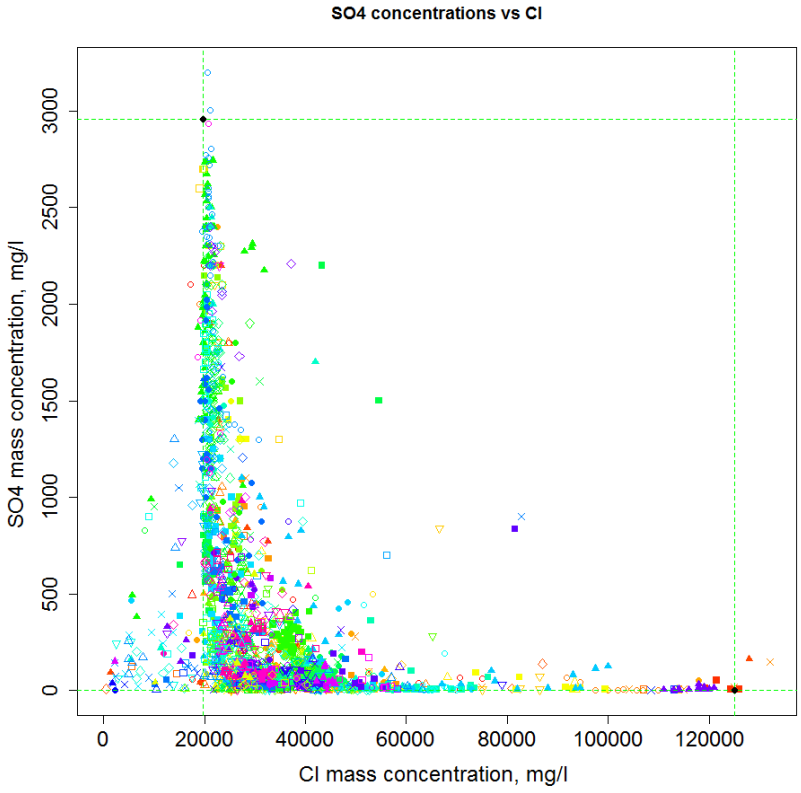

Figure 6.7 Sulphate vs Chloride (different wells identified by colours).

6.4 Modelling approach and scenarios

A one dimensional reactive transport model was developed where the single flow path from injector to producer was made up of 50 blocks in order to identify which reactions were required to reproduce observed produced water chemistry data. The first solution (North Sea water) was defined and injected into first block. The second kind of solution (Ekofisk formation water) was defined to be initially present in each block and they would be mixed and displaced by injected seawater. The initial reservoir mineralogy (calcite predominantly) was specified as well in all 50 blocks and CO_2 gas phase was also initially defined so as to consider the partitioning of CO_2 from the hydrocarbon phase into the brine within the reservoir. The thermal model in PHREEQC was included in some modelling scenarios to consider temperature front and effects. The mineral precipitation and dissolution reactions in **Table 6.1** were included in the model and discussed in detail later based on the simulation results of different modelling scenarios.

Table 6.1 Mineral reactions included in the model.

Mineral	Chemical formula	Mineral reactions
Barite	$BaSO_4$	$BaSO_4 = Ba^{2+} + SO_4^{2-}$
Celestite	$SrSO_4$	$SrSO_4 = Sr^{2+} + SO_4^{2-}$
Anhydrite	$CaSO_4$	$CaSO_4 = Ca^{2+} + SO_4^{2-}$
Calcite	$CaCO_3$	$CaCO_3 = CO3^{2-} + Ca^{2+}$
Magnesite	$MgCO_3$	$MgCO_3 = CO3^{2-} + Mg^{2+}$
Dolomite	$CaMg(CO_3)_2$	$CaMg(CO_3)_2 = Ca^{2+} + Mg^{2+} + 2\ CO_3^{2-}$
Huntite	$CaMg3(CO_3)_4$	$CaMg_3(CO_3)_4 + 4\ H^+ = Ca^{2+} + 3\ Mg^{2+} + 4\ HCO_3^-$

6.4.1 Heat transport

In actual reservoirs with seawater injection, the reservoir rock is cooled by cold injection water and in turn the injected seawater heats up in the reservoir. Therefore, the reservoir temperature constantly decreases. However, the change in temperature does not occur at the same speed as the propagation of the brine mixing front, since it is retarded due to heat exchange with reservoir rock. The extent of retardation is determined by the porosity and thermal properties of reservoir rocks, which are primarily heat capacity, thermal conductivity and diffusivity.

In the one dimensional reactive transport model developed in this study, an exchange of heat is allowed to take place that will cause the temperature of the cell to change as transport progresses. Two parameters which can be defined for calculating the diffusive part of heat transport are the temperature retardation factor and the thermal diffusion coefficient (Equation 1.30 and 1.31).

6.4.2 Initial carbonate chemical equilibrium

6.4.2.1 Formation water

The concentration of bicarbonate, the amount of dissolved CO_2 and the pH were not measured for the formation water samples in the field. The results of the measurements are probably not to be considered as a representation even if they were available, as there is a large difference in the carbonate species concentration between standard and reservoir conditions. Normally water samples may be collected under downhole or more usually surface conditions, but are certainly measured in the onshore laboratory at standard conditions.

In theory, there exists a chemo-physical equilibrium between initial formation water, oil, and gas and reservoir rock at the initial reservoir conditions before oil production. The carbonate system in the reservoir is composed of carbonated species and calcium concentration in formation brine, CO_2 in the hydrocarbon phase and calcite in the reservoir rock. Calcite would not tend to precipitate or dissolve initially, but had reached the chemical equilibrium, which indicates that saturation index (SI) of calcite should be zero under the initial reservoir conditions. Therefore, a set of equilibrium conditions can be calculated on the basis of fixed calcium (known) concentration in formation water and varying CO_2 content in the reservoir which is unknown to us for the Ekofisk field. Equation 6.1 and 6.2 present the relationship between the Saturation Index of CO_2 and the partial pressure of CO_2 which is the product of the reservoir pressure and the CO_2 content.

$$SI(CO_2) = \log_{10} P_{CO_2} \tag{6.1}$$

$$P_{CO_2} = P_{Reservoir} \times n_{CO_2} \tag{6.2}$$

For each equilibrium listed in **Table 6.2**, carbonate species in the formation water were obtained based on one specific value for CO_2 content. This is a reasonable method to

identify the carbonate concentration in formation water, and I use this on the premise that I have no information on the accurate measurement of carbonate concentration (CO_2, CO_3^{2-}, HCO_3^- and pH) in the reservoir.

Table 6.2 Initial carbonate concentration in formation water equilibrated with calcite and CO_2 gas phase.

PCO_2 atm	$SI(CO_2)$	Total C mol/kwg	HCO_3 mol/kwg	Dissolved CO_2 mol/kwg	pH
0.1452	-0.83803	0.000692	0.000178	0.000512	5.492
2.42	0.383815	0.009218	0.000722	0.008495	4.881
4.84	0.684845	0.01792	0.001017	0.0169	4.731
14.52	1.161967	0.05147	0.001732	0.04974	4.494
24.2	1.383815	0.08348	0.002198	0.08128	4.385

6.4.2.2 Injected seawater

Seawater is equilibrated with air containing only 0.03% CO_2 under standard atmospheric condition at 1 atm and 25°C. However, the initial equilibrium will be broken if seawater is injected into the subsurface where it is under reservoir conditions (484 atm and 131°C in the case of Ekofisk field). CO_2 may be dissolved into the seawater from the hydrocarbon phase and calcite may be dissolved (on contact with seawater) or precipitated as a result of the variation in the composition and temperature of the injected seawater.

Voidage is normally replaced during water flooding, so it is reasonable to assume that reservoir pressure remains approximately constant. However, reservoir temperature would be decreased during continuous seawater injection at low temperature (25^{o}C). Both isothermal and non-isothermal models will be developed and run so as to make comparison to highlight the effects of temperature on the geochemical reactions.

Table 6.3 shows concentrations of carbonate species in seawater equilibrated with CO_2 gas whose partial pressure ranges from 0.15 to 24.2 atm (corresponding to CO_2 content ranging from 0.03% to 5.00%). It is noted that reacted seawater would be under-saturated with carbonate minerals if the CO_2 content in the reservoir is slightly higher than 0.1452 atm (atmospheric condition). CO_2 partial pressure is determined by both of reservoir pressure and CO_2 content, so the high reservoir pressure (484 atm) in the Ekofisk field

could lead to a large amount of CO_2 being dissolved in the injected seawater even if the reservoir fluids do not contain a high concentration of CO_2.

Table 6.3 Carbonate concentration in reacted seawater equilibrated with CO_2 gas phase in the reservoir at 131°C

CO2 content	PCO2 atm	SI(CO2)	Total C mol/kgw	HCO3 mol/kgw	Dis CO2 mol/kgw	CO3 mol/kgw	H+ mol/kgw	OH- mol/kgw	Alkalinity	pH	SI(Calcite)
0.03%	0.15	-0.84	3.15E-03	2.32E-03	8.11E-04	6.01E-06	4.02E-07	1.75E-05	2.34E-03	6.58	0.21
0.05%	0.24	-0.62	3.68E-03	2.32E-03	1.35E-03	3.62E-06	6.67E-07	1.05E-05	2.34E-03	6.36	-0.01
0.10%	0.48	-0.32	5.03E-03	2.34E-03	2.68E-03	1.84E-06	1.32E-06	5.31E-06	2.34E-03	6.06	-0.31
0.50%	2.42	0.38	1.57E-02	2.35E-03	1.34E-02	3.72E-07	6.56E-06	1.07E-06	2.34E-03	5.37	-1
1.00%	4.84	0.68	2.90E-02	2.35E-03	2.66E-02	1.88E-07	1.30E-05	5.39E-07	2.34E-03	5.07	-1.29
3.00%	14.52	1.16	8.11E-02	2.38E-03	7.88E-02	6.51E-08	3.80E-05	1.84E-07	2.34E-03	4.60	-1.75
5.00%	24.20	1.38	1.31E-01	2.40E-03	1.28E-01	4.10E-08	6.13E-05	1.14E-07	2.34E-03	4.40	-1.94

The temperature of injected seawater is normally at 25ºC, so the regions close to the injector will be gradually cooled by the injected seawater. The concentrations of carbonate species, pH and saturation index of calcite for reacted seawater with equilibrated with varying CO_2 partial pressure have been calculated and presented in **Table 6.4**.

Table 6.4 Carbonate concentration in reacted water equilibrated with CO_2 gas phase in the reservoir at 25°C.

CO2 content	PCO2 atm	SI(CO2)	Total C mol/kgw	HCO3 mol/kgw	Dis CO2 mol/kgw	CO3 mol/kgw	H+ mol/kgw	OH- mol/kgw	Alkalinity	pH	SI(Calcite)
0.03%	0.15	-0.84	4.78E-03	2.34E-03	2.44E-03	9.33E-07	1.59E-06	2.12E-08	2.34E-03	5.89	-1.59
0.05%	0.24	-0.62	6.39E-03	2.34E-03	4.04E-03	5.64E-07	2.64E-06	1.28E-08	2.34E-03	5.67	-1.81
0.10%	0.48	-0.32	1.04E-02	2.35E-03	8.06E-03	2.84E-07	5.25E-06	6.42E-09	2.34E-03	5.37	-2.11
0.50%	2.42	0.38	4.23E-02	2.36E-03	4.00E-02	5.82E-08	2.58E-05	1.31E-09	2.34E-03	4.68	-2.79
1.00%	4.84	0.68	8.11E-02	2.40E-03	7.87E-02	3.03E-08	5.02E-05	6.71E-10	2.34E-03	4.39	-3.07
3.00%	14.52	1.16	2.28E-01	2.48E-03	2.25E-01	1.14E-08	1.38E-04	2.43E-10	2.34E-03	3.95	-3.47
5.00%	24.20	1.38	3.55E-01	2.55E-03	3.53E-01	7.71E-09	2.10E-04	1.59E-10	2.34E-03	3.78	-3.62

I have performed a series of simulations (shown in **Table 6.5**) to study the presence of calcite as a primary mineral, dolomite and huntite mineral reactions, thermal effects of injection water and impact of CO_2. The Ekofisk field has similar formation water composition to the Gyda field. Both of them have relatively high calcium, barium and strontium concentrations. The mineralogical composition of the Ekofisk reservoir is

dominated by calcite (>95%) as it is a carbonate reservoir field, but calcite is only present in calcite stringers (<1%) or cements in the Gyda field. The substantial source of initial calcite in the Ekofisk reservoir carbonate rocks provides the opportunity for injected seawater to dissolve calcite continuously, so it is necessary to investigate what factors affect calcite dissolution and what effect dissolving calcite has on the other geochemical reactions.

Table 6.5 Modelling scenarios.

Modelling scenario	Initial calcite	Dolomite + Huntite reactions	Thermal effects	CO_2 in gas phase	CO_2 Partial pressure, atm
1	×	×	×	negligible	4.84
2	×	×	✓	negligible	4.84
3	✓	×	×	negligible	4.84
4	✓	×	×	excess	4.84
5	✓	×	✓	negligible	4.84
6	✓	×	✓	excess	4.84
7	✓	✓	✓	excess	4.84

6.5 Modelling results

6.5.1 Presence of initial calcite

In modelling Scenario 1, there are only three sulphate scaling reactions: barite, celestite and anhydrite precipitate that were included, and the entire system is at the relatively high temperature of 131ºC. Barite, celestite and anhydrite were all precipitated due to brine mixing of formation water containing barium, strontium and calcium and injected seawater rich in sulphate, and both of celestite and anhydrite would then dissolve in pure seawater.

Calcite mineral precipitation and dissolutions reactions were allowed to occur in the modelling scenario 3 where calcite was initially present in each block. Temperature change induced by injection was not considered in the case. **Figure 6.8** shows how calcite and anhydrite change and pH behaviour against injected pore volume in the first block. A small amount of calcite is precipitated from the injected seawater due to constant reservoir temperature of 131ºC and unavailability of a CO_2 gas phase in the model. pH sharply increases from 5.5 (formation water) to 7.5 (injected seawater) due to brine mixing, subsequently keeping a stable and slow increase as calcite precipitates. In this

scenario, not much difference is observed due to the sulphate scaling reactions (barite, celestite and anhydrite) from. The following scenarios (4 and 5) model the impact of CO_2 and temperature changes respectively, which are believed to be the two main factors that affect the calcite mineral reaction.

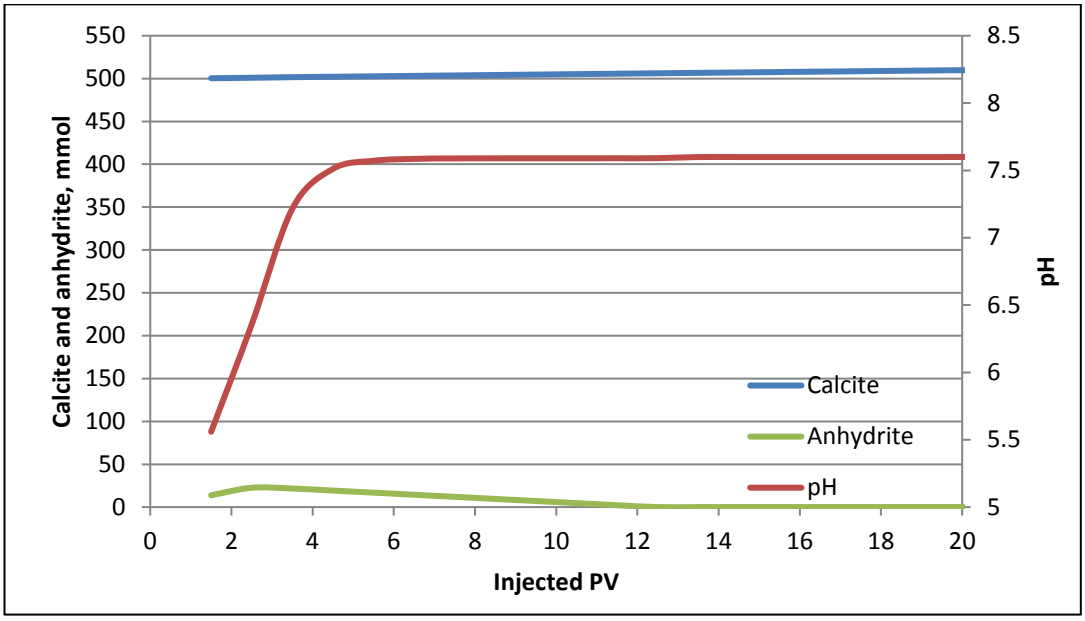

Figure 6.8 Simulation results at first block from modelling scenario 1.

6.5.2 Thermal effect

The simulation results from scenario 5 are shown in **Figure 6.9**. The temperature in the first block is rapidly deceased to 25°C due to cool seawater injection. The solubility of calcite increases as temperature decreases, so we can observe that a small amount of calcite dissolves into injected seawater at 25°C. Compared with scenario 3, a greater increase in pH is achieved which is caused by calcite dissolution. Anhydrite does not precipitate as much due to its higher solubility at lower temperature (25°C). In this case, in which the thermal model is included but CO_2 is not present in the gas phase, the initial calcite defined as the primary mineral phase is dissolved into injected cool seawater. However, the small amount of calcite dissolution does not significantly affect barite, celestite and anhydrite mineral reactions.

The effects of temperature on the precipitation and dissolution of anhydrite mineral have been discussed in detail in the previous chapters, which concentrated on the investigation of geochemical reactions taking place in the Gyda field. Similar conclusions as for sandstone reservoirs could also be derived for in this chalk field without the consideration of carbonate reservoir mineralogy (>95% calcite in the primary mineral phase). The

amount of anhydrite precipitation decreases in the non-isothermal modelling scenario. This leads to more barite and celestite precipitated due to greater availability of sulphate ions in the aqueous phase. The most striking difference with the Gyda field is that anhydrite cannot be precipitated by injected seawater itself since the Ekofisk field (131°C) is not at as high temperature as the Gyda field (160°C).

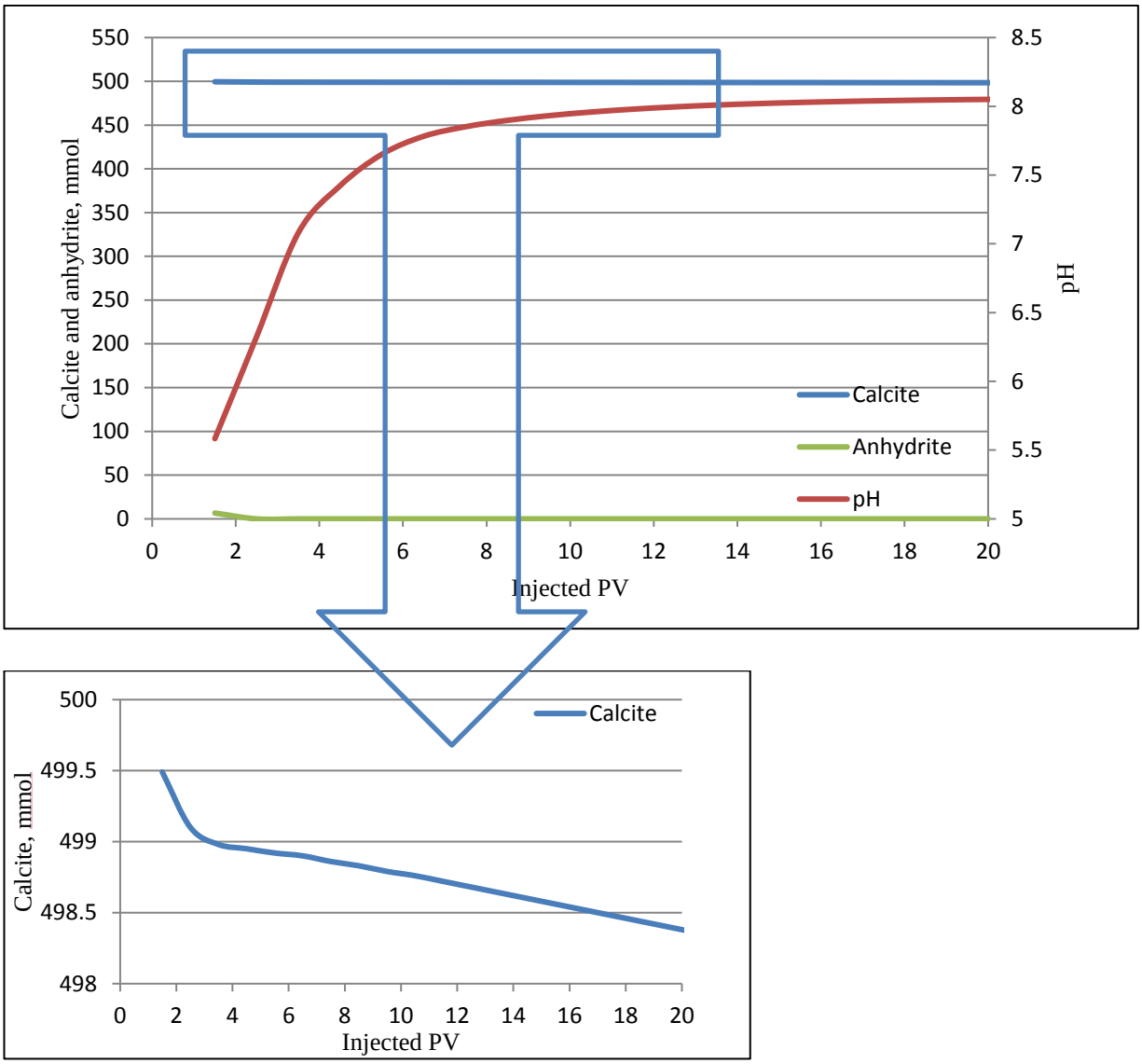

Figure 6.9 Simulation results at first block from modelling scenario 5.

6.5.3 Impact of CO_2 interaction

The impact of CO_2 interactions deep within the reservoir is often neglected in both of experimental and modelling studies. However, in reality, the partitioning of CO_2 from the

hydrocarbon phase into injected seawater has a significant impact on the carbonate aqueous chemical and mineral reactions. In carbonate reservoirs, such as the Ekofisk field focused on here, calcite dominates the mineralogy of the reservoir rocks (>95%), which indicates a large source of potentially reactive mineral is present in the reservoir. The calcite will be dissolved provided the pH of the injected seawater decreases due to more dissolution of CO_2. Therefore, the impact of CO_2 interactions deep in the reservoir must be considered and the initial CO_2 in the hydrocarbon phase needs to be included in the model. Otherwise, the dissolution of calcite will be significantly underestimated.

The model presented in this chapter was developed using PHREEQC, which is a one dimensional single phase reactive transport model that does not have the capability to model gas (CO_2) transport. This indicates that the gas phase would be equilibrated with the solution entering the specific block but it would not be displaced into the next block. Therefore, the assumption we made in this study is that there is unlimited CO_2 available for equilibrating with injected seawater, which will thus immediately reach the equilibrium with the CO_2 phase (in the hydrocarbon) once contacting with the CO_2 gas phase, and the transport of the gas phase (including CO_2 and hydrocarbon) is not considered. The partitioning of CO_2 from the hydrocarbon phases into injected brine and its impact on the dissolution of calcite within the reservoir will be studied and discussed in detail through developing the CMG GEM model in the next chapter since detailed hydrocarbon composition can be defined in the reservoir compositional model.

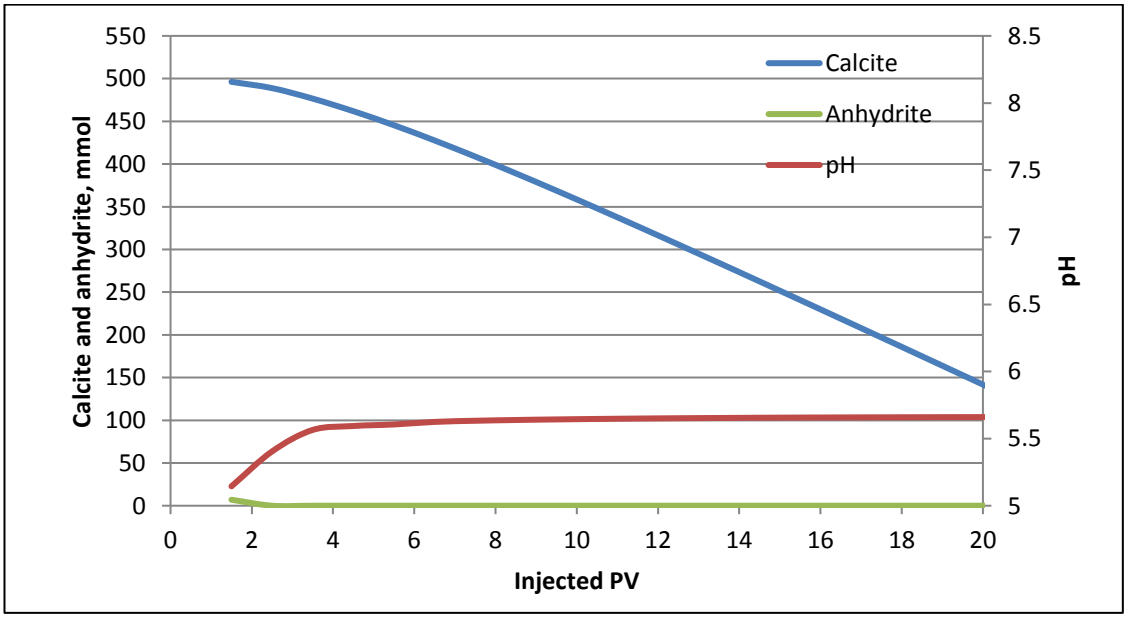

Figure 6.10 Simulation results at first block from modelling scenario 6.

It is worth noting that using the CO_2 buffer model most likely approximates conditions within the hydrocarbon-leg or close to the OWC. Between 1-5 mol% CO_2 is appropriate given the reservoir temperature so we would expect injected seawater to be a sink for CO_2 originally in the hydrocarbon phases. In the modelling Scenario 6, the excess CO_2 is added into the gas phase on the basis of the previous case (Scenario 5) in order to make sure that CO_2 present in the hydrocarbon phase is dissolved into injected seawater. It can be easily found from **Figure 6.10** that in the first block (injector) a large amount of calcite dissolves into seawater in this case and lower pH is retained when all of the initial formation water is displaced, due to the presence of CO_2. There is still not much anhydrite precipitated around the injector (first block) due to the low temperature (25^{o}C).

Figure 6.11 presents how calcite and anhydrite are precipitated or dissolved and how the temperature front propagates towards the production well. First of all, the temperature front is displaced more slowly than the mixing front. Therefore, at seawater breakthrough anhydrite precipitates due to mixing of formation water and injected seawater, and it will then dissolve when the (cool) temperature front reaches the location. On the other hand, the dissolution of calcite upstream (See **Figure 6.10**) provides a substantial source of calcium, leading to high calcium concentration in the equilibrated brine downstream. More and more calcite precipitates as temperature decreases because anhydrite has a higher solubility than calcite at relatively low temperature.

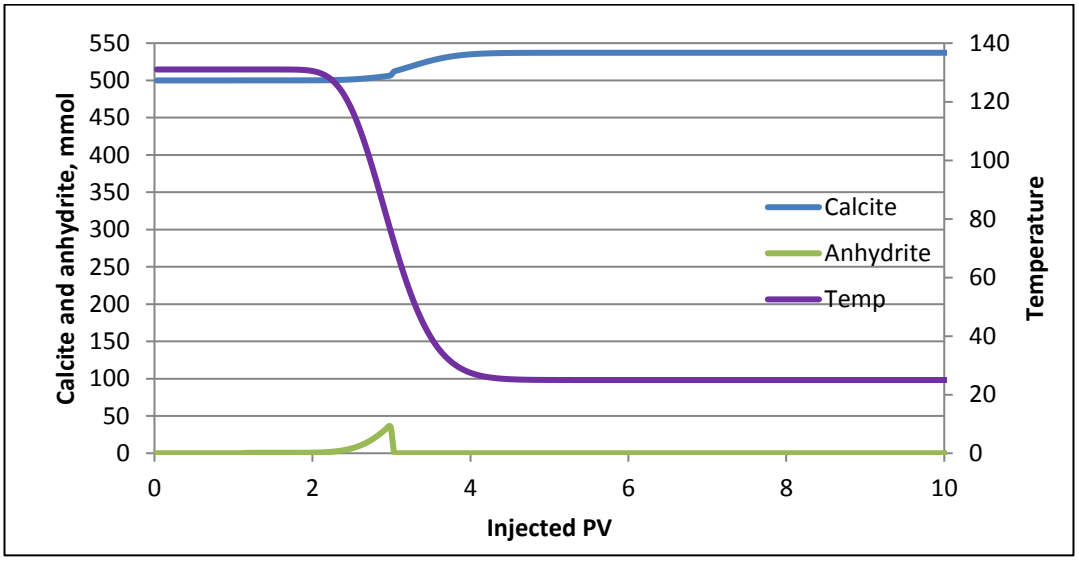

Figure 6.11 Simulation results at last block from modelling scenario 7.

6.5.4 Other carbonate mineral reactions (dolomite and huntite)

I have observed that calcite precipitated downstream due to calcite dissolution upstream from modelling scenario 6 in which calcite dissolution and precipitation is the only carbonate mineral reaction allowed to occur in the model. The calcite dissolving upstream gives rise to higher calcium and carbonate concentrations in the downstream flow (than initial calcium concentration in seawater) which will then trigger more carbonate mineral reactions as fluid temperature increases. Therefore, it is interesting to look into the solubility of some potentially reactive carbonate minerals, which commonly include magnesite, dolomite and huntite.

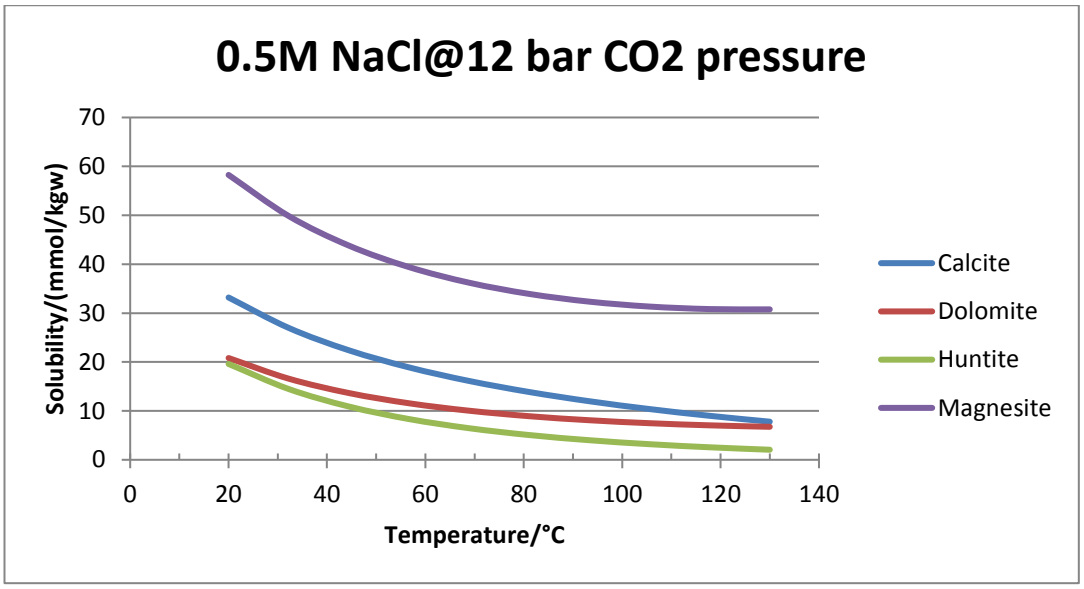

Figure 6.12 The solubility of calcite, dolomite, huntite and magnesite in 0.5 mol NaCl brine at 12 bar CO_2 partial pressure.

Figure 6.12 illustrates the solubility of calcite, dolomite, huntite and magnesite at different temperatures in 0.5 mol NaCl brine (equivalent to injected seawater) at 12 bar CO_2 pressure. First of all, the solubilities of the four minerals all decrease with increasing temperature, which suggests that heating up the injected seawater in the reservoir may lead to some precipitation. The solubility of magnesite is higher than 30 mmol per kg water and this is much higher than for the other three minerals. This indicates that magnesite is less likely to be precipitated in competition for the carbonate/bicarbonate with the other three minerals, even though magnesite precipitation was detected by SEM-EDS analysis in the core flooding experiments implemented by Madland et al. (2011).

The reservoir rock is constantly cooled by cold injection water, and thus more calcite will be dissolved in the brine over time. This is another reason why injected seawater dissolves

calcite in the reservoir, other than the pH of injected brine decreasing due to dissolution of CO_2 which has been discussed above. Calcite has higher solubility than dolomite and huntite, so dolomite and huntite are probably deposited when calcite is dissolved. I can find from **Figure 6.12** that at high temperature, the solubility of dolomite is higher than that of huntite and very close to that of calcite, but it gets closer to that of huntite and lower than that of calcite with the decrease of temperature. This observation may imply that huntite precipitation is dominant at the initial reservoir temperature of 130°C, but more and more dolomite precipitation will occur as the cool front of injection water moves towards the production well.

The dolomite and huntite mineral reactions are included in the modelling scenario 7 although both of them are commonly thought to be occurring only over the geological time scales. They are now modelled as equilibrium reactions in this study, so kinetics are not considered. **Figure 6.13** illustrates how much anhydrite, dolomite and huntite are precipitated in the last grid block from Scenario 6 and 7. Some huntite and dolomite precipitation can be found at relatively high and low temperatures, respectively.

Another important finding is that there is much more anhydrite precipitated in the Scenario 7. The explanation is that the precipitation of dolomite and huntite leads to more calcite dissolution, which indicates that there will be more calcium ions available in the brine and more anhydrite precipitates. It is evident that in the hydrocarbon-leg, conditions are primed for calcite dissolution and the extent of this reaction determines how much sulphate (a key scaling ion) is stripped in the reservoir due to anhydrite precipitation. The extent of the reaction will be determined by the nature of the carbonate sink (huntite, dolomite in our model) so it is important to understand this reaction in more detail.

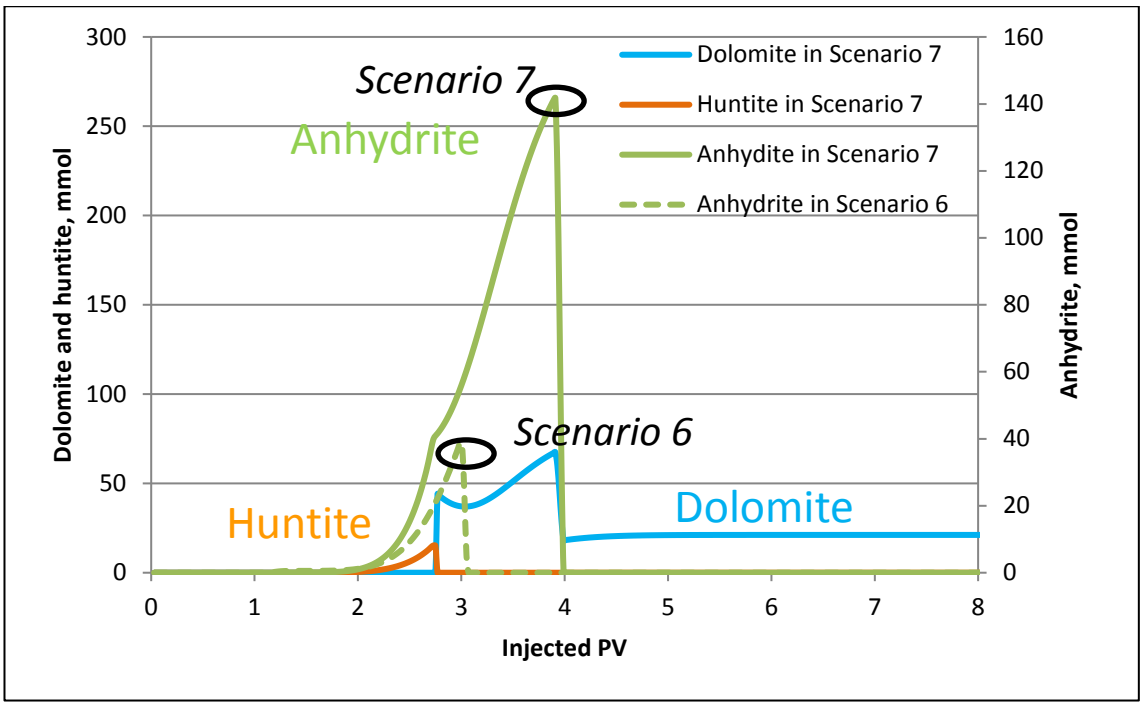

Figure 6.13 Simulation results in the last block from modelling scenario 7.

6.5.5 Comparison of modelling results with observed data

The following plots shown in **Figure 6.14** for sulphate, magnesium and barium as a function of chloride present the simulation results from a variety of modelling scenarios (1, 5, 6 and 7) compared to ion behaviours from produced water samples. Any possible geochemical reactions, thermal effects and the impact of CO_2 are all modelled in scenario 7, the calculation results provide a closer match with observed data than those from other modelling scenarios. This can give us confidence to believe that the geochemical processes modelled in scenario 7 are representative of the *in situ* reservoir interactions occurring and also demonstrate that it is necessary to consider the impact of CO_2, solubility dependent on the temperature and some carbonate mineral reactions (besides calcite) during seawater injection into a carbonate reservoir.

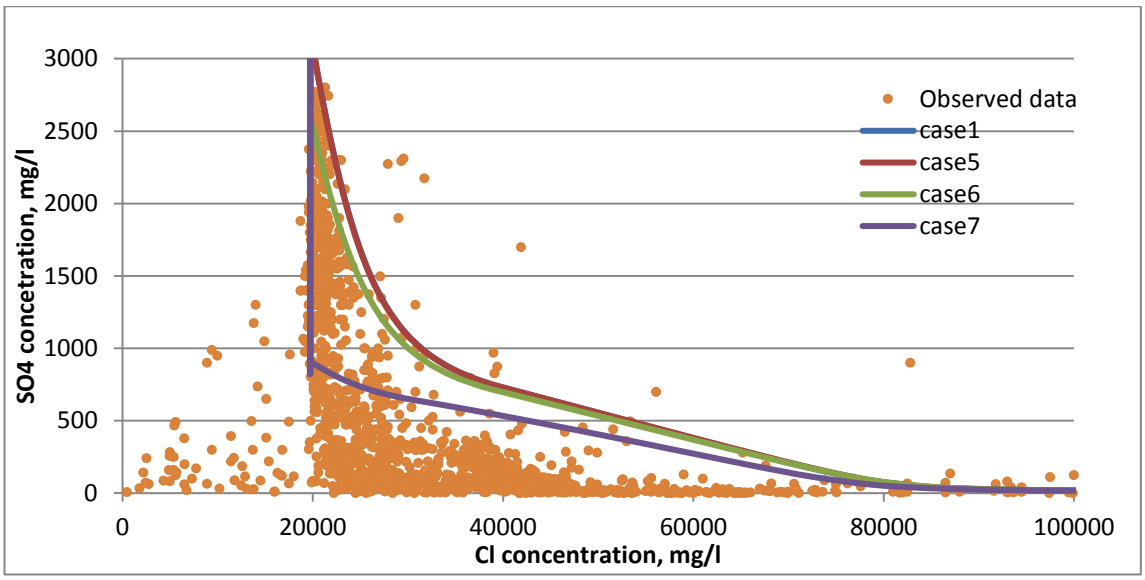

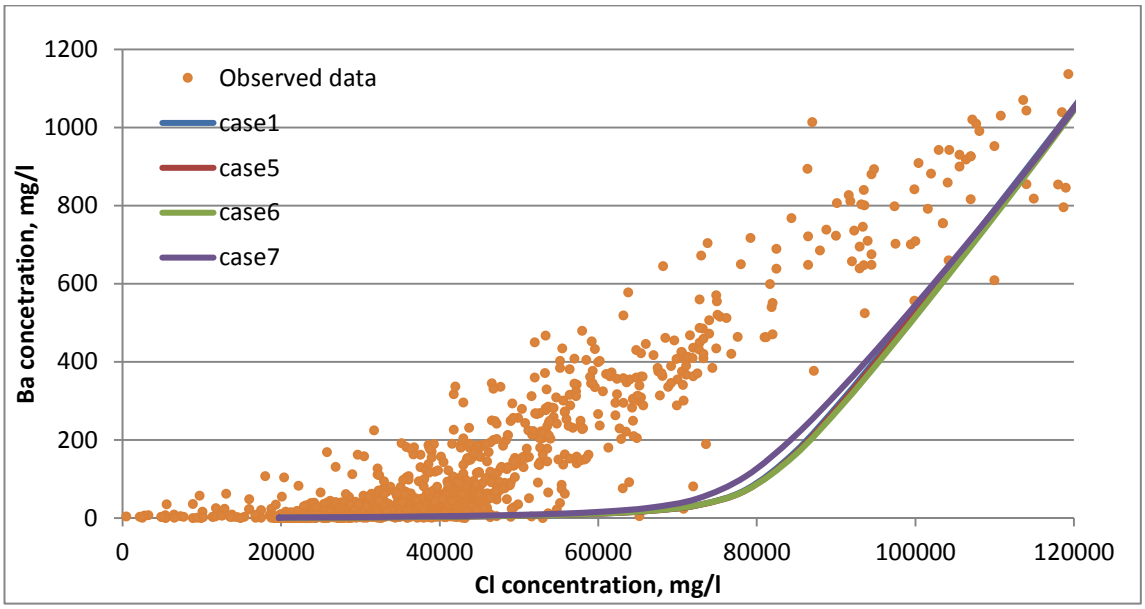

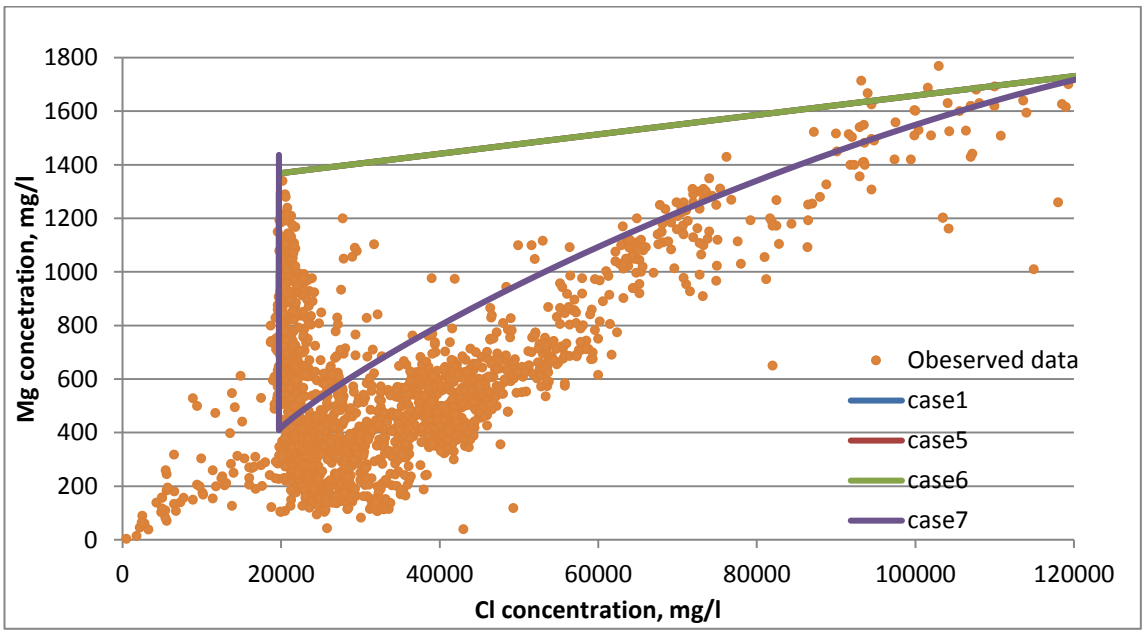

Figure 6.14 Comparison on SO_4 (top), Ba (middle) and Mg (bottom) of modelling results from scenarios 1, 5, 6 and 7 with observed data.

6.6 Sensitivity study

However, there are still some discrepancies with regard to sulphate, barium and magnesium concentrations between modelling results of scenario 7 and observed data. Regarding confidence in the model results, one concern is with the thermodynamic data being used. How reliable are the equilibrium constant data for anhydrite, huntite and dolomite? For example, evidence suggests that ordered dolomite would be the dolomite phase to precipitate (Montes-Hernandez et al., 2014), but there are no specific data on the different phases of dolomite in the PHREEQC PITZER thermodynamic database. It is therefore used to run the model and force the deposition of huntite, magnesite, and dolomite only in turn to identify the effects of each reaction on the produced water analyses. Also, some simulations can be run to look at the effects of varying the solubilities of these minerals and of calcite to assess impact of the uncertainties on the predicted produced water analyses. I also consider examining the effects of varying the solubility of anhydrite. PHREEQC appears to use a solubility that is too high at temperature over 100^{o}C for predicting anhydrite precipitation from seawater (Appendix). This type of work can highlight the importance of uncertainties in the thermodynamic data and demonstrate whether or not data needs to be obtained for the specific reservoir conditions.

6.6.1 Varying anhydrite solubility

As described in chapter 3, the Saturation Index of a given mineral is adjusted to change its solubility based on Equation 3.1. The results of decreasing the solubility of anhydrite in steps from 1 to 0.1 times from its initial value (default) is shown in **Figure 6.15**. More anhydrite is precipitated as the anhydrite solubility declines. Barium is competing with calcium to react with sulphate in order to form barite as sulphate available in seawater is the limiting ion. There are few available sulphate ions to react with barium when more sulphate ions are consumed by the depletion of calcium sulphate. Thus, a higher barium concentration may be found in the produced water. I have demonstrated that significant sulphate stripping is predominantly caused by anhydrite precipitation rather than by barite precipitated in the previous chapters of this thesis. Therefore, the produced water has a lower sulphate concentration if more anhydrite but less barite precipitates (decreasing the solubility of anhydrite).

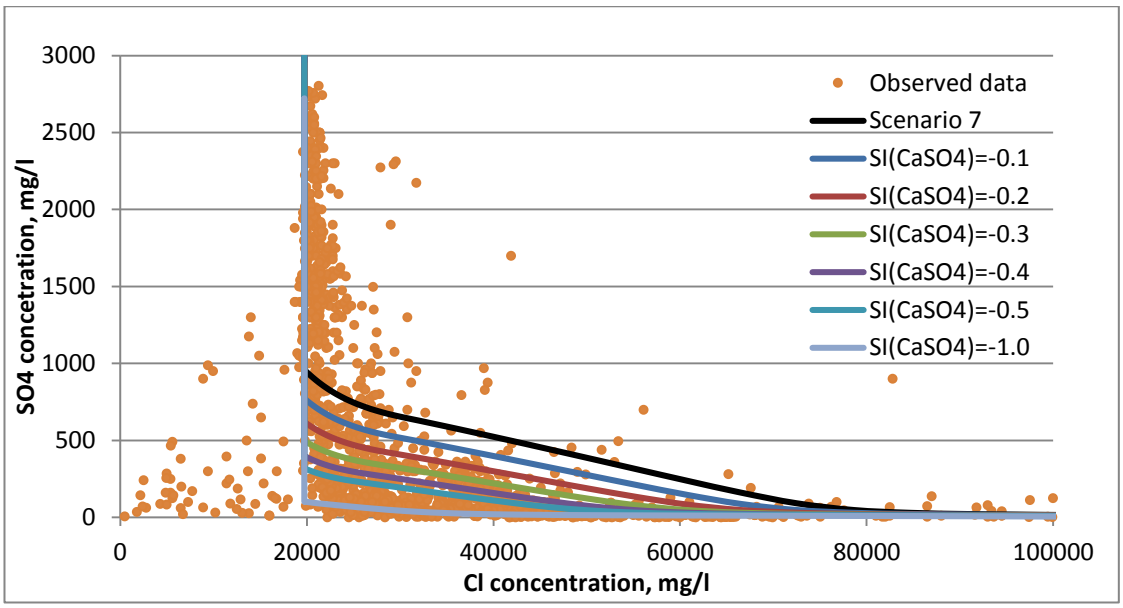

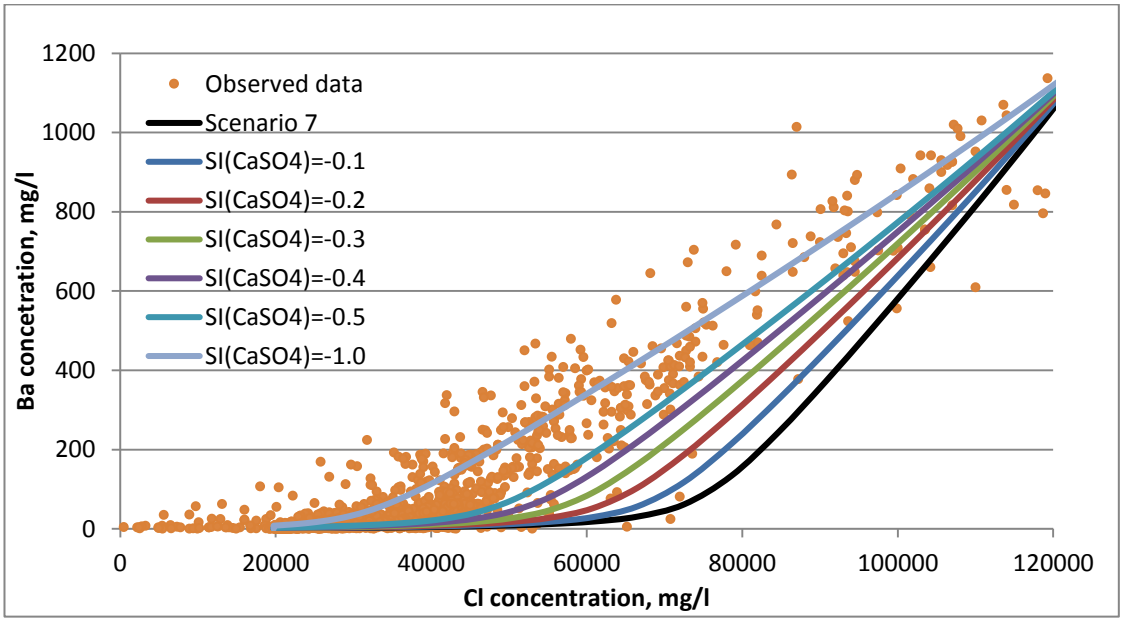

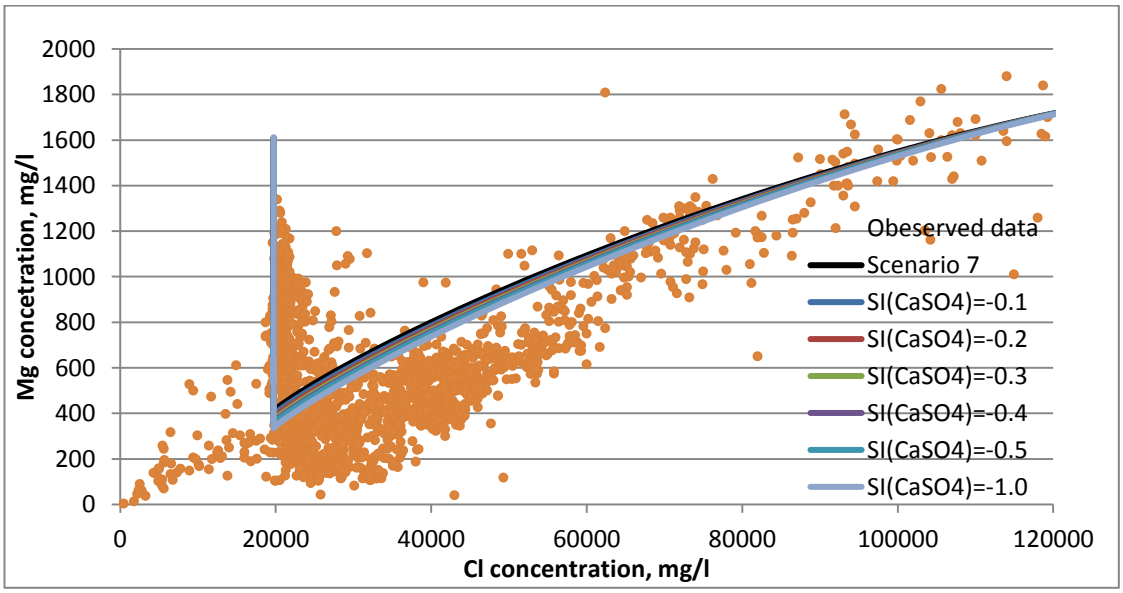

Figure 6.15 SO_4 (top), Ba (middle) and Mg (bottom) vs Cl plots where solubilities of anhydrite is varied in scenario 7, compared to observed data.

It is observed that varying the solubility of anhydrite affects the produced magnesium trend somewhat. Calcium in the formation water is in excess during the anhydrite precipitation reaction, so the calcite precipitation reaction (and other carbonate precipitation reactions) will not depends strongly on the extent of the anhydrite reaction.

6.6.2 Varying carbonate minerals (magnesite, dolomite, huntite) solubility

The solubilities of magnesite, dolomite and huntite are decreased to force greater precipitation. I can observe significantly more magnesium removal as a result of the decline in magnesite (dolomite, huntite) solubility (**Figure 6.16**), which indicates produced magnesium behaviour is determined by the solubility of carbonate minerals. The carbonate precipitated is probably not one pure mineral phase (magnesite/dolomite/huntite), but the combination of various calcium magnesium carbonate minerals. However, the variation in the solubilities of magnesite, dolomite and huntite does not have a big impact on the produced barium and sulphate trends (shown in **Figure 6.17 and 6.18**).

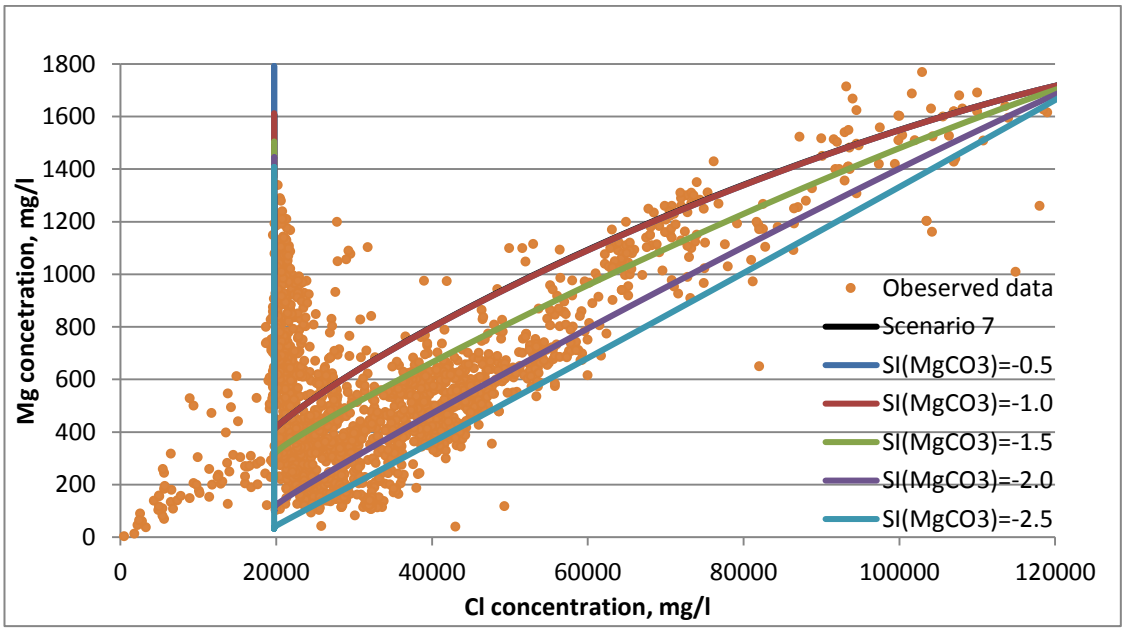

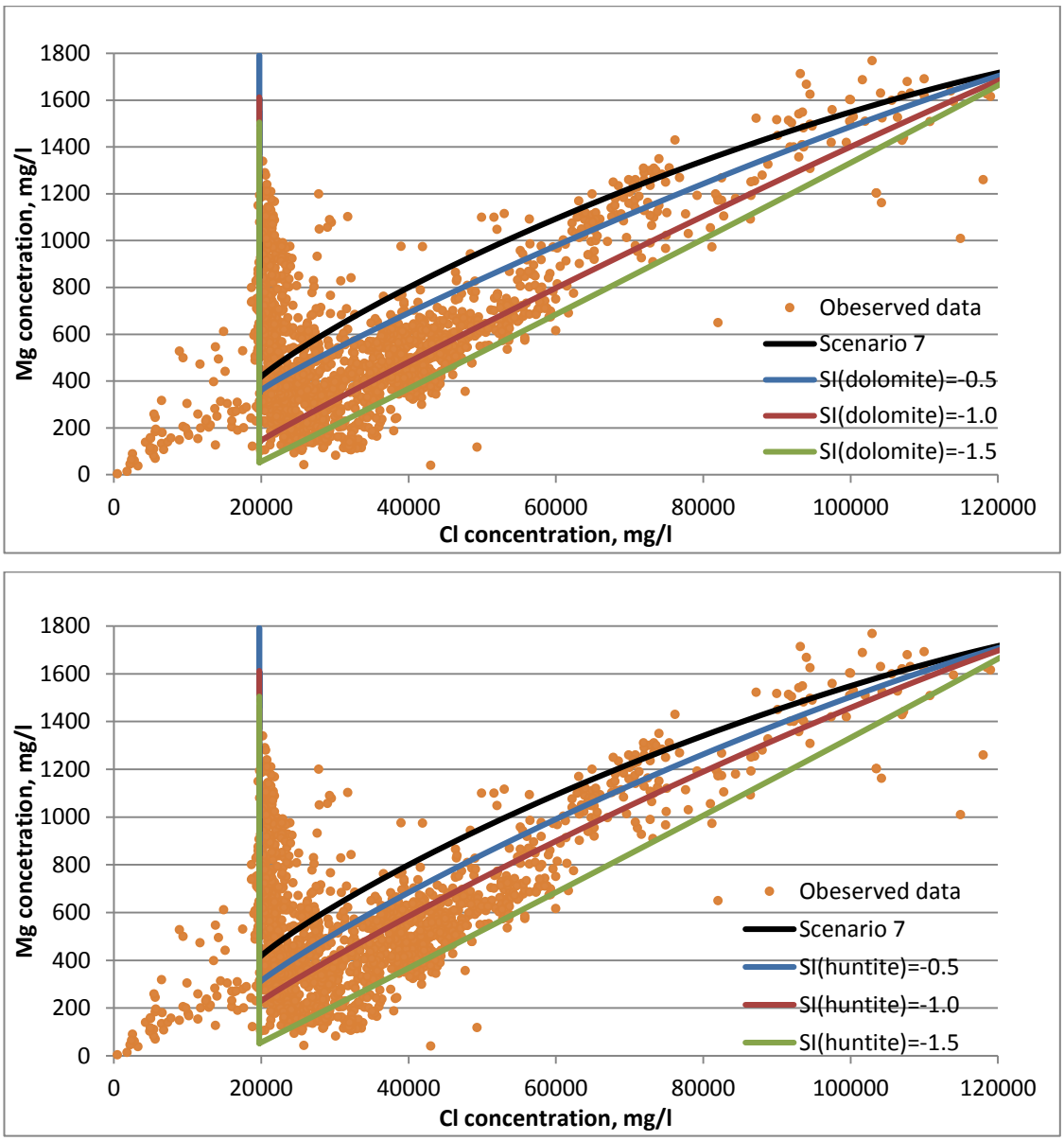

Figure 6.16 Mg vs Cl plots where solubilities of magnesite (top), dolomite (middle) and huntite (bottom) is varied in scenario 7 compared to observed data.

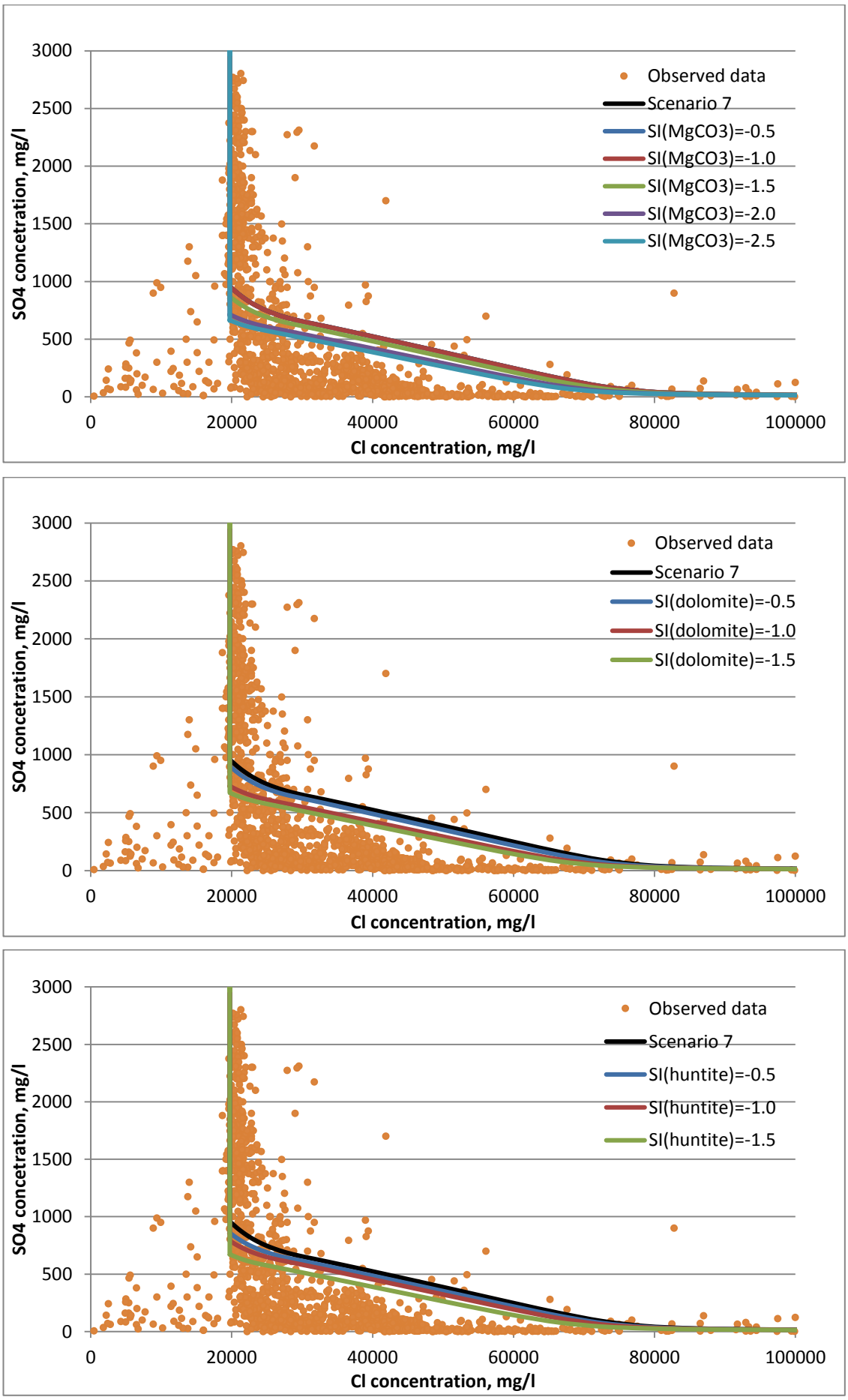

Figure 6.17 SO_4 vs Cl plots where solubilities of magnesite (top), dolomite (middle) and huntite (bottom) are varied in scenario 7, compared to observed data.

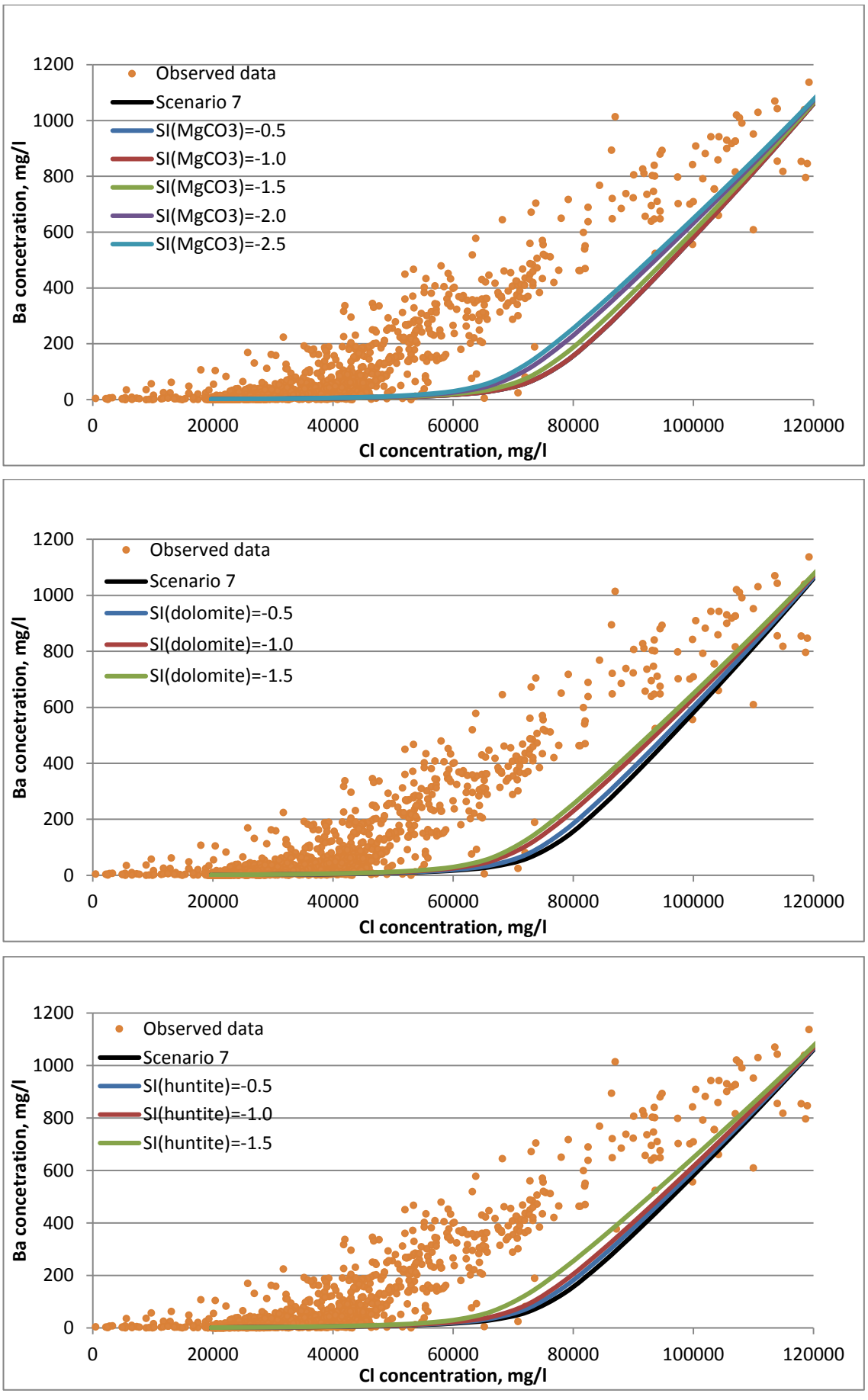

Figure 6.18 Ba vs Cl plots where solubilities of magnesite (top), dolomite (middle) and huntite (bottom) are varied in scenario 7, compared to observed data.

The increased dolomite (magnesite, huntite) deposition caused by tuning solubility consumes more calcium and carbonate, and also result in more calcite dissolution. More calcite dissolved provides substantial source of calcium which can form anhydrite precipitation. This process can be verified by observation of higher barium and lower sulphate concentration in produced water as dolomite (magnesite, huntite) solubility decreases (**Figure 6.17** and **6.18**). However, the variation in the solubilities of magnesite, dolomite and huntite does not have a big impact on the produced barium and sulphate trends.

6.6.3 Calcite exhaustion

Another uncertainty in the model relates to how much calcite is initially defined. Oil reservoirs are big enough and the mass of chalk contained in the reservoir is sufficient that it is not possible for the continuously injected seawater to dissolve all of reservoir rock. However, it is possible for the calcite surfaces exposed to seawater to become armoured with dolomite (Jonasson, 1991), so it is interesting to investigate how produced ion trends change by varying the amount of initial calcite *available to react*.

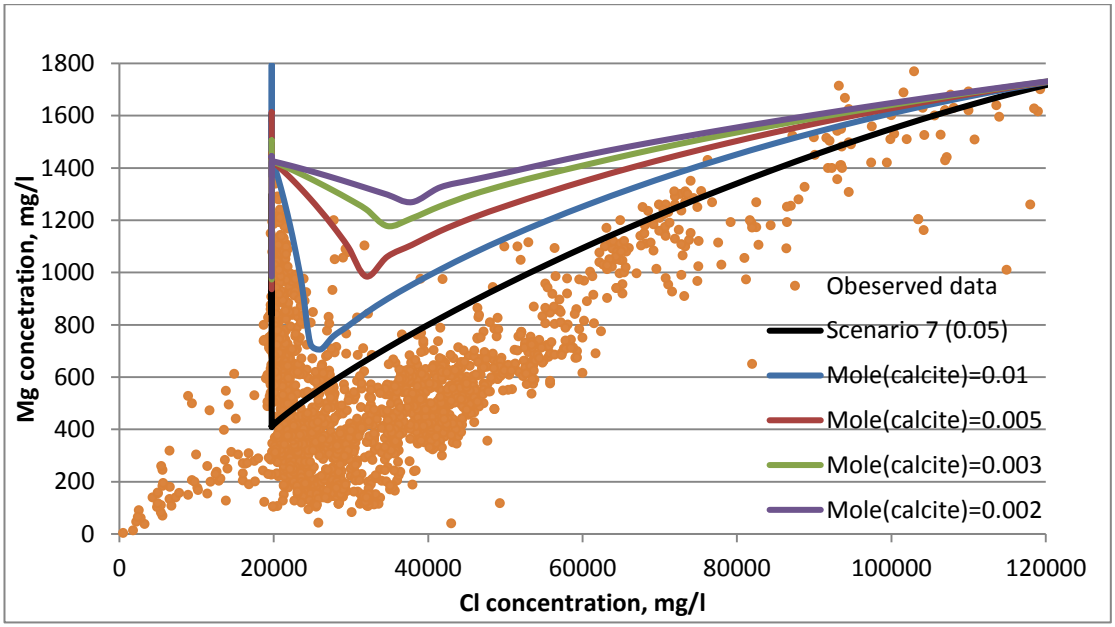

Figure 6.19 Mg vs Cl plots where the amount of calcite is varied in scenario 7, compared to observed data.

I observe from **Figure 6.19** that the lowest magnesium concentration is determined by the amount of calcite initially present. How much magnesium calcium carbonate is precipitated is dependent on how much calcite is available for dissolution. Decreasing the

moles of initial calcite supresses the deposition of carbonate mineral (magnesium stripping). It can be seen from the observed data that there is a large mass of calcite available in the reservoir rock available to be reacted with injection water.

6.6.4 Ion exchange in carbonate reservoirs

Multi-component ion exchange is an exchange of ions between two electrolytes or between an electrolyte solution and a complex. The ions that are initially attached to the rock surface are in equilibrium with the initial brine contacting the rock. Therefore, the ions will potentially be desorbed from the surface into the brine or absorbed from brine onto the rock surface if the composition of the brine changes.

It has been reported in many publications that ion exchange usually takes place in sandstone reservoir rock when this contains significant clays with high specific surface areas (Smith 1978; Bazin et al., 1991; Carlyle et al., 2004), but only limited literature can be found about occurrence of ion exchange on the surface of calcite in chalk reservoirs (Fabricius et al., 2005; Alam et al., 2010). Some lab experiments demonstrated that calcium ions could be replaced by magnesium or sodium ions on the calcite surface, and that this phenomenon was not caused by the dissolution of calcite because the brine injected into the core was prepared from samples equilibrated with calcite solution (Alam et al., 2010; Madland et al., 2011). The Equation 6.3 below was also proposed by Alam et al. (2010) to calculate the cation exchange capacity (CEC) of chalk grains and their study on Ekofisk and Tor Formation chalk samples from South Arne field of the North Sea indicated that the calcite grains have considerable CEC.

$$CEC_{rock} = \left\{CEC_{ir} \times IR\frac{SSA_{ir}}{SSA} + CEC_{calcite} \times (1 - IR \times \frac{SSA_{ir}}{SSA})\right\} \times (1 - \emptyset) \quad (6.3)$$

Where CEC_{ir} and $CEC_{calcite}$ are the CEC of non-carbonates and the calcite part of the chalk respectively. IR is the fraction of irreducible residue by weight ($IR = 1 - CaCO_3$) fraction.

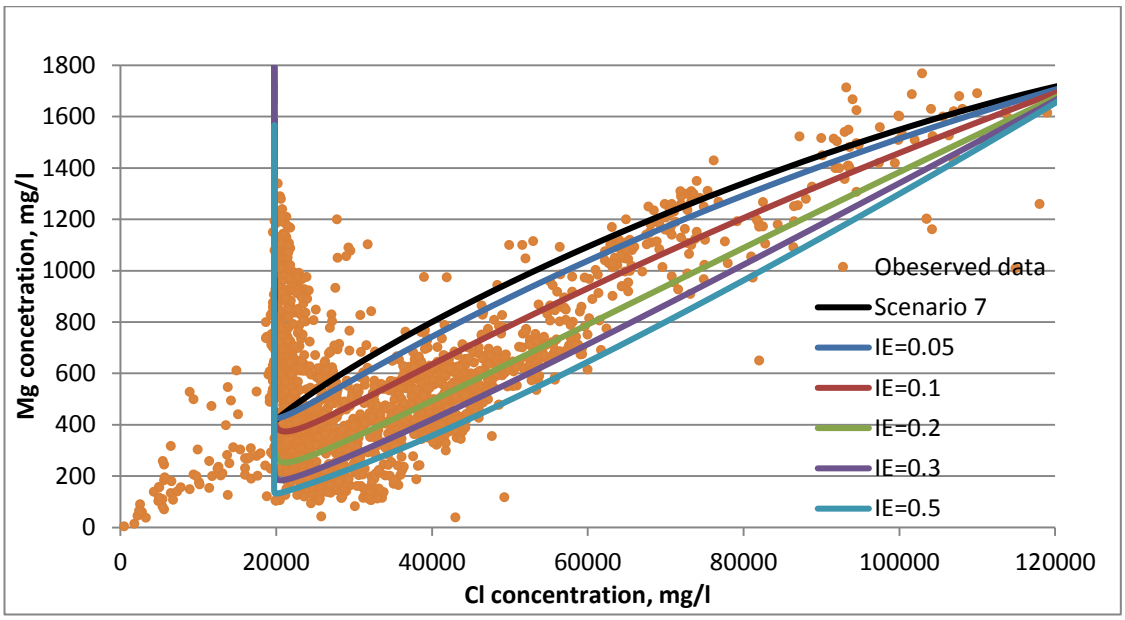

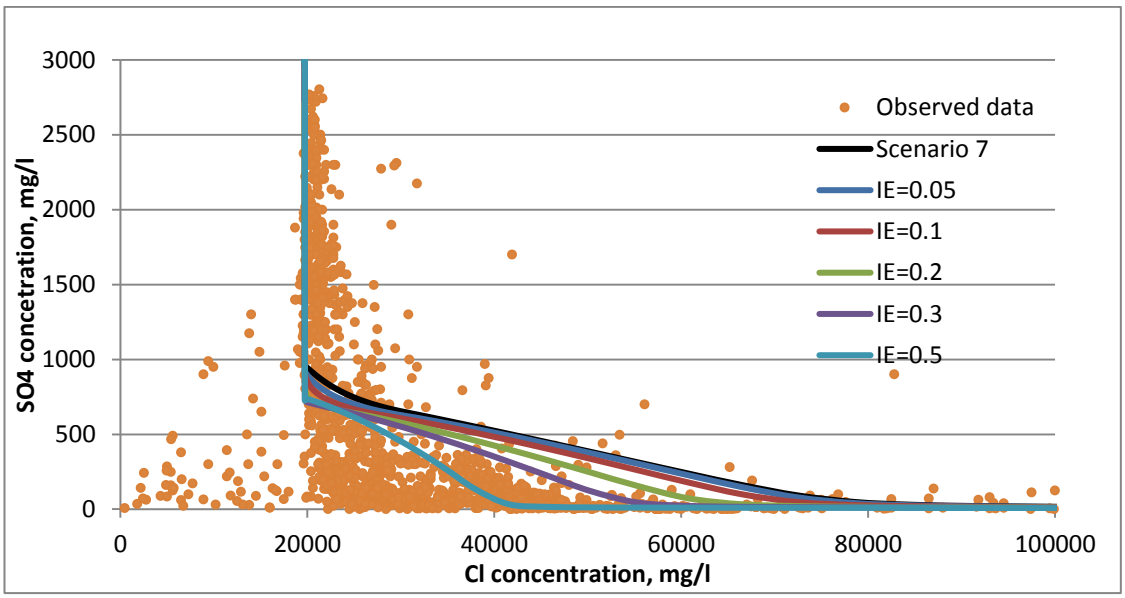

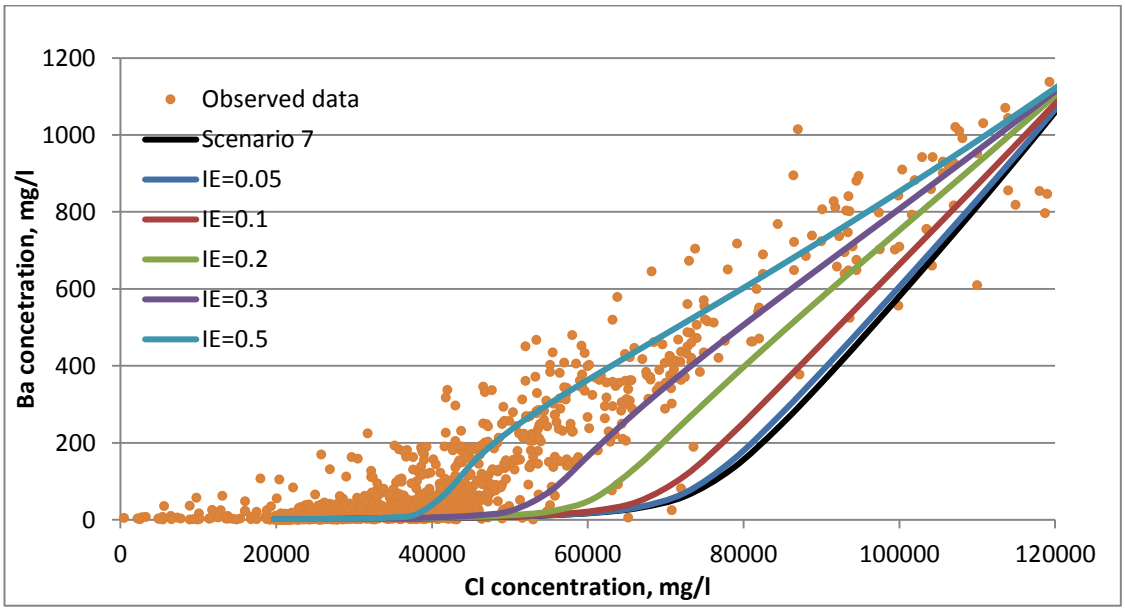

Figure 6.20 Mg (top), SO_4 (middle) and Ba (bottom) vs Cl plots obtained by varying the amount of exchangers in scenario 7, compared to observed data.

The model of ion exchange reaction used in this study is based on clay surface chemistry that is demonstrated by Appelo and Postma (2009), so the cation exchange capacity and selectivity coefficient may not be applicable for chalk, but the results can give us some approximate values as a reference and also help us understand the ion exchange occurring on the chalk surface through comparison with observed field data.

The inclusion of ion exchange reactions leads to more magnesium, sulphate and less barium depletion, through which a better match with observed data is achieved. Magnesium absorbing onto the rock surface and calcium releasing into the brine is the main process in this ion exchange reaction. The liberated calcium can react with sulphate, which leads to more anhydrite (lower sulphate concentration) and less barite (higher barium concentration). (**Figure 6.20**)

6.7 Conclusions

The produced water dataset from a carbonate reservoir under seawater flooding is analysed, investigated and explained for the first time. It can be shown from the plots of each ion against chloride that both magnesium and sulphate concentrations are significantly depleted relative to their pure mixing lines, and other ions such as sodium, barium, strontium and calcium almost lie on their mixing lines.

I can draw some conclusions based on the one dimensional reactive transport model which is developed using PHREEQC to identify the relevant geochemical processes within the carbonate reservoir during seawater flooding.

1. The seawater can take up CO_2 from the hydrocarbon phases (containing CO_2) once it is injected into the oil leg or close to the oil water contact. The reacted seawater becomes acidic and then dissolves calcite. The initial high reservoir temperature (131^oC) is lowered by cool injection water (25^oC). The dissolution of calcite is favoured by the decline in temperature around the injector.
2. Calcite is the predominant mineral in the chalk reservoir rock and is widely present. It will be dissolved when flushed by the reacted seawater due to low temperature and dissolved CO_2. The dissolution of calcite significantly suppresses barite and celestite precipitation but leads to more anhydrite precipitation, as substantial calcium can be provided and sulphate in the injected seawater becomes

the limiting ion. The dissolving calcite needs to be considered even if sulphate mineral reactions are modelled and studied.

3. Calcite dissolution triggers carbonate mineral precipitation (calcium magnesium carbonate) as a substantial source of calcium and carbonate is provided by calcite dissolution and seawater is rich in magnesium. The deposition of various carbonate minerals, in return, results in further calcite dissolution. Carbonate mineral precipitation (huntite and dolomite), for which the presence of calcite is a precondition, contributes to the significant magnesium stripping in the produced water since the chalk is mainly made up of calcite in the Ekofisk field. However, it is found that ion exchange may also deplete magnesium ions from brine through comparing calculation results with observed data
4. The thermal front plays a key role in the mineral reactions of anhydrite, calcite, dolomite and huntite. Huntite tends to precipitate at the relatively high temperature and dolomite is the dominant precipitation reaction at low temperature in the thermal model which considers calcite dissolution. Therefore, more huntite precipitation will take place during longer periods of time if the change in temperature is retarded.

The comparison between calculation results from a variety of modelling scenarios and observed data from produced water samples is made, which highlights the importance of the impact of temperature changes and CO_2 dissolution during geochemical processes occurring in the reservoir. Uncertainties in the thermodynamic data in the reactive transport model are studied through tuning the solubility of minerals involved, and the effects of relative geochemical reactions on the produced water compositions are also investigated.

CHAPTER 7 MINERAL SCALING AND CHEMICAL EOR IN CARBONATE RESERVOIRS

7.1 Introduction

Extensive studies have confirmed that altering ionic composition of injection water has a big impact on the ultimate oil recoveries. Different mechanisms have been proposed to explain the positive effects of Smart Water injection, but none is universally accepted as the dominant mechanism. Therefore, this chapter presents a three-dimensional reactive transport modelling study to investigate the geochemical processes during seawater/ altered seawater flooding with different sulphate concentrations being injected into a carbonate reservoir. This can help our understanding of the possible mechanisms behind Smart Water injection. A series of calcite and anhydrite mineral reactions are the key in situ chemical reactions included in the study. At the early stages of transport, CO_2 partitioning from the hydrocarbon phase into the brine causes significant calcite dissolution. This process can be enhanced by increasing the sulphate concentration in the injection water. Sulphate concentration in the injection water has a significant impact on whether the calcite is continuously dissolved or not after the CO_2 front passes by. In the modelling cases including thermal transport, reservoir rock is cooled by injection water, and compared with isothermal cases, thus anhydrite precipitation and calcite dissolution are decreased. The purpose of the study conducted in this chapter is not to model how much incremental oil recovery can be achieved, but trying to investigate possible geochemical reactions behind altered seawater injection, a enhance oil recovery method.

7.2 Background and aim

In recent years, extensive core flooding studies have shown that altering the chemical composition of injection water can increase oil recovery in sandstones and carbonates, and several mechanisms, such as multicomponent ion exchange, wettability alteration, mineral dissolution and fines migration, are proposed (Fjelde, 2012; Yousef, 2014; Al-Shalabi et al, 2014; Austad et al, 2015). It is generally agreed that reaching a better understanding of the geochemical processes during smart water/low salinity water injection is of importance, although there is some debate as to which mechanisms are the dominant ones.

Zahid et al (2012) observed a substantial increase in oil recovery in Middle East corefloods at 90^{o}C and no EOR effect at 25^{o}C. Attar et al (2013) demonstrated that

increasing calcium concentration in the injected brine resulted in decreased ultimate oil recovery, but an increase in sulphate concentration led to improved oil recovery. An additional recovery was shown in a series of Middle Eastern carbonate core flooding tests when the sulphate concentration in the injected seawater was increased, as was reported by Awolayo et al (2015). Fewer modelling studies of tuning injection water composition in carbonates have been conducted compared to sandstones, probably since a series of more complex fluid/rock/gas/oil interactions may be occurring in the carbonate systems.

Here I consider that a hydrocarbon fluid element that was bound to the chalk matrix after ageing would be mobilised if the part of the chalk matrix it was bound to dissolves. The more of the matrix that is dissolved, the more hydrocarbon would be mobilised. Injection of lower salinity brine will promote the dissolution of calcite, and the expansion of the double layer may also reduce the adhesive forces binding the hydrocarbons to the matrix and increase the opportunity for mineral reactions at the solid surface. Furthermore, I demonstrate that the addition of sulphate to the brine will serve to promote calcite dissolution. In this chapter I present a simulation study using a three-dimensional reactive transport model to investigate what key *in situ* chemical reactions occur in carbonate reservoirs during Smart Water flooding (seawater with altered sulphate concentration).

7.3 Model setup

In this study, a quarter five spot water flood model was developed. The model consists of 25 x 25 x 10 grid cells, with cell dimensions of 100 m x 100 m x 5 m. **Table 7.1** shows the initial reservoir properties. Porosity is 0.2, and horizontal permeability 600 mD. The kv/kh ratio of 0.1 exists throughout the system. The reservoir top is at a depth of 4155m, and the model area considers the oil leg. A four component EoS model is used to describe the hydrocarbon phases. Thermal calculations are performed and thermal properties of typical carbonate systems are assumed.

Table 7.1 Reservoir properties.

Property	Assigned Value
Initial Reservoir Pressure, Kpa	49000
Initial ReservoirTemperature, C	131
Porosity	0.2
X-Permeability, mD	600
Y-Permeability , mD	600
Kv/Kh	0.1
Initial water saturation	0.0894

Figure 7.1 shows the oil water relative permeability curves. Oil-water capillary pressure is set to zero, and the system does not go below the bubble point pressure at any stage, so there is no free gas in the system. CO_2 is allowed to dissolve in all phases, including water. Aqueous and mineral reactions that constitute the basic carbonate reactive system are applied. (shown in **Table 7.2**)

Table 7.2 Chemical and mineral reactions included in the model.

Aqueous equilibrium reactions	Mineral reactions
$CO_2(aq) + H_2O = (H^+) + (HCO_3^-)$	Calcite + $(H^+) = (Ca^{2+}) + (HCO_3^-)$
$(OH^-) + (H^+) = H_2O$	Barite = $(Ba^{2+}) + (SO_4^{2-})$
$(CO_3^{2-}) + (H^+) = (HCO_3^-)$	Anhydrite = $(Ca^{2+}) + (SO_4^{2-})$
	Celestite = $(Sr^{2+}) + (SO_4^{2-})$

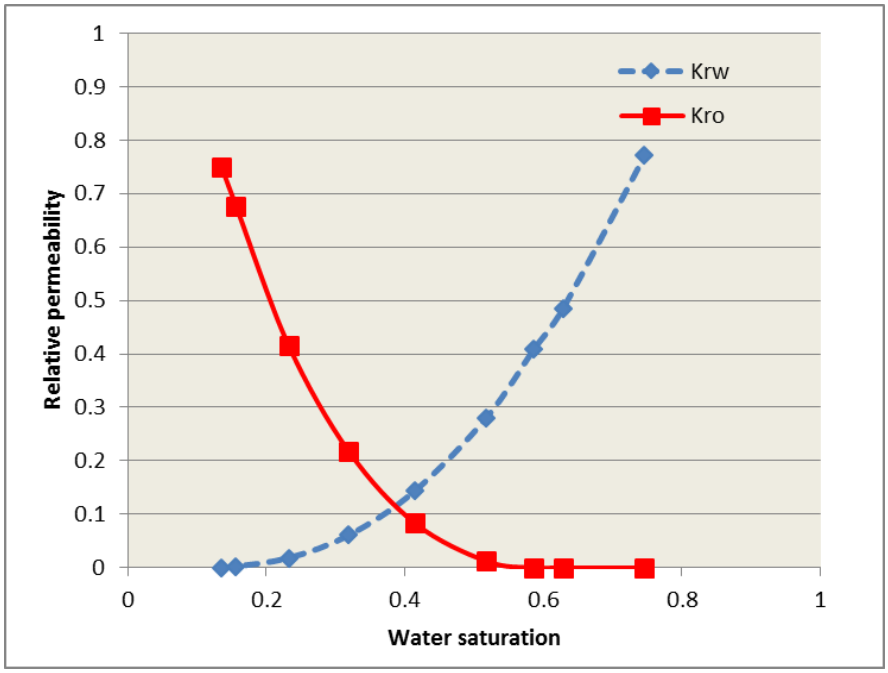

Figure 7.1 Oil and water relative permeability curves.

One injector and four producers are located in the centre and four corners of the simulation model, respectively. The injector and production wells are operated under constant bottom-hole pressure of 59000 kPa and 38000 kPa. Seawater and altered seawater (varying sulphate concentration) is the injection fluid (Shown in **Table 7.3**). The simulation is run for 20 years (from 1st January 2000 to 1st January 2020).

Table 7.3 Formation water, seawater and altered seawater compositions used in the study.

Ion	Formation water (mol/l)	Injected seawater (IW)(mol/l)	IW0S (mol/l)	IW0.1S (mol/l)	IW0.5S (mol/l)	IW2S (mol/l)
Na	2.39	0.4989	0.4989	0.4989	0.4989	0.4989
Ca	0.549	0.01068	0.01068	0.0107	0.01068	0.0107
Mg	0.07	0.0563	0.0563	0.0563	0.0563	0.0563
Ba	0.0087	0	0	0	0	0
Sr	0.018	0	0	0	0	0
Cl	3.526	0.5557	0.5865	0.5834	0.5711	0.5249
SO4	0	0.0308	0	0.0031	0.0154	0.0616
HCO3	0.00036	0.0023	0.0023	0.0023	0.0023	0.0023
pH	4.92	7.3	7.3	7.3	7.3	7.3

7.4 Base case model

An initial model was defined in which the initial global molar fraction of CO_2 is set to 0.01 (1% CO_2 content in hydrocarbon phase), in which a fraction of the solid rock volume equivalent to 0.0088 is defined to be reactive calcite (the rest of the rock volume is considered to be inert), and the injection brine is North Sea seawater, the formation brine is equilibrated with the hydrocarbon phase in terms of the CO_2 concentration and calcite initially present in the reservoir rocks. The injection brine is assumed to have been degassed at standard conditions prior to injection. Various figures are used to display the advance of various fronts through the reservoir, snapshots being taken after 10 years (left) and 20 years (right) of production. **Figure 7.2** shows the advance of the saturation and tracer fronts in this system.

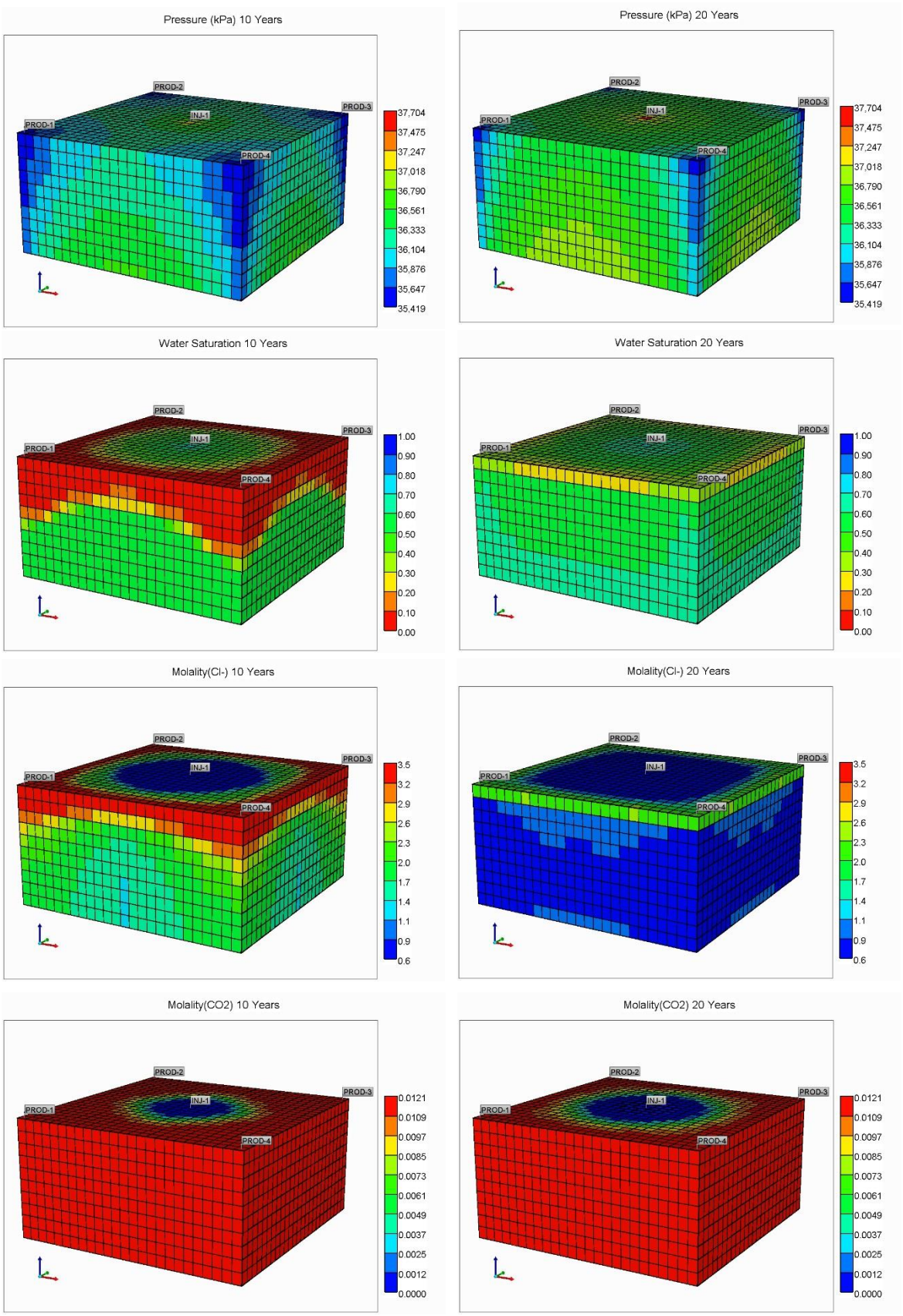

Figure 7.2 Pressure, water saturation, injected tracer (Cl) and molality of CO_2 fronts in base case model.

7.5 Sensitivity study

7.5.1 Impact of CO_2 content initially in the reservoir

The CO_2 present in the hydrocarbon phases at the initial reservoir conditions is sometimes neglected in geochemical simulation studies, but actually it affects the geochemical reactions occurring in the reservoir and the chemical composition of produced brine as well. Therefore, here I first consider what impact the CO_2 initially in the hydrocarbon phases is having on the dissolution of calcite (carbonate reservoir rocks) during seawater injection.

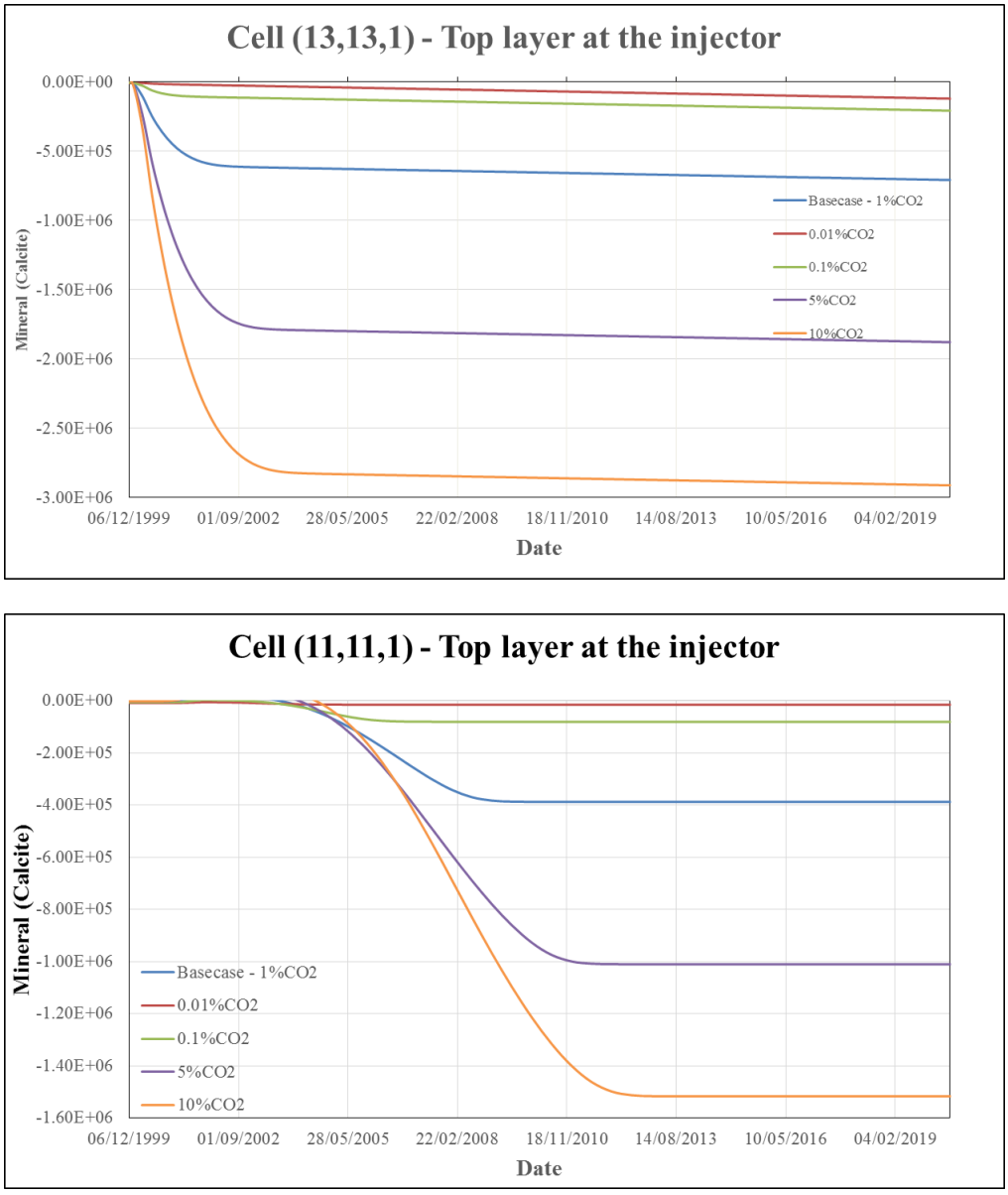

Figure 7.3 The change of calcite mineral at the cell (13,13,1) and cell (11,11,1) which are in the top layer at the injector and one point between the injector and producer. Sensitivity is the CO_2 volume fraction in the initial oil.

It can be easily found from **Figure 7.3** that much more dissolution of calcite is observed during the early stages if the liquid hydrocarbon phase contains more CO_2. In the case where the CO_2 global mole fraction was set to near zero (0.0001), the calcite hardly dissolves.

In **Figure 7.4,** we plot the molality of CO_2 at the two positions in the reservoir identified above. In each case as seawater breaks through the depletion of CO_2 has not yet occurred. This indicates that CO_2 is gradually partitioning from the oil phase into the seawater. Thereafter, the front of decreasing CO_2 concentration starts to break through, and the local pH increases, eventually reaching the injection pH value.

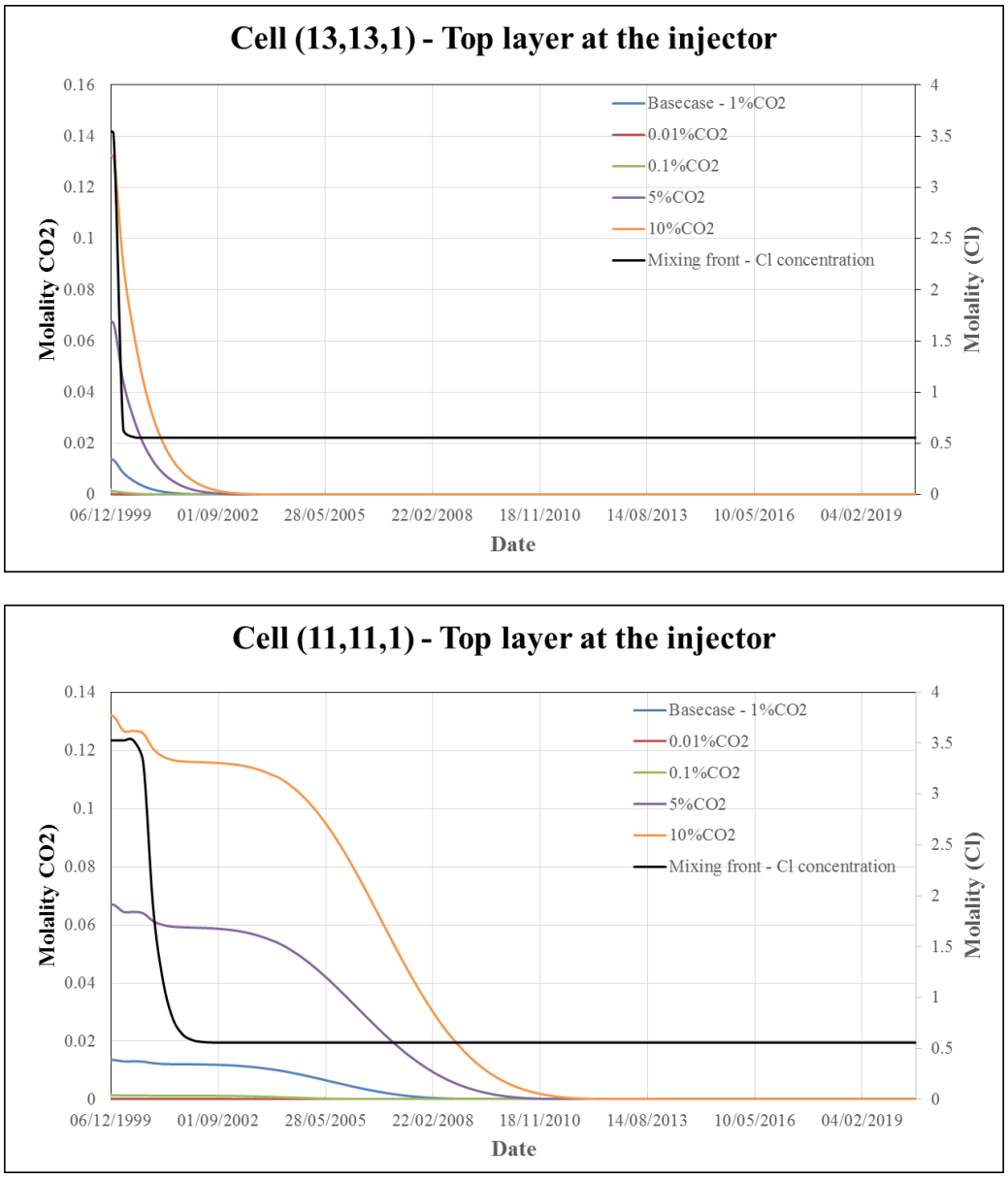

Figure 7.4 The propagation of CO_2 in the water phase at the cell (13,13,1) and cell (11,11,1) which are in the top layer at the injector and one point between the injector and producer.

7.5.2 Effect of varying sulphate concentration - constant reservoir temperature

The following plots present how the calcite and anhydrite mineral change at the injector (top layer) as (altered) seawater with varying sulphate concentrations is injected into reservoir system at constant reservoir temperature of 130^{o}C (no cooling effect at the injector). **Figure 7.5** shows the calcite dissolution behaviour in the top layer adjacent to the injector. In the absence of any other reactions, calcite will be precipitated from the injection water (equilibrated at 25^{o}C on surface) as it heats up in the reservoir (to 131^{o}C) because the solubility of calcite decreases as temperature increases. However, as the injected brine comes into contact with residual oil, the result will be that CO_2 partitions into the brine, reducing the pH and causing calcite dissolution instead. Once all the CO_2 has been stripped out of the residual oil, in the cases where the injection water contains lower sulphate concentrations (*red*, *green* (overlying red) and *purple* lines), calcite will now start to precipitate out of the injection water, and so the amount of calcite in the system starts to rise again.

However, the presence of sulphate in the injection water also leads to anhydrite precipitation at the reservoir temperature. It is evident from **Figure 7.5** that the higher the sulphate concentration, the more anhydrite that is precipitated. This lowers the calcium concentration in the brine, and so drives the calcite dissolution: especially at high sulphate concentrations (light blue). Interestingly, at the sulphate concentration equal to seawater (dark blue line), once the CO_2 has been stripped out of the residual oil there is almost no subsequent net change in the amount of calcite.

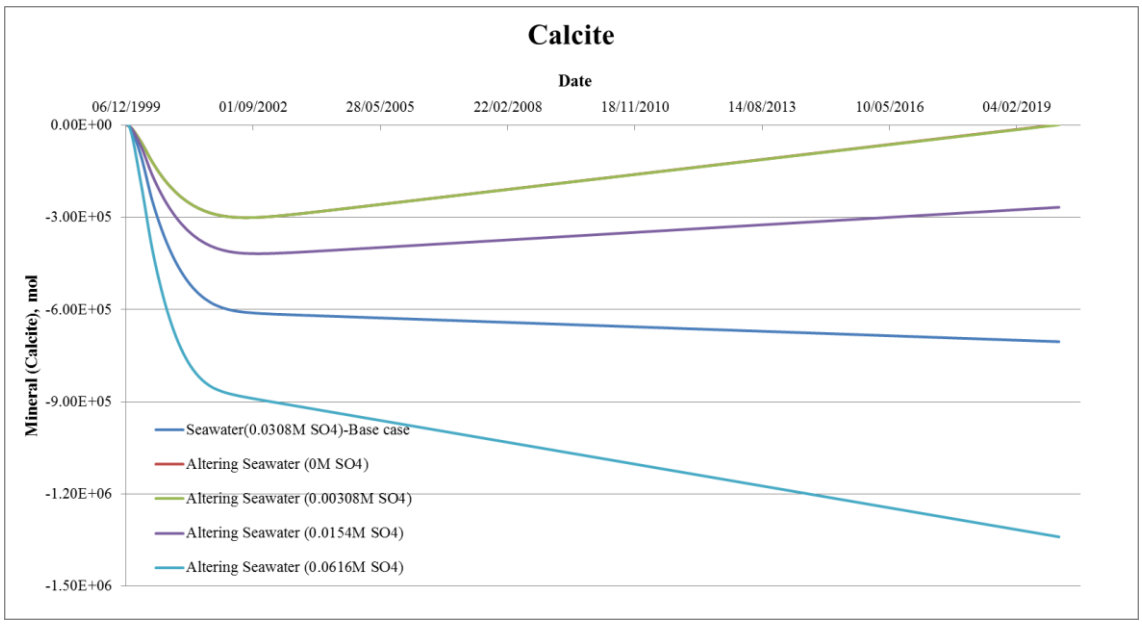

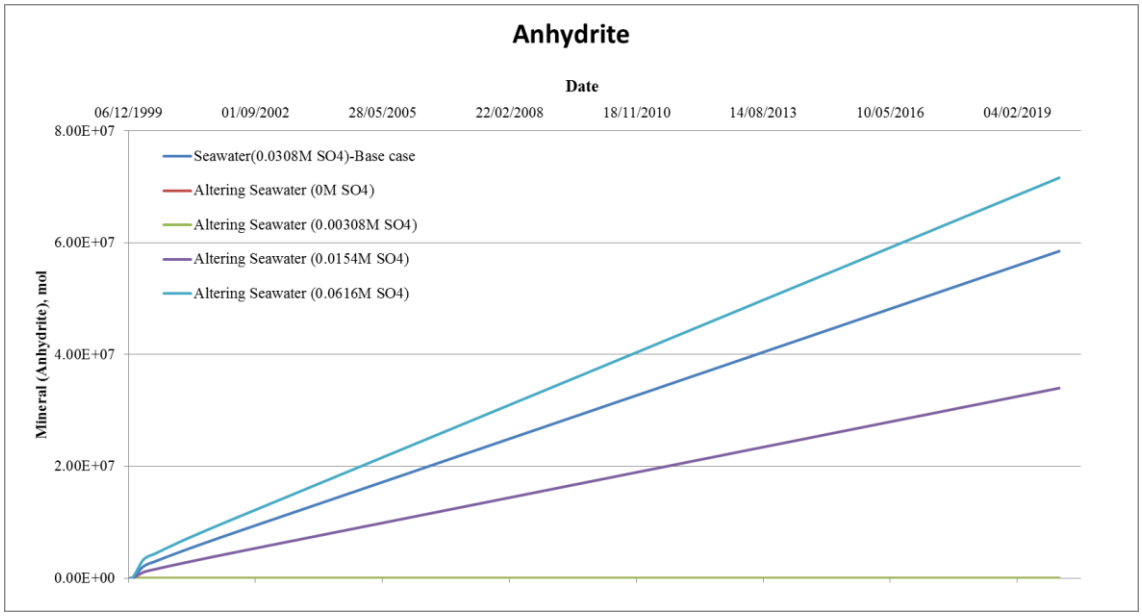

Figure 7.5 The mineral change of calcite (top) and anhydrite (bottom) in the top layer at the injector. Sensitivity is the SO_4 concentration in injected seawater. Cell (13, 13, 1)

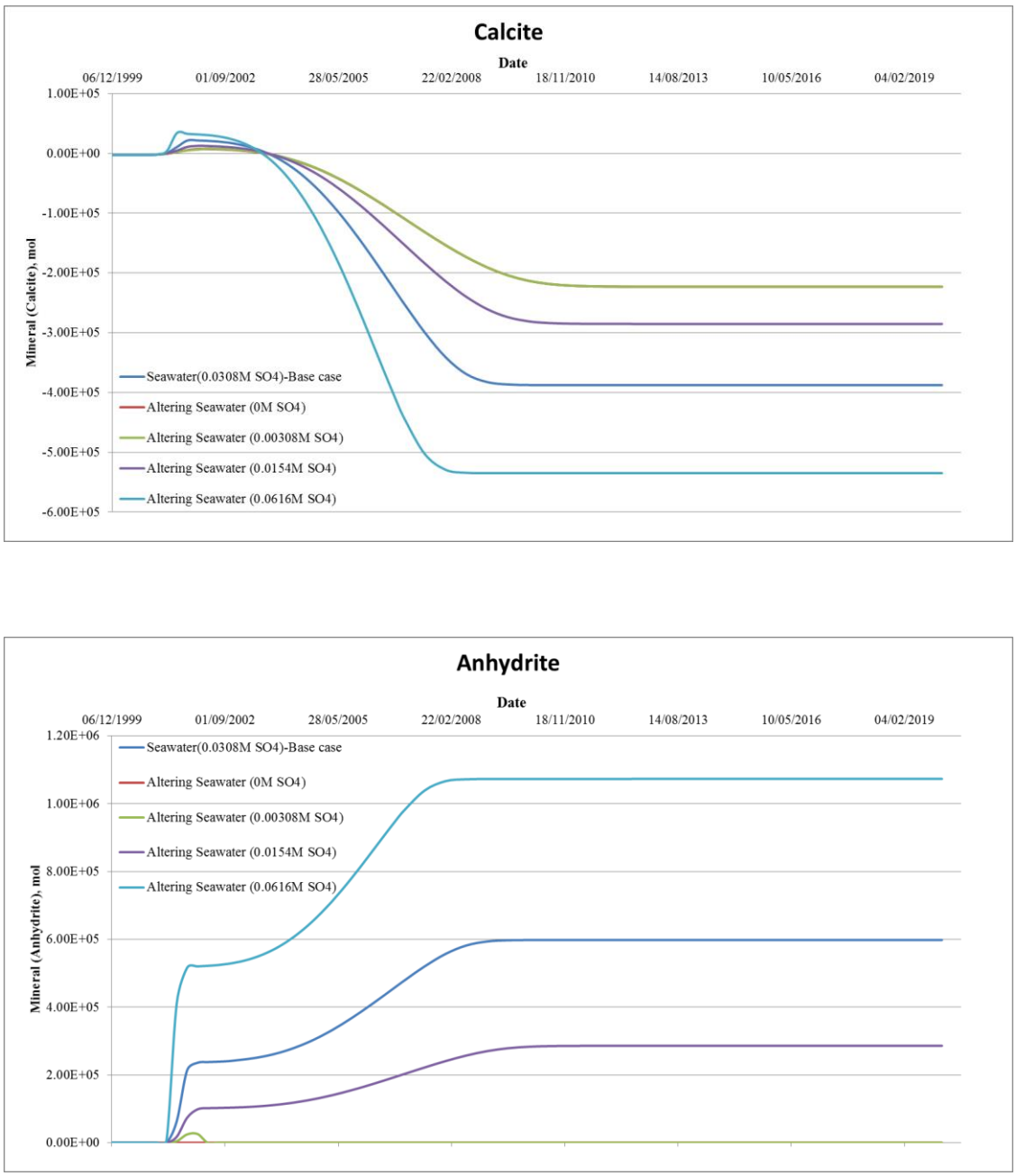

Figure 7.6 The mineral change of calcite (top) and anhydrite (bottom) in the top layer of a point between the injector and the producer. Cell (11, 11, 1)

Figure 7.6 shows that 250m away from the injector there is some initial precipitation of calcite when injection water breaks through (as identified by the change in chloride concentration in **Figure 7.7**). The precipitation is due to the increase in calcium concentration during calcite dissolution upstream and the mixing with bicarbonate in the formation water. When the formation water is completely displaced, the calcite precipitation stops, and dissolution starts, as upstream at the injection well. As before,

higher sulphate concentrations lead to greater calcite dissolution due to the coupled anhydrite reaction. However, once there is no more CO_2 from the partitioning, there are no further changes in the amount of calcite present; the excess sulphate in the injection water is all consumed upstream, and so there is no longer a driving force for anhydrite precipitation and hence for calcite dissolution.

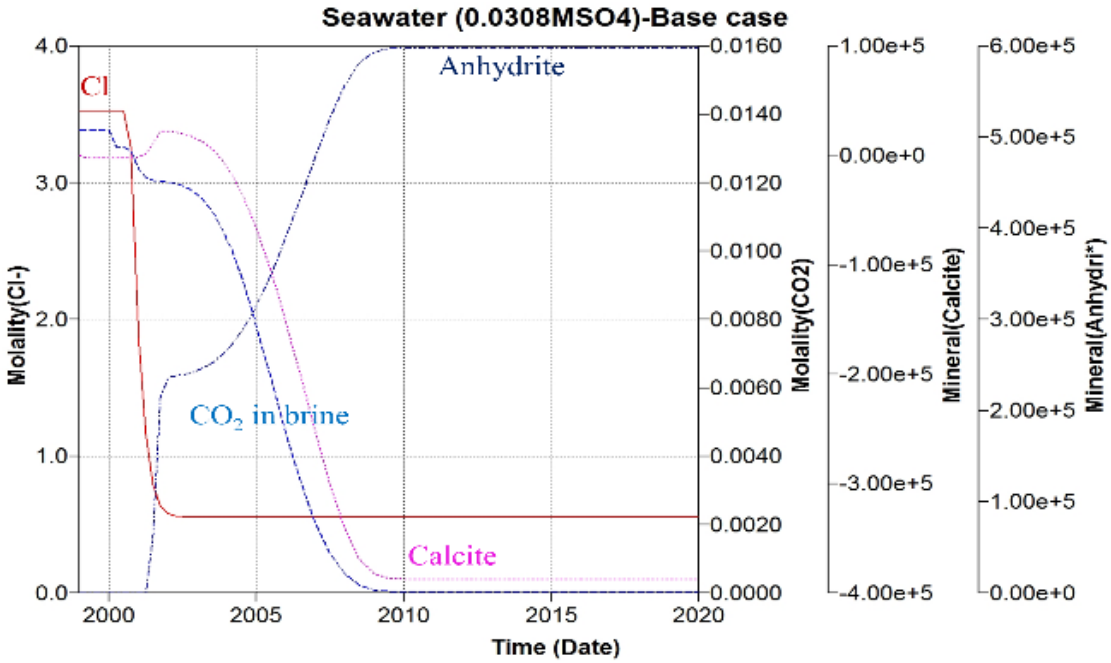

Figure 7.7 The development of chloride, CO_2 in brine, the changes of calcite and anhydrite minerals at the cell (11,11,1).

In summary, the calcite dissolution and anhydrite precipitation are coupled reactions, due to calcium being an ion common to both reactions. The calcite dissolution is accelerated when the residual oil is a source of CO_2, which by partitioning to the aqueous phase acidifies it, but even when the CO_2 is consumed the dissolution of calcite will continue if anhydrite precipitation is ongoing – albeit more slowly. On the other hand, the anhydrite precipitation reaction requires sulphate, which is the limiting ion in these conditions. Thus, the extent of anhydrite precipitation is dependent on the concentration of sulphate in the injection brine, and therefore so also is the extent of calcite dissolution.

7.5.3 Cooling effect of injection water

Injected seawater normally has a temperature of about 20-30^{o}C as it enters the reservoir, depending on depth and injection rate – it is not instantly heated to reservoir temperature

as the above calculations assume. Indeed, on entering the reservoir there will be heat exchange, such that the seawater heats up, but in the process cools the near wellbore reservoir rocks. Therefore, the cooling effect on the geochemical reactions should be considered, since both the calcite and anhydrite reactions are temperature sensitive. The temperature front generally advances much slower than the brine mixing front (or indeed most of the compositional fronts), unless, of course, the temperature change induces a geochemical reaction that alters the brine composition.

In this section, the temperature of injected brine is set to 25^{o}C and the reservoir temperature gradually decrease from 131^{o}C to 25^{o}C as seawater is displaced and flows from the injector to producer. The changes of mineral calcite and anhydrite at the cell (13,13,1) are illustrated in **Figure 7.8**. The same conclusion with the isothermal modelling study I can make is that addition of sulphate into seawater causes more anhydrite precipitation and calcite dissolution. However, when the temperature front breaks through and the system is all at a temperature of 25^{o}C, very little dissolved calcite can be found no matter how much sulphate is added to the injected water. This indicates that anhydrite mineral reaction has a big impact on the dissolution reaction of calcite. At 25^{o}C, anhydrite is more soluble, and the previously precipitated anhydrite is dissolved in all cases with the exception of the last one (*black line*), thus there is no more anhydrite deposition to drive the calcite dissolution.

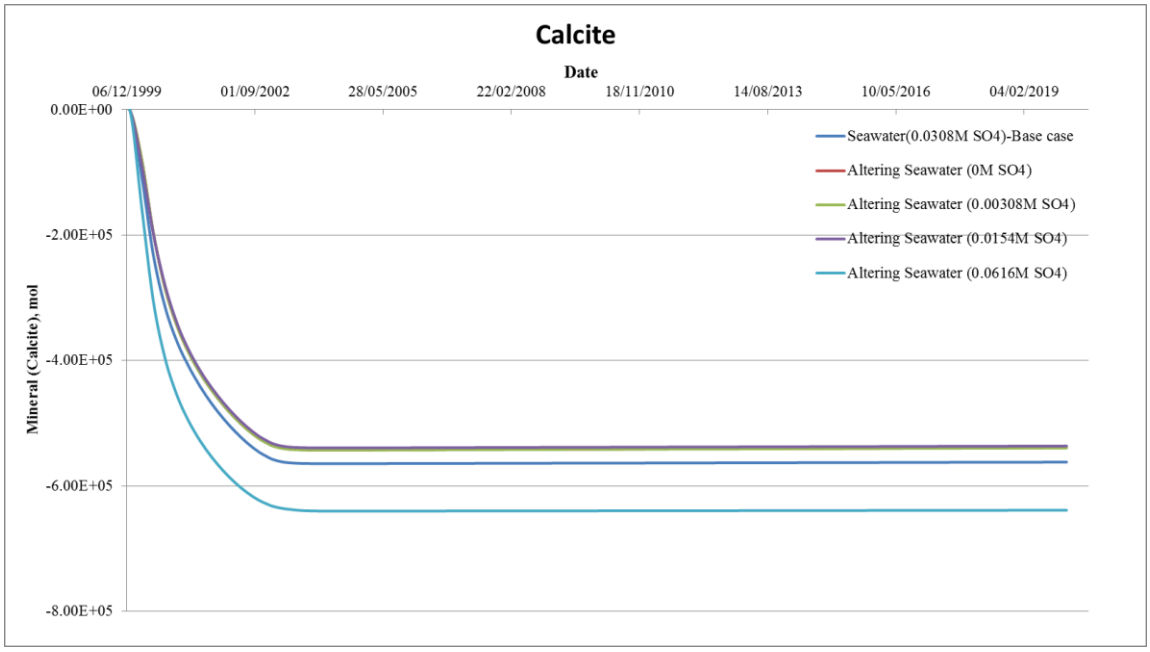

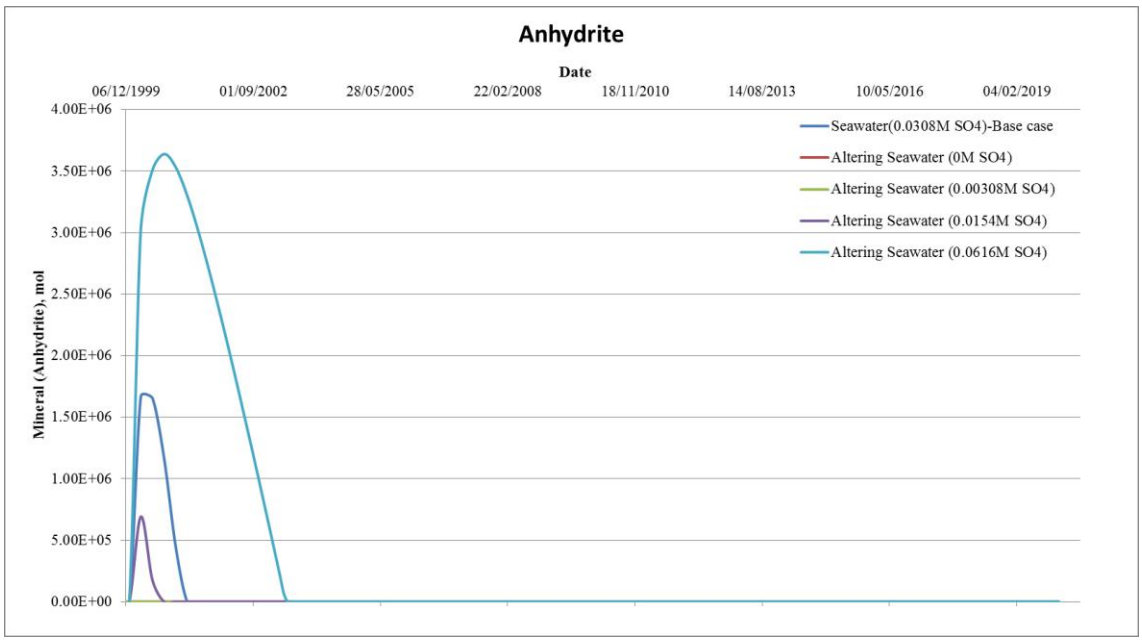

Figure 7.8 The mineral change of calcite (top) and anhydrite (bottom) in the top layer of the injector. Cell (13,13,1)

Figure 7.9 shows the behaviour of calcite and anhydrite minerals downstream. The calcite change is more or less similar with what we have presented in the isothermal case, but anhydrite is dissolved after hitting the peak of deposition as the temperature is gradually lowered by the advancing cool injection water.

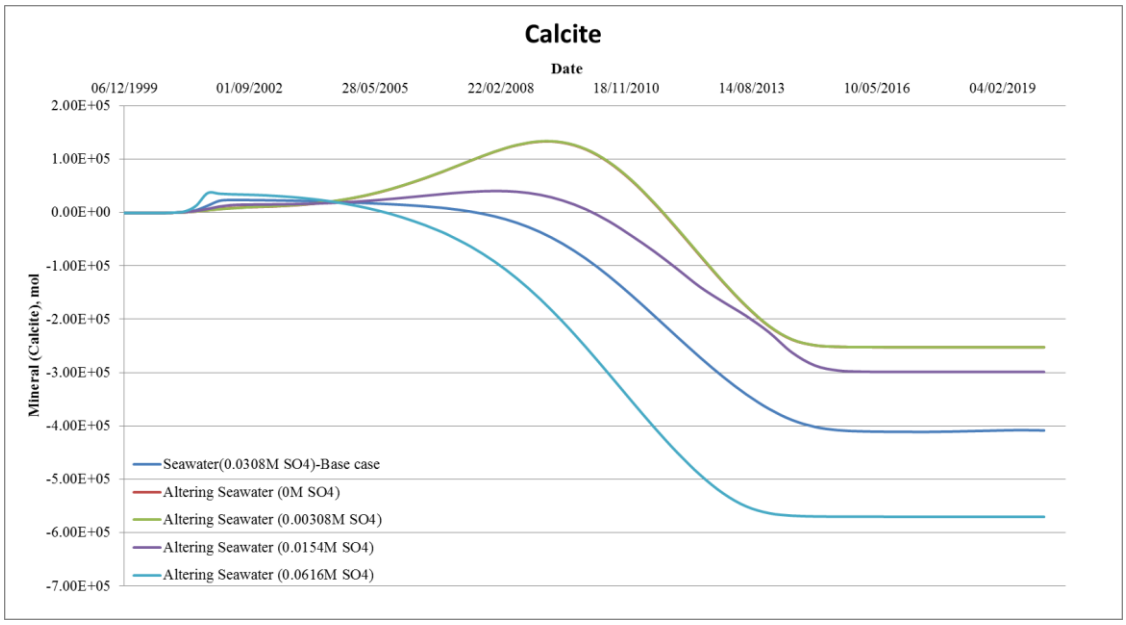

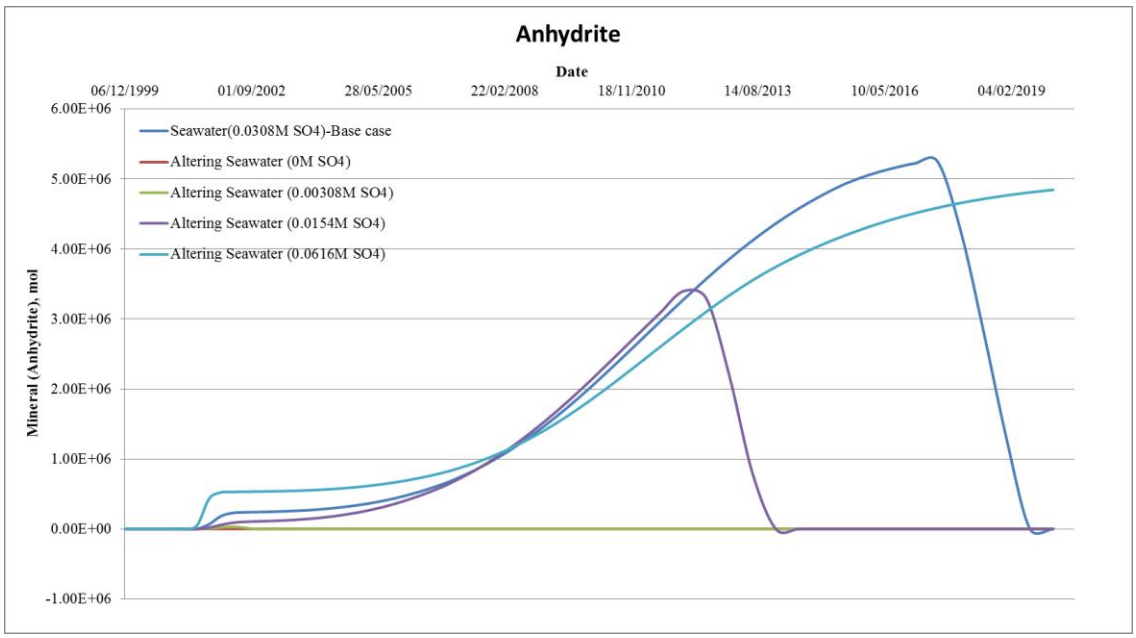

Figure 7.9 The mineral change of calcite (top) and anhydrite (bottom) in the top layer of one point between the injector and the producer. Cell (11,11,1)

A comparison of the amount of calcite dissolved around the injection well during seawater injection when heat transfer is included (*dotted* lines) and when it is not (*solid* lines) is presented in **Figure 7.10**. Although high sulphate concentration (*green lines*) always leads to more calcite dissolution than low sulphate concentration (*red lines*), the difference when thermal cooling is accounted for is much smaller. This is because anhydrite is more soluble at lower temperature.

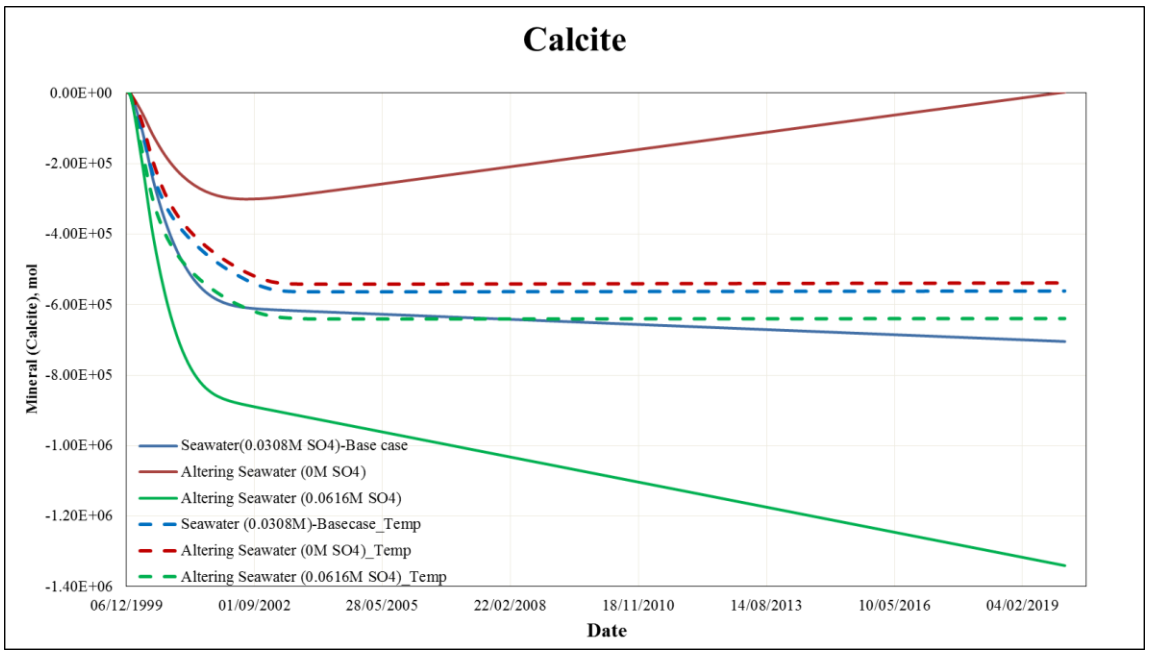

Figure 7.10 The amount of dissolved calcite with thermal modelling (dotted lines) and without thermal modelling (solid lines) for the cell with the injection well.

Figure 7.11 shows the development over time of the chloride concentration (red), the molality of CO_2 (light blue), temperature (green), calcite (pink) and anhydrite (blue) mineral change at cell (11,11,1) in the seawater injection case. It indicates that away from the injector, the partitioning of CO_2 into the brine phase is reduced as the rock cools, and in this case the complete consumption of CO_2 is delayed by some five years compared to the isothermal model. This means that calcite is being dissolved for a longer period. Almost an order of magnitude more anhydrite precipitates than in the isothermal case, despite the reduced solubility at the lower temperature. As noted previously sulphate availability is the limiting factor in this reaction. Since calcite is dissolving at later time when there will have been more sulphate injected, the mass of anhydrite precipitated is greater. However, when the temperature reduces sufficiently (to below 40^{o}C), all the anhydrite then re-dissolves, and there will be no further dissolution of calcite.

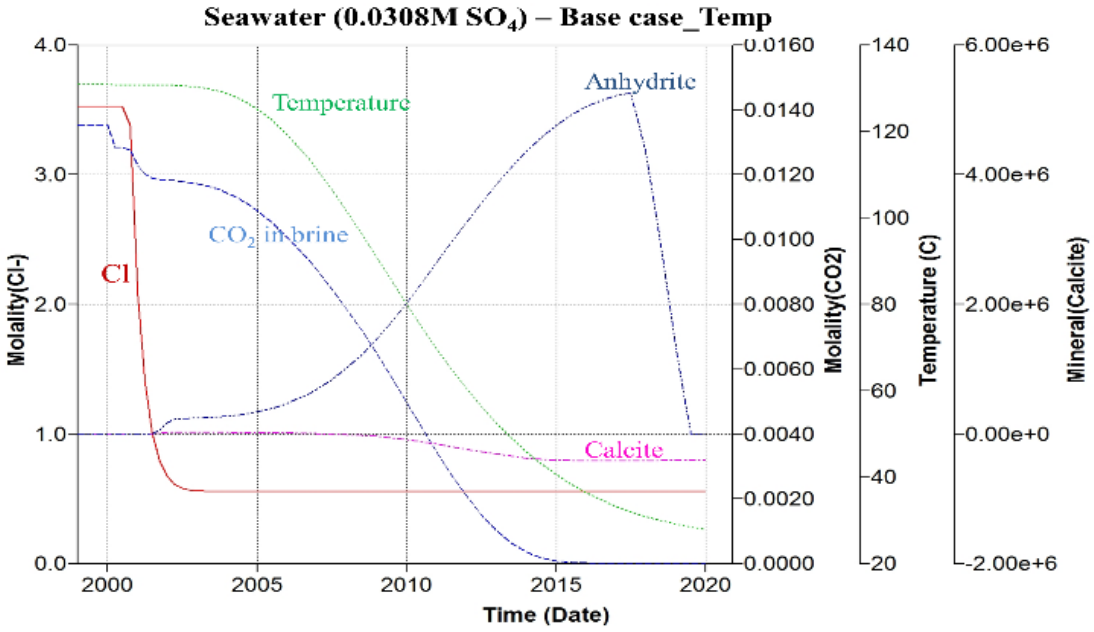

Figure 7.11 The development of chloride, CO_2 in brine, temperature, the changes of calcite and anhydrite minerals at cell (11,11,1).

Figure 7.12 illustrates the distribution of minerals across the reservoir in the non-isothermal cases. In the case that accounts for thermal cooling, less calcite is dissolved, as noted above. Effectively, a bank of anhydrite will be deposited in the hot zone and be dissolved again by the cold front. Thus this bank will propagate ahead of the thermal front, and provide a continuous supply of calcium and sulphate ions at its leading edge. From the perspective of scale precipitation this is crucial, since the sulphate ions are constrained to travel at the leading edge of the thermal front, where the abundance of calcium ions due to the anhydrite dissolution upstream causes re-precipitation of anhydrite, and therefore retardation of the sulphate. In the isothermal scenario, the maximum mass of anhydrite and barite precipitation generally occurs around the production wells, as is commonly observed in clastic reservoirs, but in the non-isothermal calculations (shown in **Figure 7.12**) the sulphate front is still distant from the producers.

3 Years

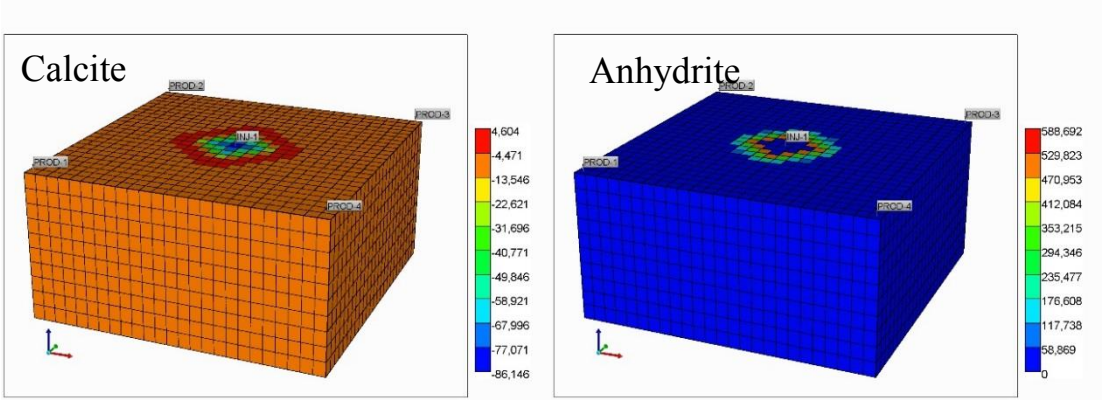

9 Years

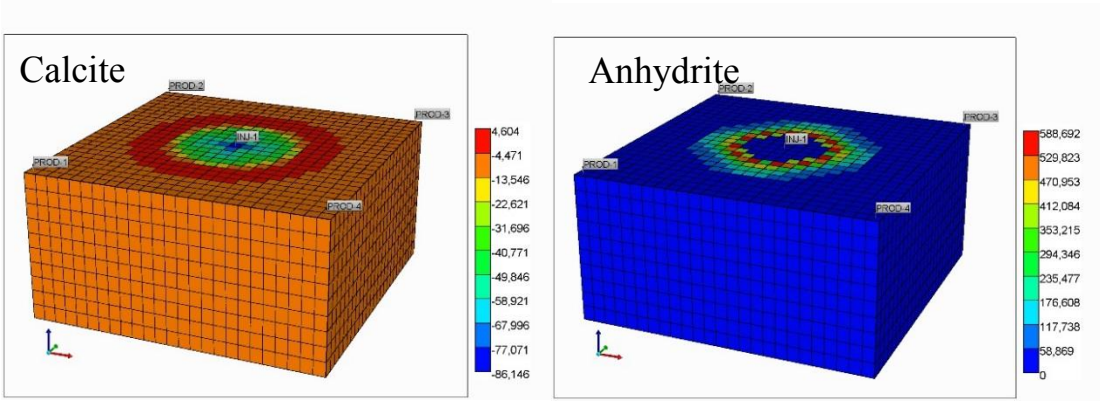

Figure 7.12 Calcite (left) and anhydrite (right) mineral distributions (in gmole) across the chalk reservoir after 3 (top) and 9 years (bottom) of seawater flooding (Non-isothermal model).

7.6 Implications for chemical EOR

When a brine that is undersaturated with respect to calcite at the various temperature and pressure conditions observed in the reservoir is injected into a chalk reservoir, it may dissolve some chalk as it enters the reservoir, but as the calcium and bicarbonate concentrations increase it will quickly become buffered, and further reactions will be prevented. It may come into contact with residual oil, with the result that some CO_2 partitions into the brine, reducing the pH and causing some more calcite dissolution, but again it will equilibrate quickly and cease to react during the rest of its transit across the reservoir.

What effect does that have if some sulphate is added to the brine prior to injection? The formation water will have a certain calcium concentration because it is in equilibrium with the chalk matrix, and so there may be some mixing between the formation water and the sulphate rich injection water. This may lead to gypsum or anhydrite precipitation.

However, this will be limited because the reservoir is not an efficient reaction vessel for fluid-fluid contact: if this litre of brine has been preceded by a million other litres of brine injected before it, it may not contact any formation water at all. However, if calcite is being dissolved, this will be a much more effective source of calcium to drive the gypsum or anhydrite precipitation. The reaction now being impacted by the fact that the subsurface formation is a very efficient reaction vessel for fluid rock contact. However, importantly, not only will the calcite dissolution serve to drive the gypsum or anhydrite precipitation, but they, in turn, will serve to drive the calcite dissolution. The calcite that is being loaded into the brine by the calcite dissolution reaction will be stripped out of the brine by the gypsum or anhydrite precipitation reaction, which means that the brine does not become equilibrated with respect to calcite, and so further calcite dissolution will occur.

As we stated previously, it has been demonstrated by some published experimental results that the dissolution of calcite was considered one of the important mechanisms to enhance the oil recovery (Nasralla et al., 2014; Ouden et al., 2015) and the addition of sulphate to the brine will serve to promote the calcite dissolution as well. The problem then becomes, what happens when the sulphate is consumed. This may not occur in the single pore volume of the static experiment, but when one litre of injection brine is displaced through the reservoir, it will quickly become depleted in sulphate, so this mechanism alone will not assist the recovery significantly.

However, sulphate would be re-introduced into later injected brine if the deposited gypsum or anhydrite re-dissolves again. Obviously, this alone would be of no benefit, as the mobilisation of oil requires calcite dissolution which requires gypsum or anhydrite precipitation, not dissolution. Also why would the gypsum or anhydrite dissolve? The answer is temperature. The original series of reactions described above would occur at the leading edge of the front, which is at reservoir temperature, since the cooling effect of the injection brine is more strongly retarded by interaction with the rock than any of the saturation or compositional fronts. The reactions will continue until the sulphate is depleted, or sufficient gypsum or anhydrite has deposited to coat the rock surface. By this stage any incremental oil will have been mobilised in this locality. However, when the cold front eventually reaches this part of the reservoir, the precipitated gypsum or anhydrite will re-dissolve due to the increase in solubility. The released calcium and sulphate ions will then be mobilised, and, crucially, be able to travel faster than the

thermal front, and so be propagated into the hot zone, where the whole process can begin again, releasing more oil.

Effectively, a bank of gypsum or anhydrite will be deposited in the hot zone and be dissolved again by the cold front. Thus this bank will propagate ahead of the thermal front, and provide a continuous supply of calcium and sulphate ions at its leading edge which. If this mechanism is correct, it can mobilise the oil. It then becomes a matter of economics as to how long to keep the flood going, but incremental oil should be expected until the gypsum or anhydrite front reaches the production well. This effect may already be occurring in Ekofisk field but has not been identified.

7.7 Conclusions

A 3D reactive transport model was developed to carry out an investigation of the geochemical process during (altered) seawater injection into carbonate reservoirs. Calcite and anhydrite mineral reactions are identified to be key geochemical reactions and should be focused on in this study although there is some barite and celestite precipitation due to mixing of formation and injection water.

The main finding of this work is that calcite dissolution is promoted by the increase in sulphate concentration in the injection water, since this drives an anhydrite precipitation reaction that consumes calcium. The injected water has stronger ability to dissolve calcite at higher temperature since anhydrite precipitation that is favoured by the increase in temperature significantly drives more calcite dissolution. This temperature dependent process will affect oil that is bound to the chalk surface. Also, the scaling risk at production wells will be delayed by the retardation of sulphate.

CHAPTER 8 SUMMARY, CONCLUSIONS AND FUTURE RECOMMENDATIONS

8.1 Summary and conclusions

Thermodynamic modelling (batch models) and 1D/2D/3D reactive transport models in combination with analysing produced water chemistry data from five selective fields were used to develop a deep understanding of what geochemical reactions are taking place within different reservoir scenarios, other relevant data were identified as the reservoir rock mineralogies, formation water compositions, injection water compositions and physical conditions (temperature and pressure). The geochemical models which have been developed using PHREEQC, FrontSim and CMG GEM provide support for the identification of reactions based on the initial analysis of the produced water chemistry data. This study identifies that these models should be used as learning tools to improve our understanding of the reservoir system under study, and they provide some degree of validation of the choice of reaction mechanisms to explain produced brine compositional trends.

8.1.1 Geochemical reactions

Some barite precipitation, due to chemical incompatibility of injected seawater rich in sulphate and formation water containing barium, commonly takes place within each of the reservoir system studied here, although dissolution of initial barite minerals (if present) or re-dissolution of deposited barite have not been observed. For the typical sandstone reservoirs, such as Field X and the Miller Field, barium sulphate deposition occurring within the reservoir leads to significant barium stripping and produced water having lower barium concentration; while the trends of produced *sulphate* concentrations show no strong deviation from the sulphate mixing line. The occurrence of barite precipitation deep within the reservoir is beneficial for lowering the scaling risk in the near wellbore region and the production wellbore itself. In contrast to the typical sandstone reservoirs, in the Ekofisk field (a chalk reservoir) and the Gyda field (a sandstone where there is formation water with extremely high calcium concentration), barium levels in the produced brine do not vary much below the mixing line, and thus very little barium sulphate precipitation is occurring within the reservoir.

In the Miller and X fields, small amounts of strontium sulphate were shown to have precipitated at low IWFs, but some of this was then re-dissolved at higher IWFs. It also

can be noted that strontium stripping due to strontium sulphate precipitation is weaker than the depletion in barium as a result of barium sulphate scale formation in the reservoir.

Calcium sulphate has been precipitated within the reservoir in the cases of the Gyda and Ekofisk fields. Theoretical and real anhydrite scaling tendencies demonstrate that the saturation ratio and maximum precipitation were significantly reduced, and most of the anhydrite was precipitated in the reservoir. The high reservoir temperatures (160℃ and 131℃ respectively) and high calcium concentrations provide a strong driving force for calcium sulphate precipitation. The precipitated calcium sulphate was shown to have dissolved as the local reservoir temperature is lowered by cool injection water; the calcium and sulphate due to dissolution re-precipitate as anhydrite and gypsum downstream as the brine flows through more quickly than the temperature front propagates.

Calcite was dissolved in the Ekofisk field as the injected seawater takes up CO_2 and becomes acidic. The precipitation of calcium magnesium carbonate mineral is usually accompanied by calcite dissolution, as it occurs due to there being a substantial source of calcium, so it is more likely to take place in chalk reservoirs (such as the Ekofisk field), and less likely to occur in pure sandstone reservoirs (such as Field X).

Calcium release and magnesium stripping induced by multicomponent ion exchange is identified as a plausible mechanism to cause lower magnesium concentration produced in the effluent since clays are usually present in sandstone reservoirs (X, Miller and Gyda fields). The extent of ion exchange reaction occurring in the sandstone reservoirs is determined by the clay content. Ion exchange occurring in the Ekofisk field was also proposed to fully explain the extent of magnesium depletion in the reservoir.

The process of using the model to match the observed produced water chemistry data enables Cation Exchange Capacity to be determined. This may be of importance for chemical EOR methods, such as low salinity waterflooding, which may depend on ion exchange for mobilisation of oil.

Analysis of layered model in the Gyda case shows that flow thorough segregated layer of different permeability reduce the extent of mixing in the reservoir relative to homogeneous model, and thus more mixing will take place in the wellbore itself in layered systems.

8.1.2 Implications of scale management

The scaling risk of barium sulphate deposition *at producer wells* is not ever eliminated even though it is lowered by barite precipitated within the reservoir for the X and Miller fields. Even in the X Field, where there have been very low produced barium concentrations (<10mg/l) in the produced water due to barium stripping, the analyses shows there is still a risk of scale precipitation in the wellbore that needs to be managed. Therefore, caution has to be taken in evaluating and predicting barium concentrations in the produced brine - reservoir stripping does not eliminate the problems at the well. However, these data are helpful for determination of MIC (minimum inhibitor concentration) during squeeze treatments since chemical remediation requirement are very sensitive to brine composition.

To varying degrees, magnesium was absorbed onto the rock surface and calcium was released into the brine during ion exchange process as in all four fields studied. This implies that magnesium is not a conservative tracer and cannot be used to calculate the IWF. For some operators who calculate the IWF based on magnesium, the timing of the seawater breakthrough would be underestimated and squeeze treatment would not be implemented in a timely fashion.

The implications from the Gyda and Ekofisk studies are that although the barium concentrations in the formation brines are high, the presence of calcite and the high calcium concentrations in the formation brines, coupled with the high formation temperature, result in anhydrite precipitation *in situ*, which in turn strips sulphate from the injection water deep within the reservoir, and thereby initially reduces the barite and anhydrite scaling tendencies at the producers. However, this *in situ* stripping process is not merely a consequence of brine mixing deep within the reservoir – it is also dependent on brine-rock interactions, and on the propagation of the thermal front. Thus the reactions are more extensive than if purely induced by brine mixing, and hence lead to the observation that sulphate can be completely stripped out of the brine up to seawater fractions of up to 90%. Effectively a bank of anhydrite is laid down in the reservoir and then removed, the leading edge occurring at the seawater-formation water mixing front, the trailing edge occurring at the cooling front.

The benefit to the operator is that the sulphate scaling risk at the production wells is initially reduced. However, caution is required, since a late life anhydrite scaling risk is to be expected, and this will grow as the cooling front propagates through the reservoir, allowing precipitated anhydrite to dissolve and then re-precipitate, ever closer to the

production wells. In contrast to conventional systems where the sulphate scaling risk tends to decrease as seawater fraction exceeds 50%, in the Gyda field it is to be expected that this scaling risk will increase.

For the Miller Field, streamline modelling, in which barite precipitation is assumed possibly throughout the reservoir might up to the sandface of the producer well, the difference between modelled data and observed data, which included the effect of squeeze treatment that protect the near well formation, is used to assess the effectiveness of the squeeze treatment.

This body of work has described the initial development of database of produced water composition, and the development of modelling technique to assist in the analysis of these data. The method has been demonstrated for four fields, with insights gained that impact scale management in these and analogues systems.

8.2 Future recommendations

Data from fields in which produced water chemistry data have been collected into our produced water database are from sandstone reservoirs located in the North Sea region where seawater has been injected. I recommend extending the range of such fields as much as possible, and I would also emphasise the need to process data from more fields around the world with different brine compositions, rock mineralogies, reservoir conditions and where the fields are naturally or artificially flooded with brines of different compositions, or are steam flooded, so as to reveal and identify more trends and reservoir interactions occurring in the reservoir across these systems.

The reactive transport model I used in this thesis could be improved in a variety of ways in the future through coping with the limitations of those models. The GEM geochemical model used in Chapters 5 and 7 needs to be improved. First of all, the equilibrium model could be included as an alternative approach to describe mineral reactions as in most cases the flow rate of the brine deep within the reservoir is so slow relative to the reaction rate that the reservoir brine could reach the equilibrium in the reservoir (fluid/gas/rock) system. Secondly, the activity models that are available to be used in GEM are IDEAL, DEBYE-HUCKEL and B-DOT models. However, these models consider only the interaction of the species with the solution medium and therefore have limited accuracy in highly saline solutions. The PITZER model calculates activity coefficients by incorporating short-range interactions between ion pairs and triplets, and thus can accurately model them in solutions up to 6 mol/kgw (Pitzer, 1987). Therefore, the introduction of the PITZER

activity model in systems with salinities of 0.5 mol/kgw and above would be helpful for more accurate modelling of chemical and mineral reactions.

The PHREEQC model that has been used in Chapters 3 and 6 has a good capability to simulate geochemical processes in a 1D flow path, but its main limitation is the inability to simulate two/three dimensional multiphase (oil and gas phase) flow. In reality, complicated geological parameters affecting fluid flow in porous media need to be considered and the effects of the hydrocarbon phases on geochemical reactions are also necessary. Hence coupling the PHREEQC with a reservoir simulator would greatly help accurately identify and model geochemical reactions occurring deep within the reservoir.

For all reactive transport models, one of the biggest challenges is the lack of experimental data to validate and improve the applicability of an equilibrium model at actual reservoir conditions (high temperature, high pressure and high salinity) and a kinetic model. The thermodynamic equilibrium constants used in the model are often not appropriate for oilfield systems, and the kinetic reaction rate parameters are certainly not accurate either. Thus more reliable data obtained from experiments are essential for improvement of current thermodynamic/kinetic models and better simulating reservoir interactions.

REFERENCES

Agarwal, B., Hermansen, H. and Sylte, J.E., 1999. Reservoir characterization of Ekofisk Field: A Giant, Fractured Chalk Reservoir in the Norwegian North Sea – History Match. Paper SPE 68096 presented at the SPE Reservoir Simulation Symposium held in Houston, Texas, 14-17 February 1999.

Alam, M.M., Ahsan, R., Shaik, A.K. and Fabricius, I.L., 2010. Surface charge of calcite and its influence on the electrical conductivity in chalk. Paper presented at the 2010 Annual Meeting of SEG.

Al-Attar, H.H., Mahmoud, M.Y., Zekri, A.Y, Almehaideb, R. and Ghannam, M., 2013. Low-salinity flooding in a selected carbonate reservoir: experimental approach. J Petroleum. Exploration and Production Technology 3 (2), 139-149.

Al-Mayshi, N.M., Snippe, J., Rucci, F., and Linthorst, S., 2012, Water Injection Subsurface Challenges and Reactive Transport Modelling. Paper SPE 154457 presented at the SPE EOR Conference at Oil and Gas West Asia held in Muscat, Oman, 16-18 April.

Al-Shalabi, E.W., Sepehrnoori, K. and Delshad, M., 2014. Mechanisms behind low salinity water injection in carbonate reservoirs. Fuel 121, 11–19.

Andersen, P.Ø. Evje, S., Madlan, M.V. and Hiorth, A., 2012. A geochemical model for interpretation of chalk core flooding experiments. Chemical Engineering Science 84 (2012), 218-241.

Appelo, C. A. J., 2014. Equations for calculating hydrogeochemical reactions of minerals and gases such as CO2 at high pressures and temperatures. Geochim. Cosmochim. Acta 125: 49-67.

Appelo, C. A. J., 2015. Principles, caveats and improvements in databases for calculating hydrogeochemical reactions in saline waters from 0 to 200 °C and 1 to 1000 atm. Applied Geochemistry 55: 62 – 71.

Austad, T., Shariatpanahi, S.F., Strand, S., Aksulu, H. and Puntervold, T., 2015. Low Salinity EOR-effects in limestone reservoir cores containing anhydrite: a discussion of the chemical mechanism. Energy Fuels, 29 (11), 6903–6911.

Awolayo, A., Sarma, H. and AlSumaiti, A., 2015. An Experimental Investigation into the Impact of Sulfate Ions in Smart Water to Improve Oil Recovery in Carbonate Reservoirs. Transport in Porous Media 1-20.

Appelo, C.A.J and Postma, D., 2010, Geochemistry groundwater and pollution, CRC Press.

Baraka-Lokmane, S. and Hurtevent, C., 2014. Chemical Incompatibility between Formation Water and Injection Water; Comparison between Modeling and Site Observations in Fields Operated by TOTAL. Paper SPE 161314 presented at the SPE Abu Dhabi International Petroleum Exhibition & Conference held in Abu Dhabi, UAE, 11-14 November 2014.

Bazin, B. and Labrid, J., 1991. Ion Exchange and Dissolution/ Precipitation Modeling: Application to the Injection of Aqueous Fluids Into a Reservoir Sandstone. SPE Reservoir Engineering (May 1991) 6(02), 233-238.

Bedient, P., Rifai, H. and Newell, C., 1999. Ground water contamination – transport and remediation. 2nd edition, Prentice Hall PTR, New Jersey, USA.

Bethke, C.M., 1996. Geochemical Reaction Modelling, Oxford Univ. Press, New York.

Bjørlykke K. and Gran K., 1994. Salinity variations in North Sea formation waters: implications for large-scale fluid movements. Marine and Petroleum Geology (February 1994) 11(01), 5-9.

Block, J., Waters, O.B., 1968. The CaSO4–Na2SO4–NaCl–H2O system at 25–100 °C. J. Chem. Eng. Data 13, 336–344.

Blounot, C.W. and Dickson, F.W., 1969. The solubility of anhydrite (CaSO4) in NaCl-H2O from 100 to 450°C and 1 to 1000 bars. Geochimica et Cosmochimica Acta. (February 1969) 33(02), 227-245.

Blounot, C.W., 1977. Barites solubilities and thermodynamic quantities up to 300°C and 1400 bars. American Mineralogist (January 1977) 62, 942-957.

Bourne, H.M., Williams, G. and Hughes, C.T., 2000. Increasing squeeze life on Miller with new inhibitor chemistry. Paper SPE 60198 presented at the 2000 second International Symp. On oilfield scale held in Aberdeen, UK, 26-27 January 2000.

Brantley, S.L., Kubicki, J.D. and White, A.F., 2007. Kinetics of Water-Rock Interactions. Springer.

Carlyle, H.F., Tellam, J.H. and Parker, K.E., 2004. The use of laboratory-determined ion exchange parameters in the predictive modelling of field-scale major cation migration in groundwater over a 40-year period. Journal of Contaminant Hydrology (January 2004) 68(1-2), 55-81.

Charleston, J., 1968. Scale Removal in the Virden, Manitoba Area. Paper SPE 2160 presented at 43rd Annual SPE Meeting, 1968, Houston, Texas.

Christian, T.M., Currie, J.C., Lantz, T.G., Rismyhr, O. and Snow, S.E., 1993. Reservoir management at Ekofisk field. Paper SPE 26623 prepared for presentation at the 68th Annual Technical Conference and Exhibition of the Society of Petroleum Engineers held in Houston, Texas, October 3-6, 1993.

Collins, I. R., Duncum, S.D., Jordan, M.M., Feasey, N.D., 2006. The Development of a Revolution Scale-Control Product for the Control of Near-Well Bore Sulphate Scale Within Production Wells by the Treatment of Injection Seawater. Paper SPE 100357 presented at the SPE International Oilfield Scale Symposium, 31 May-1 June 2006, Aberdeen, UK.

Computer Modeling Group Ltd, 2015. Advanced Compositional and GHG Reservoir Simulator, User's guide.

Craig, F., 1971, The Reservoir Aspects of Waterflooding, SPE monograph, Vol 3.

Dai, Z., Shi, W., Kan, A.T., Zhang, N., Tomson, M.B., 2014. Improvement of Thermodynamic Modelling of Calcium Carbonate and Calcium Sulphates at High Temperature and High Pressure in Mixed Electrolytes. Paper SPE169786 presented at the SPE International Oilfield Scale Symposium, Aberdeen, UK, 14-15 May 2014.

Datta-Gupta, A. and King, M. J., 2007. Streamline Simulation: Theory and Practice. Society of Petroleum Engineers.

Davies, C.W., 1962. Ion Association. London: Butterworths, 37–53.

Debye, P. and Hückel, E., 1923. The theory of electrolytes. I. Lowering of freezing point and related phenomena. Physikalische Zeitschrift 24, 185–206.

Delshad, M. and Pope, G.A., 2003. Effect of dispersion on transport and precipitation of barium and sulphate in oil reservoirs. Paper SPE 80253 presented at the SPE International Symposium on Oilfield Chemistry held in Houston, Teas, U.S.A., 5-7 February 2003.

Egeberg P. K. and Aagaard P., 1989. Origin and evolution of formation waters from oil fields on the Norwegian Shelf. Applied Geochemistry (March-April 1989), 4(02), 131-142.

Fabricius, I.L., Olsen, C. and Prasad, M., 2005. Log Interpretation of Marly Chalk, the Lower Cretaceous Valdemar Field, Danish North Sea: Application of Iso-frame and Pseudo Water Film Concepts. The Leading Edge, 24, No.5, 496.

Featherston,A. B., Mihram, R. G., and Waters, A. B., 1959a. Minimizationof Scale Deposits in Oil Wells by Placement of Phosphates in Producing Zones. J. Pet. Tech. 11(03), 29-32.

Featherston,A. B., 1959b. Removal and Prevention of Scale in Producing Oil Wells. Paper SPE 1238-G presented at the Drilling and Production Practices Meeting, April, 1959, Lafayette, La.

Fjelde, I., Asen, S.M., and Omekeh, A., 2012. Low Salinity Water Flooding Experiments and Interpretation by Simulations. Paper SPE 154142 presented at the SPE Improved Oil Recovery Symposium, Tulsa, Oklahoma, USA.

Fu, Y., Berk, W.V., Schulz, H.M., 2012. Hydrogeochemical Modelling of Fluid-Rock Interactions Triggered by Seawater Injection into Oil Reservoirs: Case Study Miller Fields (UK North Sea). Applied Geochemistry (March 2012), 27 (06), 1266-1277.

Fu, Y., Berk, W.V., Schulz, H.M., 2013. Temporal and spatial development of scale formation: One-dimensional hydrogeochemical transport modelling. Journal of Petroleum Science and Engineering, (November 2013), 112 (2013), 273-283.

Gomes, R.M., Mackay, E.J., Deucher, R.H., Bezerra, M.C.M., Rosario, F.F. and Jordan, M.M., 2012, Impact of Reservoir Reactions on Thermodynamic Scale Predictions. Paper SPE 155255 presented at the SPE International Conference and Exhibition on Oilfield Scale, Aberdeen, U.K., 30-31 May.

Hallenbeck, L.D., Sylte, J.E. and Ebbs, D.J., 1991. Implementation of the Ekofisk Field Waterflood. SPE Journal (September 1991), 6(03), 284 – 290.

Hardie, L. A., 1967. The gypsum-anhydrite equilibrium at one atmosphere pressure. The American Mineralogist, Vol, 52, January-February.

Hassane, T., 2013. The application of streamline reservoir simulation calculations to the management of oilfield scale. Heriot-Watt University PhD Thesis, June 2013.

Helgeson, H.C., 1969, Thermodynamics of hydrothermal systems at elevated temperatures and pressures. Am J Sci, 267, 729-804.

Houston, S.J., Yardley, B.W.D and Smalley, P.C. and Collins, I., 2006, Precipitation and Dissolution of Minerals During Waterflooding of a North Sea Oil Field. Paper SPE 100603 presented at the 2006 SPE International Oilfield Scale Symposium, Aberdeen, UK, 30 May-1 June.

Huseby, O., Chatzichchristtos, C., Sagen, J., Muller, J., Kleven, R., Bennett, B. and Larter, S., 2005. Use of natural geochemical tracers to improve reservoir simulation models. Journal of Petroleum Science and Engineering, 48 (2005), 241– 253.

Ishkov, O., Mackay, E.J., and Sorbie, K. S., 2009, Reacting Ions Method to Identify Injected Water Fraction in Produced Brine. Paper SPE 121701 presented at the SPE Oilfield Chemistry Symposium, The Woodlands, Texas, 20-22 April 2009.

Jonasson, R.G., 1991. Interaction of Phosphonate Scale Inhibitors with Mineral Surfaces during the Steam Stimulated Recovery of Bitumen. Paper presented at the Proceedings of the 6th IFP Exploration and Production Research Conference, held in Saint-Raphaël, September 4-6, 1991.

Kaasa, B., 1998, Prediction of pH, mineral precipitation and multiphase equilibria during oil recovery: IUK-PhD Thesis. The Norwegian University of Science and Technology, Trondheim, Norway.

Kleven, R. and Alstad., J., 1996. Interaction of alkali, alkaline-earth and sulphate ions with clay minerals and sedimentary rocks. J. Pet. Sci. Eng., 15 (2-4), 181–200.

Kletinitz, W., Koehler, M., and Kietzsch, G., 2001. The precipitation of Salt in Gas Producing Wells. Paper SPE 68953 Presented at the European Formation Damage Conference, The Hague, Netherlands, 21-22 May.

Kokal, S. and Kaabi, A., 2010. Enhanced oil recovery: challenges & opportunities. World Petroleum Council: Official Publication.

Langmuir, D., 1997. Aqueous environmental geochemistry. Prentice Hall.

Lasater, R. M., Gardner, T. R., and Glasscock, F. M., 1968. Scale Deposits are Controlled Now with Liquid Inhibitors. Oil and Gas Journal, (Jan., 1968), 66(03).

Levenspiel, O., 1986. The Chemical Reactor Omnibook, O.S.U., Book Store Inc,New York, USA.

Lide, D, R. (Editor-in-Chief), 1995. CRC Handbook of Chemistry and Physics, 75th Ed. CRC Press Inc.

Lu, J., Wilkinson, M., Haszeldine, R. S., Boyce, A.J., 2011. Carbonate cements in Miller field of the UK North Sea: a natural analog for mineral trapping in CO2 geological storage. Environ Earth Sci (Feb. 2011), 62(03), 507–517.

Machel, H. and Mountjoy, E.W., 1986. Chemistry and Environments of Dolomitization —A Reappraisal. Earth-Science Reviews, 23 (3), 175-222.

Mackay, E.J. and Sorbie, K.S., 2000, Brine Mixing in Waterflooded Reservoirs and the Implications for Scale Prevention. Paper SPE 60193 presented at the SPE 2nd International Symposium on Oilfield Scale, Aberdeen, UK, 26-27 January.

Mackay, E.J., Graham, G.M., 2002. The use of flow models in assessing the risk of scale damage. Paper SPE 80252, SPE International Symposium Oilfield Chemistry, Houston, Texas, USA (2002), 20-21 February.

Mackay, E. J., 2003a. Modeling in-situ scale deposition: the impact of reservoir and well geometries and kinetic reaction rates. SPE Production and Facilities, 18(01), 45-56.

Mackay, E., 2003b. Predicting in situ sulphate scale deposition and the impact on produced ion concentrations. Chemical Engineering Research and Design, 81(03), 326-332.

Mackay, E. J., Jordan, M. M. and Torabi, F., 2003c. Predicting brine mixing deep within the reservoir and the impact on scale control in marginal and deepwater developments. SPE Production and Facilities. 18(03), 210-220.

Mackay, E. J., and Graham, G.M., 2003d. The Use of Flow Models in Assessing the Risk of Scale Damage. Paper SPE 80252 presented at the International Symposium on Oilfield Chemistry, 5-7 February, Houston, Texas, USA, 20–21 Feb. 2003.

Mackay, E. J., Jordan, M. M., Feasey, N. D., Shah, D., Kumar, P. and Ali, S. A., 2005a. Integrated risk analysis for scale management in deepwater developments. SPE Production and Facilities, 20(02), 138-154.

Mackay, E. J. & Jordan, M. M., 2005b. Impact of brine flow and mixing in the reservoir on scale control risk assessment and subsurface treatment options: Case histories. Journal of Energy Resources Technology. 127(03), 201-213.

Mackay, E.J., Sorbie, K.S, Kavle, V., Sørhaug, Melvin, Sjursaether, Jordan, M., 2006, Impact of In-Situ Sulphate Stripping on Scale Management in the Gyda Field. Paper 100516 presented at the SPE International Symposium on Oilfield scale, Aberdeen, UK, 30 May-1 June.

Mackay, E. and Martins, S.A.P., 2014a. Modelling of CO2 and Seawater Injection in Carbonate Reservoirs to Evaluate Inorganic Scaling Risk. Paper SPE 169766 presented at the SPE International Oilfield Scale Conference and Exhibition, 14-15 May, Aberdeen, Scotland.

Mackay, E.J., Jordan, M.M. and Ishkov, O. and Vazquez, O., 2014b. Reservoir simulation, ion reactions, and near-wellbore modelling to aid scale management in a subsea Gulf of Mexico field. SPE Prod & Facilities (Aug 2014), 29 (3), 172-182.

Madland, M.V., hiorth, A., Omdal, E., Megawati, M., Hildebrand-Habel, T., Korsnes, R.I.,Evje, S., Cathles, L.M., 2011. Chemical alterations induced by rock-fluid interactions when injecting brines in high porosity chalks. Transp. Porous media (April 2011), 87(03), 679-702

Marchand, A.M.E., Haszeldine, R.S., Smaller, P.C., Macaulay, C.I., Fallick, A.E., 2001. Evidence for reduced quartz cementation rates in oil-rilled sandstones. Geology 29, 915-918.

Marchand, A.M.E., Smaller, P.C., Haszeldine, R.S., Fallick, A.E., 2002. Pore water evolution in oilfield sandstones: constraints from oxygen isotope microanalysis of quartz cement. Chem Geol (Nov. 2002), 191(04), 285-304.

McElhiney, J.E., Sydansk, R.D., Lintelmann, K.A. and Benzel, W.M., 2000. Determination of In-Situ Precipitation of Barium Sulphate During Coreflooding. Paper SPE 68309 presented at the SPE 3rd International Symposium on Oilfield Scale, Aberdeen, Scotland, 30-31 January 2000.

McCartney, R. A., Williams, J. C., & Coghlan, G. P., 2005. Processes determining the composition of produced water from subsea fields and implications for scale management - Birch Field, UKCS. Paper SPE 94869 presented at the SPE International Symposium on Oilfield Scale, 11-12 May, Aberdeen, UK.

McCartney, R. A., 2008. Conditions under which anhydrite precipitation can occur in oil reservoirs as a result of seawater injection. Paper presented at the 19th International Oilfield Chemistry Symposium, Geilo, Norway, 9-12 March.

McCartney, R. A., Melvin, K., Wright, R and Sørhaug, E., 2007. Seawater injection into reservoirs with ion exchange properties and high sulphate scaling tendencies: Modelling of reactions and implications for scale management, with specific application to the Gyda Field. Paper prepared for the 18th International Oilfield Chemistry Symposium, Geilo, Norway, 26-28 March.

McCartney, R. A., Tjomsland, T., Sandøy, B. and Fadnes, F. H., 2012. Application of multi-rate well tests (MRT) to scale management. Part 1: Interpretation of produced water analyses. SPE Production and Facilities, 27(03), 211-222.

Meister, P., Reyes, C., Beaumont, W., Rincon, M., Collins, L., Berelson, W., Stott, L., Corsetti, F. and Nealson, K.H., 2011. Calcium and magnesium-limited dolomite precipitation at Deep Springs Lake, California, Sedimentology (December 2011) 58(07), 1810-1830.

Mitchell, R.W., Grist, D.M. and Boyle M.J., 1980. Chemical Treatments Associated with North Sea Projects. J. Pet Tech (May 1980), 32 (05), 904-912.

Montes-Hernandez, G., Findling, N., Renard, F. and Auzende, A.-L., 2014. Precipitation of Ordered Dolomite via Simultaneous Dissolution of Calcite and Magnesite: New Experimental Insights into an Old Precipitation Enigma. Cryst. Growth Des. (January 2014) 14(2), 671–677.

Moss B., Barson D., Rakhit K., Dennis H., and Swarbrick R. E., 2003. Formation pore pressures and formation waters. In The Millenium Atlas: Petroleum Geology of the Central and North Sea (ed. D. Evans, C. M. Graham, A. Armour, and P. Bathurst). Geological Society.

Nasralla, R.A., Sergienko, K., Masalmeh, S.K., Van der linde, H.A., Brussee, N.J., Mahani, H., Suijkerbuijk, B. and Alqarshubi, L., 2014. Demonstrating the Potential of Low-Salinity Waterflood to Improve Oil Recovery in Carbonate Reservoirs by Qualitative Coreflood. Paper SPE 172010 presented at the Abu Dhabi International Petroleum Exhibition and Conference held in Abu Dhabi, UAE, 10-13 November 2014.

Oddo, J.E. and Tomson, M.B., 1994. Why Scale Forms in the Oil Field and Methods To Predict It. SPE Production & Facilities (February 1994) 9(01), 47-54.

Østvold, T., Mackay, E.J., McCartney, R., Davis, I.R. and Aune, E.D., 2010. Redevelopment of the Froy Field: Selection of the Injection Water. Paper SPE130567, presented at the SPE International Conference on Oilfield Scale, 26-27 May, Aberdeen, UK.

Ouden, L.D., Nasralla, R.A., Guo, H., Bruining, H. and Van Kruijsdijk, C.P.J.W., 2015. Calcite Dissolution Behaviour During Low Salinity Water Flooding in Carbonate Rock. Paper presented at the 18th European Symposium on Improved Oil Recovery.

Parkhurst, D. L., 1990. Ion association models and mean activity coefficients of various salts. In D. C. Melchior and R. L. Basset (eds). Chemical modelling of aqueous systems II. ACS Symp. Ser. 416, 30-43.

Parkhurst, D.L., and Appelo, C.A.J., 1999. User's guide to PHREEQC (version 2)—a computer program for speciation, batch-reaction, one-dimensional transport, and inverse geochemical calculations: U.S. Geological Survey. Water-Resources Investigations Report 99-4259, US Geological survey, Denver, Colorado.

Paulo, J., Mackay, E. J., Menzies, N. A. & Poynton, N., 2001. Brine mixing complicates Alba field scale management. Oil and Gas Journal. 99(35), 79-93.

Pitzer, K.S., 1987, Thermodynamic model for aqueous solutions of liquid-like density: in I. S. E. Carmichael and H. P. Eugster, eds. Thermodynamic modeling of geological materials: Minerals, fluids and melts. Reviews in Mineralogy 17, 97-142.

Poynton, N., Kelly, C. and Fergusson, A., 2004. Selection and Deployment of a Scale Inhibitor Squeeze Chemical for the BP Miller Field. Paper SPE 87466, presented at the 6th International Symposium on Oilfield Scale held in Aberdeen, UK, 26-27 may 2004.

Ralston, P. H., 1969. Scale Control with Aminomethylenephosphonates. J. Pet. Tech., 21(08), 1029-1036.

Reardon, E.J. and Armstrong, D.K., 1986. Celestite ($SrSO_4(s)$) solubility in water, seawater and NaCl solution, Geochim. Cosmochim. Acta, 51(01), 63– 72.

Reed, M.H., 1982. Calculation of multicomponent chemical equilibria and reaction processes in systems involving minerals, gases, and an aqueous phase. Geochim. Cosmochim. Acta, 46 (04), 513– 528.

Robert, W.M. and Bowyer, P.M., 1982. Water Injection Methods. Paper SPE 10028 presented at International Petroleum Exhibition and Technical Symposium, 17-24 March, Beijing, China.

Rothwell, N.R., Sorensen, A., Peak, J.L., Byskov, K. and McKean, T.A.M., 1993, GYDA: Recovery of difficult reserves by flexible development and conventional reservoir management. Paper SPE 26778 presented at the Steering Committee of the European IOR Symposium, 1993.

Sánchez-Román, M., McKenzie, J.A., de Luca Rebello Wagener, A., Rivadeneyra, M.A., and Vasconcelos, C., 2009. Presence of sulphate does not inhibit low-temperature dolomite precipitation. Earth and Planetary Science Letters, 285 (1-2), 131-139.

Schmidt, T. and Thingvoll, J., 1990. New methods for the early detection of injection water breakthrough in an oil producer. UK corrosion

Shaughnessy, C.M., Kline, W.E., 1983. EDTA Removes Formation Damage at Prudhoe Bay. Journal of Petroleum Technology, 35 (10), 1783-1791.

Siegel, F.R., 1961. Factors influencing the precipitation of dolomite of dolomitic carbonates. Geological survey of Kansa Bulletin, 152 (5), 129-158.

Sorbie, K. S. and Mackay, E.J., 2000. Mixing of injected, connate and aquifer brines in waterflooding and its relevance to oilfield scaling. Journal of Petroleum Science and Engineering (July 2000) 27 (1-2), 85-106.

Slaton, L., Lasater, R., and Knox, J., 1965. Scale Deposition and Removal. Producers Monthly (Sept., 1965).

Slentz, L.W., 1981. Geochemistry of reservoir fluids as unique approach to optimum reservoir management. Paper SPE 9582 presented at the Middle East Oil Technical Conference of the SPE held in Manama, Bahrain, March 9-12, 1981.

Smith, F.W., 1978. Ion-Exchange Conditioning of Sandstones for Chemical Flooding. Journal of Petroleum Technology (June 1978) 30(06), 959-968.

Stanghelle, K.U., 2009, Evaluation of artificial lift methods on the Gyda field. Master's thesis in the University of Stavanger.

Stiff, H. A. and Davis, L. E., 1952. A Method for Predicting the Tendency of Oilfield Waters and Deposit Calcium Sulfate. Trans. AIME 195(25), 25-28.

Sylte, J.E., Hallenbeck, L.D. and Thomas, L.K., 1988. Ekofisk Formation Pilot Waterflood. Paper SPE 18276 presented at the 63rd Annual Technical Conference and Exhibition of the Society of Petroleum Engineers held in Houston, TX, October 2-5, 1988.

Templeton, C.C., 1960. Solubility of barium sulfate in sodium chloride solutions from 25°C to 95°C. J. Chem. Eng. Data 5, 514–516.

Thiele, M.R., and Batycky, R.P. and Fenwick, D.H., 2010. Streamline Simulation for Modern Reservoir-Engineering Workflows. Journal of Petroleum Technology (January 2010) 62(01), 64-70.

Uchameyshvili, N.Y., Malinin, S.D., Khitarov, N.I., 1966. Solubility of barite in concentrated chloride solutions of some metals at elevated temperatures in relation to problems of the genesis of barite deposits. Geochem. Int. 10, 951–963.

Vazquez, O., McCartney, R., Mackay, E., 2013, Produced Water Chemistry History Matching Using a 1D Reactive Injector/Produced Reservoir Model. SPE Production and Facilities, 28(4), 369-375.

Vazquez, O., Young, C., Demyanov, V. and Arnold, D., 2015. Produced Water Chemistry History Matchin in the Janice Field. Paper SPE 164903, SPE Prod & Facilities (Nov 2015) 18 (4), 564-576.

Vetter O. J. G., 1975. Oilfield Scale- Can we Handel it?. Journal of Petroleum Technology (Dec. 1976) 28(12), 1402-1408.

Vetter, O. J. G. and Phillips, R. C., 1970. Predictionof Deposition of Calcium Sulfate Scale under Down-Hole Conditions. J. Pet. Tech. (Oct. 1970) 22(10), 1299-1308.

Warren E. A. and Smalley P. C., 1994. North Sea Formation Water Atlas. In Memoir No. 15, pp. 208. Geological Society.

Webb, P.J. and Kuhn, O., 2004. Enhanced Scale Management through the Application of Inorganic Geochemistry and Statistics. Paper SPE 87458 presented at the 6th International Symposium on Oilfield Scale held in Aberdeen, UK, 26-27 May 2004.

Weintritt, D. J. and Cowan, J. C., 1967. Unique Characteristics of Barium Sulfate Scale Deposition, J. Pet. Tech. (Oct., 1967) 19(10), 1381-1394.

Wolery, T.J., 1979. Calculation of chemical equilibrium between aqueous solution and minerals: the EQ3/6 software package. Lawrence Livermore National Laboratory, UCRL-52658 (1979).

Wylde, J.J., Williams, G.D.M, Careil, F., Webb, P., Morris, A., 2005. Deep downhole chemical injection on BP-operated Miller: "experience and learning. Paper SPE 922832 presented at the 2005 SPE International Symposium. Oilfield Chemistry Houston, Texas, USA, 2-4 February 2005.

Yeester, S. T., 1939. The Gypsum Problem in Water Flooding. Producers Monthly, (April, 1939) 27.

Yousef, A.A. and Ayirala, S.C., 2014. Optimization study of a novel water-ionic technology for smart-waterflooding application in carbonate reservoirs. Oil Gas. Facil. 3 (5), 72–82.

Yuan, M., Todd, A.C., Sorbie, K.S., 1994. Sulphate scale precipitation arising from seawater injection: a prediction study. Marine and Petroleum Geology (February 1994) 11, 24-30.

Zahid, A., Stenby, E.H. and Shapiro A.A., 2012. Smart Waterflooding (High Sal/Low Sal) in Carbonate Reservoirs. Paper SPE 154508, EAGE Annual Conference, Copenhagen, Denmark.

Zenger, D.H , Dunham, J.B., 1980. Concept and Models of Dolomitization – An introduction 1-9 in Concepts and Models of Dolomitization. SEPM Spec. Pubn, No.28, Tulsa, 1980.

Zhang, Y., and Sarma, H., 2012. Improving waterflood recovery efficiency in carbonate reservoirs through salinity variations and ionic exchanges: A promising low-cost “Smart waterflood” approach. Paper SPE 161631, International Petroleum Exhibition & Conference, Abu Dhabi, UAE.